

NASA
Technical
Paper
2430

C2
June 1985

Lee-Side Flow Over Delta Wings at Supersonic Speeds

David S. Miller
and Richard M. Wood

Property of U. S. Air Force
AEDC LIBRARY
F40600-81-C-0004 ✓

TECHNICAL REPORTS
FILE COPY

NASA

**NASA
Technical
Paper
2430**

1985

Lee-Side Flow Over Delta Wings at Supersonic Speeds

David S. Miller
and Richard M. Wood

*Langley Research Center
Hampton, Virginia*



National Aeronautics
and Space Administration

Scientific and Technical
Information Branch

Contents

| | |
|---|-----|
| Summary | 1 |
| Introduction | 1 |
| Symbols | 1 |
| Test Information | 2 |
| Models and Instrumentation | 2 |
| Wind Tunnel and Test Conditions | 2 |
| Flow-Visualization Methods | 2 |
| Discussion and Results | 3 |
| Classical Leading-Edge Vortex | 3 |
| Flow-Visualization Results | 3 |
| Pressure Results | 5 |
| Concluding Remarks | 7 |
| Figures | 8 |
| Appendix A | 17 |
| Appendix B | 19 |
| Appendix C | 116 |
| Appendix D | 129 |
| References | 150 |

Summary

An experimental investigation of the lee-side flow on sharp leading-edge delta wings at supersonic speeds has been conducted. Pressure data were obtained at Mach numbers from 1.5 to 2.8, and three types of flow-visualization data (oil-flow, tuft, and vapor-screen) were obtained at Mach numbers from 1.7 to 2.8 for wing leading-edge sweep angles from 52.5° to 75.0° . From the flow-visualization data, the lee-side flows were classified into seven distinct types, depending on the particular flow mechanism observed (e.g., shock or shockless, attached or separated, etc.). A chart was developed that defines the flow mechanism as a function of the conditions normal to the wing leading edge, specifically, angle of attack and Mach number.

Lee-side wing pressure data obtained experimentally and by a semiempirical prediction method were employed to investigate the effects of angle of attack, leading-edge sweep, and Mach number on vortex strength and vortex position. In general, the predicted and measured values of vortex-induced normal force and vortex position have the same trends with angle of attack, Mach number, and leading-edge sweep; however, the vortex-induced normal force is underpredicted by 15 to 30 percent, and the vortex spanwise location is overpredicted by approximately 15 percent.

Introduction

During the last 20 years, aerodynamicists have attempted to design aircraft wings for efficient supersonic flight using attached-flow concepts. For cruise levels of lift, linearized-theory wing-design methods (refs. 1 and 2) have successfully produced optimum twisted and cambered wings. Because of the early success of these methods, the methods have been continuously modified and refined to include the effects of component-on-wing interference (ref. 3), real-flow constraints (ref. 4), and attainable leading-edge thrust (ref. 5). Examples of applications of this low-lift wing-design technology are contained in references 6 through 8.

For maneuver levels of lift at supersonic speeds, basically two approaches are available for the design of wings. One approach is to provide an attached-flow, controlled expansion around the wing leading edge and on the upper surface. This attached-flow approach for producing efficient high lift depends on the ability to accelerate the flow around the leading edge to supercritical conditions on the upper surface and then decelerate the flow without causing separation or producing strong shocks; this high-lift, attached-flow, wing-design concept has been exper-

imentally verified, and a summary of the investigation is given in reference 9. The second approach for obtaining efficient high-lift wings uses a controlled, separated, leading-edge vortex flow which not only produces vortex lift, but when the vortex is located on the proper leading-edge shape, also produces significant levels of effective leading-edge thrust. Investigations at subsonic and transonic speeds of the fundamental vortex behavior on the leeward surface of wings have led to the design of several unique and novel leading-edge devices commonly referred to as "vortex flaps." Also, to aid in the design of vortex flaps, several computer codes with varying degrees of complexity are being developed to predict vortex location, strength, and effect on the wing. As summarized in reference 10, the development of this new wing-design technology has been extensive but has been confined mainly to subsonic and transonic flows.

The purpose of this paper is to present some fundamental vortex-flow results obtained at supersonic speeds. An experimental investigation was performed in which pressure data and three types of flow-visualization data were obtained on the leeward surface of a series of flat delta-wing models to identify the various flow mechanisms which can occur and to determine the effect of leading-edge sweep, Mach number, and angle of attack on the vortex strength and location.

Symbols

| | |
|------------|---|
| C_p | pressure coefficient |
| $C_{p,v}$ | vacuum pressure coefficient, $-2/\gamma M^2$ |
| M | Mach number |
| M_N | component of Mach number normal to leading edge, $M \cos \Lambda_{LE}(1 + \sin^2 \alpha \tan^2 \Lambda_{LE})^{1/2}$ |
| p_o | stagnation pressure |
| R | free-stream Reynolds number, per foot |
| T_D | dew-point temperature |
| T_o | stagnation temperature |
| x | longitudinal position from wing apex |
| y | spanwise position from wing centerline |
| α | angle of attack (ALPHA in computer generated tables) |
| α_N | angle of attack normal to leading edge, $\tan^{-1}(\tan \alpha / \cos \Lambda_{LE})$ |
| β | $= \sqrt{M^2 - 1}$ |
| γ | ratio of specific heat coefficients |

| | |
|----------------|--|
| Λ_{LE} | wing leading-edge sweep angle |
| η | fraction of local wing semispan (ETA in computer generated tables) |
| η_v | semispan location of vortex action point |

Test Information

Models and Instrumentation

Planform sketches of the four wind-tunnel models tested are shown in figure 1. The models consisted of a series of four delta wings, each of which had a span of 12 in. and a different leading-edge sweep angle; the leading-edge sweep angles were 52.5°, 60.0°, 67.5°, and 75.0°. To minimize the effect of airfoil shape and thickness, the leading edge was made sharp (10° angle normal to the leading edge located on the lower surface), and the upper surface was flat.

The leeward surface of each model was instrumented with a spanwise row of 19 evenly spaced pressure orifices located 1 in. forward of the wing trailing edge. The pressure orifices were located on both the right and left wing panels at locations ranging from 0 to 90 percent of the local semispan; the distance between orifices corresponded to 10 percent of the local semispan. Pressure data were obtained from a 48-port, scanning-valve, pressure-gage system mounted outside the tunnel.

The models were connected to the permanent model-actuating system of the tunnel by a dogleg sting. A typical assembly consisting of one of the models and the dogleg sting is shown in figure 2. The sting was designed to minimize support interference effects on the flat, pressure-instrumented wing surface opposite the sting attachment point. A detailed description of the sting is given in reference 11.

During the test, the angle of attack was measured with an accelerometer located in the permanent model-actuating system. The measured angle of attack was corrected for tunnel flow angularity using nominal flow-angle values obtained from reference 12. No angle-of-attack corrections were required for deflections of the dogleg sting.

Wind Tunnel and Test Conditions

The tests were conducted in the low Mach number test section of the Langley Unitary Plan Wind Tunnel, which is a variable Mach number, variable-pressure, continuous-flow, supersonic tunnel. The test cross section is approximately 4 ft by 4 ft. (See ref. 12 for a more detailed description of this facility.)

The tests were conducted at 0° sideslip and at angles of attack from 0° to 20° for the nominal test

conditions listed in the following table:

| M | p_o , lb/ft ² | T_o , °F | R , per ft |
|-----|----------------------------|------------|-----------------|
| 1.5 | 1052 | 125 | 2×10^6 |
| 1.7 | 1114 | 125 | 2×10^6 |
| 2.0 | 1254 | 125 | 2×10^6 |
| 2.4 | 1521 | 125 | 2×10^6 |
| 2.8 | 1875 | 125 | 2×10^6 |

To ensure fully turbulent boundary-layer flow over the model at attached flow conditions, according to the guidelines set forth in reference 13, transition strips composed of No. 60 carborundum grit were sprinkled on the upper surface 0.2 in. behind the model leading edge (measured normal to the leading edge). The transition strips were approximately 0.0625 in. wide.

Flow-Visualization Methods

In addition to the surface-pressure data, three types of flow-visualization data were obtained. Vapor-screen photographs were obtained to provide information on the flow field above the wing leeward surface, and both tuft and oil-flow photographs were used to examine the flow characteristics on the model surface. Because good quality vapor could not be produced at the lower Mach number of 1.5, no flow-visualization data of any type were taken at this lower Mach number.

Vapor-screen photographs were obtained by adding water in the diffuser downstream from the tunnel test section until a uniform vapor was produced in the test section. The test conditions which provided the best vapor quality for $R = 2 \times 10^6$ are given in the following table:

| M | p_o , lb/ft ² | T_o , °F | T_D , °F |
|-----|----------------------------|------------|------------|
| 1.7 | 1058 | 106 | 13 |
| 2.0 | 1228 | 124 | 19 |
| 2.4 | 1524 | 124 | 25 |
| 2.8 | 1863 | 124 | 29 |

In the preceding table, T_D is the dew-point temperature measured in the tunnel settling chamber and corrected to standard atmospheric conditions. The nominal test conditions at which pressure data were obtained correspond to a T_D value of -20°F.

Model preparation consisted of painting one coat of flat black paint over a coat of zinc-chromate primer. White dots were painted on the model upper-surface centerline at locations where vapor-screen data were desired.

A high-intensity tungsten light source mounted outside the tunnel on the sidewall was used to produce a thin light sheet across the tunnel test section. The light sheet was positioned normal to the flow and was positioned so the model could be moved longitudinally to align the light sheet with all the white dots. Photographs were taken by a camera mounted to the ceiling inside the tunnel and located approximately 3 ft downstream from the model. The relative locations of the vapor-screen apparatus are given in appendix A.

Tuft photographs were obtained by affixing fluorescent minitufts to the model surface and illuminating the model with ultraviolet light. Model preparation consisted of painting the surface flat black using the same procedure as that for vapor-screen photographs. Chordwise rows of tufts were attached to the model using a thinned solution of radio cement. The tufts were 0.75-in. lengths of 0.003-in. diameter nylon monofilament. Each chordwise row of tufts began at the downstream edge of the leading-edge grit with a longitudinal spacing of 0.75 in. between tuft-model attachment points. The longitudinal rows were spaced 0.50 in. apart in the spanwise direction, with the first row located on the model centerline. In some of the tests, tufts were affixed to both the left and right wing panels. In other tests, tufts were affixed only to the left wing panel, so that the right wing panel could be used for oil-flow photographs. Using self-developing film, tuft photographs were taken through the window by two cameras mounted outside the tunnel on the sidewall door. The model was rolled 90° (wings vertical) and was illuminated by four ultraviolet lamps also mounted on the sidewall door.

Oil-flow photographs required the same model-surface flat black painting as previously discussed. The model surface was then brushed with a mixture of 90W oil containing yellow fluorescent powder. The model was illuminated and cameras were positioned the same as for the tuft photographs. During the tunnel start-up period, the model was kept in a wings-horizontal position to prevent the oil from running; to obtain photographs the model was rolled 90° (wings vertical) and angle of attack was set by yawing the model. After the model is positioned, approximately 3 to 4 minutes is required for the oil-flow pattern to stabilize. Normally, only 3 or 4 different angles of attack can be documented before the oil must be replaced.

Discussion and Results

Flow-visualization photographs are presented in appendix B. Pressure-coefficient data are tabulated in appendix C and plotted in appendix D.

Classical Leading-Edge Vortex

In supersonic flow, it is well-known that at most moderate angles of attack an uncambered wing with a highly swept (subsonic) sharp leading edge will develop separated flow on the lee side, which results in a classical leading-edge vortex. Although most supersonic wing designs try to avoid flow separation, the leading-edge vortex has lift-producing characteristics which could possibly be integrated into a supersonic wing design. The basic leading-edge-vortex characteristics are shown in figure 3. The figure illustrates a typical spanwise pressure distribution and a sketch of the spanwise flow produced by a classical leading-edge vortex. As shown in the sketch, when the flow attempts to expand around a sharp leading edge, it separates and forms a region of rotational flow referred to as the "primary vortex." The highly rotational primary vortex induces surface velocities which can decrease the wing pressure distribution, relative to the attached-flow pressure distribution (see fig. 3), and produce vortex lift. In the classical situation, the primary vortex is above the wing and induces flow which reattaches at a point where there is streamwise flow on the inboard side of this point and outward spanwise flow on the outboard side. The outward spanwise flow can separate into a secondary vortex and modify the pressure distribution, as illustrated by the shaded area in figure 3.

Since the classical vortex is only one of several types of flow that can exist on the lee side of delta wings in supersonic flow, the flow-visualization photographs of this test were used to identify the various types of flow and the conditions under which they exist. The pressure data were used to investigate vortex strength and positioning.

Flow-Visualization Results

In previous experimental tests, a limited amount of flow-visualization information, with or without pressure data, was employed to explain the behavior of lee-side flows about delta wings; however, in this experiment, pressure data and three types of flow-visualization information were obtained. Both tuft and oil-flow photographs were used to examine the flow characteristics on the model surface and a vapor-screen flow-visualization technique was used to examine the flow field above the wing. The surface flow direction is determined by the alignment of the tufts or the streaking of the oil; however, the tufts tend to reflect the velocity direction at the edge of the boundary layer, and the direction of oil streaking is influenced not only by the surface velocity but also by the pressure distribution. The vapor-screen flow-visualization technique provides information on the

shape and location of vortices and shocks in the flow field above the wing. The dark areas in the vapor-screen photographs indicate regions having less water condensate (droplets) than the light regions. The reason for this lack of condensate has not been scientifically explained and is still under investigation for both shocks and vortices; however, several reasons have been hypothesized. In the case of vortices, one hypothesis is that the highly rotational vortex velocities eject the condensate. Another hypothesis is that the condensate does not penetrate through the shear layer into the boundary layer which feeds the vortex; thus, the condensate never gets into the vortex. In the case of shocks, one hypothesis is that there is less condensate simply because there are fewer particles as the result of the shock-wave-produced density decrease. Another possible explanation is that the condensate undergoes a phase change and vaporizes due to the temperature increase produced by the shock. Regardless of the reason, in vapor-screen photographs, shocks and vortices can be identified by dark regions caused by less condensate.

The matrix of test data points of the present study is presented in figure 4 as a function of conditions measured normal to the wing leading edge, specifically, normal angle of attack α_N and normal Mach number M_N . In a previous study, Stanbrook and Squire (ref. 14) reported that near $M_N = 1$, a boundary existed (shaded region in fig. 4) which divided the flow into two distinct regions. To the left of the boundary, the flow was characterized by a leading-edge, separated, rolled-up-vortex flow; to the right, it was characterized by an attached flow with possible shock-induced separation. The classification into just two types of flow provided by the Stanbrook-Squire boundary was revised by Ganzer, Hoder, and Szodruch (ref. 15); however, this latter effort was based on a single leading-edge sweep of 73° and flow conditions which either coincide with or lie to the right of the Stanbrook-Squire separation boundary. In the present study, several values of leading-edge sweep were used to examine the type of flow on both sides of the Stanbrook-Squire boundary, and the flow has been clearly divided into seven categories. (See fig. 5.) This classification procedure would not have been possible with only oil-flow, tuft, and pressure data; the vapor-screen flow-visualization data were critical in determining the existence and type of shock-vortex systems. Except for the no-shock/no-separation flow, the types of flow are discussed with the aid of figures 6 through 11. Each figure shows a sketch of oil-flow, tuft, vapor-screen, and pressure data which are typically associated with a particular type of flow.

The classical vortex of figure 6 is characterized

by a primary and secondary vortex with no shock. The oil-flow and tuft patterns are similar in that they both exhibit streamwise flow between the wing centerline and the primary vortex reattachment line which divides this inboard region of streamwise flow and the adjacent region of primary-vortex-induced, outward spanwise flow. Both surface flow visualization techniques also distinctly show the secondary-vortex separation line which is the outboard boundary for the primary-vortex-induced flow region. The oil-flow data indicate the position of the secondary vortex by an oil-accumulation line nearest the wing leading edge. This third boundary is not found in the tuft data. The pressure distribution shows the significant negative pressures induced by the vortex.

For large values of angle of attack, the vortex-with-shock situation (fig. 7) is a common occurrence for subsonic and supersonic leading edges. In this flow class, the shock is located on top of the vortex, and the presence of the shock is not indicated in either the oil-flow or tuft patterns. The general surface-flow pattern of the vortex-with-shock class is similar to the classical vortex surface-flow pattern of figure 6 when shifted inboard, and the inboard streamwise flow of figure 6 is no longer present in figure 7. Apparently, the effect of the shock is limited to the flow region above the wing; no shock effects are indicated in either the surface-flow pattern or surface-pressure distributions.

Figure 8 shows typical results for a leading-edge separation bubble with no shock. In contrast to the vortex, a separation bubble is defined as having its entire rotational flow contained within its boundaries, and it exhibits no secondary separation. Except for a small amount of oil accumulation along the leading edge, the oil-flow and tuft photographs exhibit only two distinct flow patterns—streamwise flow inboard, and spanwise flow outboard, where the dividing line corresponds to the termination of the separation bubble. Thus, the effects of the separation bubble are much more confined to the leading edge than those of the classical vortex, and the pressure distribution reflects a considerable amount of lifting-pressure augmentation.

As in the case of the vortex, the situation can occur where the separation bubble develops a shock located on top. (See fig. 9.) The tuft-flow pattern in figure 9 is identical to that in figure 8, with no indication that a shock has developed; however, the oil-flow pattern of the two figures is distinctly different with an obvious oil-accumulation line present in the vicinity of the shock. Unlike the vortex-with-shock situation, the effect of the shock on top of the bubble is clearly evident in both the oil-flow patterns and the surface pressures. The shock is distinguished in the

oil-flow pattern by an oil-accumulation line located within the bubble-induced spanwise flow region and in the surface pressures by the large pressure gradient.

For sharp leading-edge wings, the last two types of flow occur for supersonic leading-edge conditions only. For both types, the flow on and immediately behind the leading edge is attached and directed inboard until a shock is encountered, as shown in the vapor-screen data of figures 10 and 11. If the shock is weak, it simply deflects the flow downstream with no separation (see fig. 10); however, if the shock is strong, it induces separation in the form of a separation bubble located immediately inboard of the shock (see fig. 11). In both types of flow, it is very difficult to detect a shock from the oil-flow or tuft patterns, and the vapor-screen data were the principal means of detecting shocks. However, the tufts tend to flutter at the shock location, and this fluttering appears as random wiggles in the tuft-flow patterns of the types shown in figure 10. Without vapor-screen data, and except for the fluttering of the tufts at the shock location, the oil-flow and tuft patterns of figure 10 could be misinterpreted as shockless attached flow, and the patterns of figure 11 could be misinterpreted as the classical vortex flow of figure 6.

To summarize all the test data according to flow type, each of the test conditions shown in figure 4 was classified according to one of the seven flow types shown in figure 5, and the results are shown in figure 12. The α_N - M_N space is clearly divided into regions where the flow type is indicated by the vapor-screen sketch placed in each region. As an added feature to provide additional information, flows with or without shocks are denoted by open or closed symbols, respectively. Also, the symbol shape is used to identify the character of the rotational flow—the circular symbols denote flows with primary and secondary vortices, and the square symbols denote flows containing separation bubbles. As shown by the solid triangles in the figure, the only flow conditions which produced shockless attached flows were angles of attack of zero ($\alpha_N = 0$); however, this may have occurred because the next smallest angle of attack in the test matrix was 4° . The results of figure 12 can be used to interpret oil-flow or tuft patterns where there is some question about the flow type; for example, the tuft-flow pattern of figure 11 should not be mistakenly identified as a classical vortex because the conditions of $\Lambda_{LE} = 60^\circ$, $M = 2.8$, and $\alpha = 8^\circ$ correspond to $M_N = 1.4$ and $\alpha_N = 15.7^\circ$; which lies in the shock-induced separation region of figure 12. Because the two most effective types of separated flow being considered for performance enhancements

are the shockless bubble and shockless vortex, it is interesting to note that these two types of flow occupy the majority of the region for $M_N < 1$. Also, above a normal angle of attack of approximately 23° , the upper boundary of the region decreases towards $M_N = 0$ with increasing α_N .

Pressure Results

In the development of vortex-flap technology, the flap loads and moments, and thus the vortex strength and position, are very important. Aerodynamically, the vortex strength and location are important because it is desirable to maximize effectiveness through the selection of wing planform, flap planform, and flap deflection. Structurally, loads and moments are required for the selection and sizing of the actuator mechanism. Thus, it is necessary to understand the behavior of the vortex flow and, specifically, to know how the vortex strength and location vary with wing-flap shape and flow conditions. For the present delta-wing study, the only wing-shape parameter is the leading-edge sweep Λ_{LE} . The flow condition parameters are simply Mach number and angle of attack. In the remainder of this paper, the effect of leading-edge sweep, Mach number, and angle of attack on the vortex strength and location is discussed.

The vortex strength and location information was extracted from the measured and predicted upper-surface spanwise pressures. (See fig. 13.) The theoretical pressures are predicted using the computational method of reference 16 which predicts both attached-flow (theory without vortex) and separated-flow (theory with vortex) results. The attached flow is represented by linearized theory which has been modified to account for attached-flow nonlinearities occurring on wings at large angles of attack. The separated flow is represented by a semiempirical technique which uses the Polhamus suction analogy to determine the leading-edge-vortex force and then modifies the upper-surface attached-flow pressures to distribute this additional force over the wing upper surface. The location and distribution of the vortex-induced pressures are determined by empirical relationships, and the total upper-surface pressure is constrained by the vacuum limit. To examine the vortex strength, the one experimental spanwise pressure distribution and the two theoretical distributions have been integrated across the span to yield a section normal-force parameter $\int_0^1 \frac{\bar{C}_p}{\bar{C}_{p,v}} d\eta$. For variations in leading-edge sweep, Mach number, and angle of attack, the vortex strength can then be examined in terms of the normal-force parameter by comparing the experimental and theory-with-vortex increments

with the theory-without-vortex values. Although the vortex location is normally defined in terms of its position in space, the vortex location in this study is defined as the point on the wing at which the vortex normal-force vector should be placed to give the same moment as the vortex-induced pressure distribution. This latter definition of vortex location is referred to as the vortex action point η_v , and the method for computing it from the upper-surface pressures is shown in figure 13. As shown in figure 14, a range of planform and flow-condition parameters was selected to encompass the entire region designated to exhibit the classical vortex-type flow. For each variation of a given parameter, the other two parameters were held constant. For example, for the α variation, the Mach number and leading-edge sweep had values of 1.7 and 75.0° , respectively. Results for other combinations of parameters were examined, and those presented here are considered typical.

The effect of angle of attack on vortex strength is shown in figure 15. For three angles of attack, inset sketches of the pressure distributions used to obtain the normal-force parameter are also shown in the figure. The difference between the theory-without-vortex values and either experimental or theory-with-vortex values represents, respectively, the experimental or theoretical vortex-induced normal-force increment. For the entire angle-of-attack range, the vortex accounts for approximately a 50-percent increase in the upper-surface attached-flow normal force. In terms of the vortex-force increment, the theory consistently underpredicts the experimental values by 15 to 30 percent. The pressure distributions indicate that at the lower three-fourths of the angle-of-attack range, the theory predicts nearly the correct pressure-distribution shape, but, as reflected in the normal force, underpredicts the level. At the larger value of α , where the normal-force agreement is best, the theory incorrectly predicts both the shape and level of the pressure distribution. Also, the vortex normal forces increase linearly with angle of attack, and not quadratically as with the full-suction analogy.

In figure 16, it is shown that the section normal-force parameter increases at a slightly decreasing rate with Mach number, and this trend with Mach number is predicted by the theory. The experimental vortex normal-force increment has a constant value of 0.125, which apparently does not vary with Mach number; however, the theoretically predicted increment is 30 to 50 percent less than the experimental value. The corresponding spanwise pressure distributions are also shown in the figure; the most outstanding observation is that the theory tends to underpredict the pressure parameter $C_p/C_{p,v}$ in the vortex-

affected region regardless of Mach number. The theory also tends to overpredict the pressure parameter in the inboard attached-flow region, and this overprediction becomes more pronounced with increasing Mach number.

The effect of leading-edge sweep on vortex strength can be deduced by the normal-force parameter variations shown in figure 17. The two theoretical curves are coincident up to $\Lambda_{LE} = 60.0^\circ$ at which point they depart at an increasing rate with leading-edge sweep; this departure is due to the absence of any theoretical vortex force below 60.0° . However, it appears that the experimental normal-force and pressure distributions indicate that a small amount of experimental vortex force may exist even at the smallest leading-edge sweep value and that the vortex force increases with increasing leading-edge sweep. From the location of the smallest two values of Λ_{LE} in figure 14, it is clearly possible that a shock-induced separation bubble could exist, which is responsible for the larger experimental normal force shown in figure 17.

The effects of angle of attack, Mach number, and leading-edge sweep on the vortex action point are shown in figure 18. As shown in the sketch, the vortex action point is identified as the fraction of the local wing semispan η_v . The vortex action point is the semispan position at which the vortex normal-force vector should be placed to give the same moment as produced by the vortex-induced pressures. The theoretical value shown was computed from the method of reference 16, which is an empirical formulation and, as shown in the figure, is only a function of the angle of attack. The experimental value was obtained using the expression given in figure 13, where the vortex $C_p/C_{p,v}$ values correspond to the experimental data. As indicated by both experimental and theoretical results, the most pronounced change occurs for the inboard movement of the vortex action point with increasing angle of attack. Typically, the vortex action point moves from a location near 80 percent semispan to a location near 50 percent semispan as angle of attack changes from 4° to 20° . As the vortex action point moves inboard, according to the method of reference 16, a larger portion of the vortex influence region moves off the wing and becomes ineffective in producing normal force. This phenomenon may explain why the vortex normal-force increment deduced from experimental data increases linearly with angle of attack, and not quadratically according to the full-suction analogy. The full-suction analogy assumes that the entire vortex influence region is not distributed, but is concentrated at the wing leading edge. According to the method of reference 16, there is no change in the vortex action point with either

Mach number or leading-edge sweep. Experimentally, only a very small inboard movement was observed with increased Mach number; however, the variation with leading-edge sweep is somewhat erratic. This erratic behavior is probably caused by the fact that the two smallest sweep values correspond to conditions at which the type of flow is changing from a classical vortex into other regions as indicated in figure 14. In general, the experimental vortex location is usually inboard of the theoretically predicted location, and the two values agree within 15 percent.

Concluding Remarks

An experimental investigation of the upper-surface flow on sharp leading-edge delta wings at supersonic speeds has been conducted. Pressure data and three types of flow-visualization data (oil-flow, tuft, and vapor-screen) were obtained at Mach numbers M from 1.7 to 2.8 for wing leading-edge sweep angles Λ_{LE} from 52.5° to 75.0° .

From the flow-visualization data, the upper-surface flows were classified into seven distinct types, depending on the particular flow mechanism observed (e.g., shock or shockless, attached or separated, etc.). A chart is presented which defines the flow mechanism as a function of the conditions normal to the wing leading edge, specifically, angle of attack α and Mach number.

Measured and predicted upper-surface wing pressure data were employed to investigate the effects of angle of attack, leading-edge sweep angle, and Mach number on vortex strength and vortex position. In general, the vortex induces an incremental normal force which, in some cases, increases the attached-flow normal force (upper-surface contribution) by as much as 50 percent. The location of the vortex action point was most sensitive to variations in angle of attack; in general, the action point moved from near 80 percent to near 50 percent of the local span as the angle of attack changed from 4° to 20° . These changes in location of the vortex action point may explain why the observed vortex-induced normal force increased linearly with angle of attack, and not quadratically according to the full-suction analogy.

Experimental results were compared with results of one semiempirical prediction method. In general, the predicted and measured values of normal force and vortex location have the same trends with α , M , and Λ_{LE} ; however, the vortex normal force is underpredicted by 15 to 30 percent, and the vortex location is overpredicted by approximately 15 percent.

NASA Langley Research Center
Hampton, VA 23665
February 25, 1985

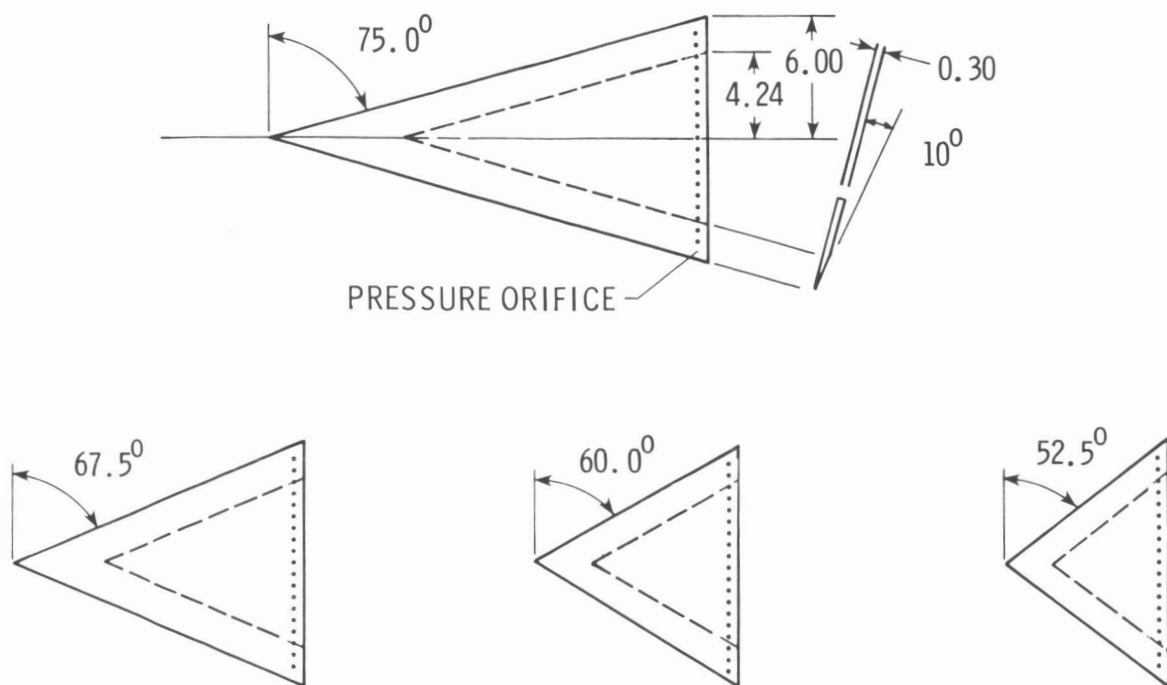


Figure 1. Model planform series. (Linear dimensions in inches.)

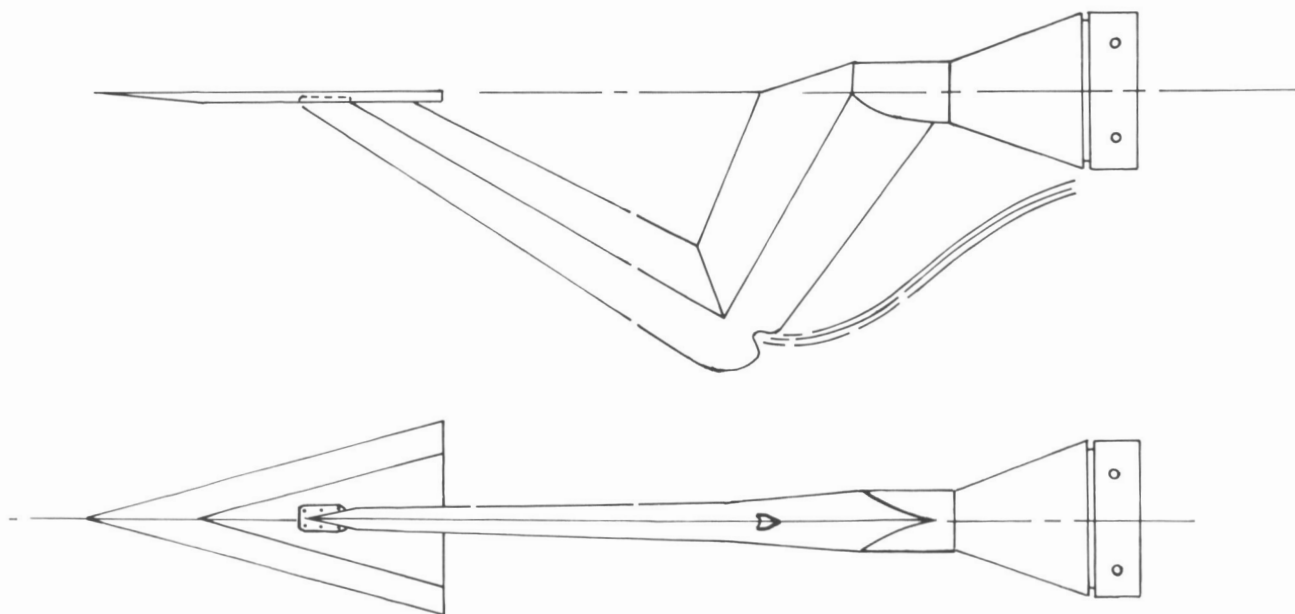


Figure 2. Typical assembly of model and dogleg sting.

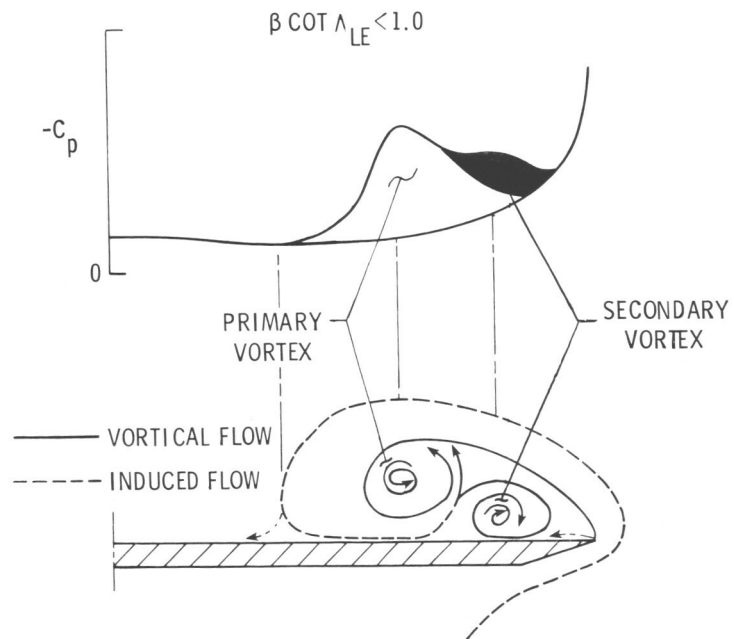


Figure 3. Basic characteristics of a leading-edge vortex.

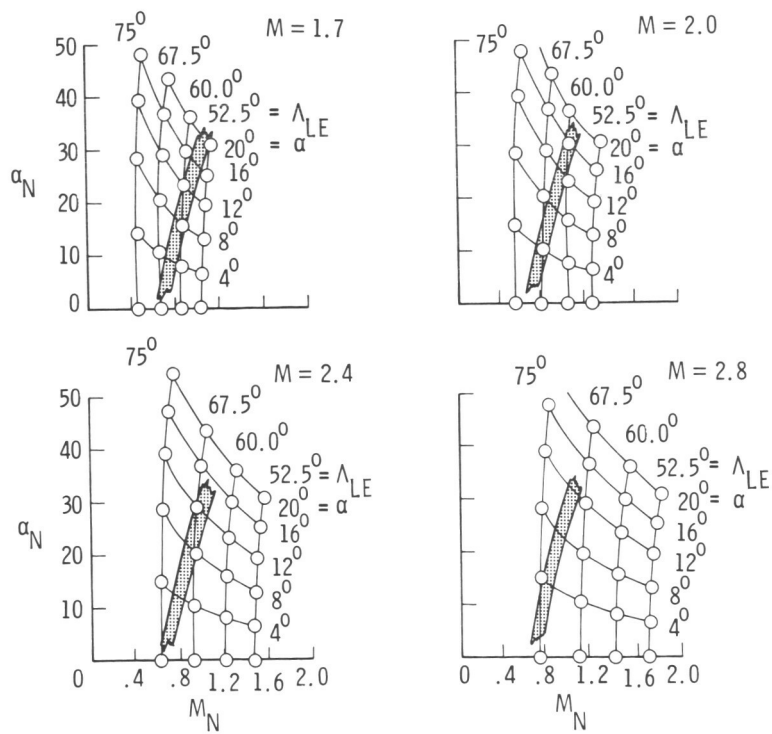
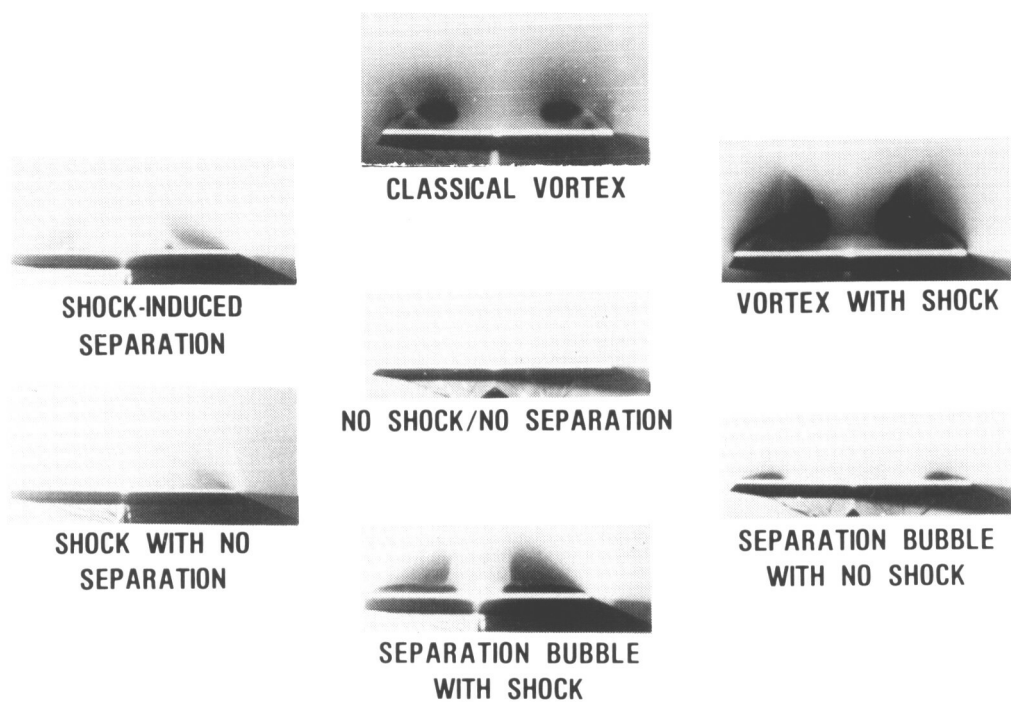


Figure 4. Matrix of test conditions.



L-83-8124

Figure 5. Flow classifications.

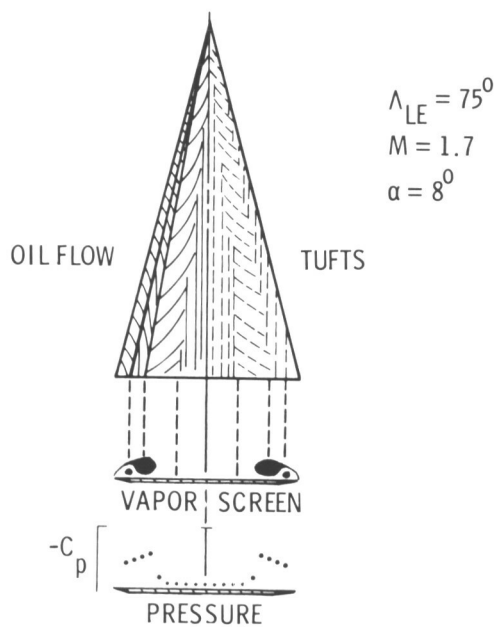


Figure 6. Classical vortex.

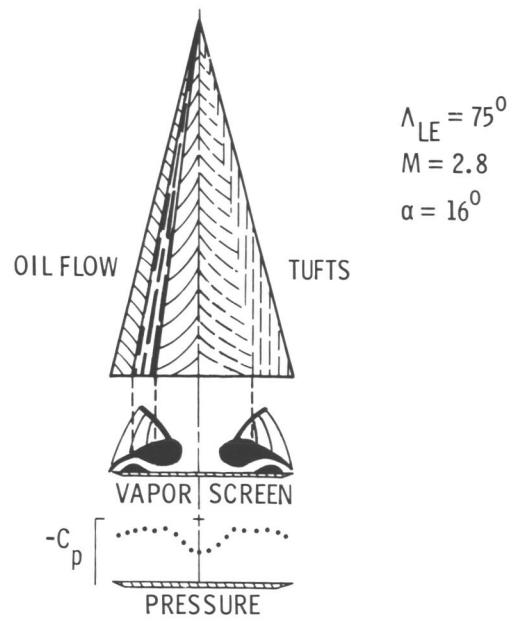


Figure 7. Vortex with shock.

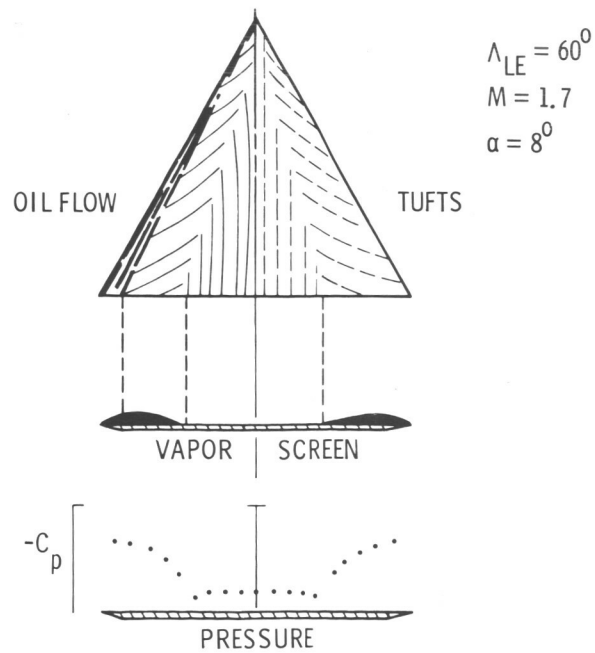


Figure 8. Separation bubble with no shock.

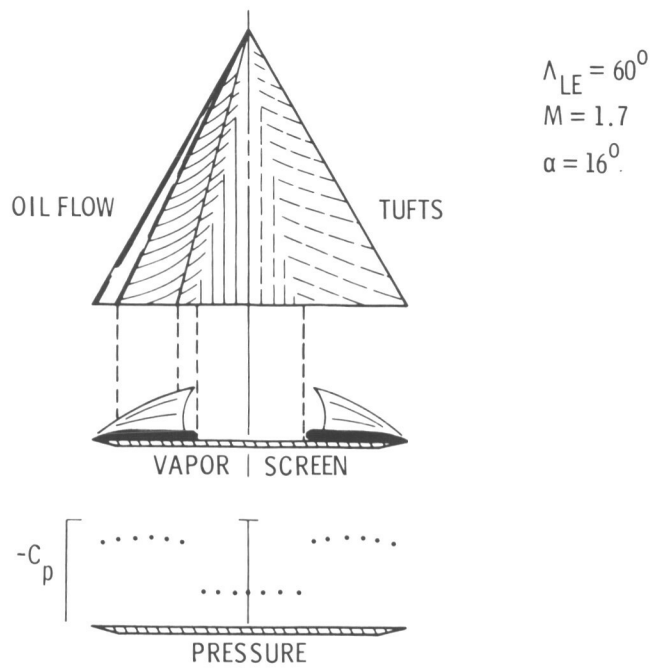


Figure 9. Separation bubble with shock.

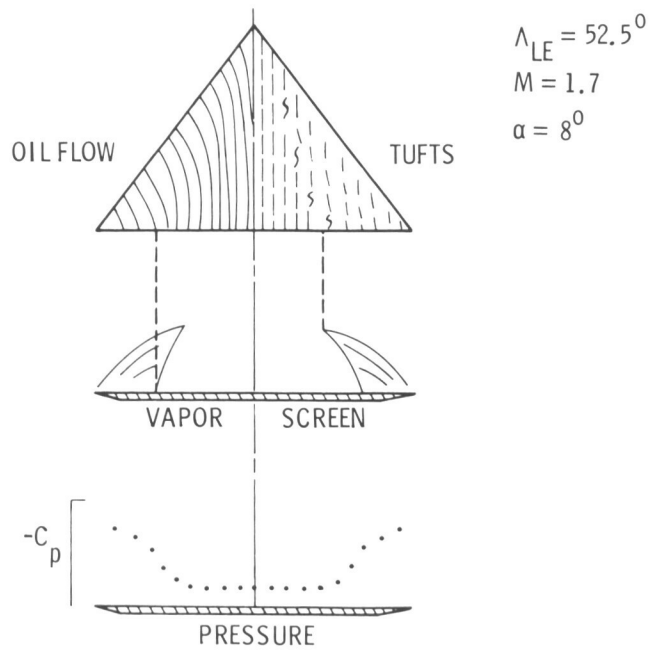


Figure 10. Shock with no separation.

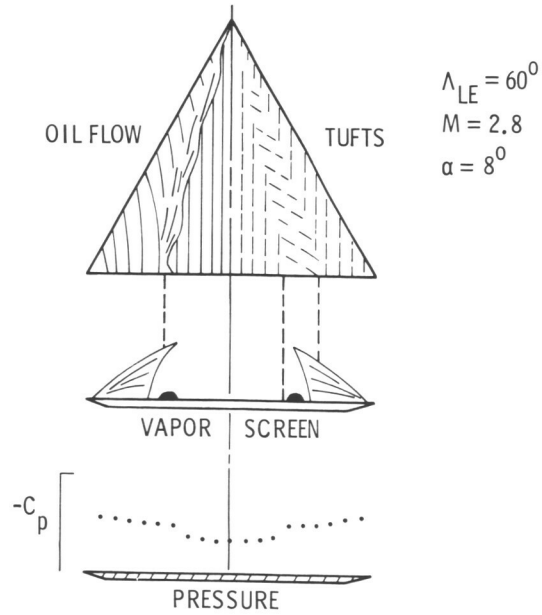


Figure 11. Shock-induced separation.

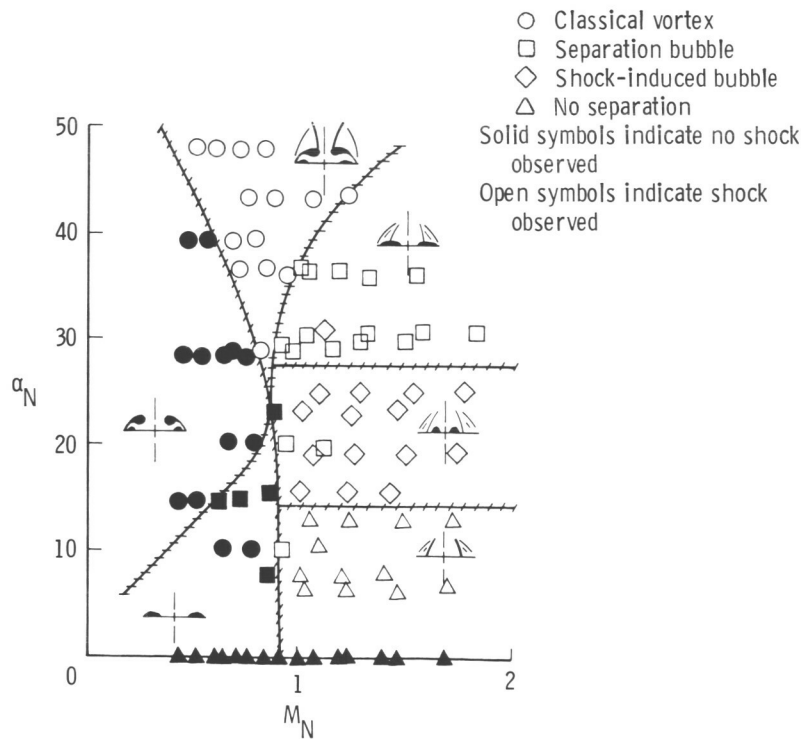


Figure 12. Classification of test data.

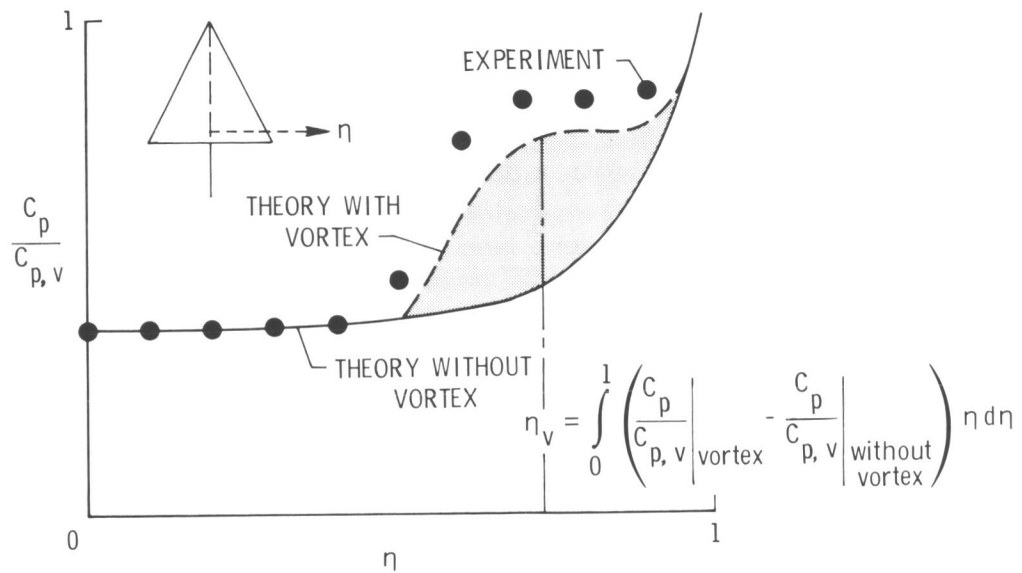


Figure 13. Typical spanwise upper-surface pressure distributions.

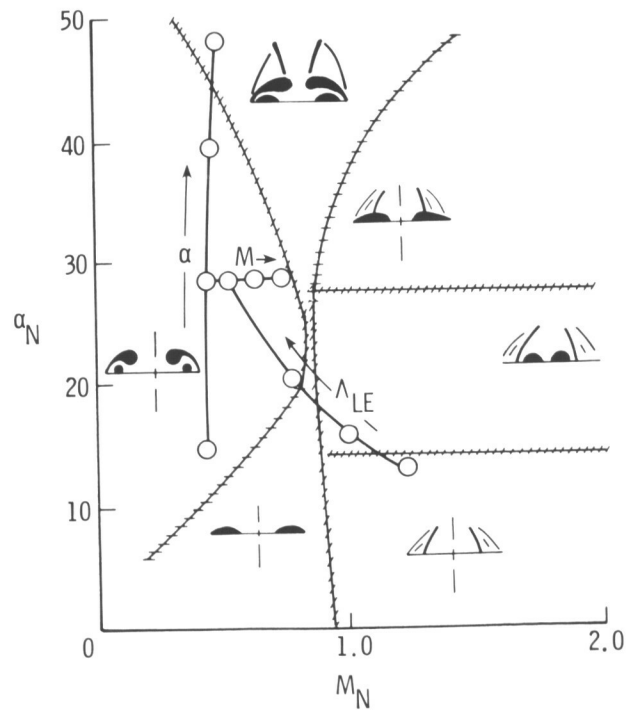


Figure 14. Variation of α , Λ_{LE} , and M for parametric study.

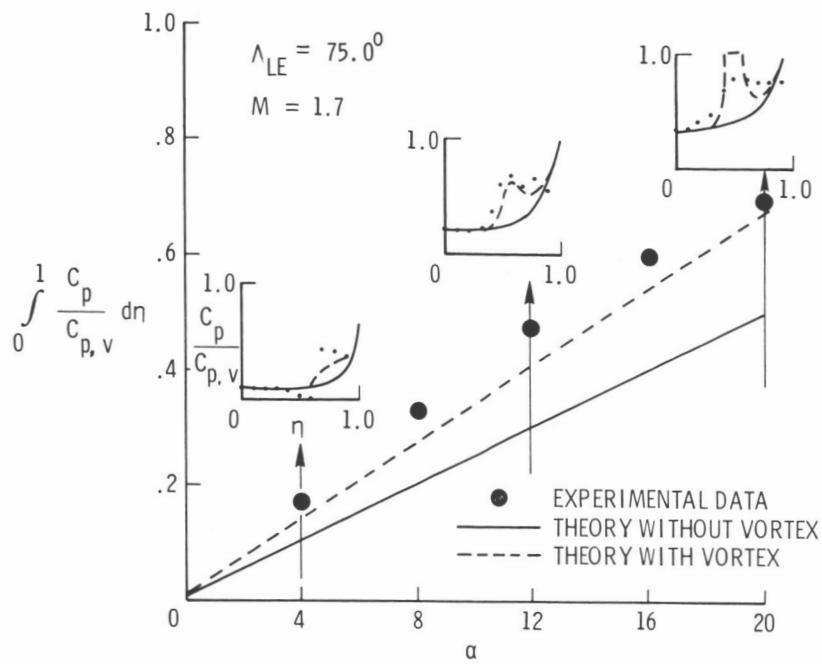


Figure 15. Effect of angle of attack on vortex strength.

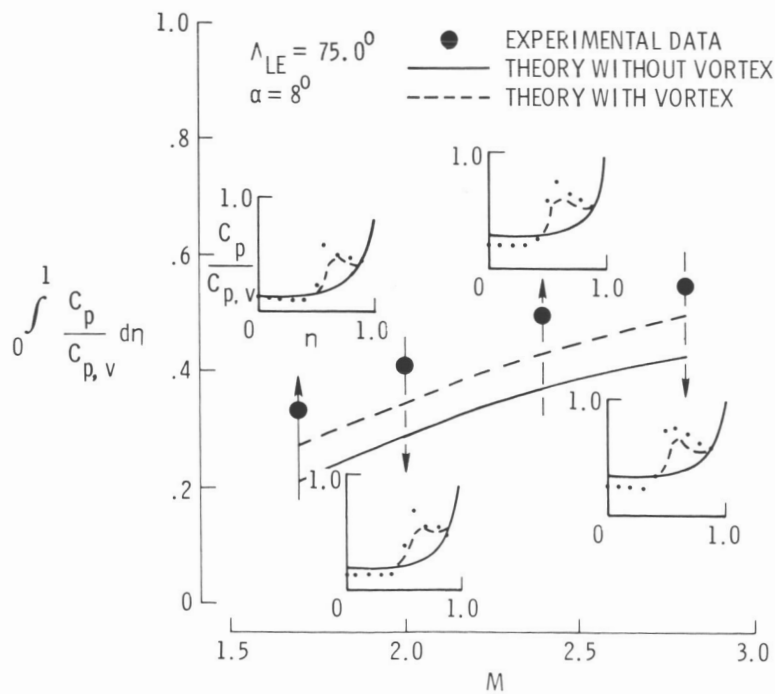


Figure 16. Effect of Mach number on vortex strength.

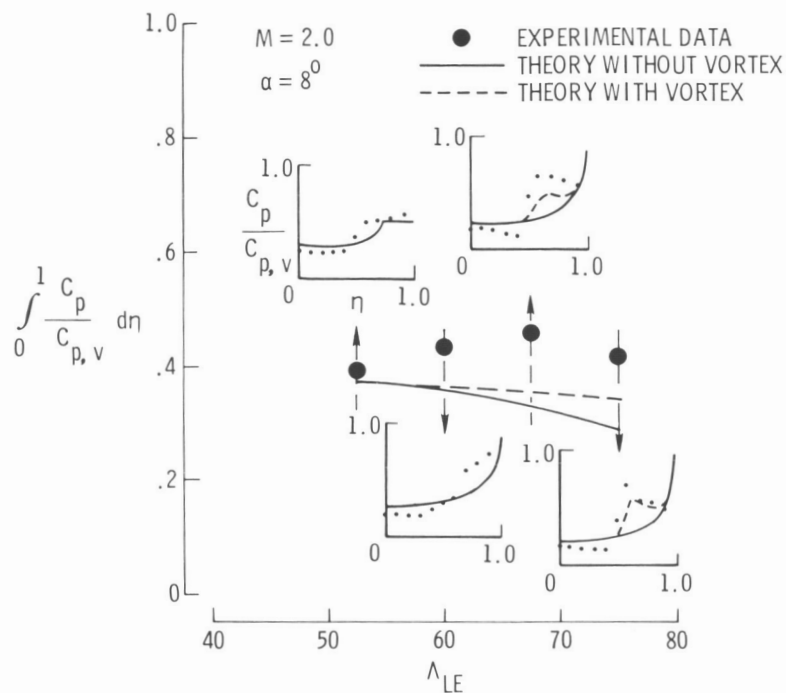


Figure 17. Effect of leading-edge sweep angle on vortex strength.

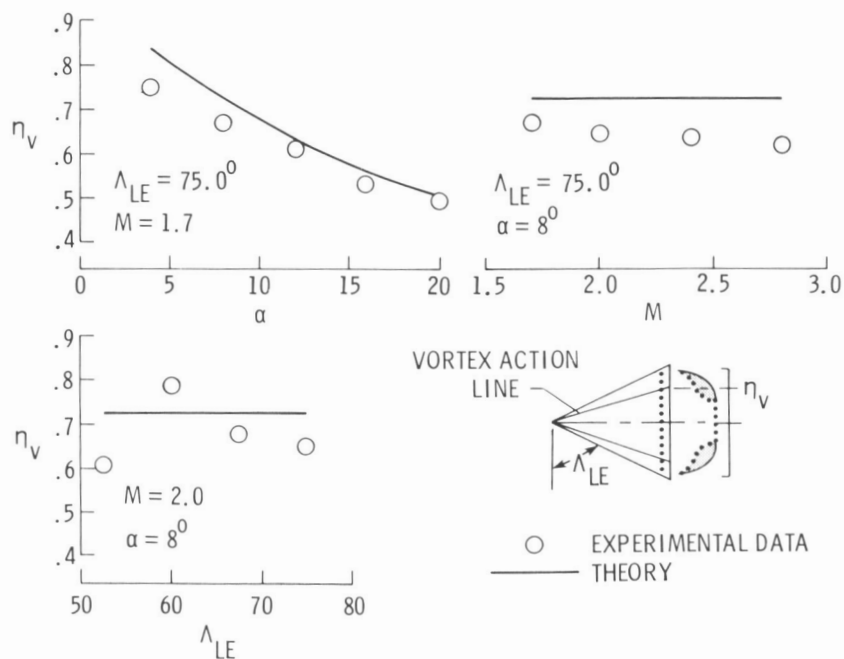


Figure 18. Location of vortex action line.

Appendix A—Vapor-Screen Photographic Apparatus

Vapor-screen photographs were obtained using a high-intensity tungsten light source mounted outside the tunnel and a camera mounted to the ceiling inside the tunnel. The light source was used to produce a thin light sheet across the tunnel test section, and the model was located to align the light sheet with the pressure-orifice location. The relative locations of the model, light sheet, and camera are shown in the following sketch, and the values of the distances (in.) and angles (deg) are given in tables A1, A2, A3, and A4 for models having leading-edge sweep values of 75.0° , 67.5° , 60.0° , and 52.5° , respectively:

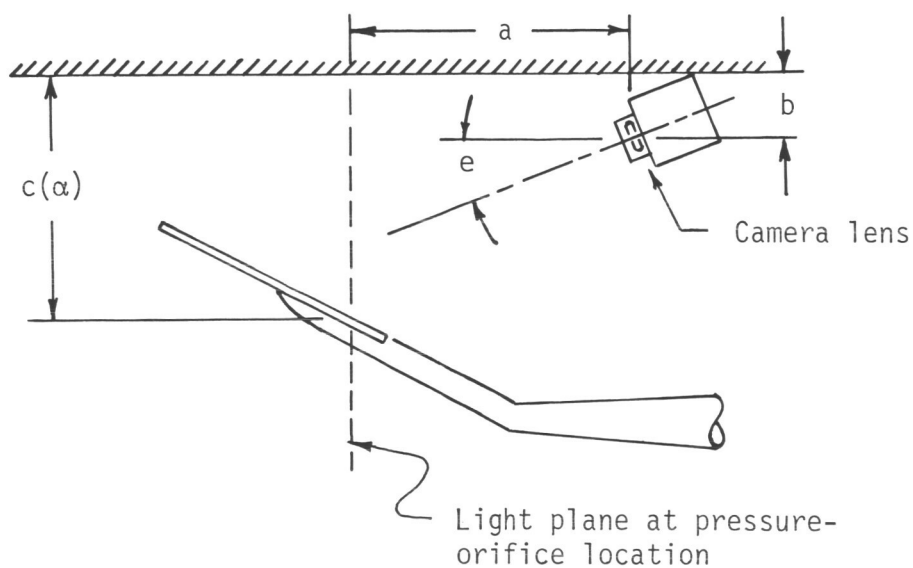


TABLE A1. LOCATIONS OF VAPOR-SCREEN APPARATUS FOR DELTA WING WITH $\Lambda_{LE} = 75.0^\circ$

$[e = 14.27^\circ; b = 8.55 \text{ in.}; a = 32.78 \text{ in.}]$

| $\alpha, \text{ deg}$ | $c(\alpha), \text{ in., at—}$ | | | |
|-----------------------|-------------------------------|-----------|-----------|-----------|
| | $M = 1.7$ | $M = 2.0$ | $M = 2.4$ | $M = 2.8$ |
| 0 | 25.25 | 25.20 | 25.15 | 25.30 |
| 4 | 26.00 | 25.85 | 25.85 | 26.27 |
| 8 | 27.10 | 26.90 | 26.90 | 27.25 |
| 12 | 28.10 | 27.90 | 27.90 | 28.25 |
| 16 | 28.50 | 28.50 | 28.50 | 28.50 |
| 20 | 28.30 | 28.37 | 28.37 | 28.27 |

TABLE A3. LOCATIONS OF VAPOR-SCREEN APPARATUS FOR DELTA WING WITH $\Lambda_{LE} = 60.0^\circ$

$[e = 14.27^\circ; b = 8.55 \text{ in.}; a = 36.78 \text{ in.}]$

| $\alpha, \text{ deg}$ | $c(\alpha), \text{ in., at—}$ | | | |
|-----------------------|-------------------------------|-----------|-----------|-----------|
| | $M = 1.7$ | $M = 2.0$ | $M = 2.4$ | $M = 2.8$ |
| 0 | 25.30 | 25.30 | 25.28 | 25.35 |
| 4 | 25.75 | 25.65 | 25.65 | 25.85 |
| 8 | 26.53 | 26.40 | 26.40 | 26.60 |
| 12 | 27.20 | 27.10 | 27.10 | 27.20 |
| 16 | 27.35 | 27.38 | 27.35 | 27.35 |
| 20 | 26.80 | 26.95 | 26.95 | 26.75 |

TABLE A2. LOCATIONS OF VAPOR-SCREEN APPARATUS FOR DELTA WING WITH $\Lambda_{LE} = 67.5^\circ$

$[e = 14.27^\circ; b = 8.55 \text{ in.}; a = 36.78 \text{ in.}]$

| $\alpha, \text{ deg}$ | $c(\alpha), \text{ in., at—}$ | | | |
|-----------------------|-------------------------------|-----------|-----------|-----------|
| | $M = 1.7$ | $M = 2.0$ | $M = 2.4$ | $M = 2.8$ |
| 0 | 25.30 | 25.25 | 25.25 | 25.35 |
| 4 | 25.75 | 25.75 | 25.75 | 25.95 |
| 8 | 26.80 | 26.60 | 26.60 | 26.85 |
| 12 | 27.55 | 27.45 | 27.45 | 27.60 |
| 16 | 27.80 | 27.80 | 27.80 | 27.80 |
| 20 | 27.40 | 27.50 | 27.50 | 27.35 |

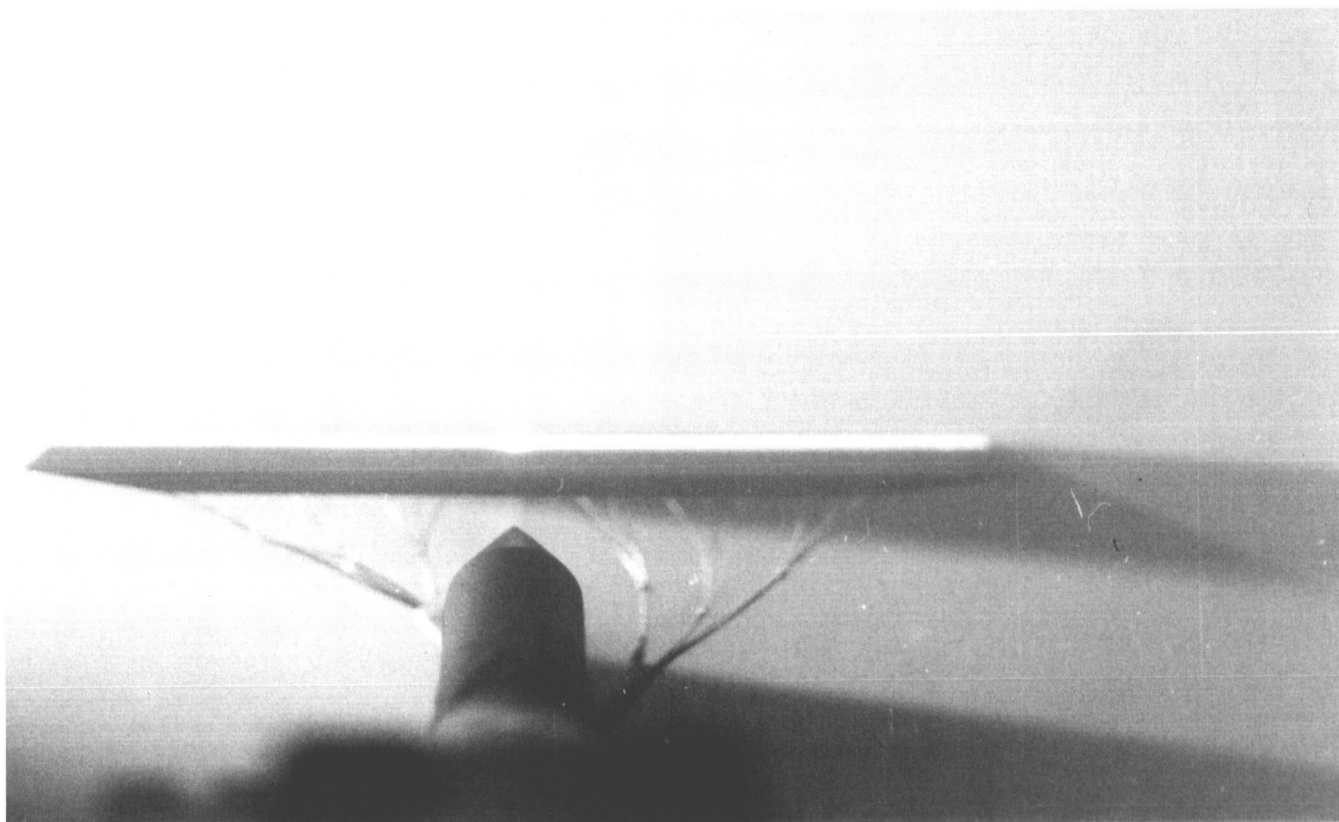
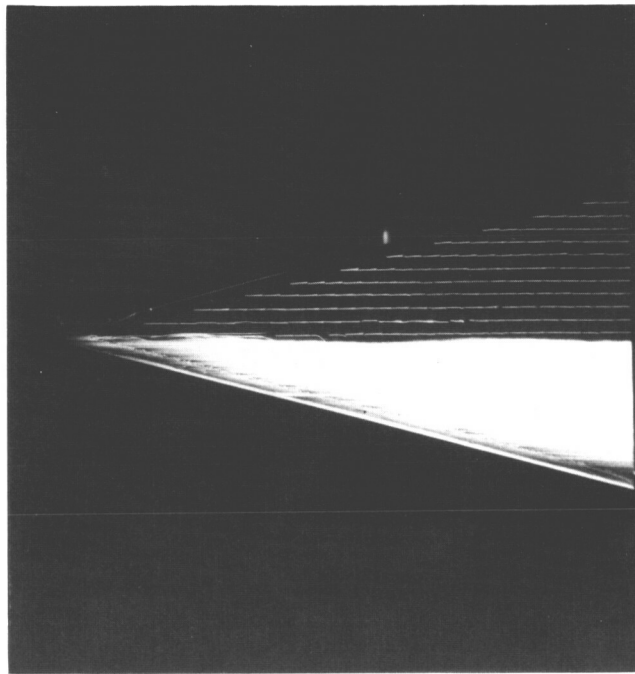
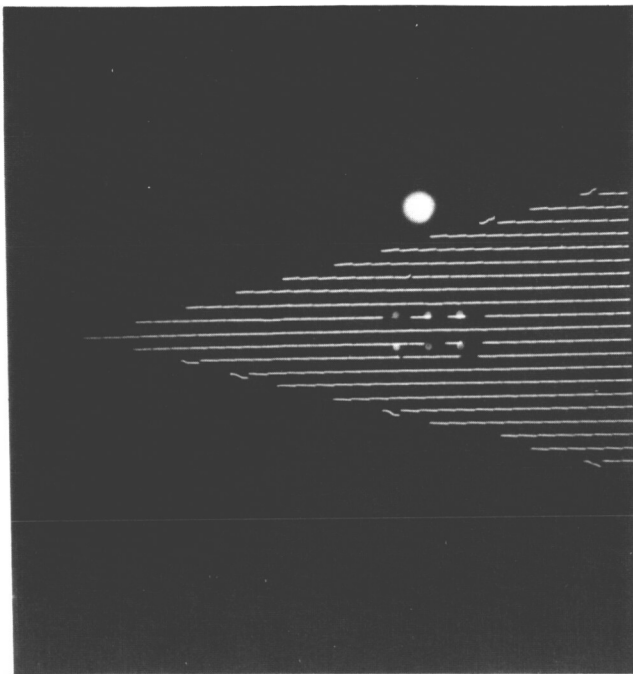
TABLE A4. LOCATIONS OF VAPOR-SCREEN APPARATUS FOR DELTA WING WITH $\Lambda_{LE} = 52.5^\circ$

$[e = 14.27^\circ; b = 8.55 \text{ in.}; a = 36.78 \text{ in.}]$

| $\alpha, \text{ deg}$ | $c(\alpha), \text{ in., at—}$ | | | |
|-----------------------|-------------------------------|-----------|-----------|-----------|
| | $M = 1.7$ | $M = 2.0$ | $M = 2.4$ | $M = 2.8$ |
| 0 | 25.30 | 25.30 | 25.30 | 25.30 |
| 4 | 25.75 | 25.65 | 25.60 | 25.80 |
| 8 | 26.45 | 26.30 | 26.30 | 26.55 |
| 12 | 27.10 | 27.00 | 27.00 | 27.10 |
| 16 | 27.15 | 27.20 | 27.20 | 27.15 |
| 20 | 26.60 | 26.80 | 26.80 | 26.55 |

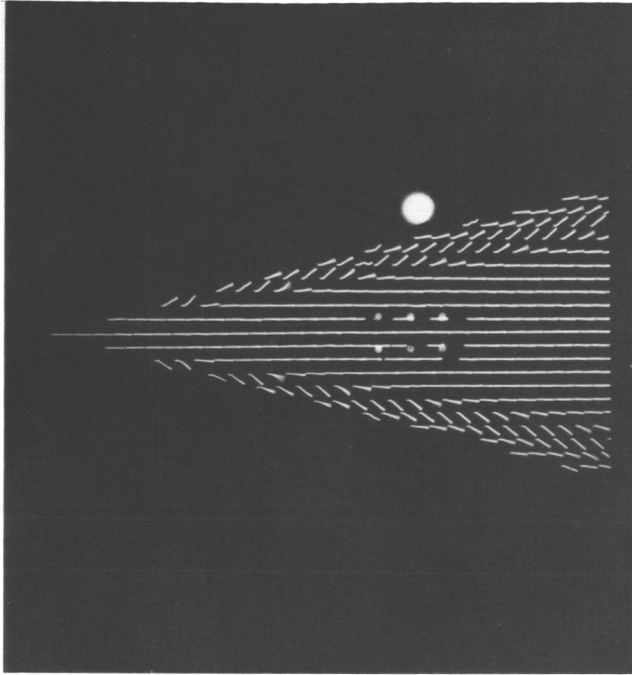
Appendix B—Flow-Visualization Photographs

Flow-visualization photographs for the four delta wings with leading-edge sweep values of 75.0° , 67.5° , 60.0° , and 52.5° are presented in figures B1, B2, B3, and B4, respectively.

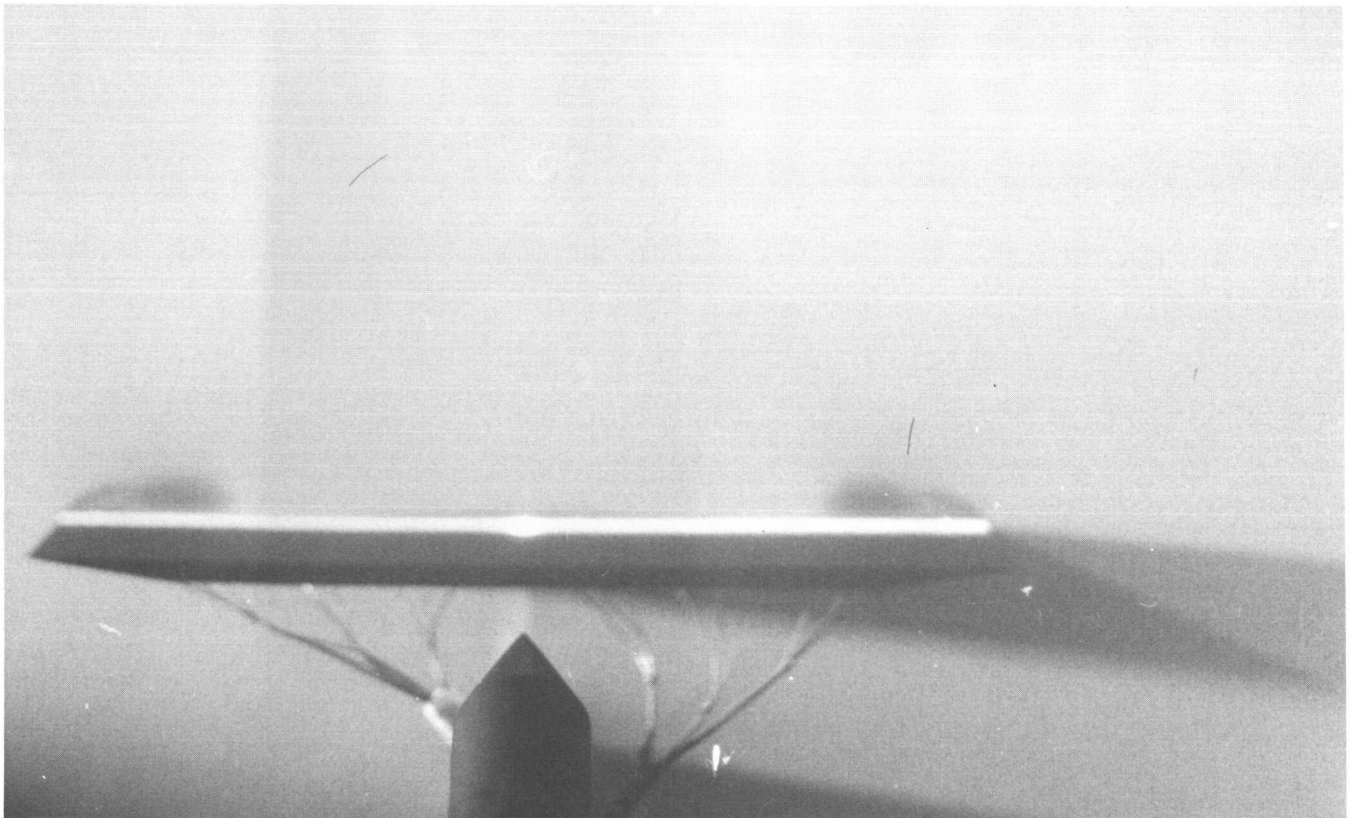


(a) $M = 1.7$, $\alpha = 0^\circ$.

Figure B1. Flow-visualization photographs for delta wing with $\Lambda_{LE} = 75^\circ$.

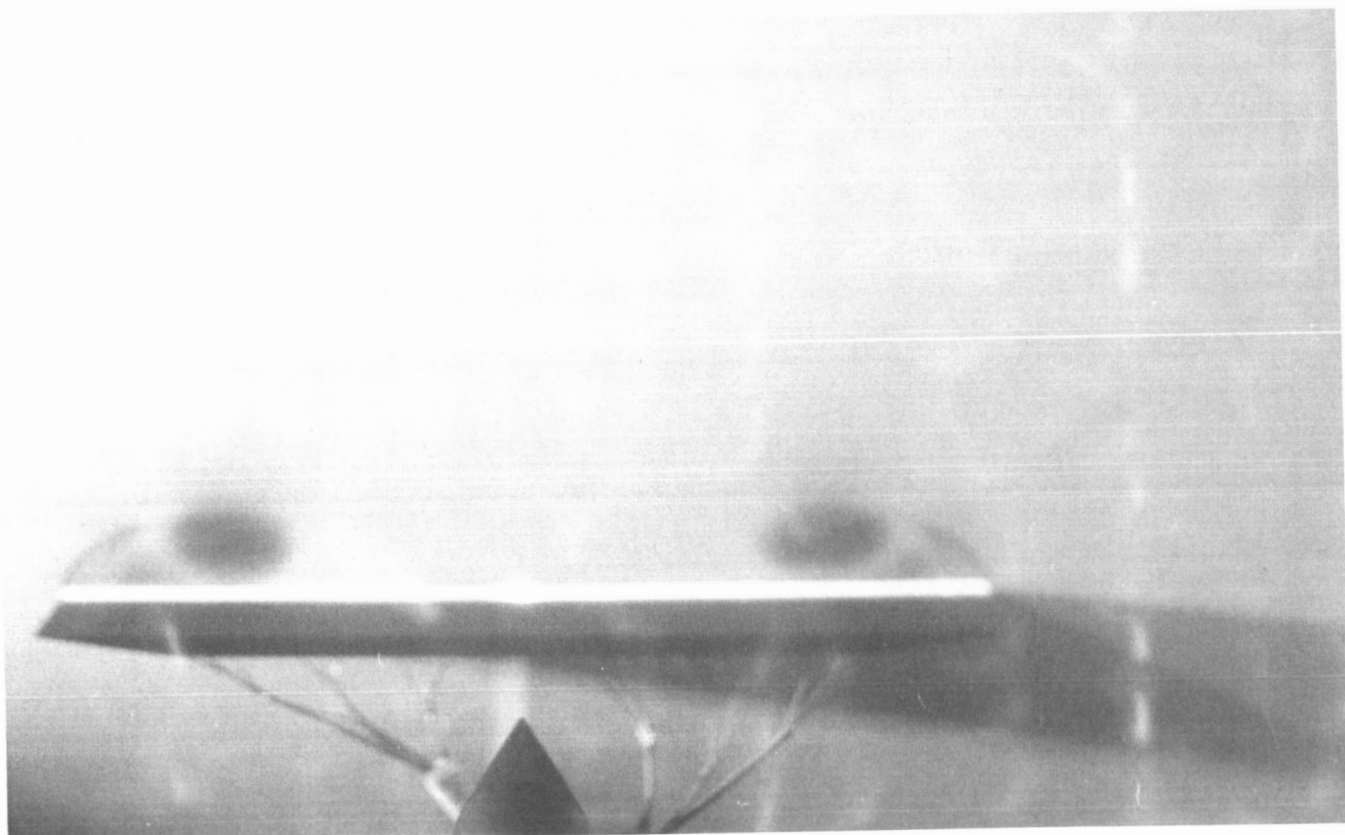
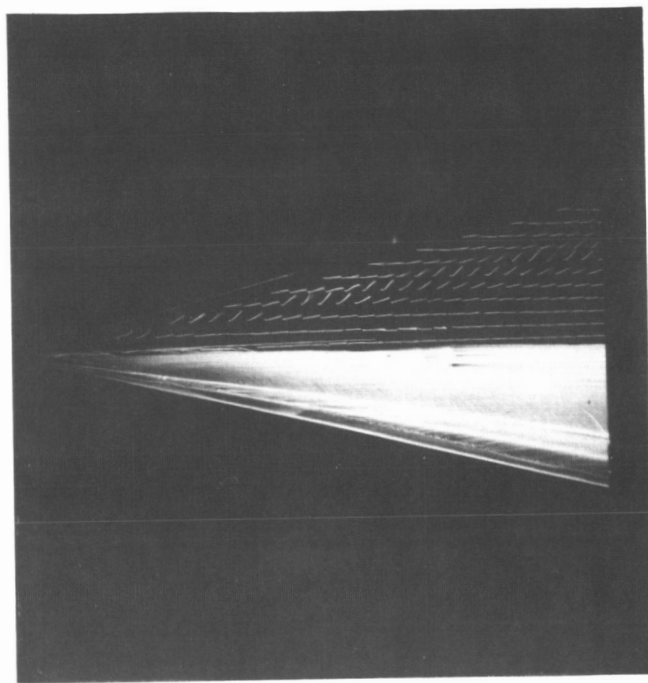
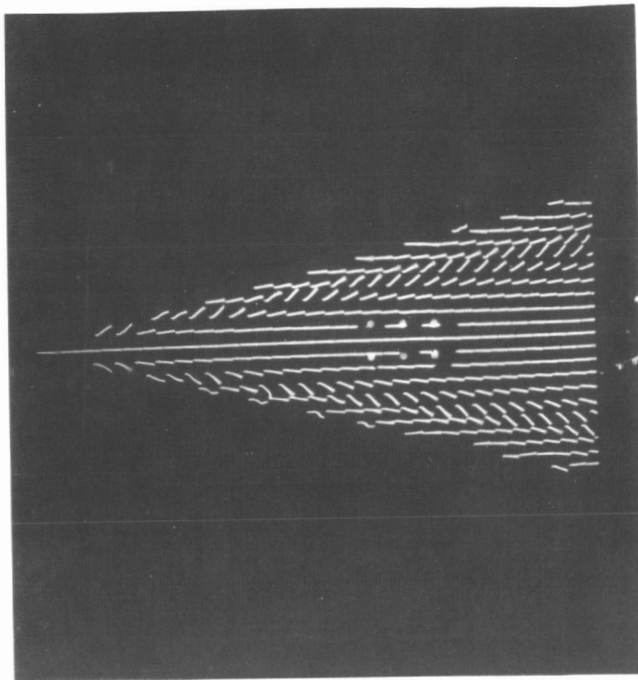


NO DATA



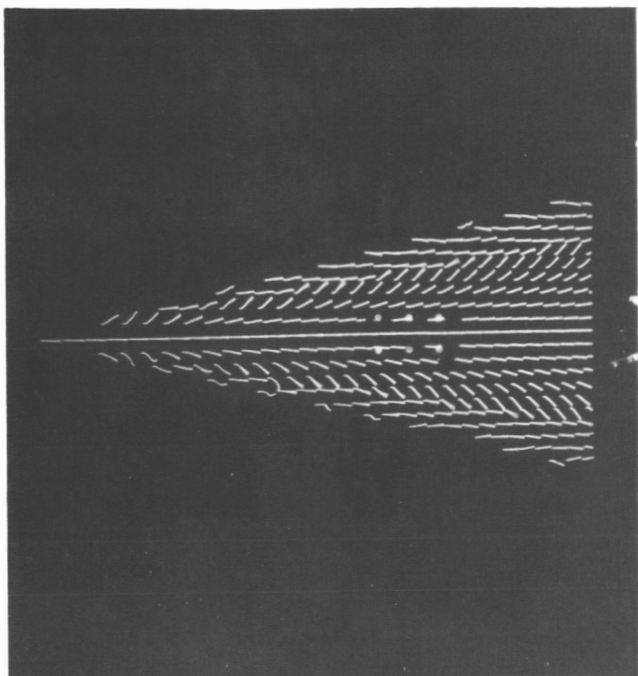
(b) $M = 1.7$, $\alpha = 4^\circ$.

Figure B1. Continued.

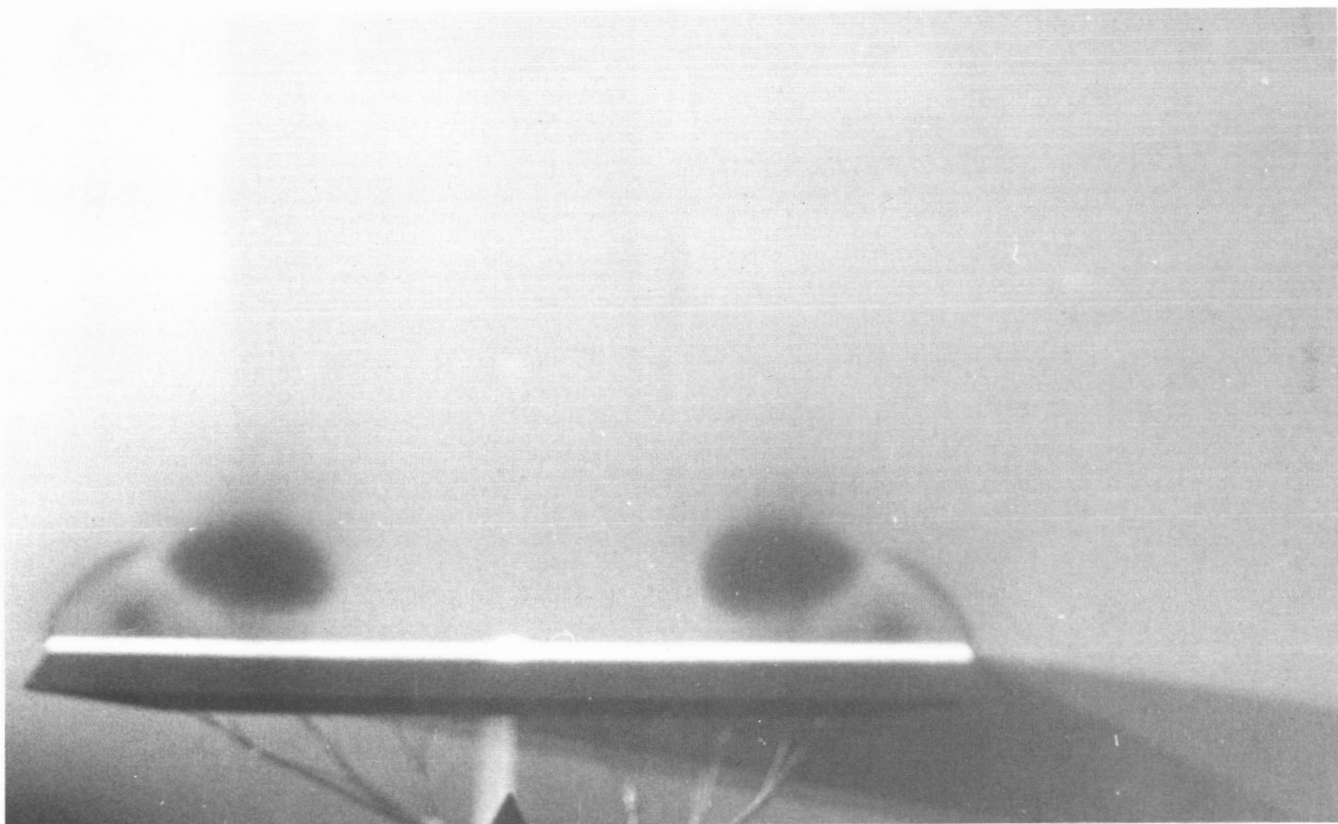


(c) $M = 1.7$, $\alpha = 8^\circ$.

Figure B1. Continued.

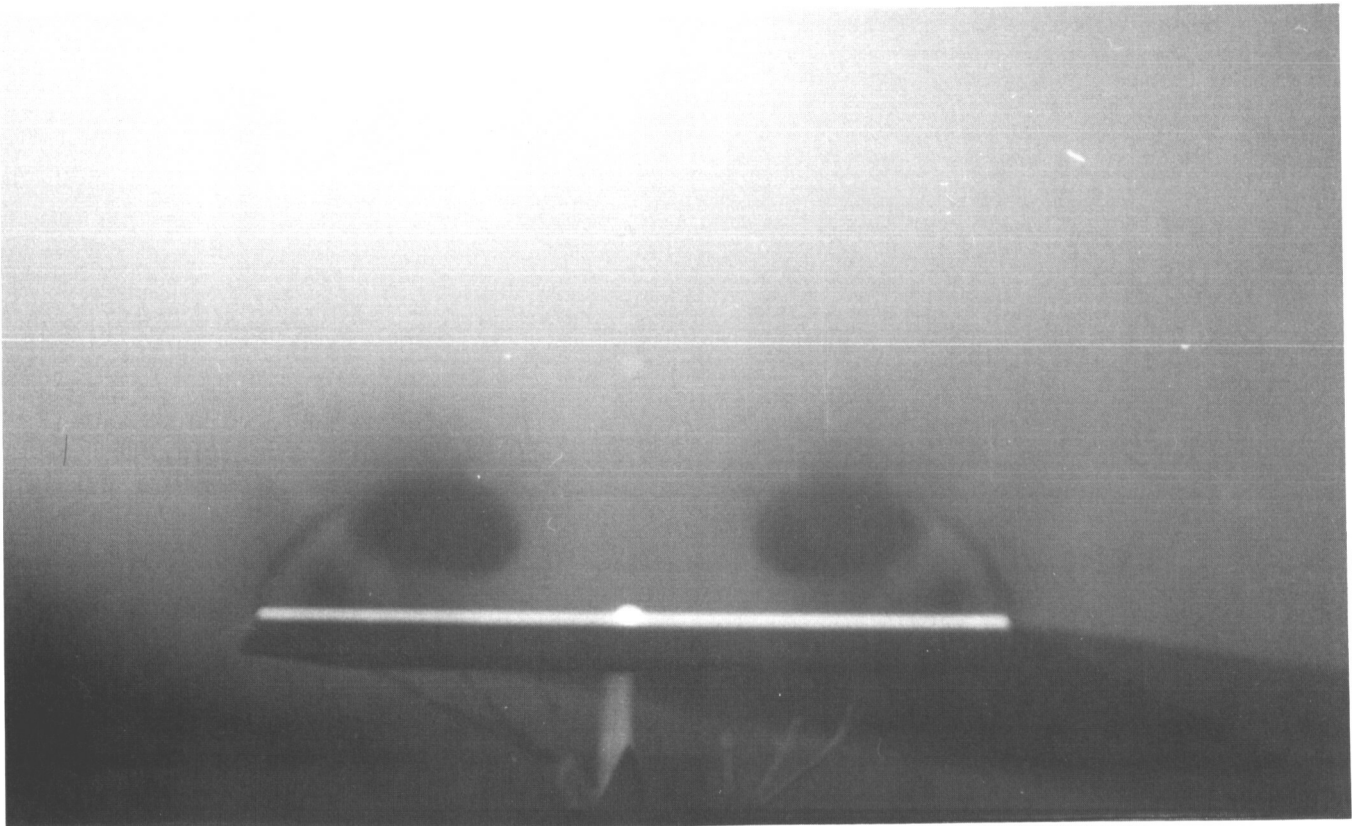
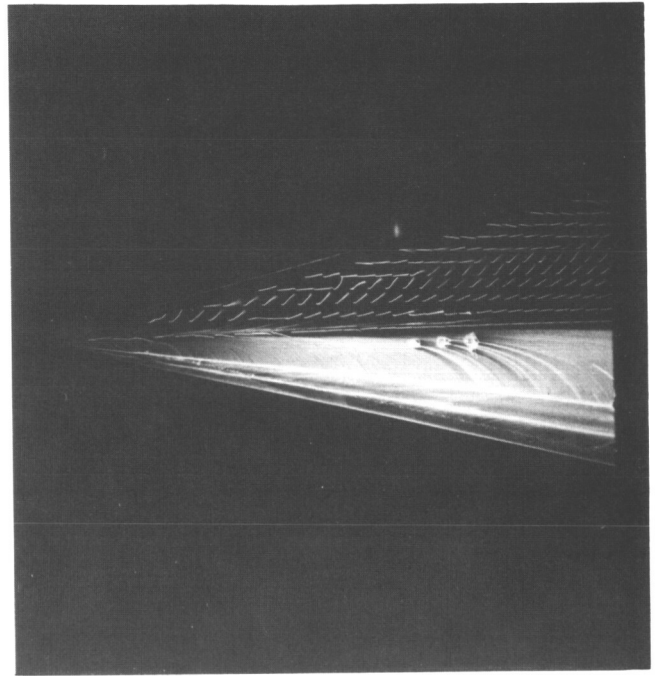
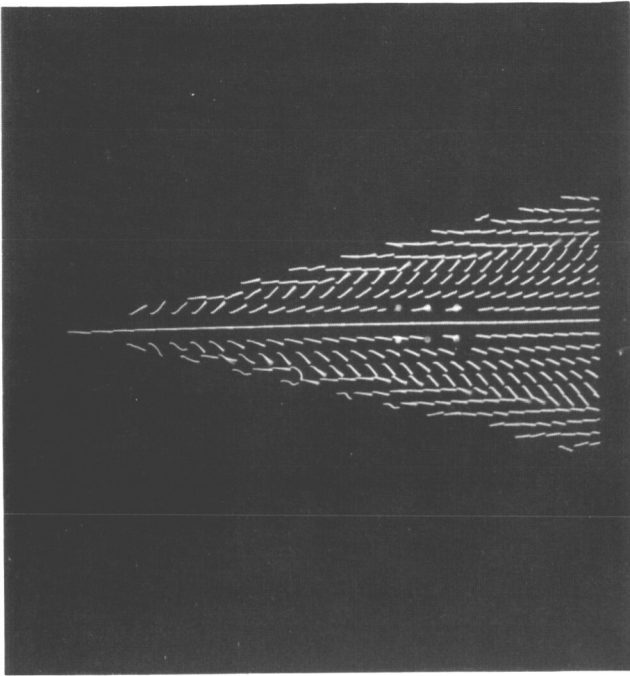


NO DATA



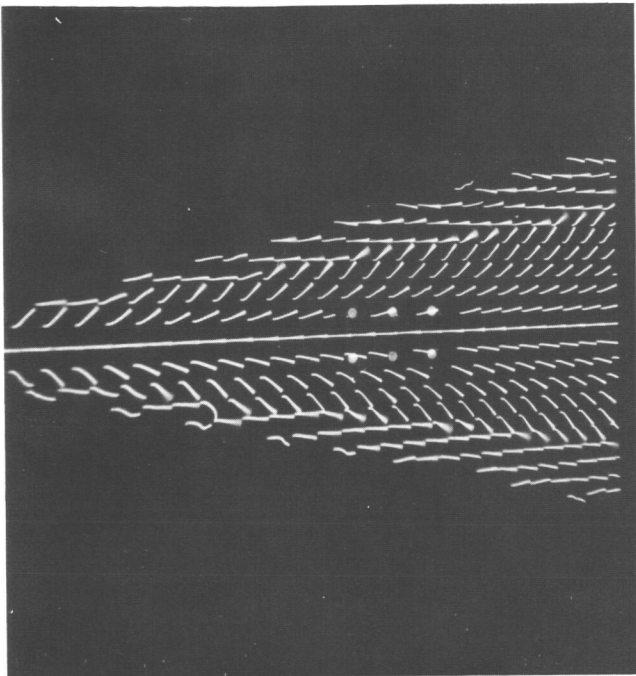
(d) $M = 1.7$, $\alpha = 12^\circ$.

Figure B1. Continued.

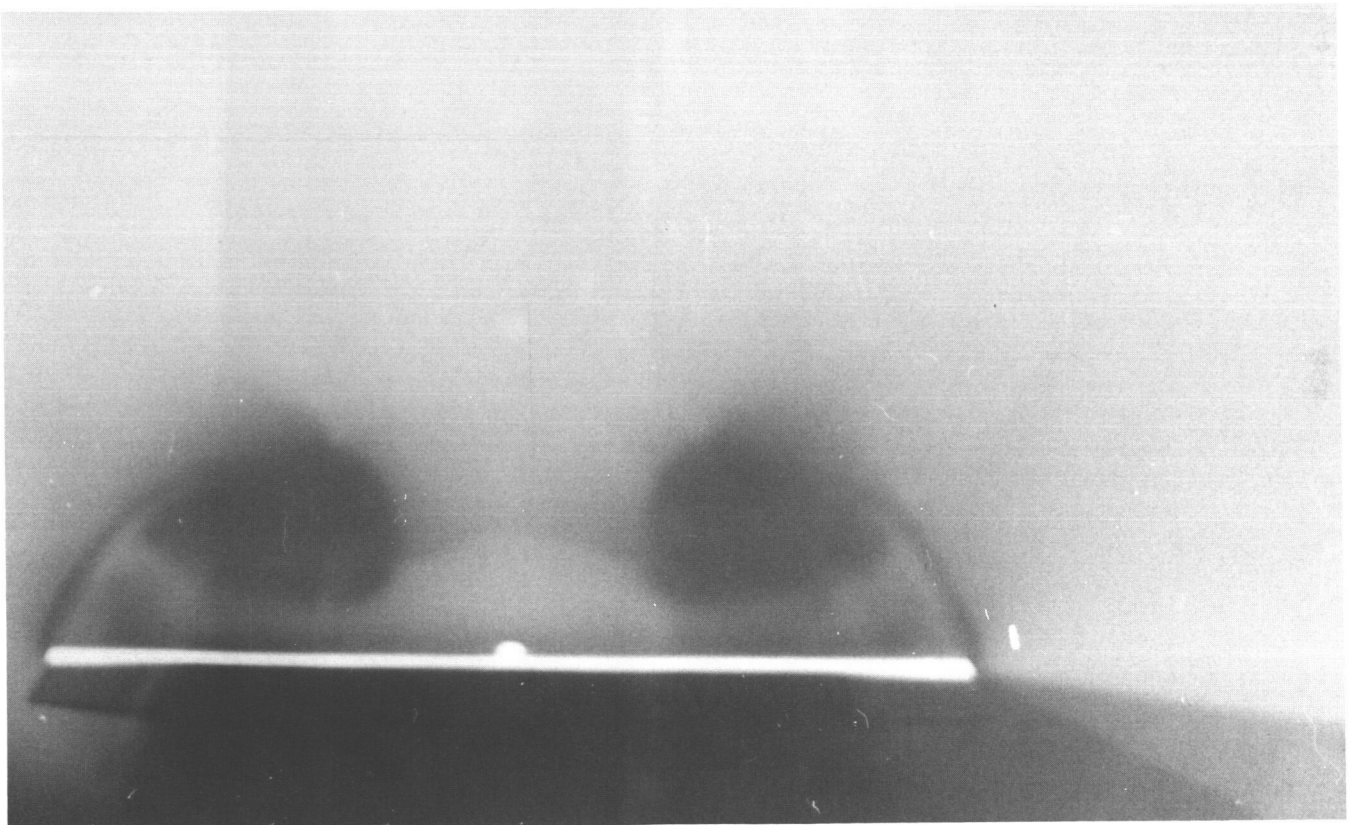


(e) $M = 1.7$, $\alpha = 16^\circ$.

Figure B1. Continued.

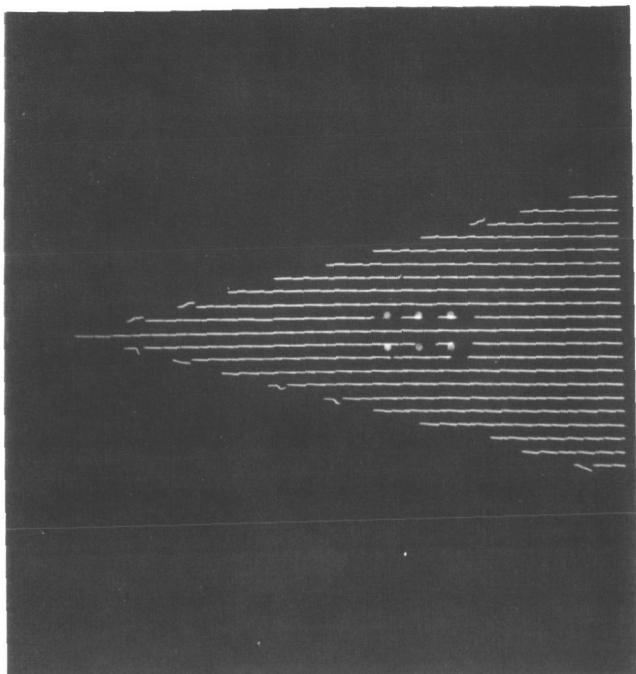


NO DATA

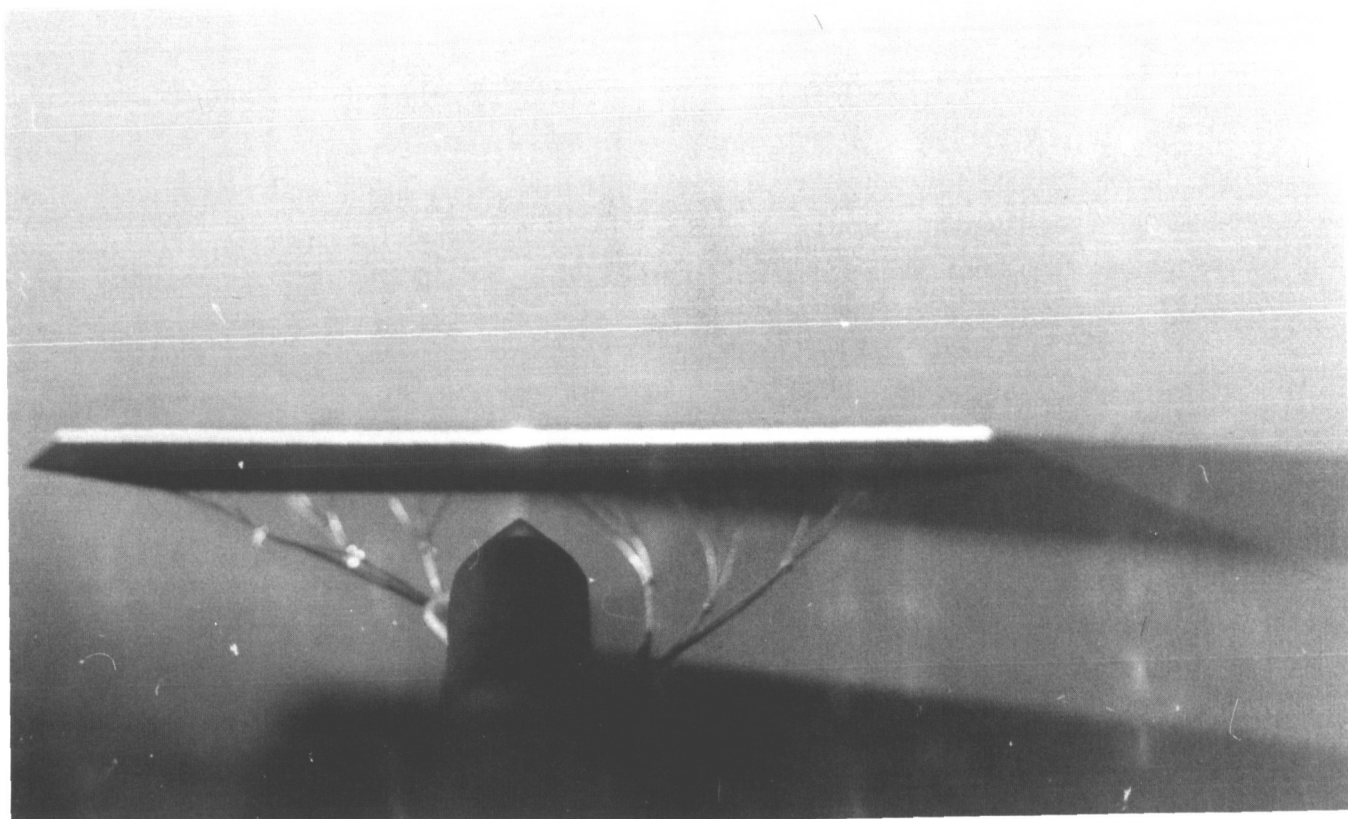


(f) $M = 1.7$, $\alpha = 20^\circ$.

Figure B1. Continued.

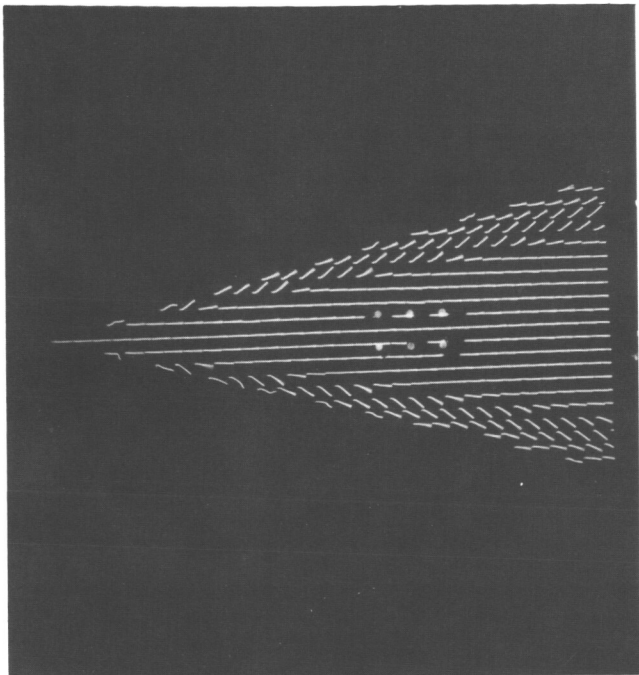


NO DATA

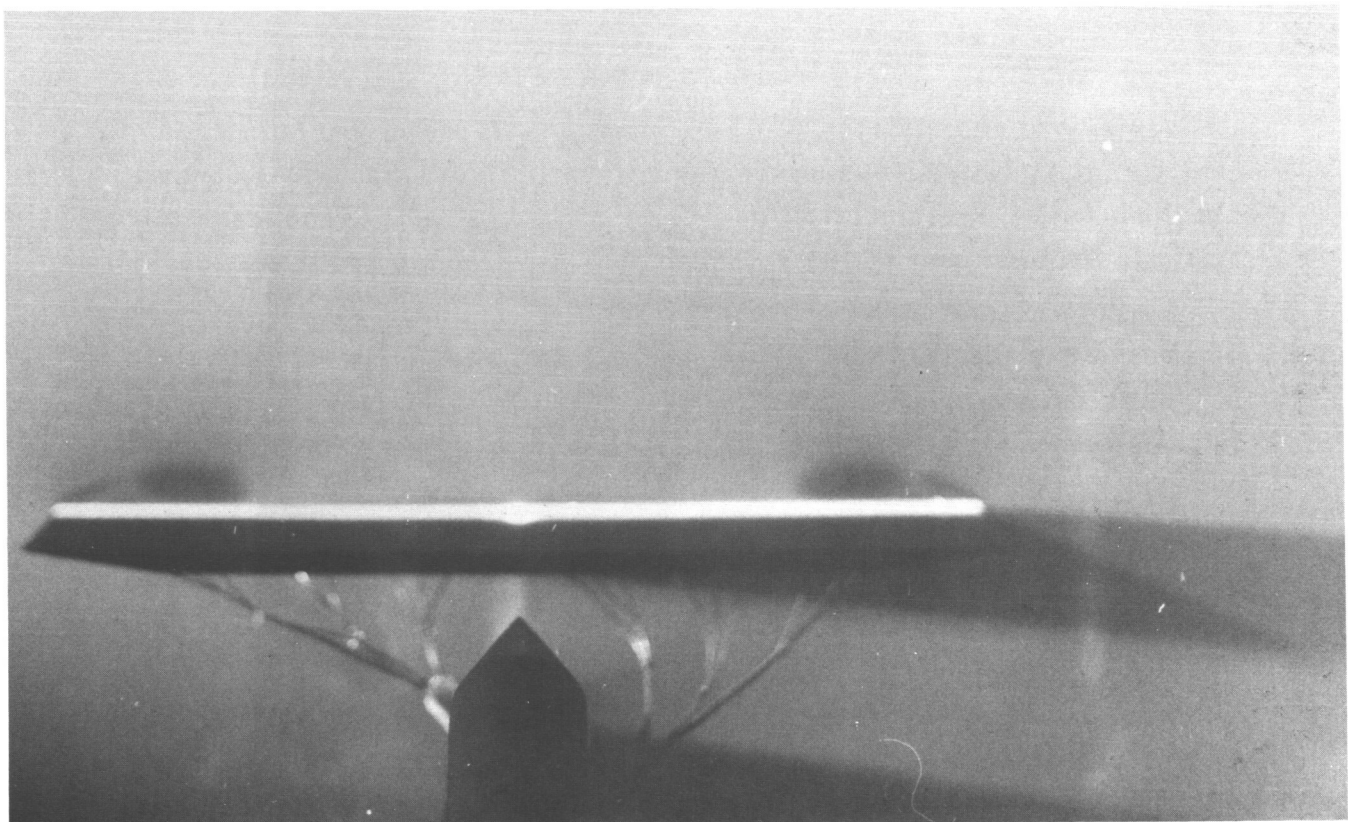


(g) $M = 2.0$, $\alpha = 0^\circ$.

Figure B1. Continued.

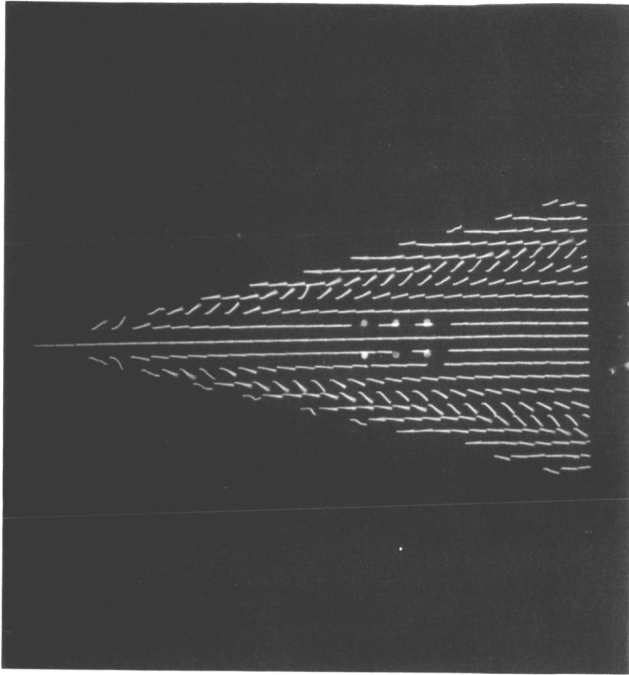


NO DATA

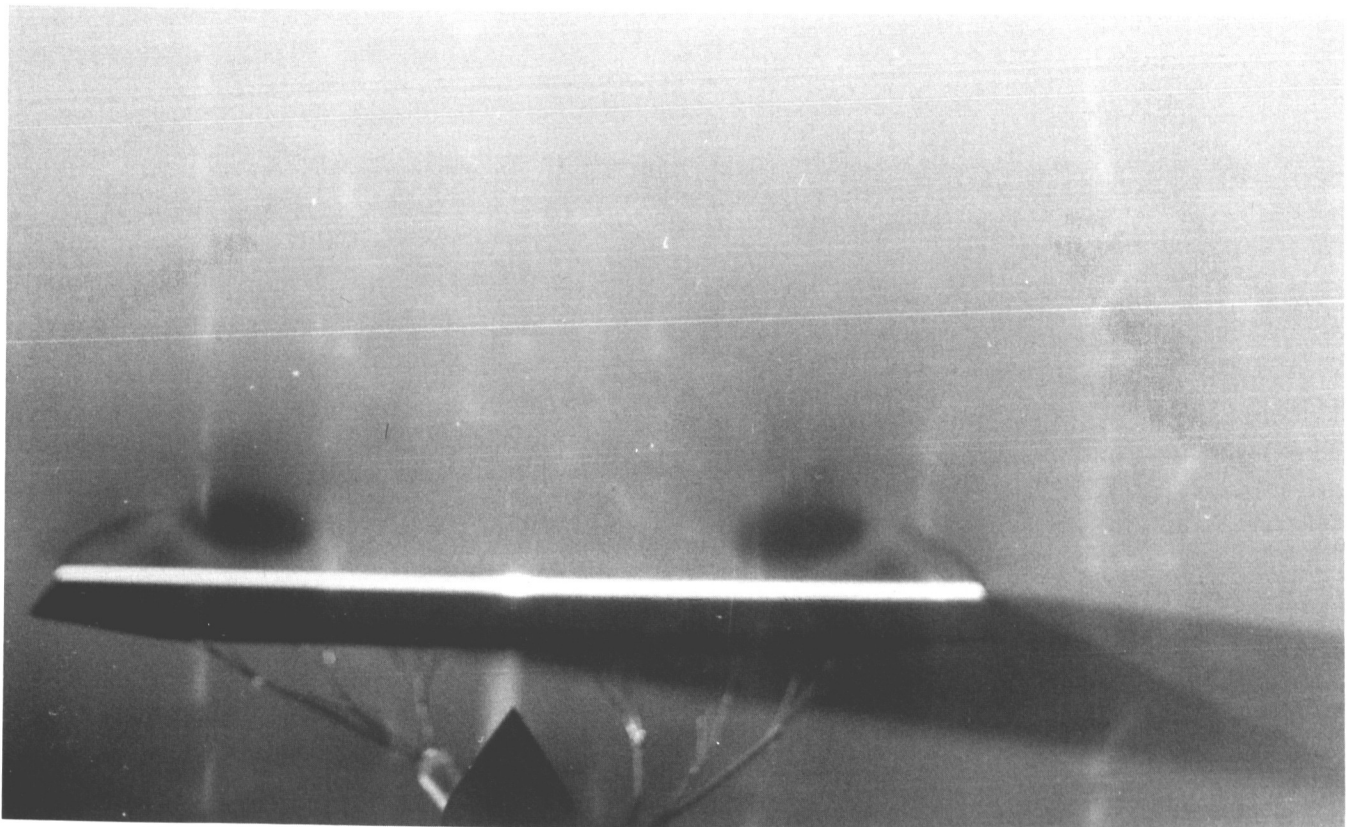


(h) $M = 2.0$, $\alpha = 4^\circ$.

Figure B1. Continued.

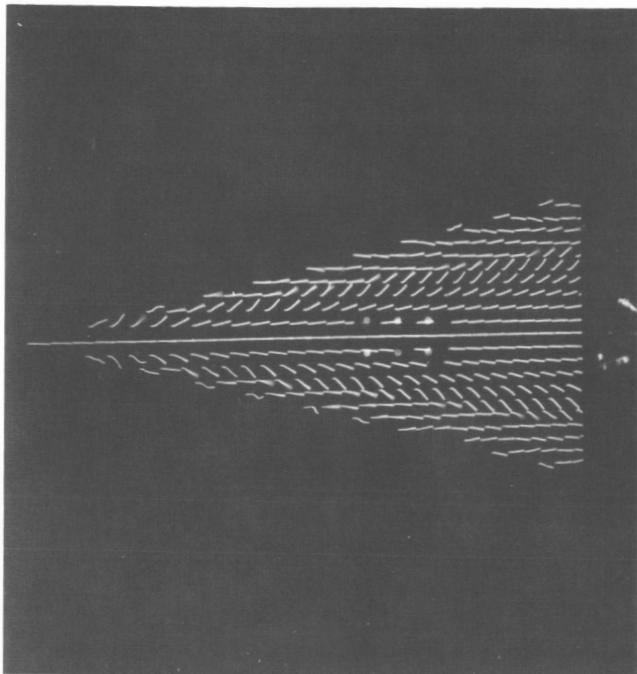


NO DATA

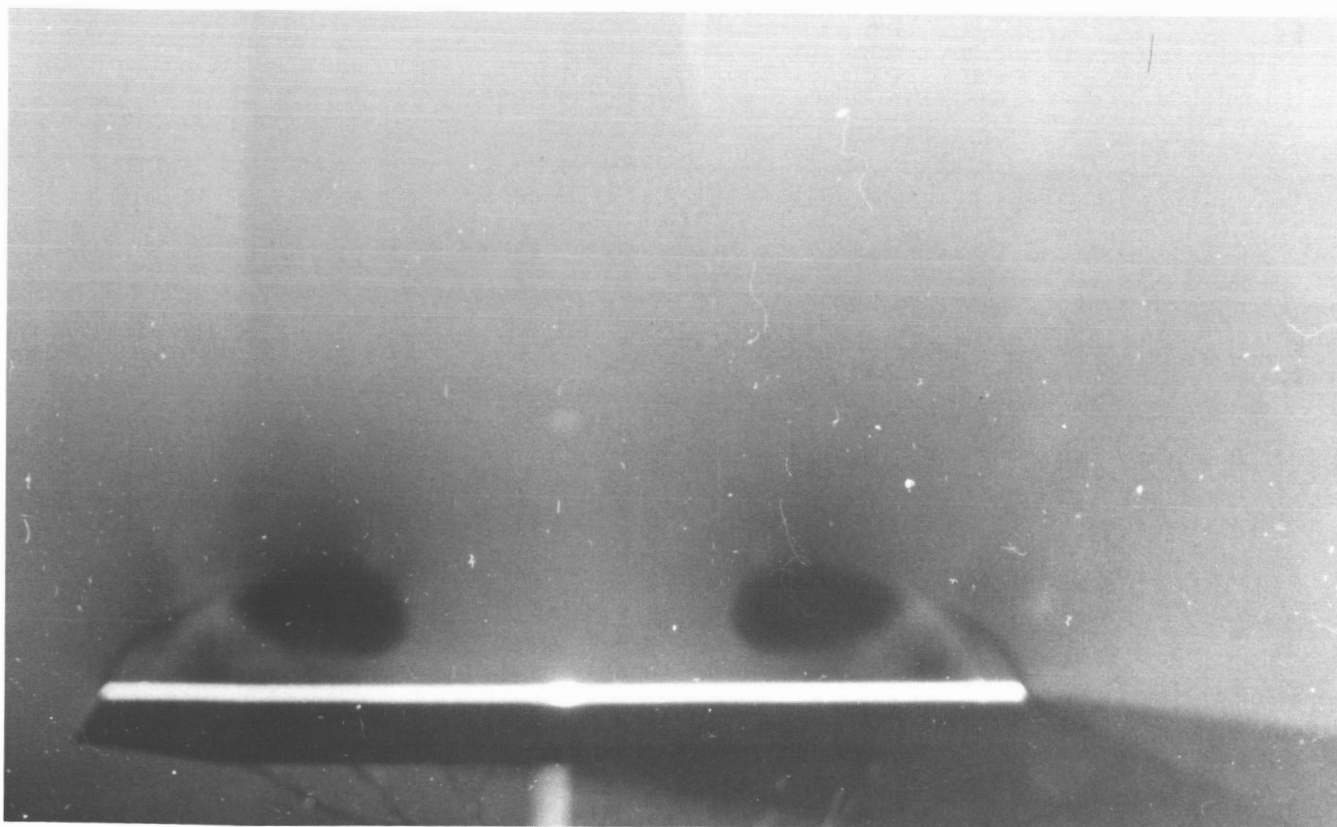


(i) $M = 2.0$, $\alpha = 8^\circ$.

Figure B1. Continued.

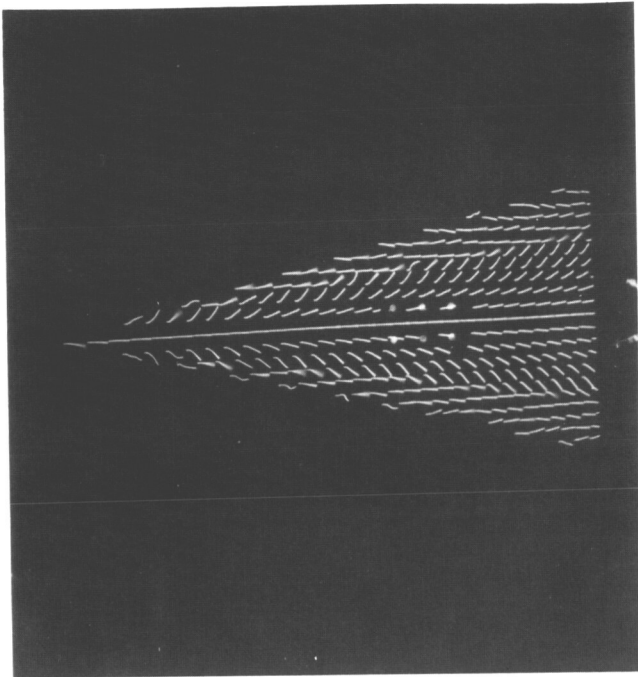


NO DATA

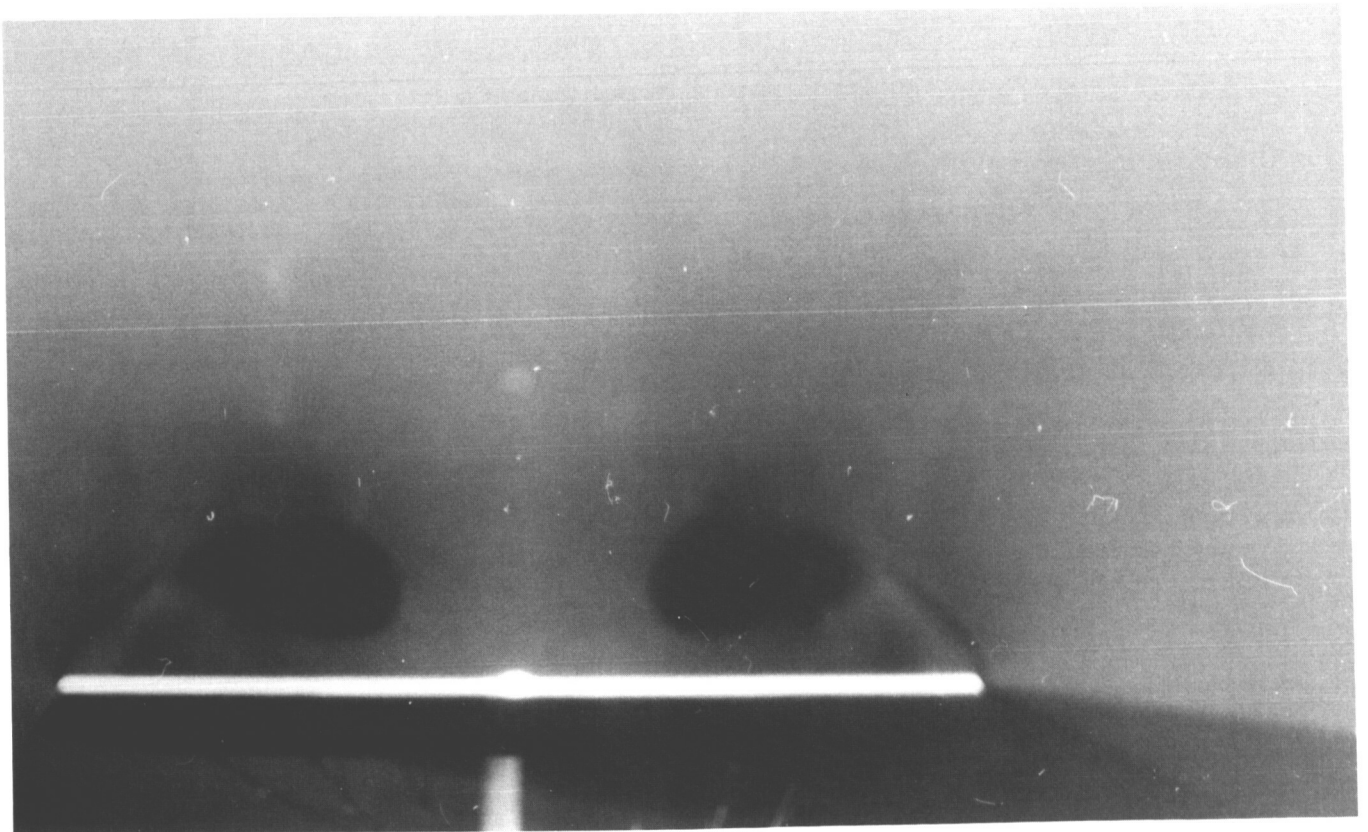


(j) $M = 2.0$, $\alpha = 12^\circ$.

Figure B1. Continued.

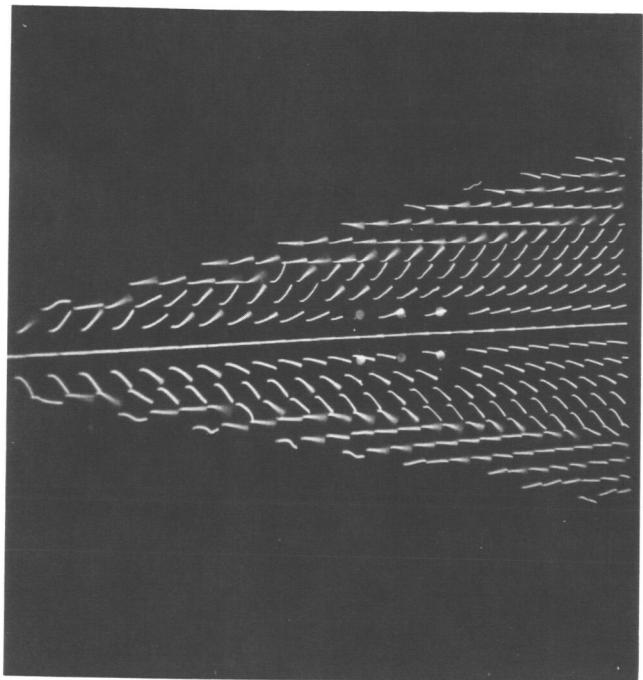


NO DATA

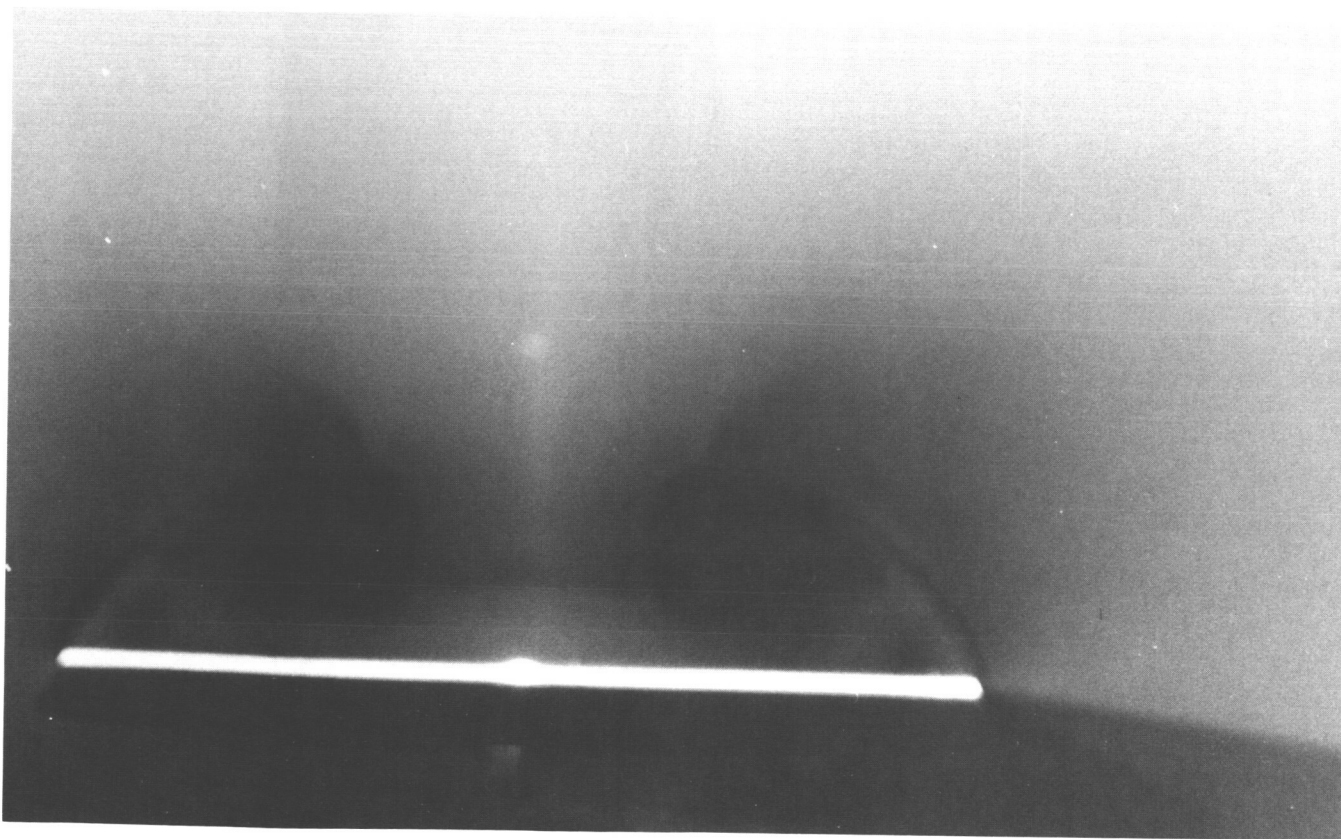


(k) $M = 2.0$, $\alpha = 16^\circ$.

Figure B1. Continued.

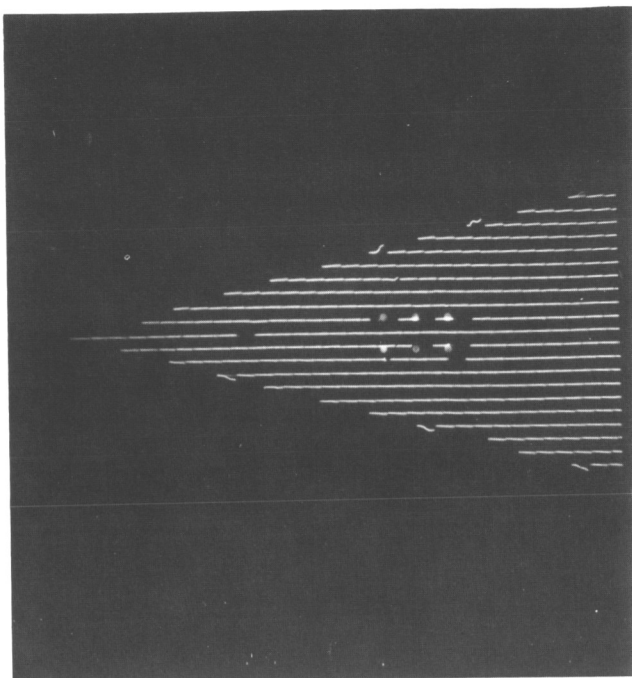


NO DATA

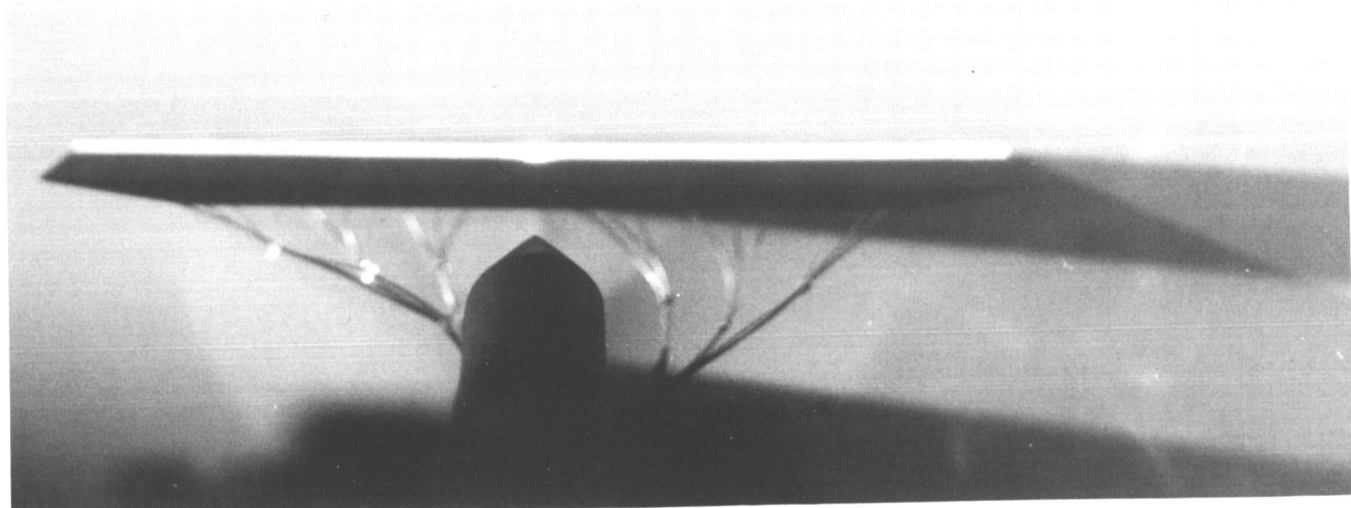


(1) $M = 2.0$, $\alpha = 20^\circ$.

Figure B1. Continued.

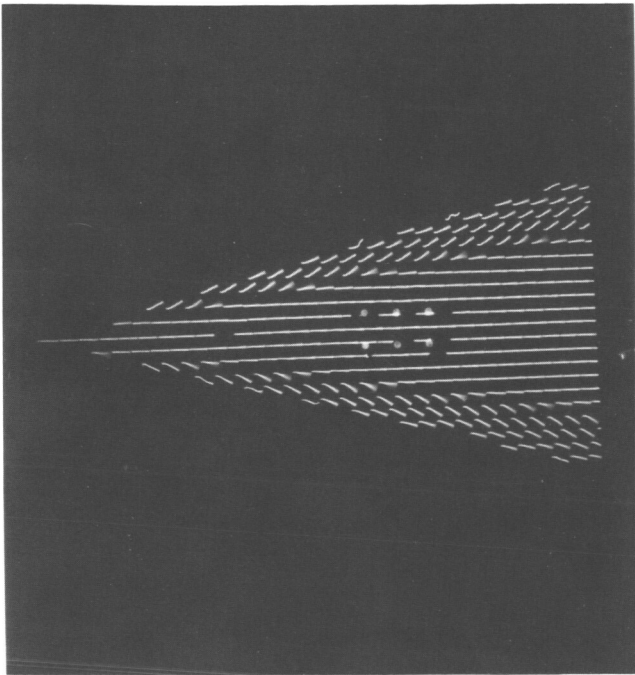


NO DATA

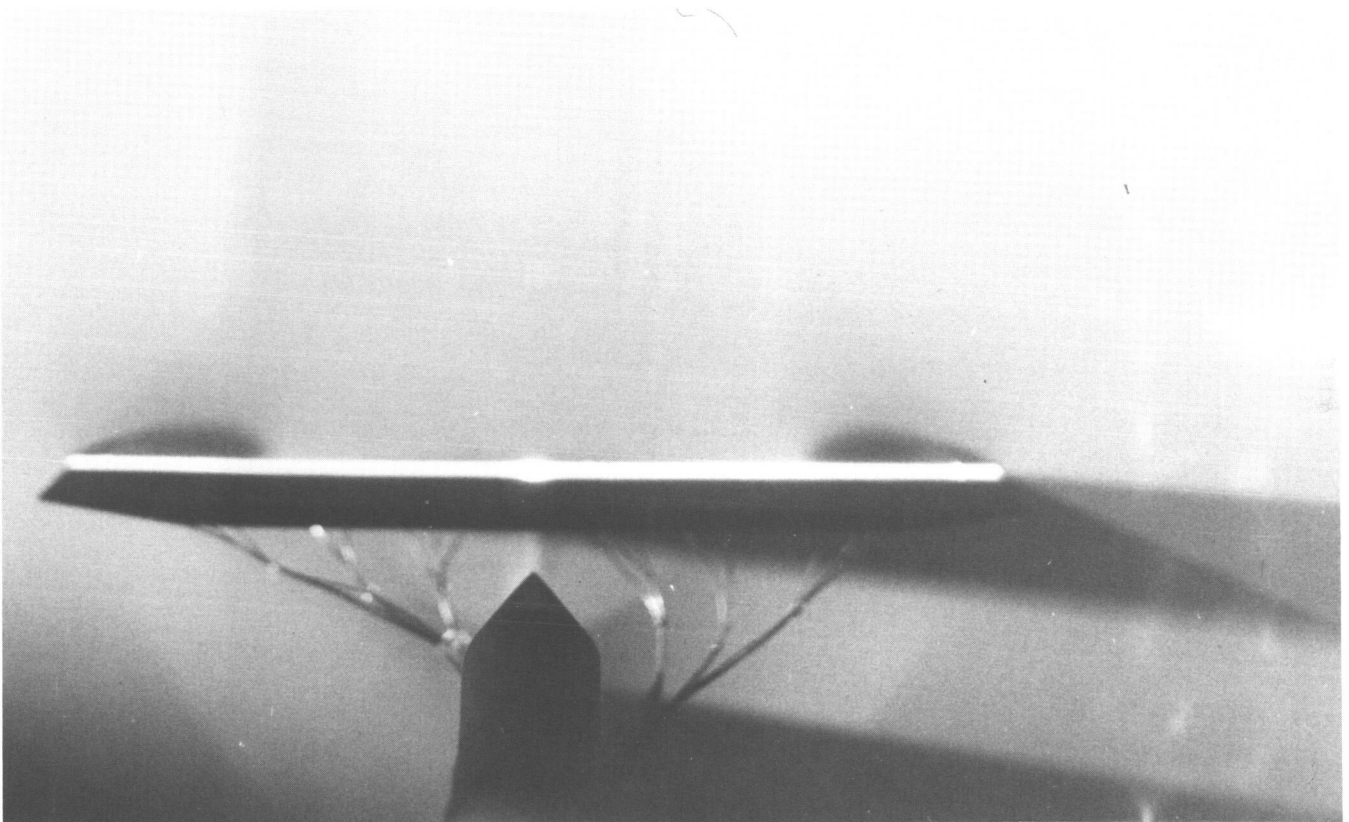


(m) $M = 2.4$, $\alpha = 0^\circ$.

Figure B1. Continued.

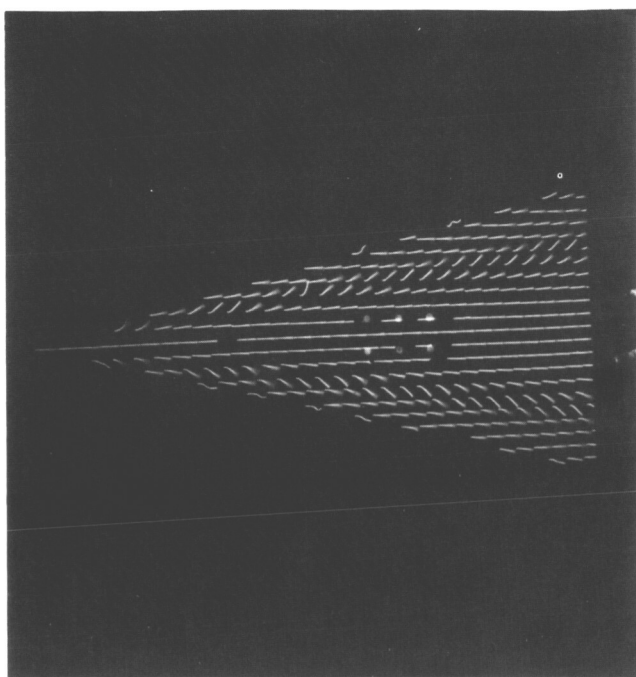


NO DATA

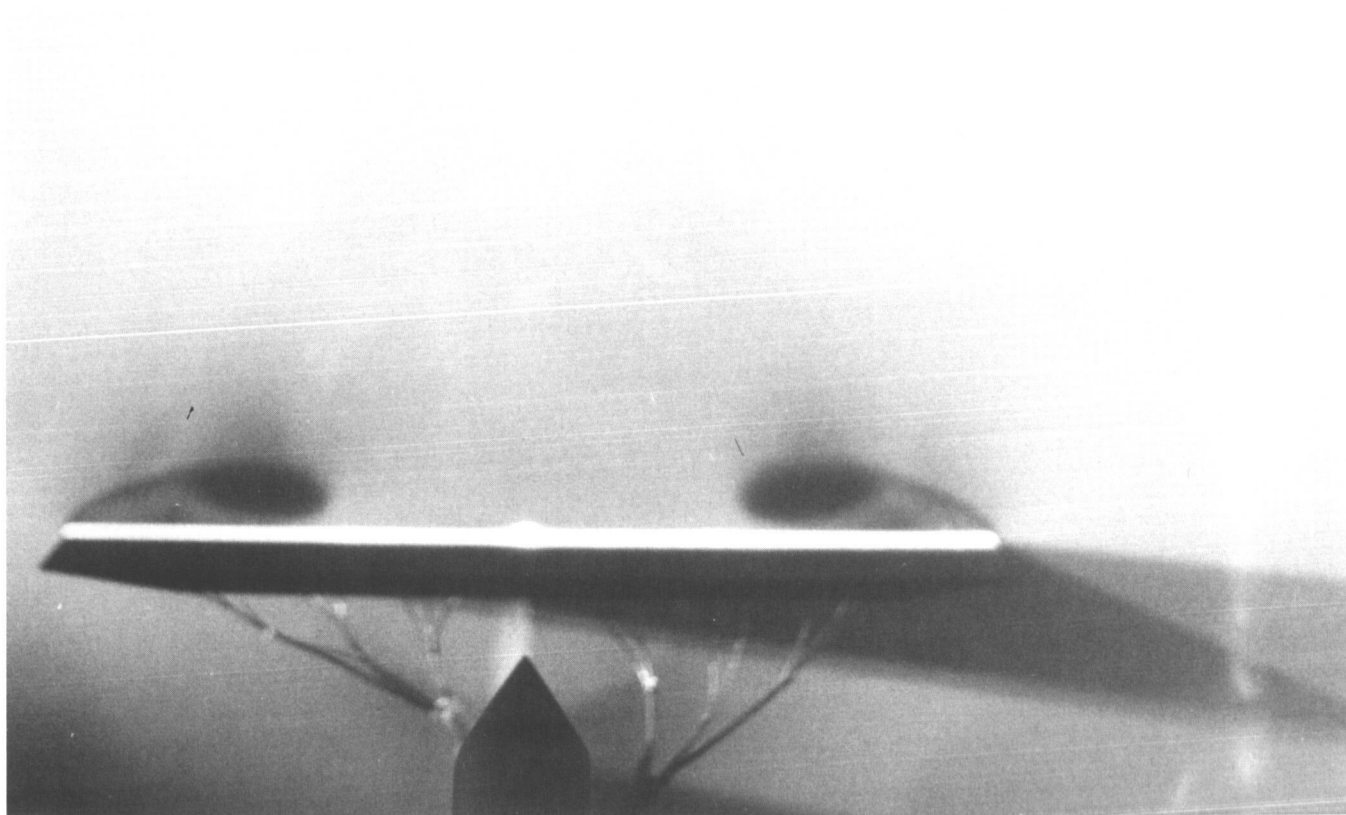


(n) $M = 2.4$, $\alpha = 4^\circ$.

Figure B1. Continued.

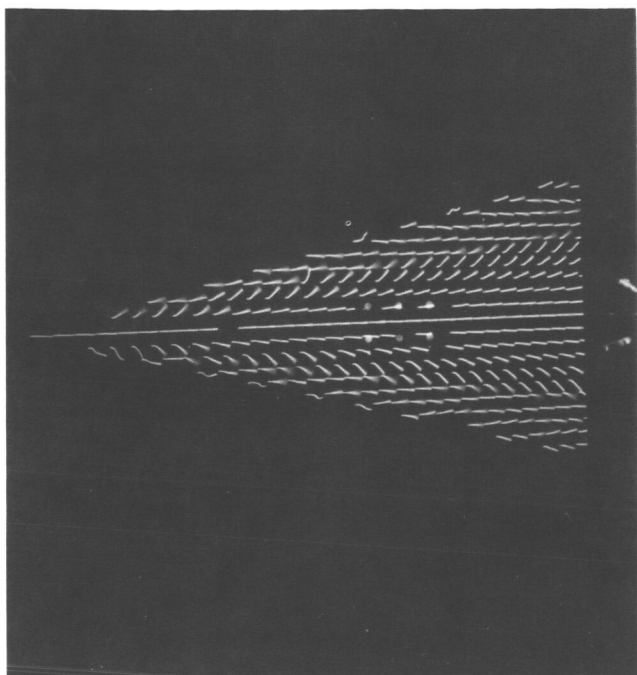


NO DATA

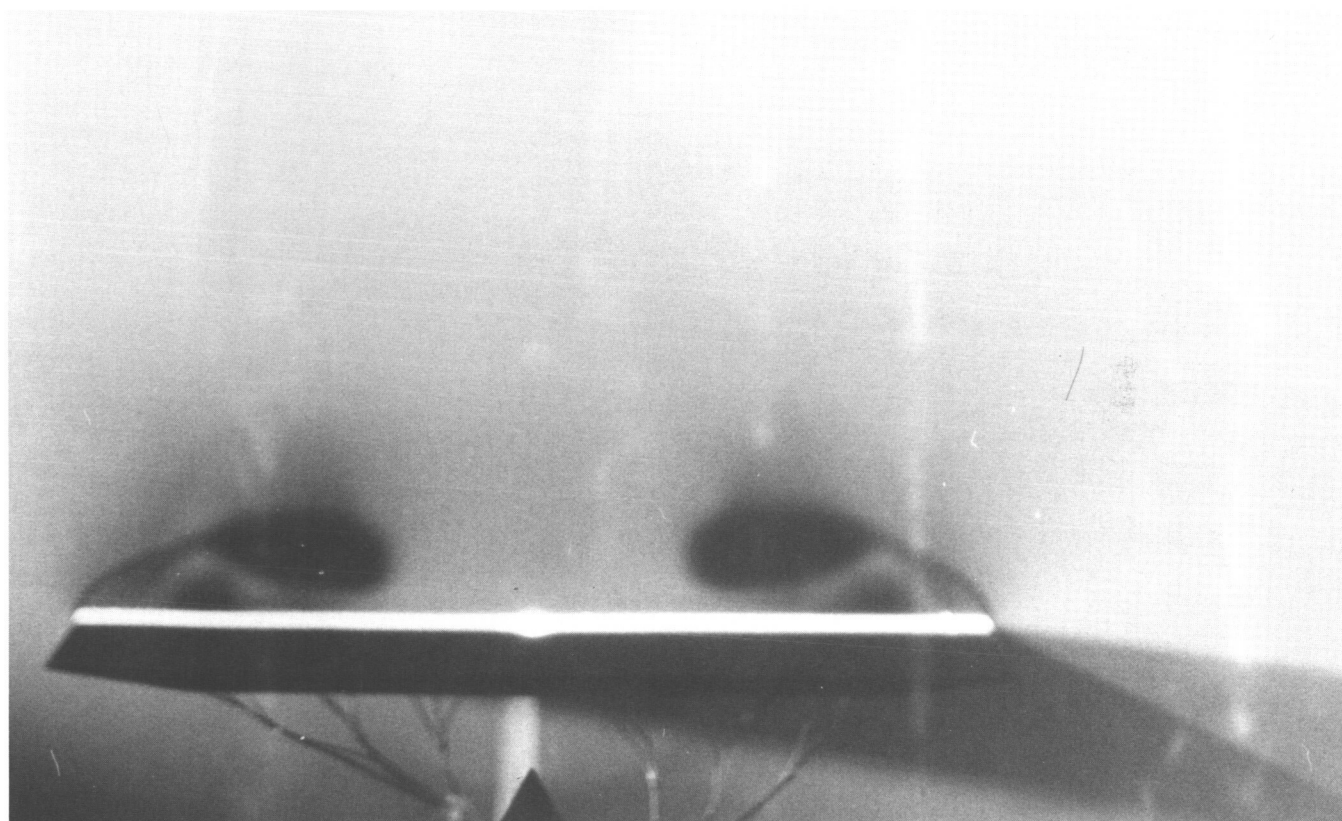


(o) $M = 2.4$, $\alpha = 8^\circ$.

Figure B1. Continued.

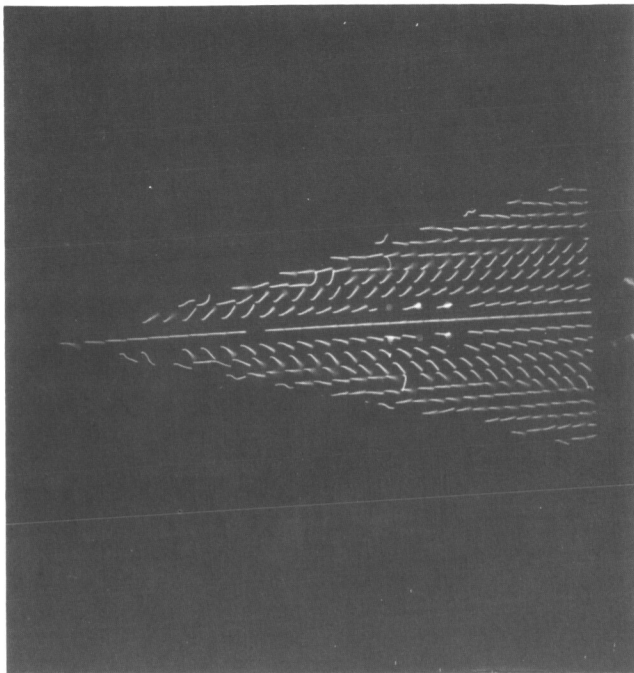


NO DATA

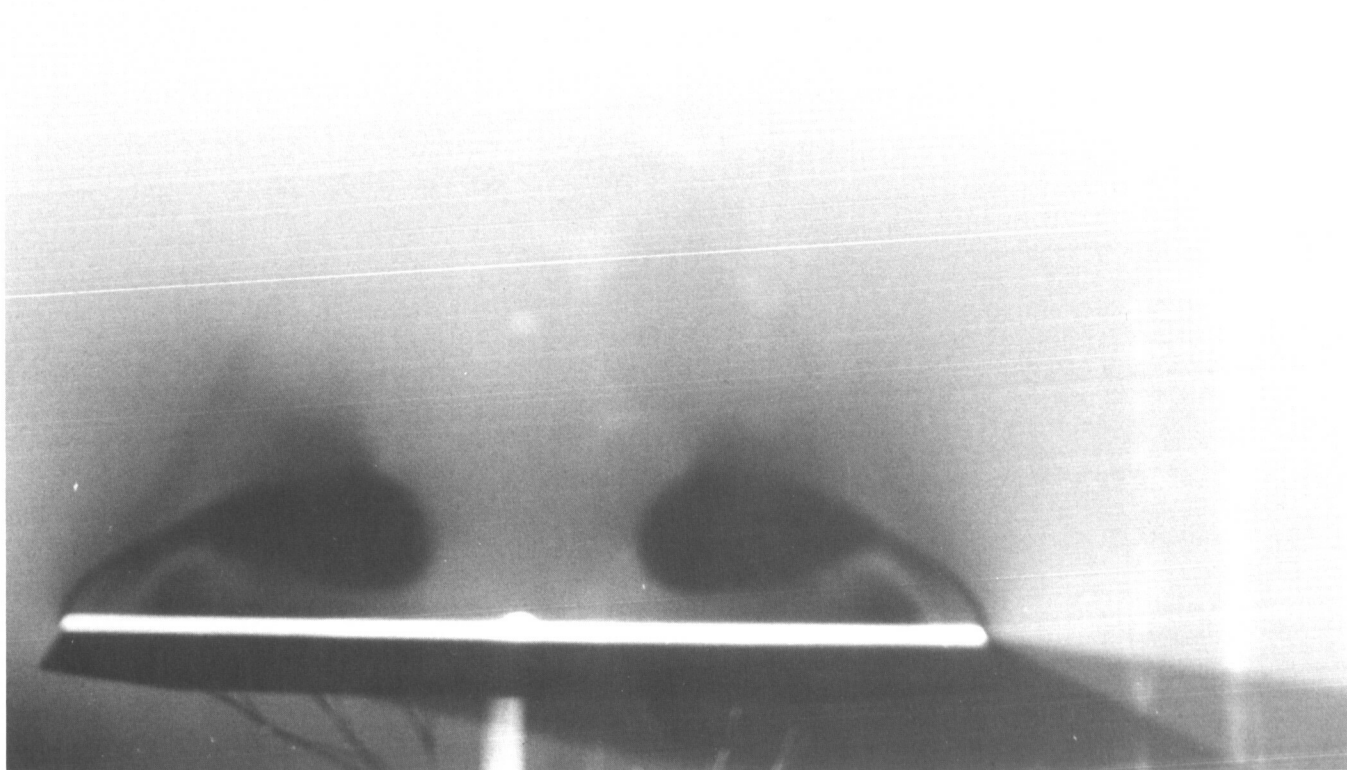


(p) $M = 2.4$, $\alpha = 12^\circ$.

Figure B1. Continued.

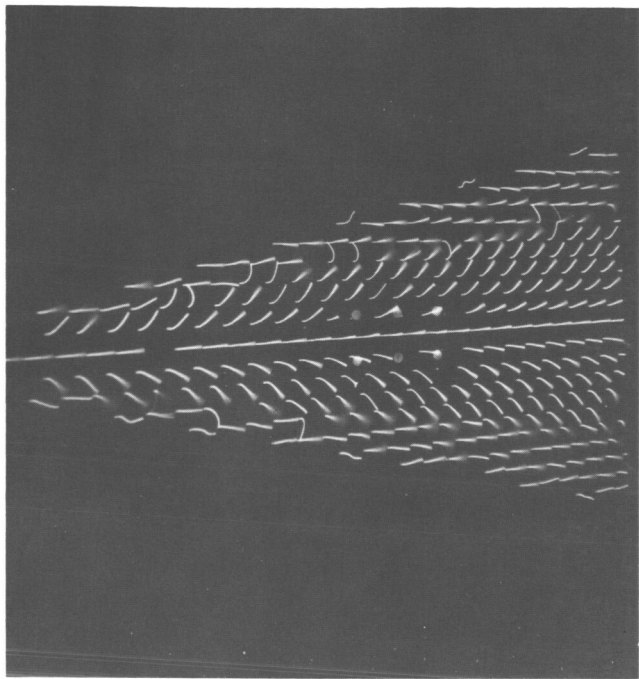


NO DATA

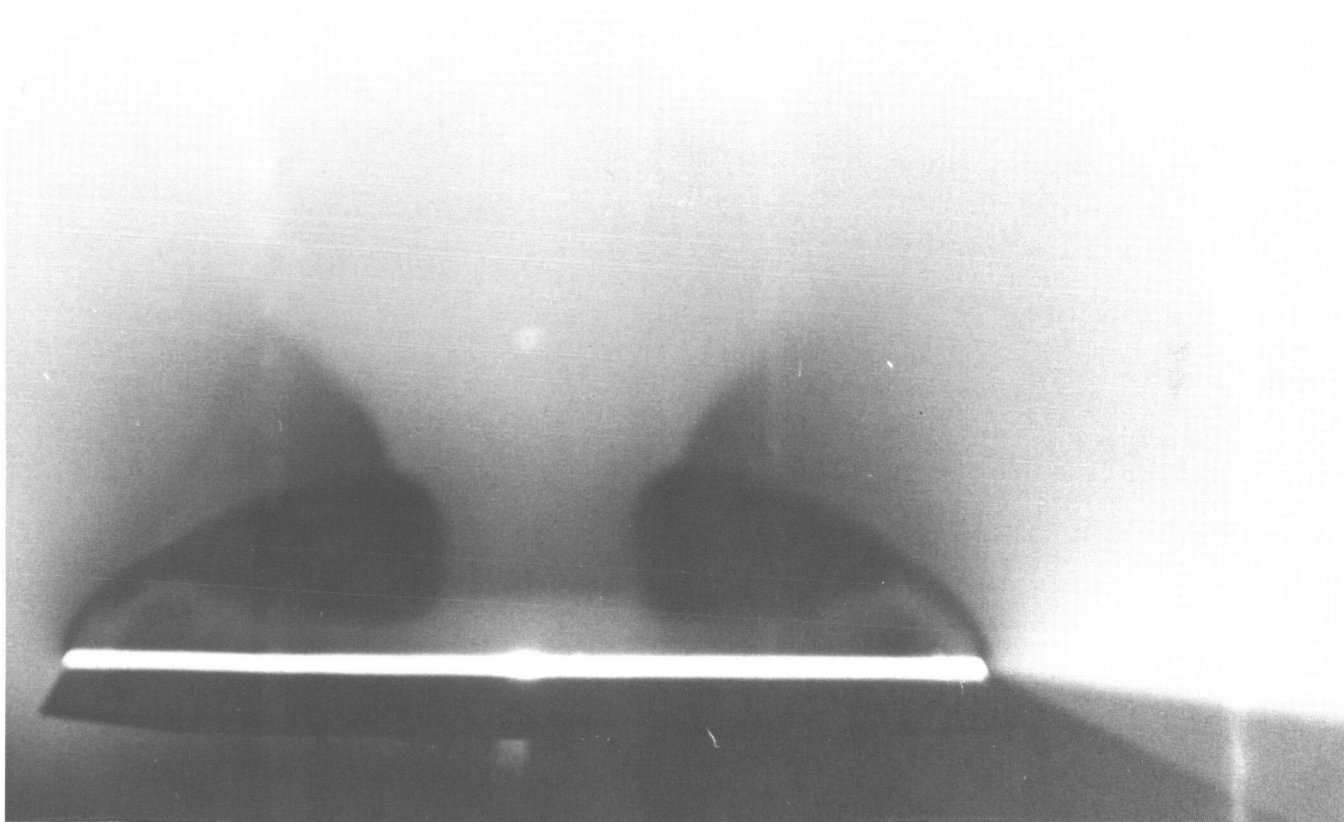


(q) $M = 2.4$, $\alpha = 16^\circ$.

Figure B1. Continued.

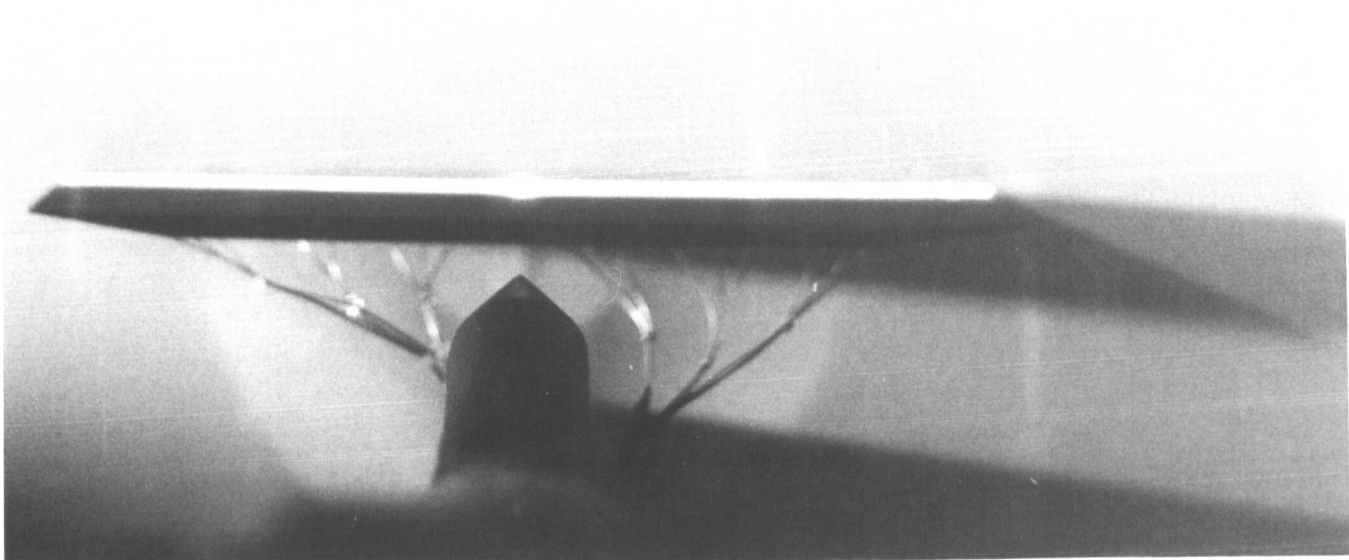
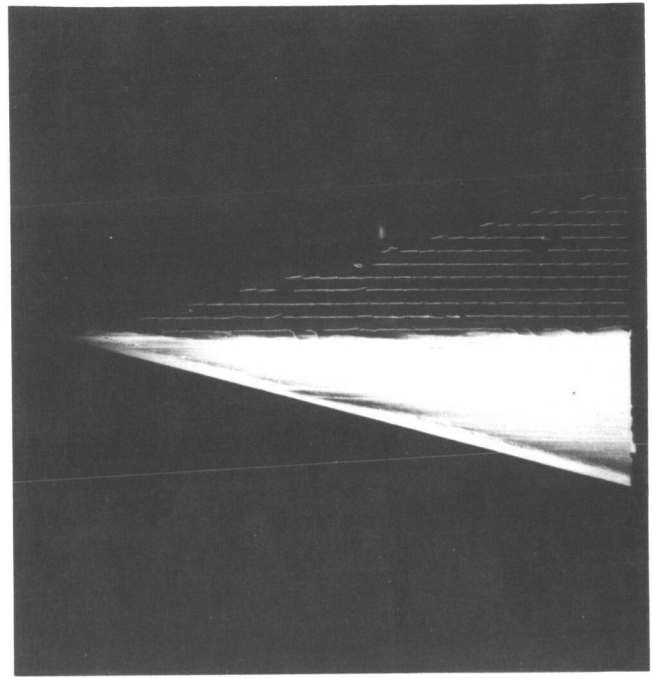
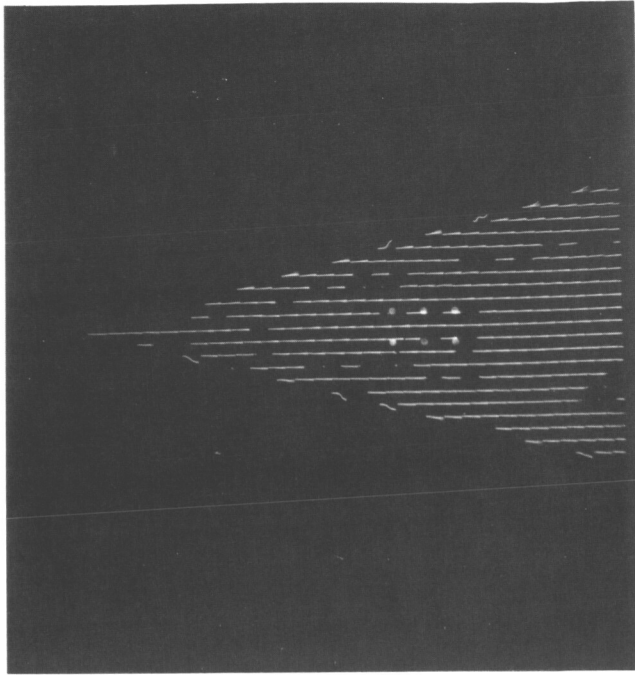


NO DATA



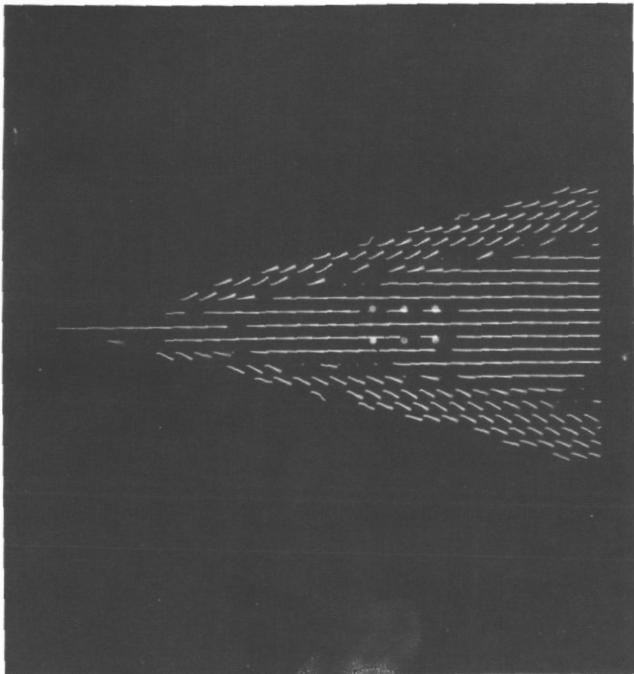
(r) $M = 2.4$, $\alpha = 20^\circ$.

Figure B1. Continued.

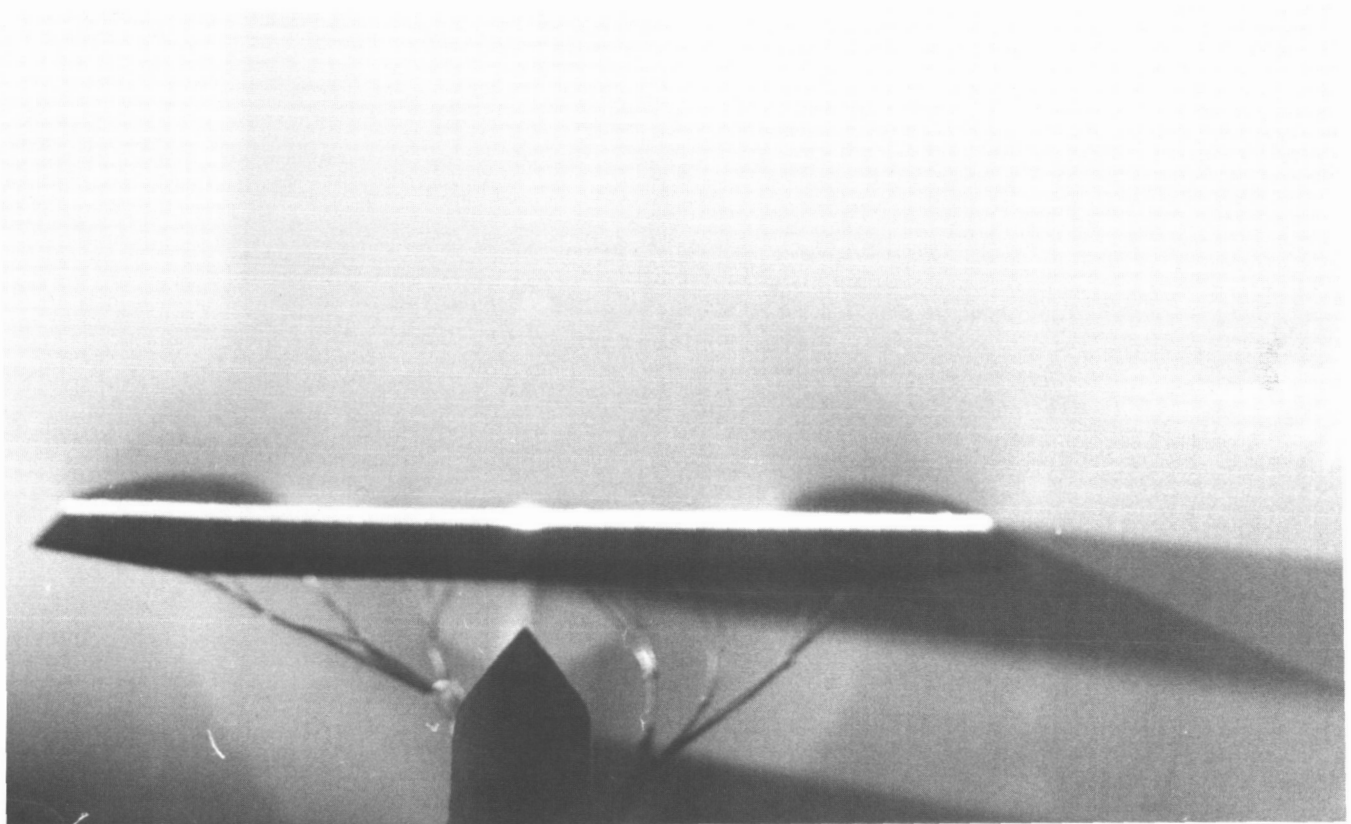


(s) $M = 2.8$, $\alpha = 0^\circ$.

Figure B1. Continued.

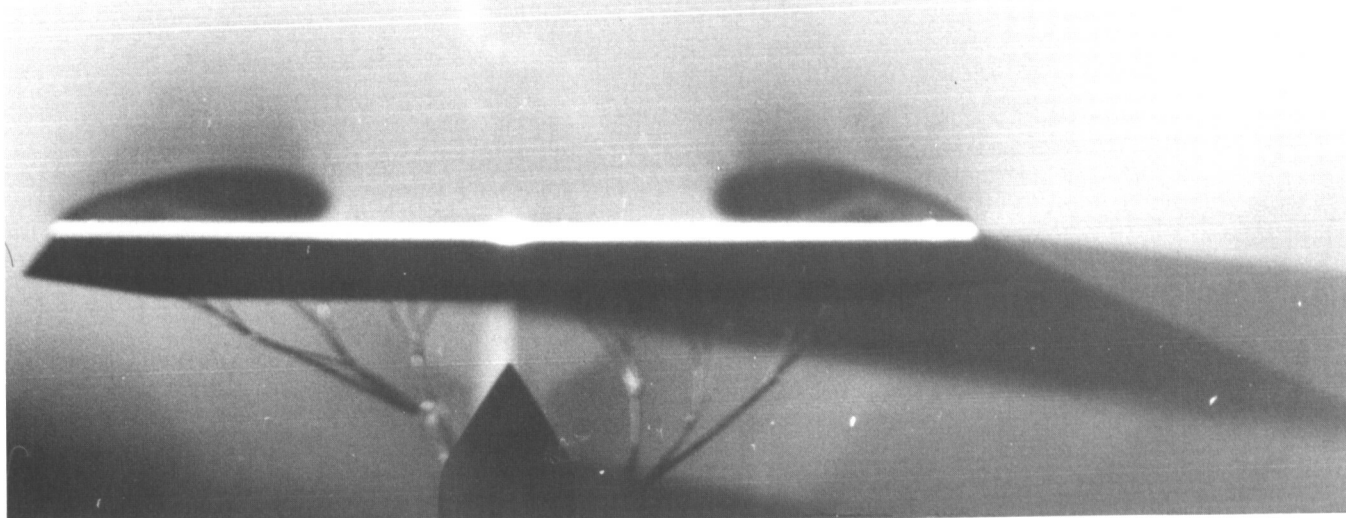
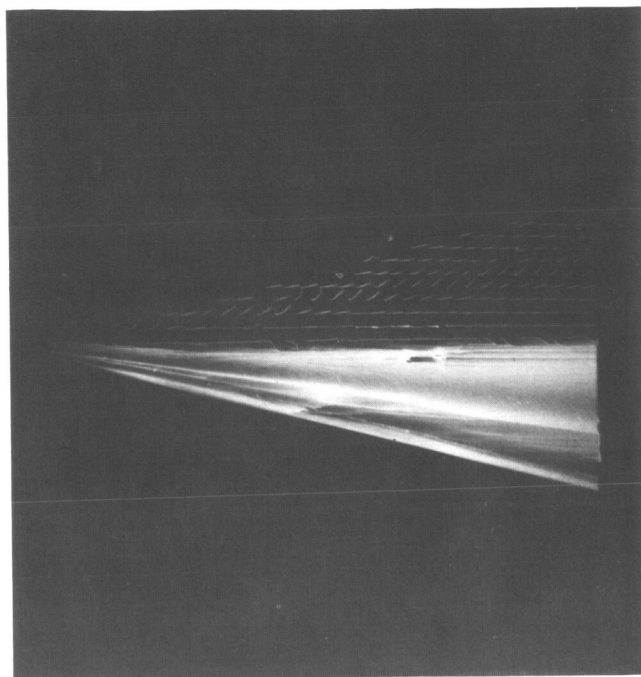
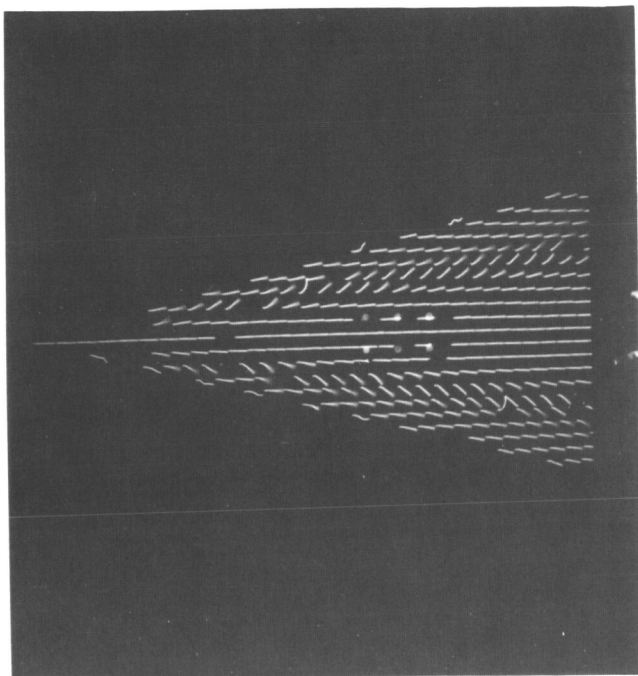


NO DATA



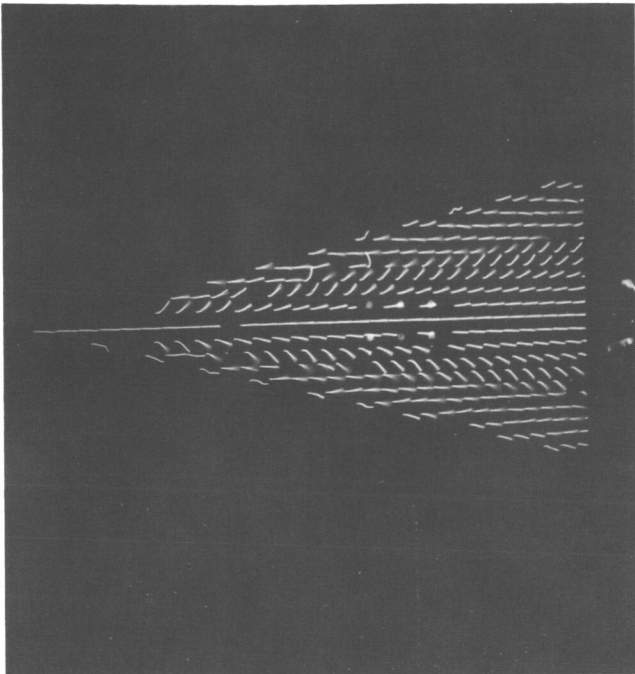
(t) $M = 2.8$, $\alpha = 4^\circ$.

Figure B1. Continued.

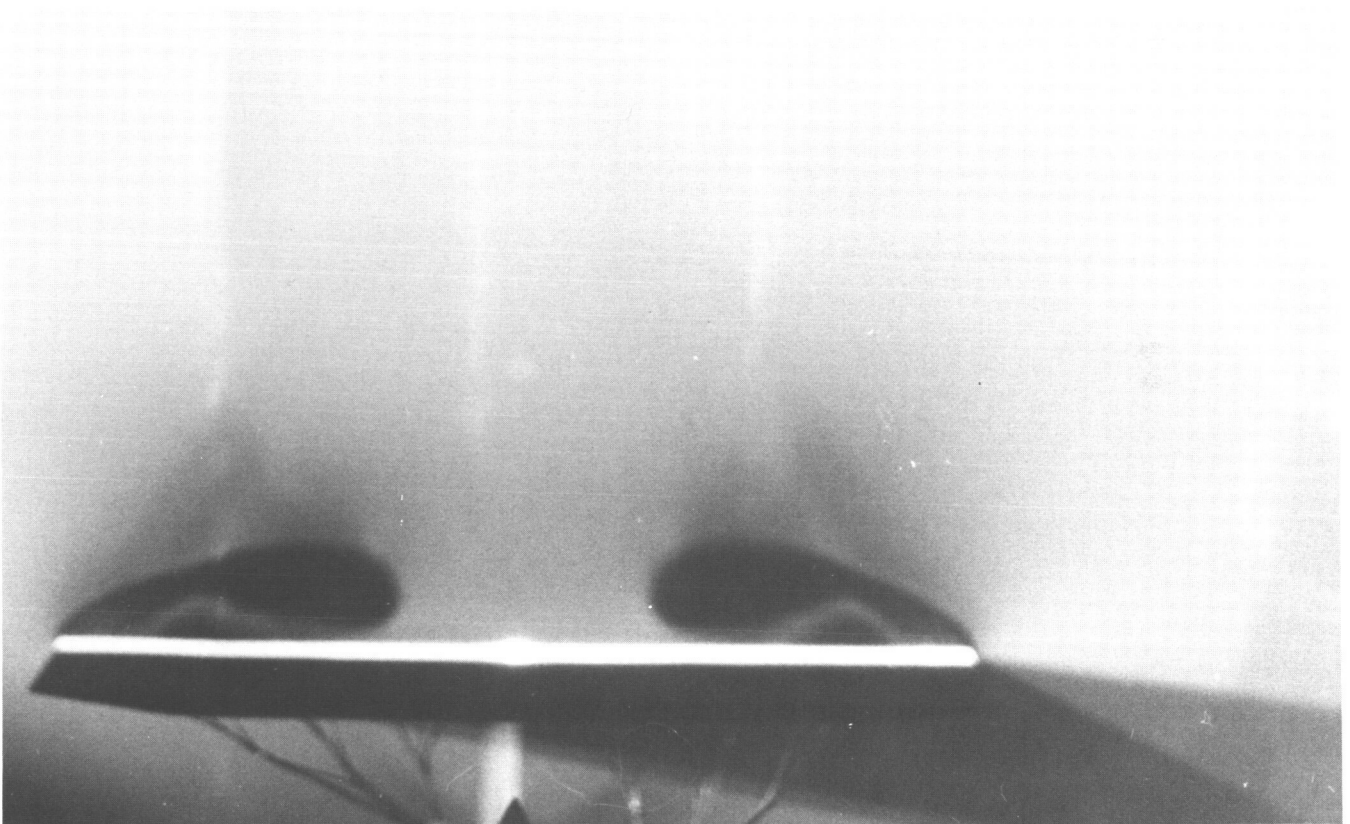


(u) $M = 2.8$, $\alpha = 8^\circ$.

Figure B1. Continued.

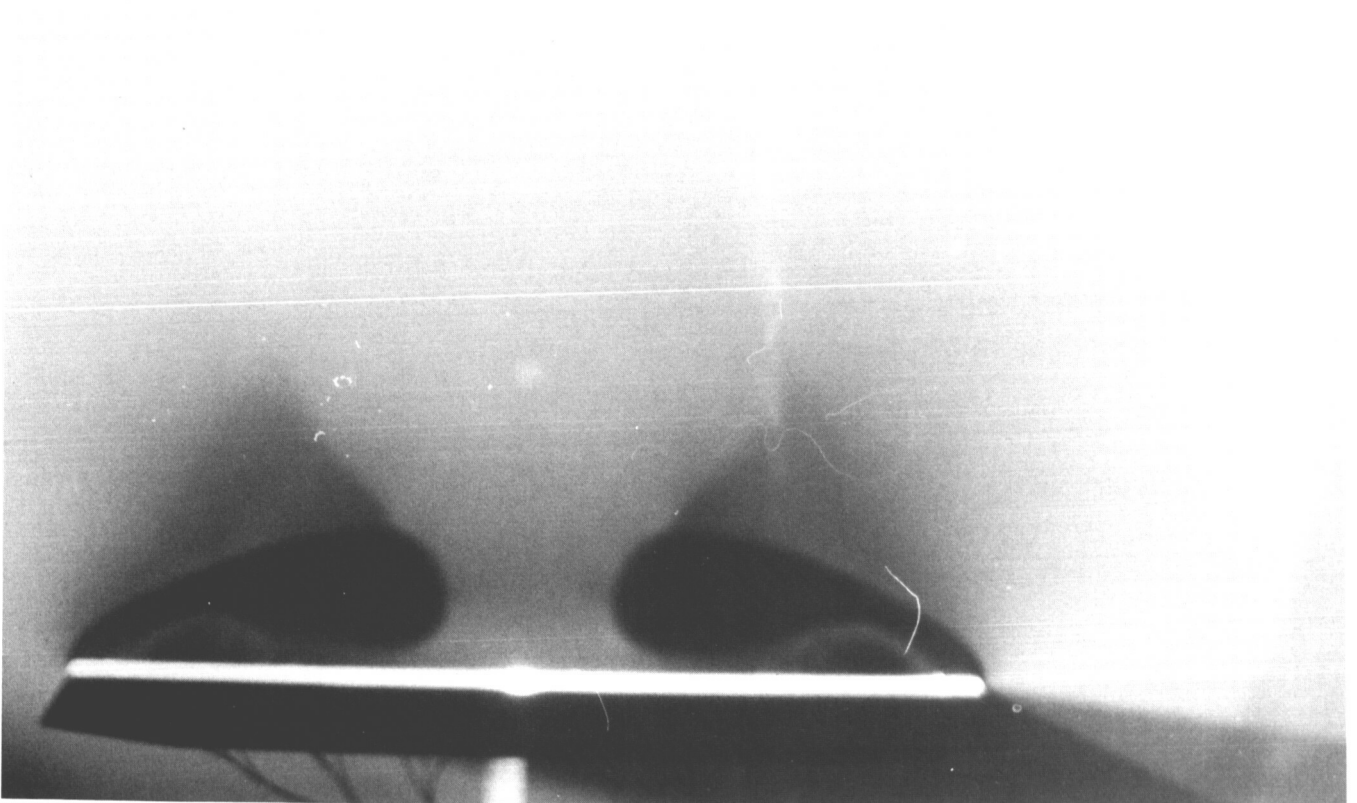
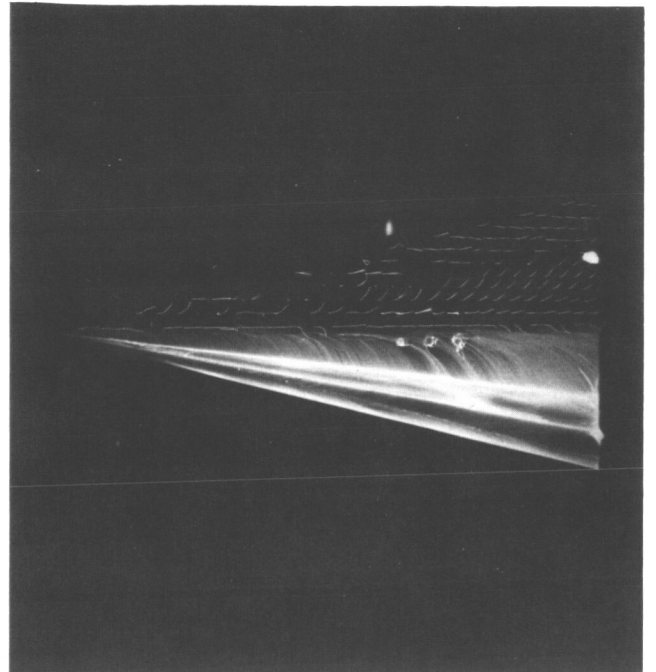
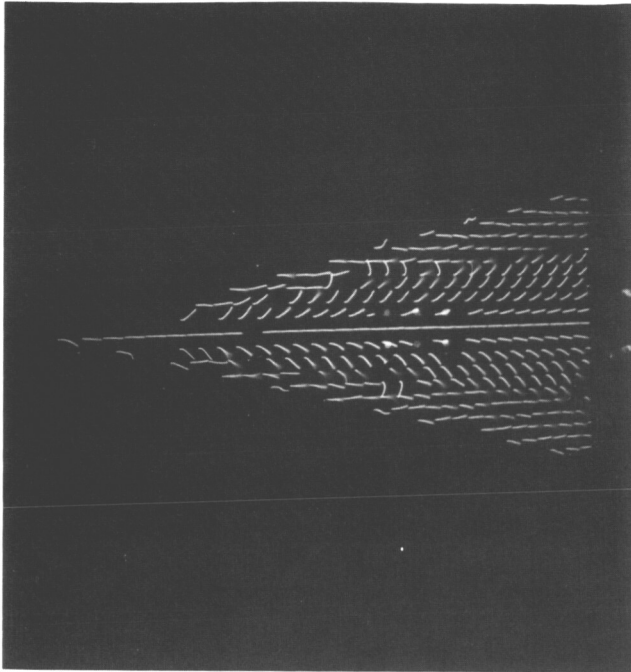


NO DATA



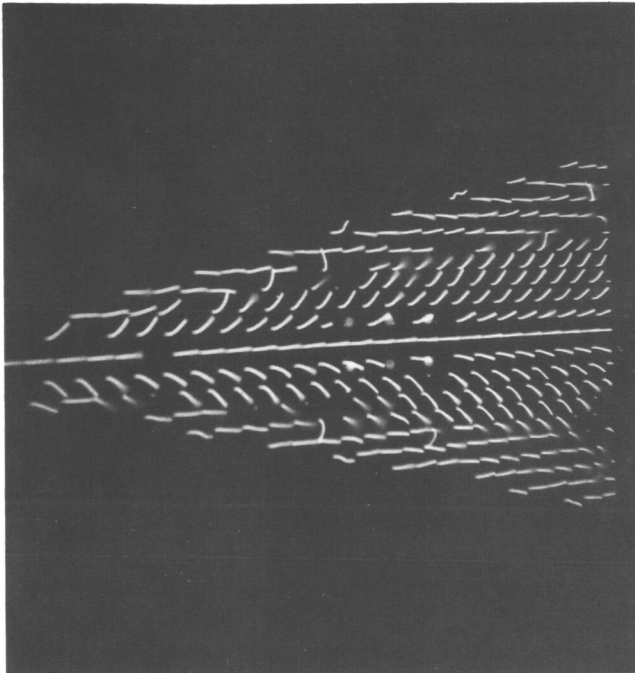
(v) $M = 2.8$, $\alpha = 12^\circ$.

Figure B1. Continued.

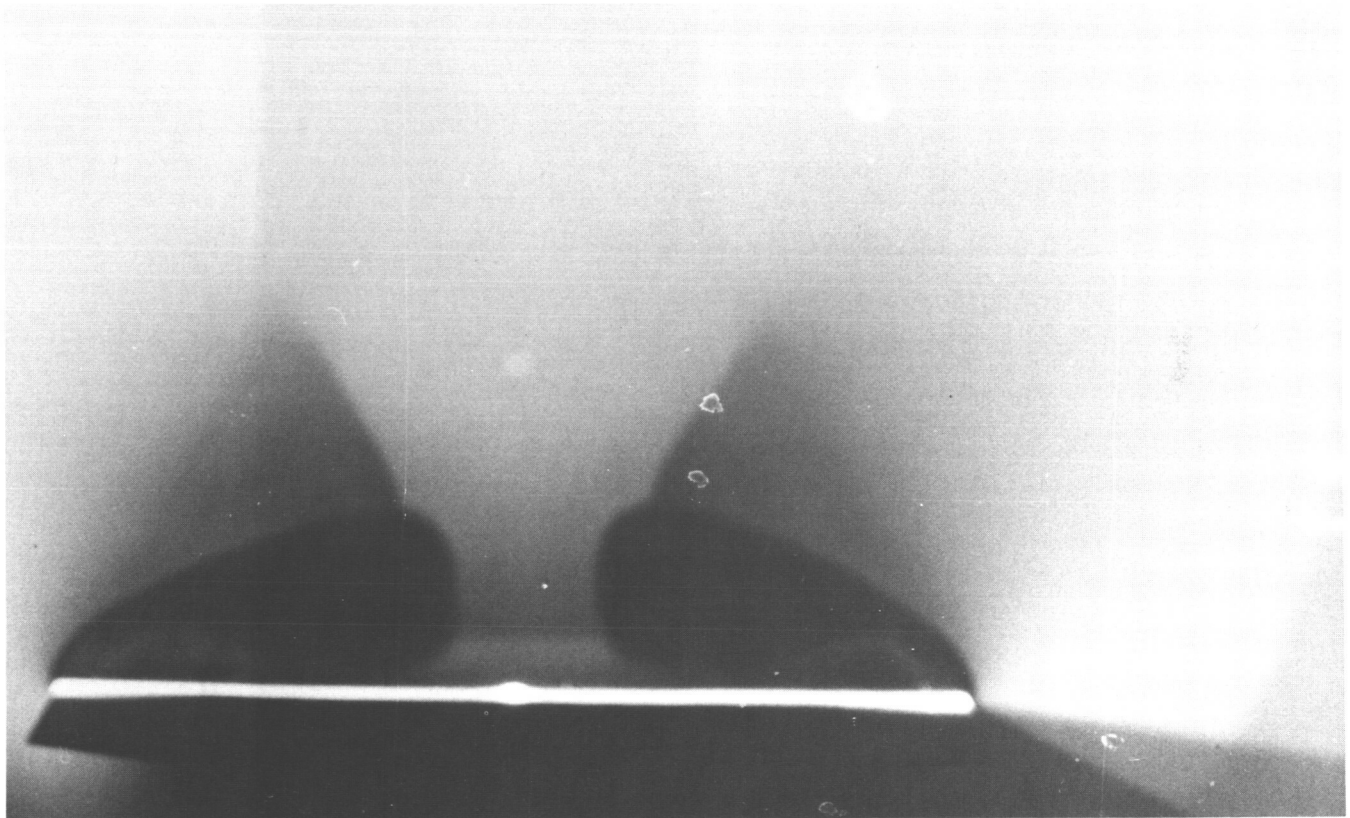


(w) $M = 2.8$, $\alpha = 16^\circ$.

Figure B1. Continued.

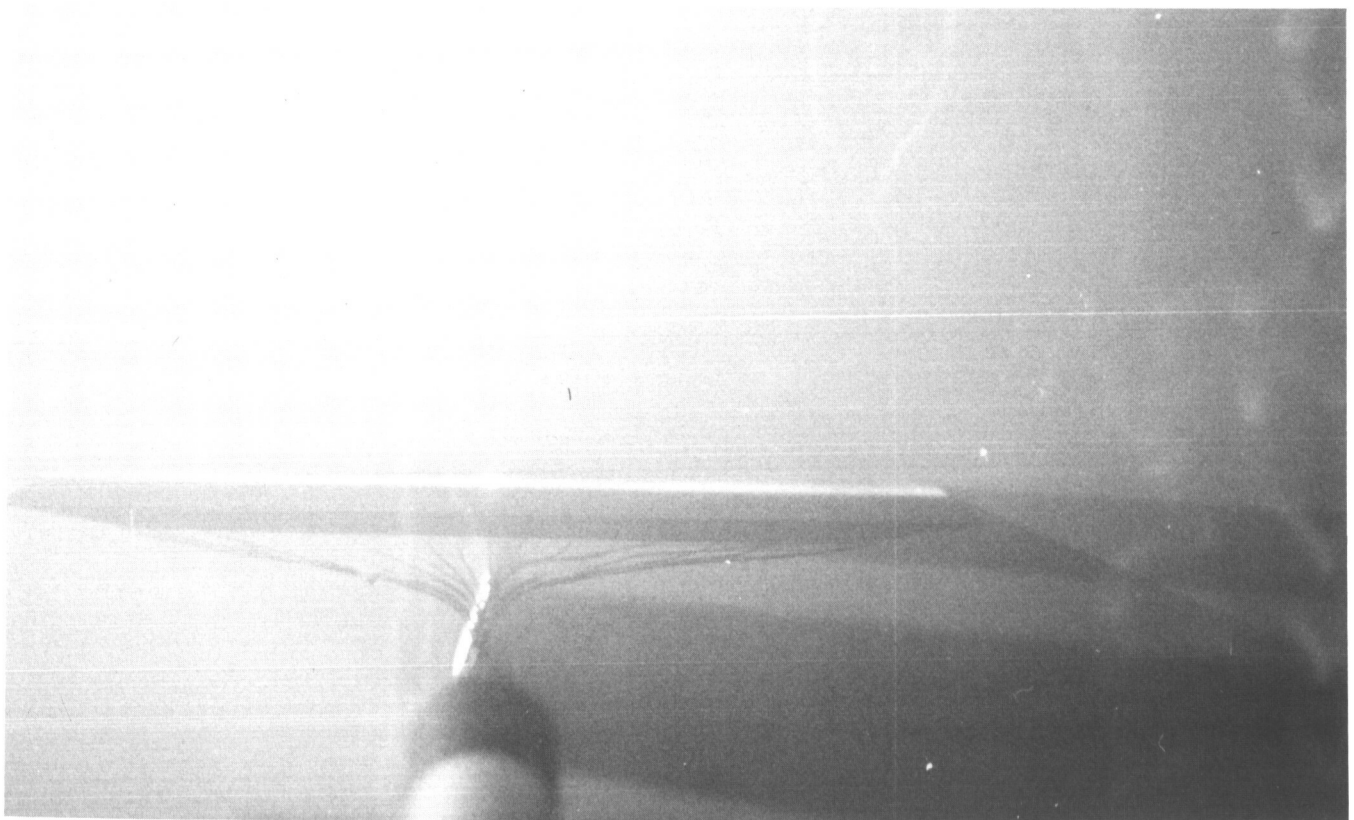
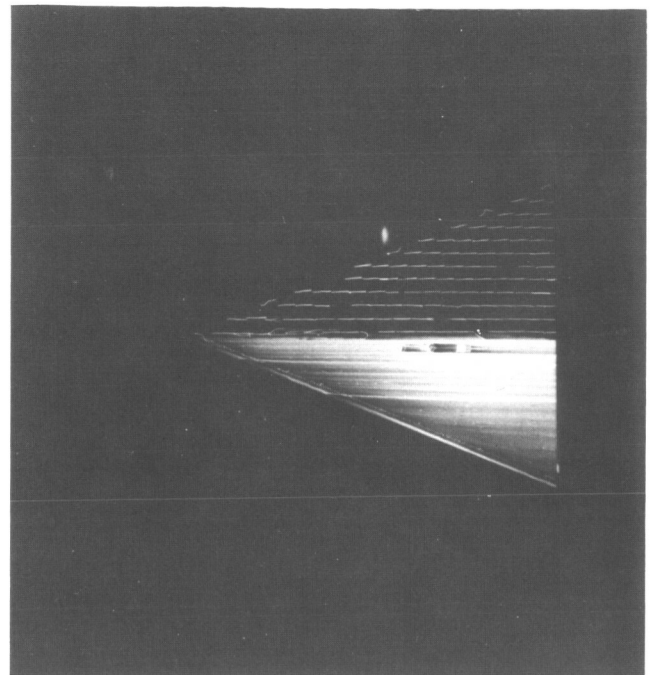
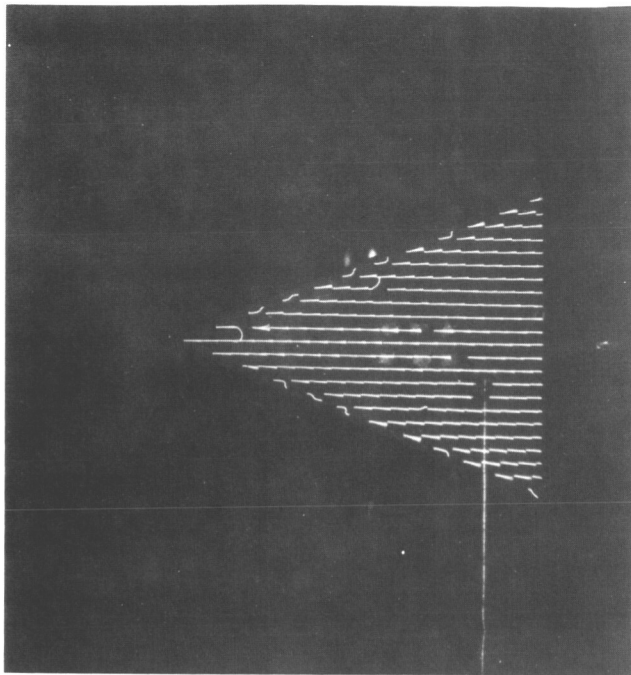


NO DATA



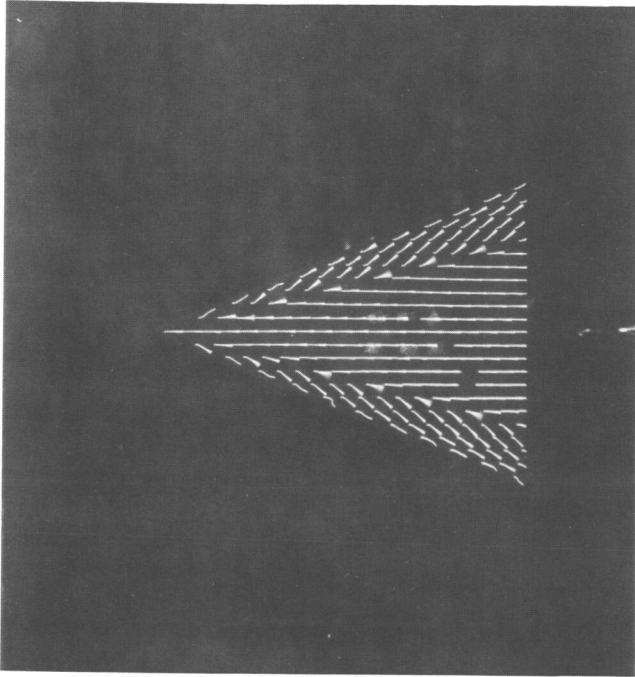
(x) $M = 2.8$, $\alpha = 20^\circ$.

Figure B1. Concluded.

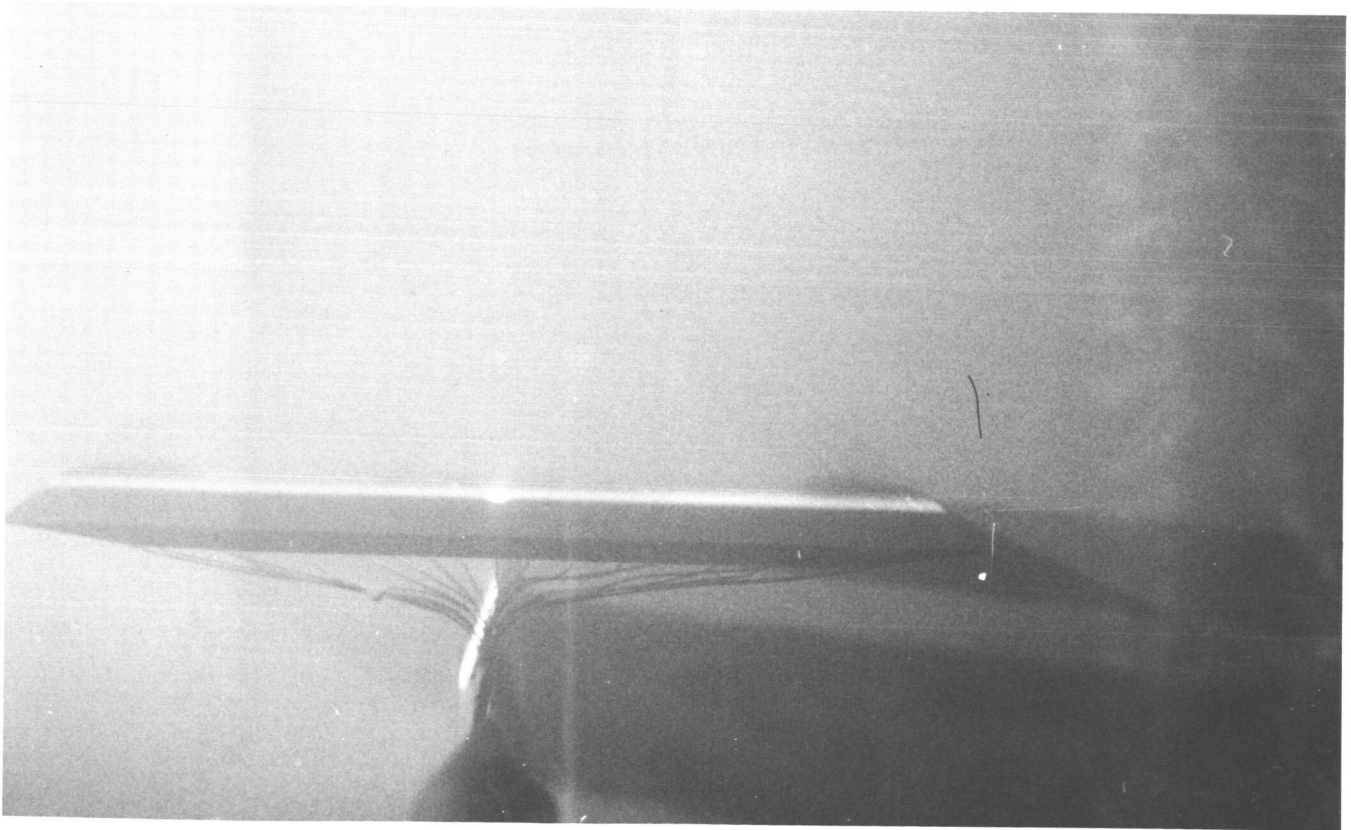


(a) $M = 1.7$, $\alpha = 0^\circ$.

Figure B2. Flow-visualization photographs for delta wing with $\Lambda_{LE} = 67.5^\circ$.

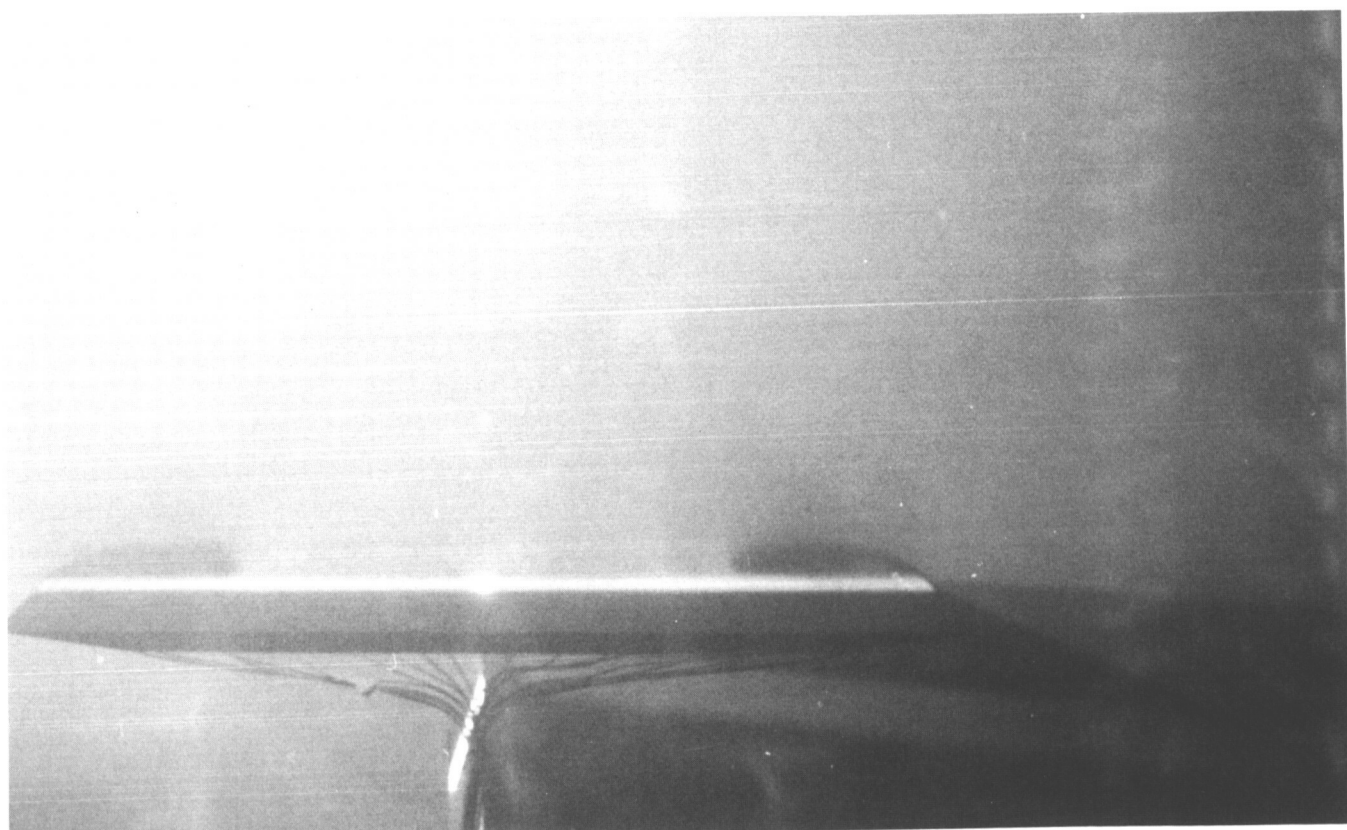
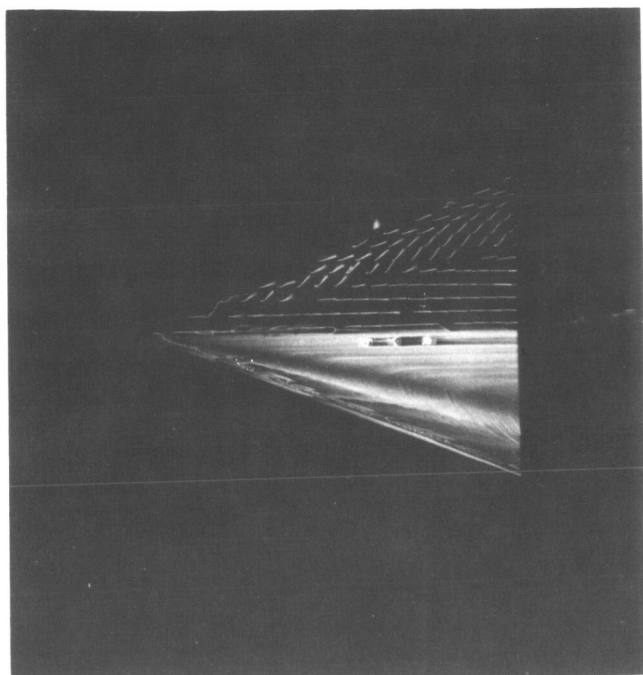
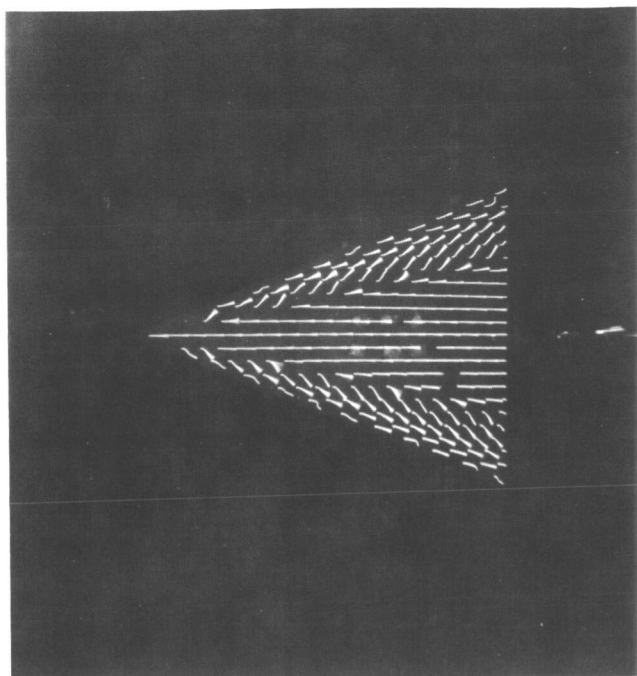


NO DATA



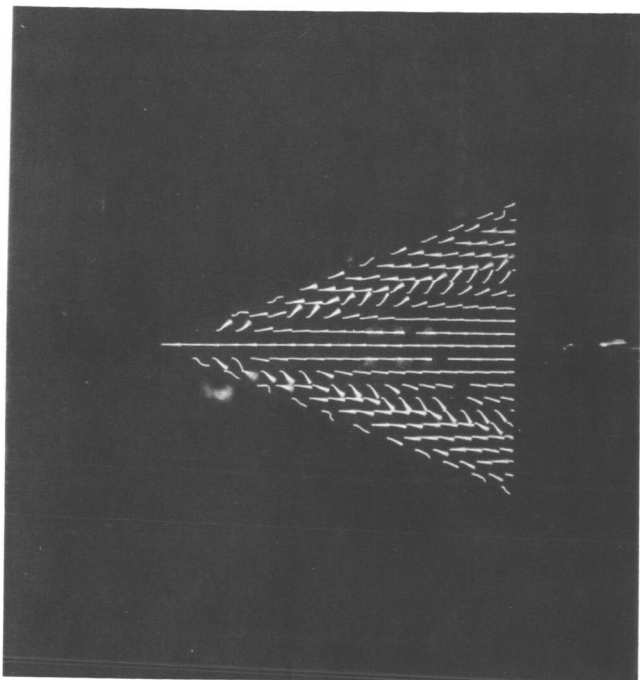
(b) $M = 1.7$, $\alpha = 4^\circ$.

Figure B2. Continued.

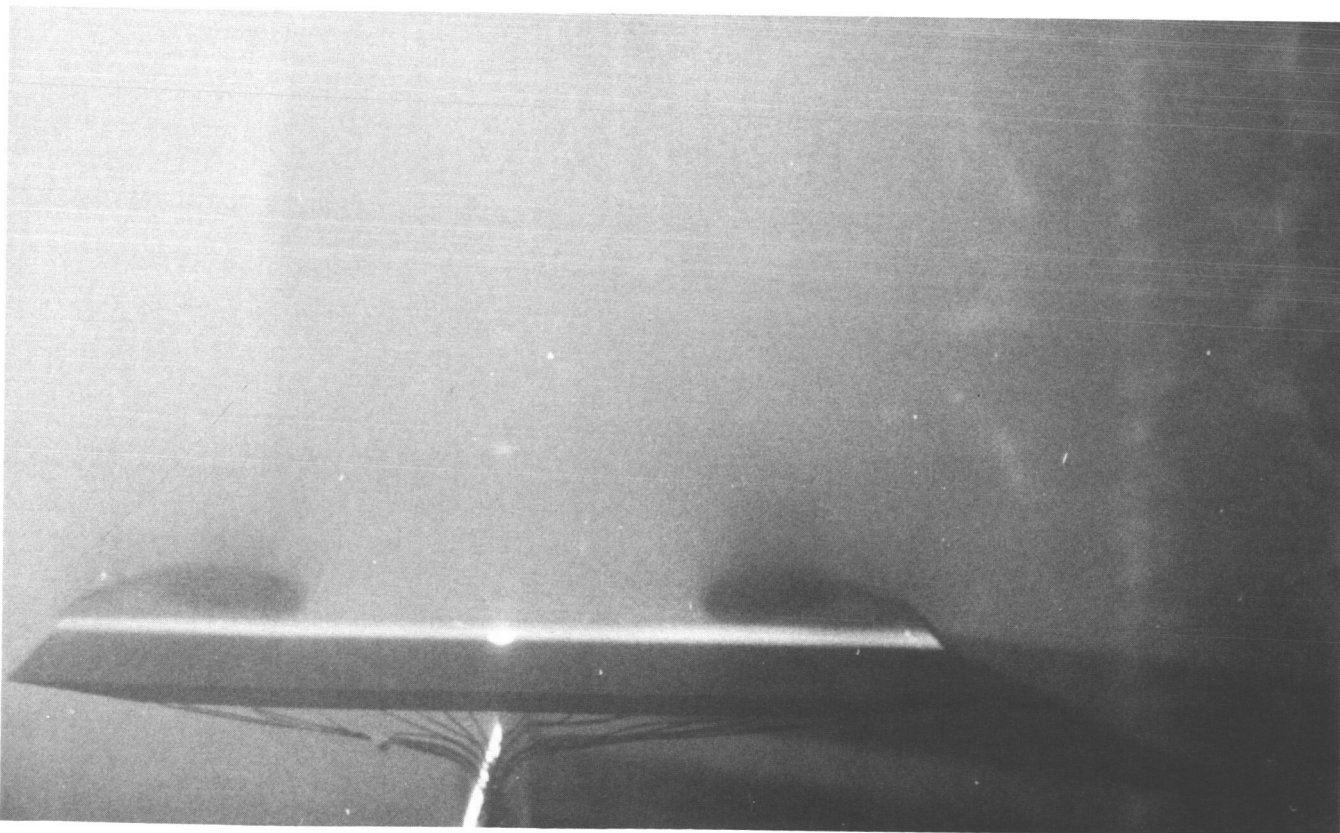


(c) $M = 1.7$, $\alpha = 8^\circ$.

Figure B2. Continued.

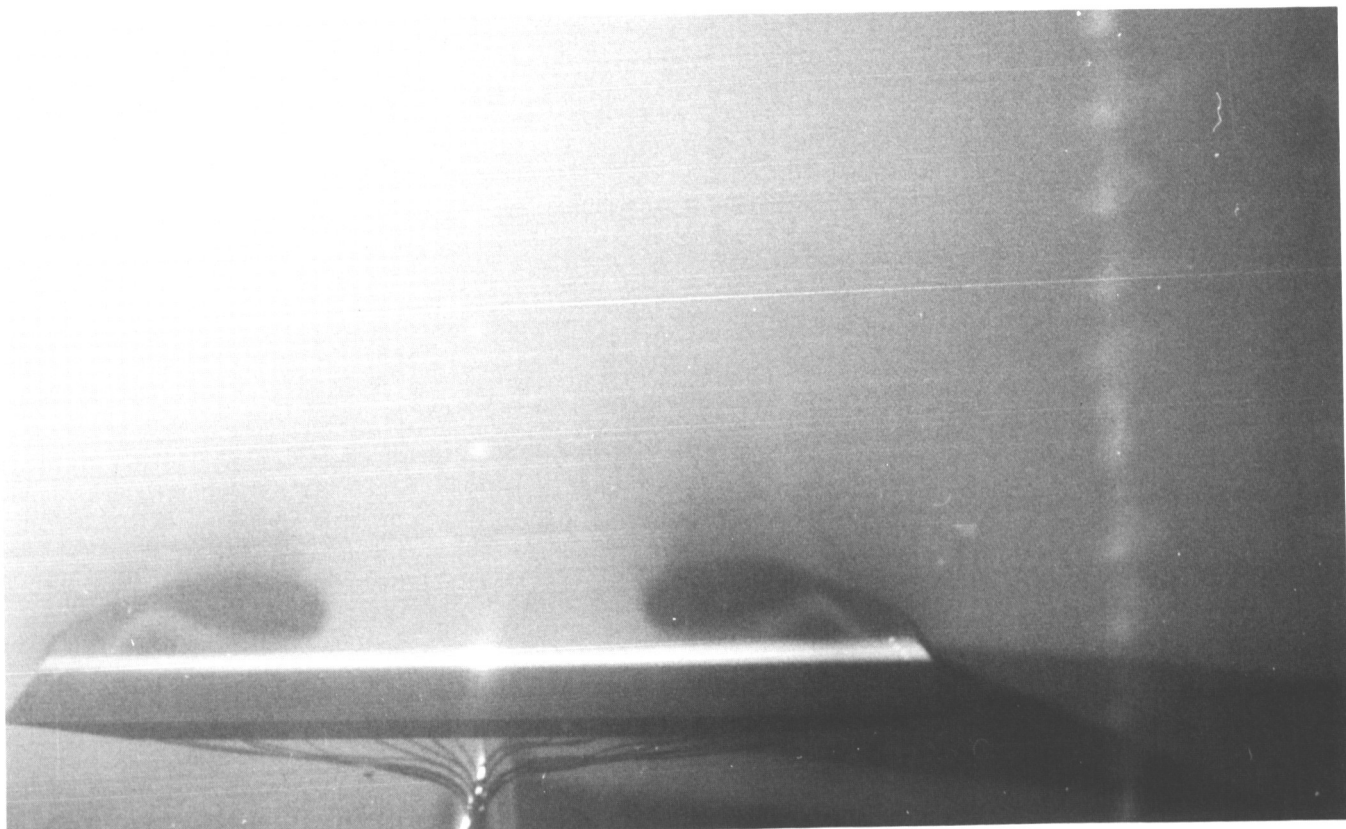
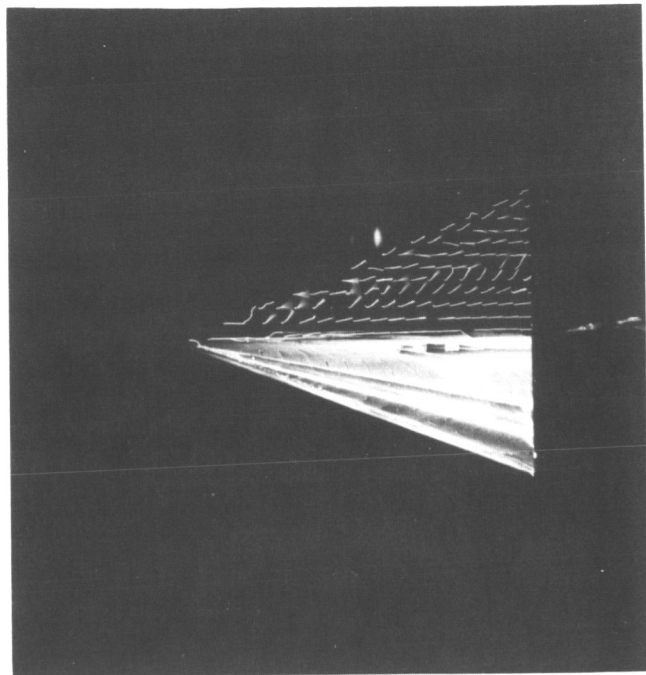
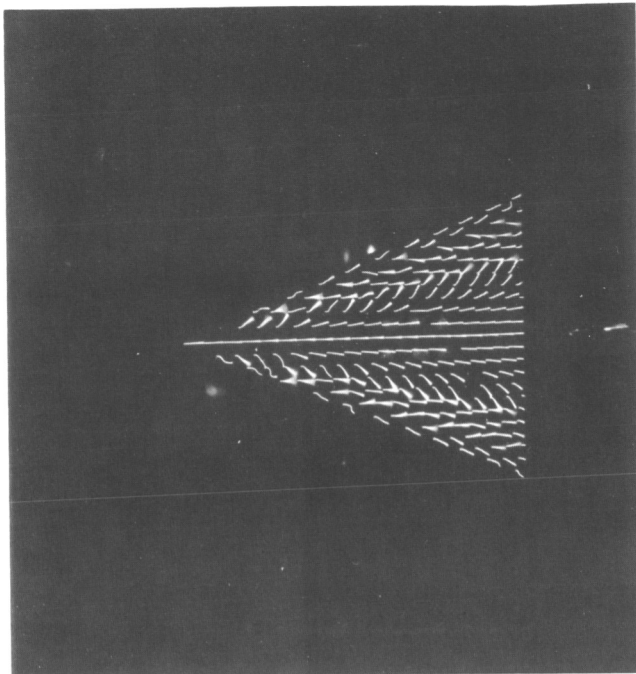


NO DATA



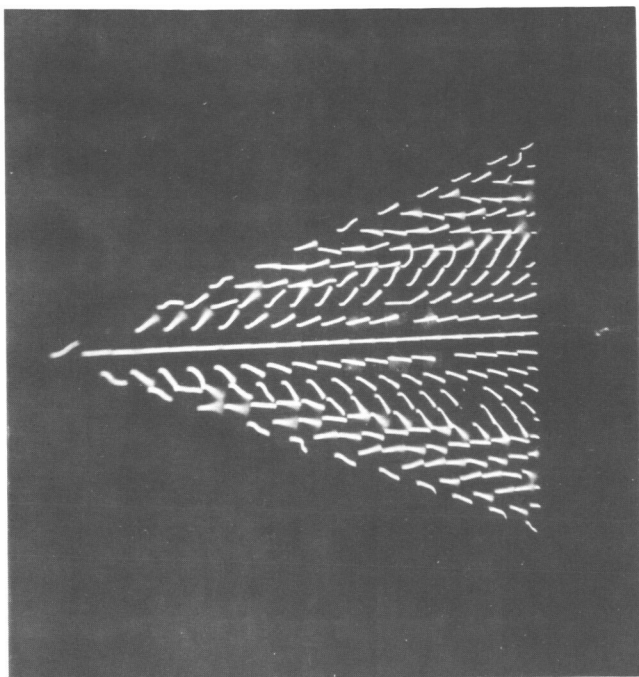
(d) $M = 1.7$, $\alpha = 12^\circ$.

Figure B2. Continued.

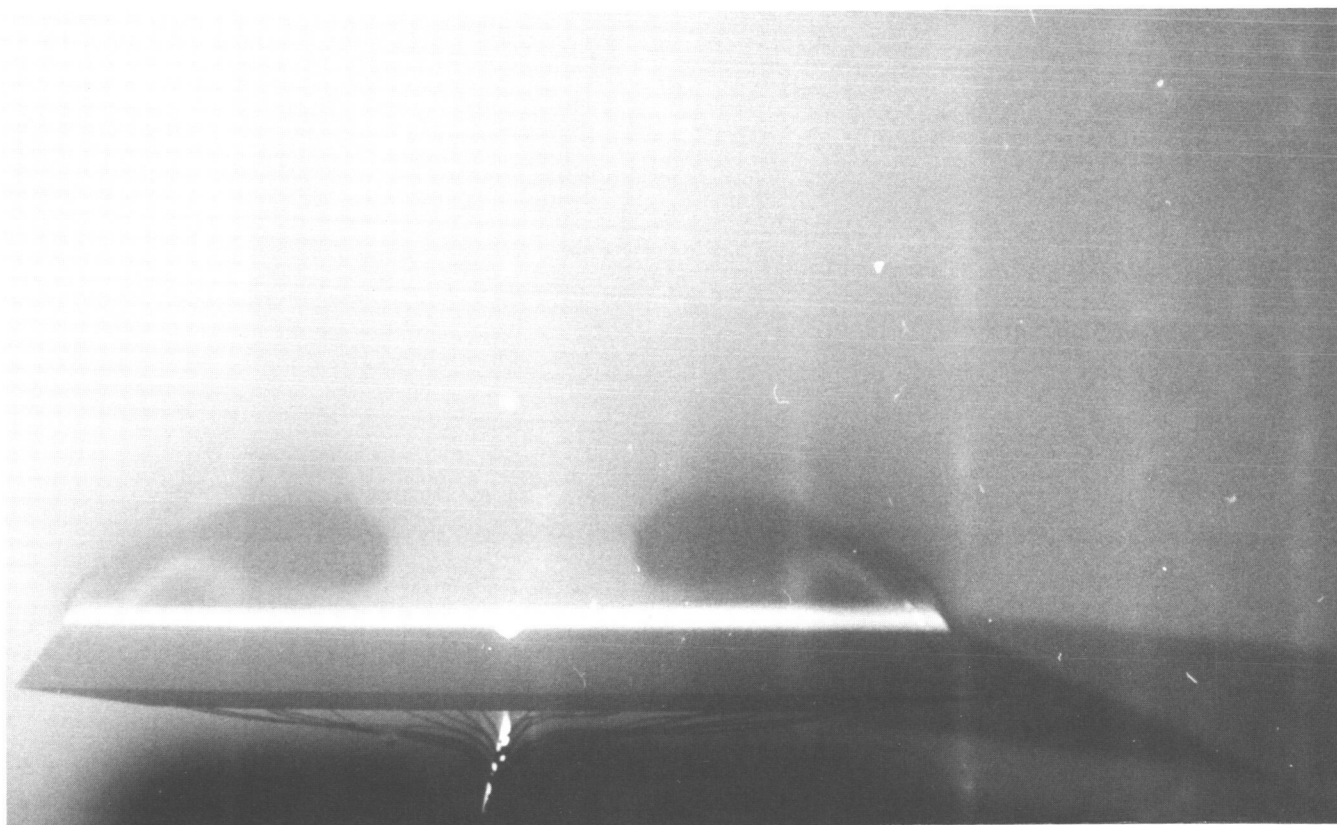


(e) $M = 1.7$, $\alpha = 16^\circ$.

Figure B2. Continued.

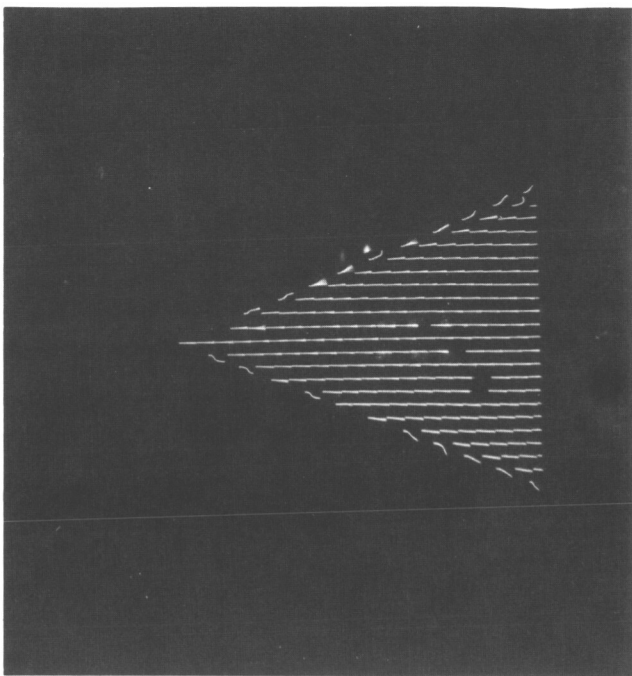


NO DATA

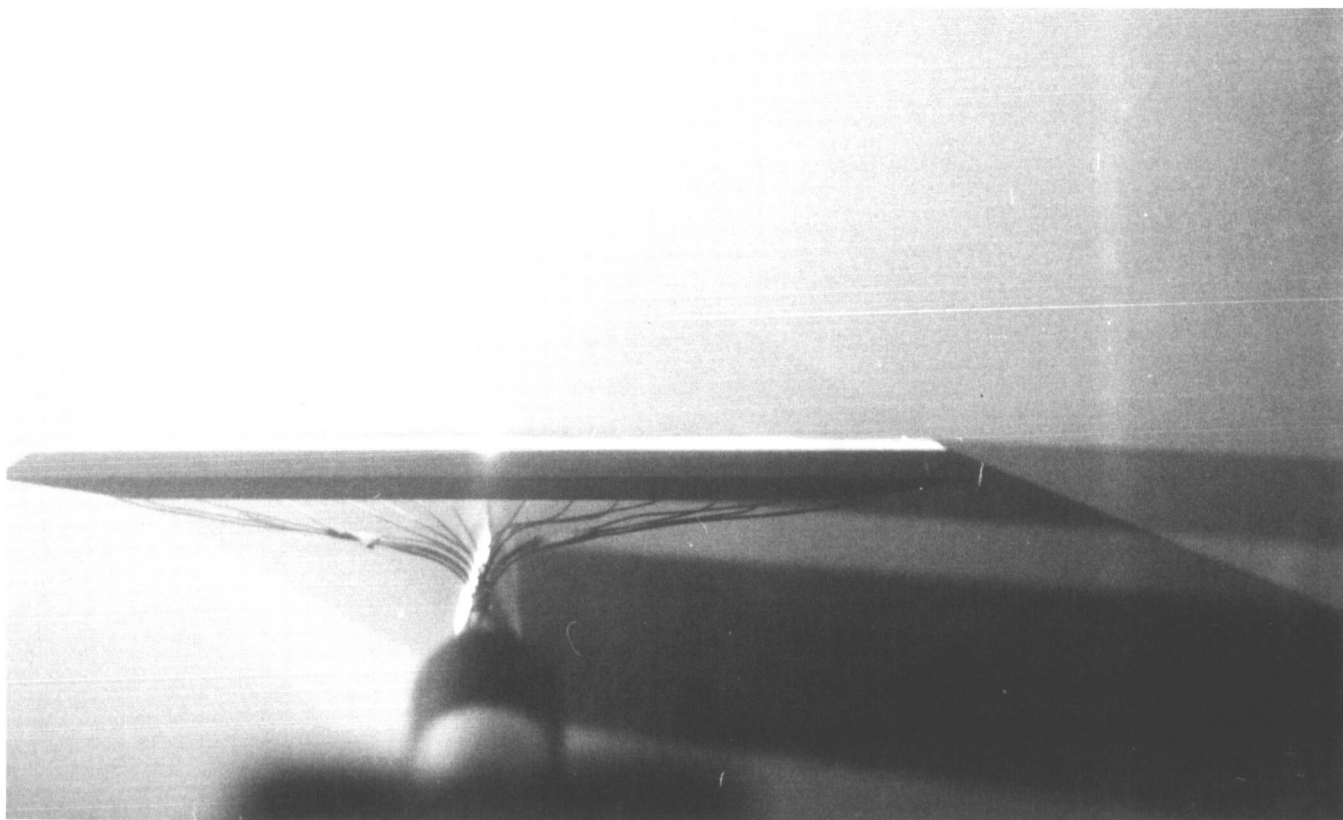


(f) $M = 1.7$, $\alpha = 20^\circ$.

Figure B2. Continued.

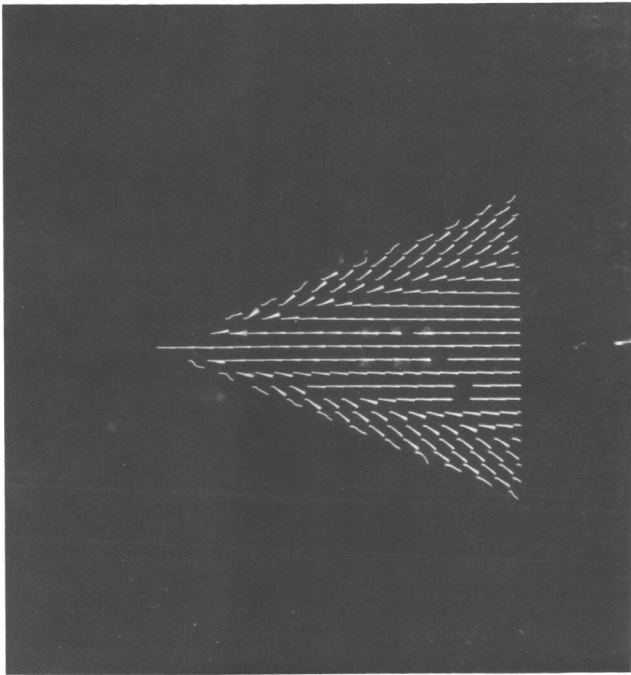


NO DATA

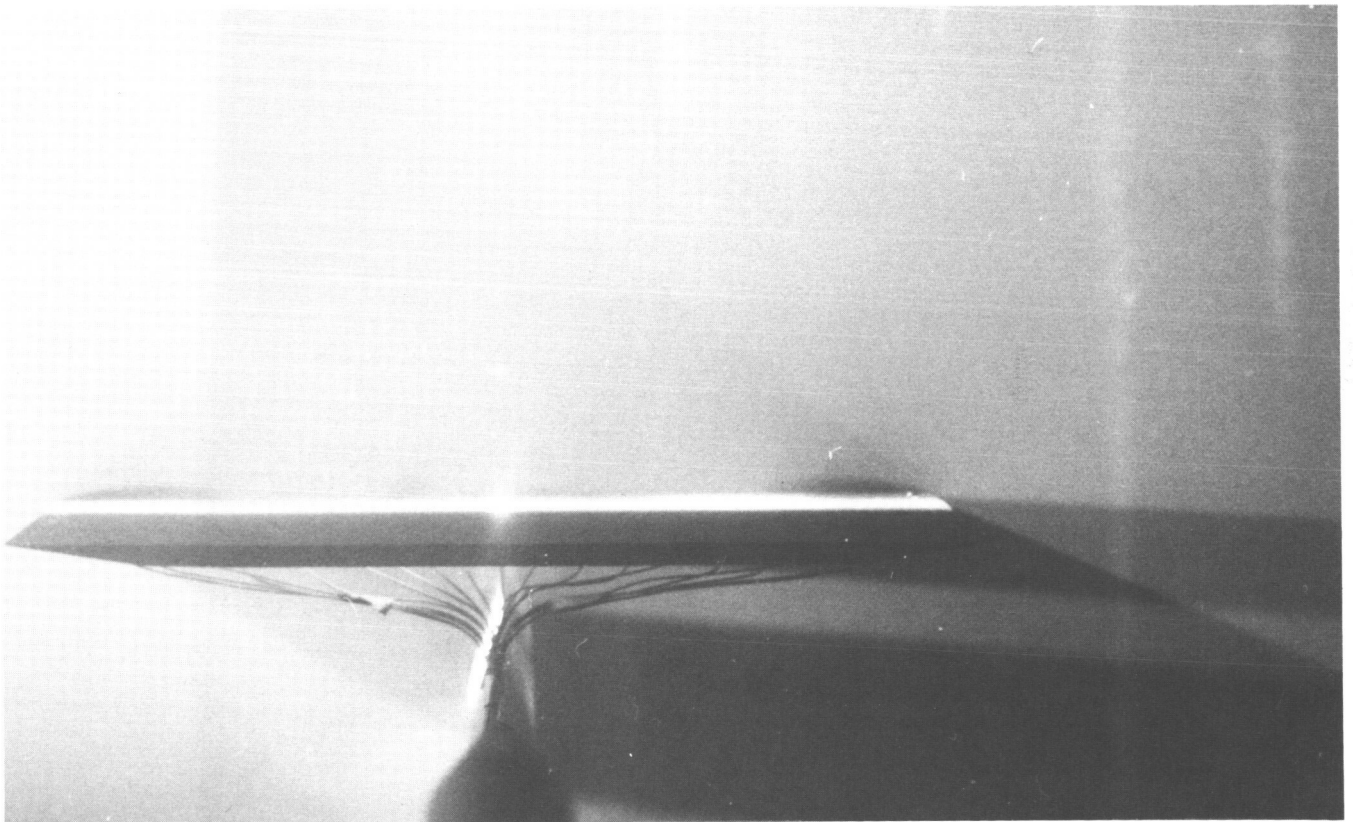


(g) $M = 2.0$, $\alpha = 0^\circ$.

Figure B2. Continued.

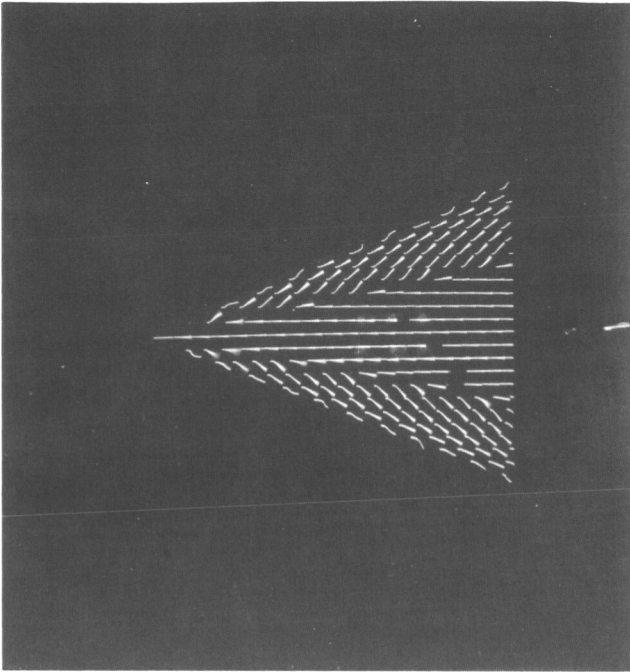


NO DATA

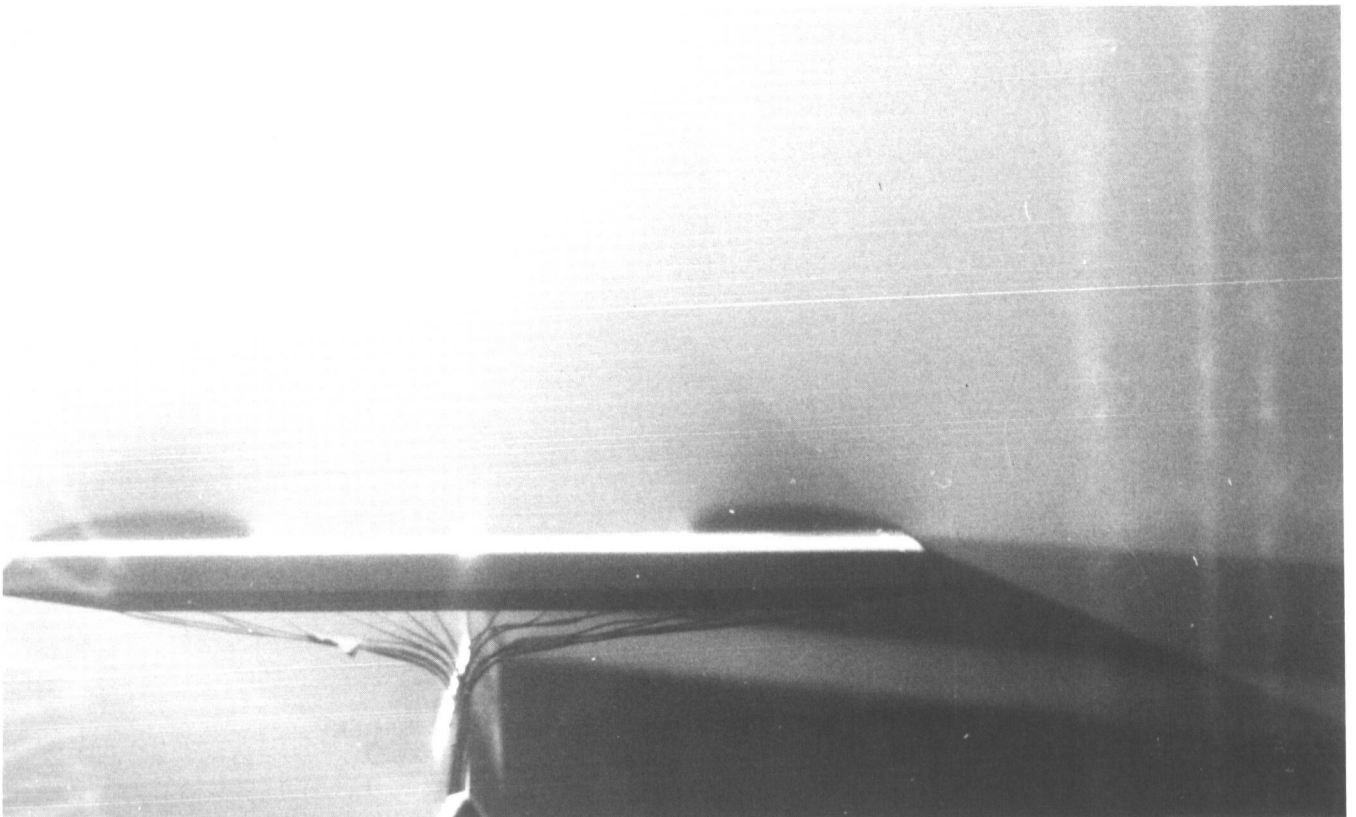


(h) $M = 2.0$, $\alpha = 4^\circ$.

Figure B2. Continued.

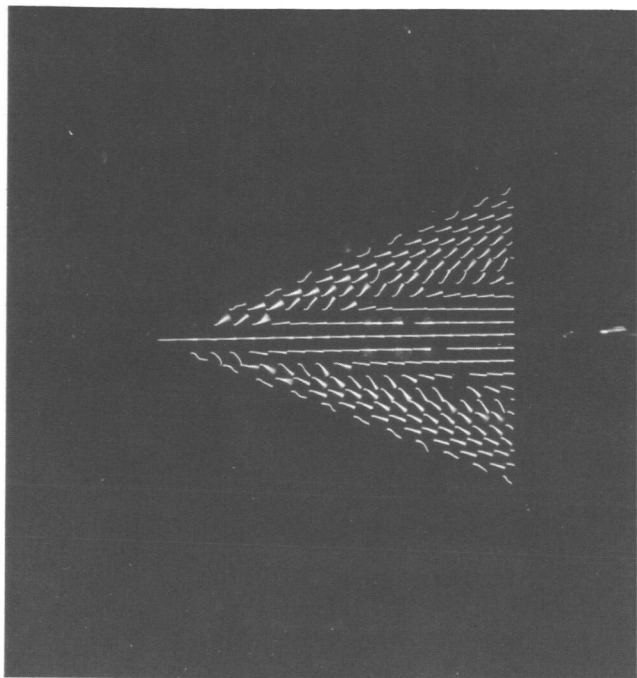


NO DATA

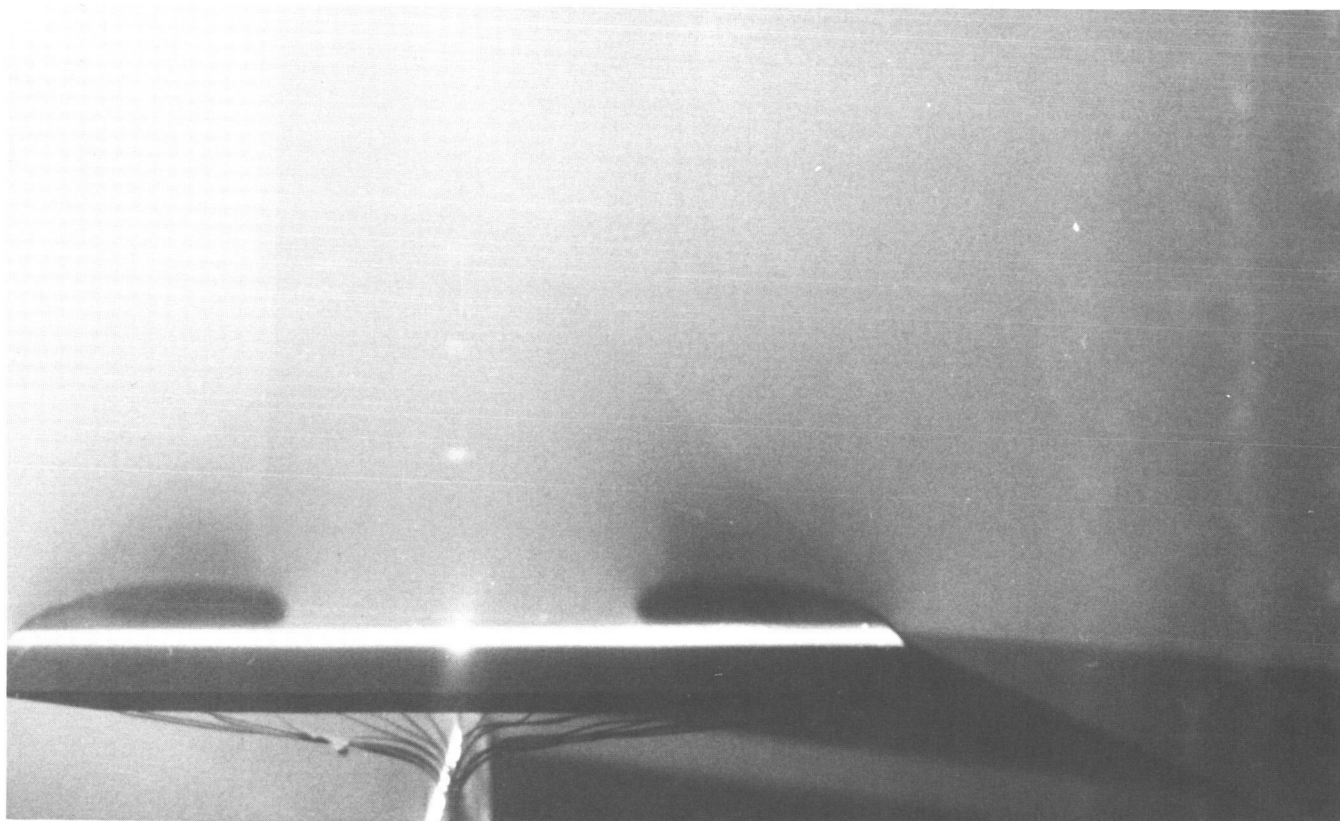


(i) $M = 2.0$, $\alpha = 8^\circ$.

Figure B2. Continued.

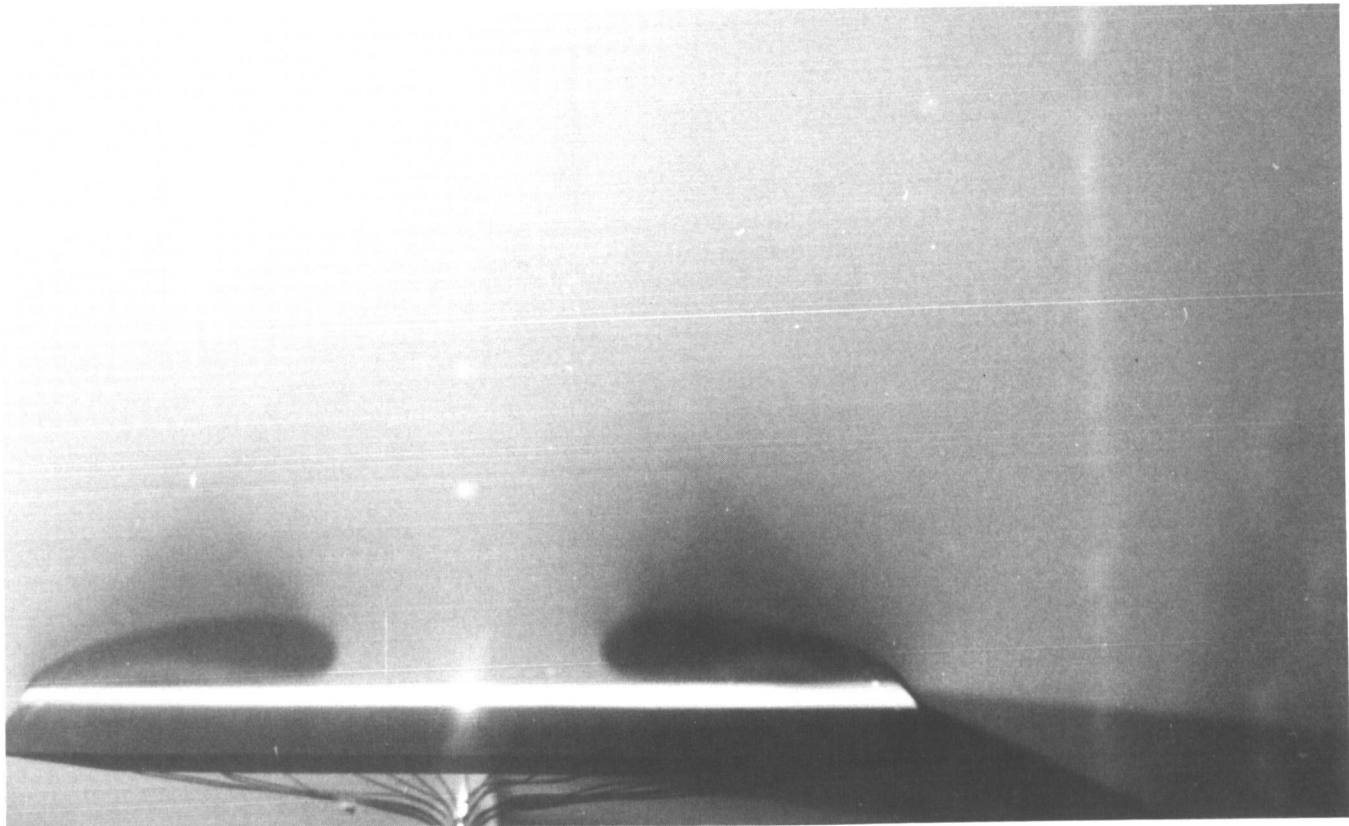
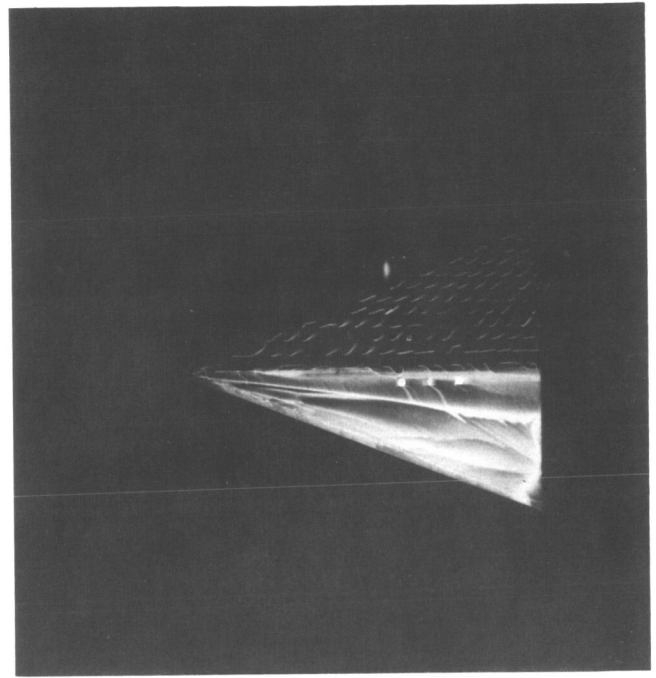
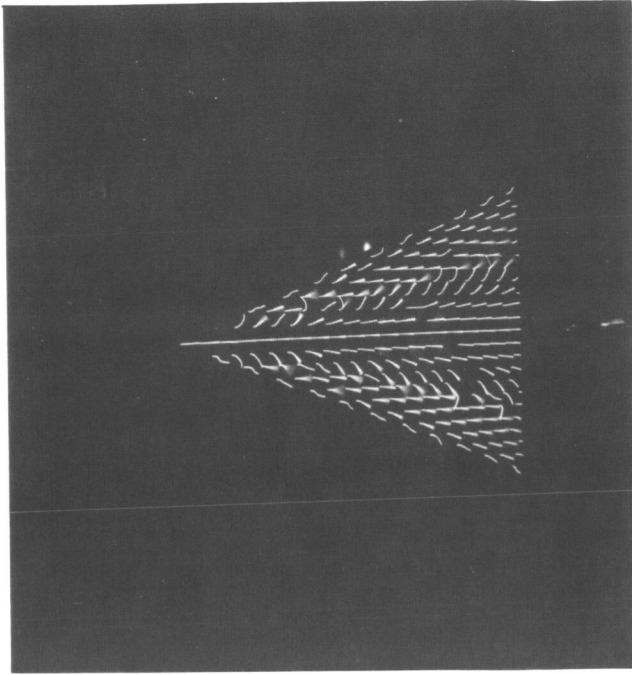


NO DATA



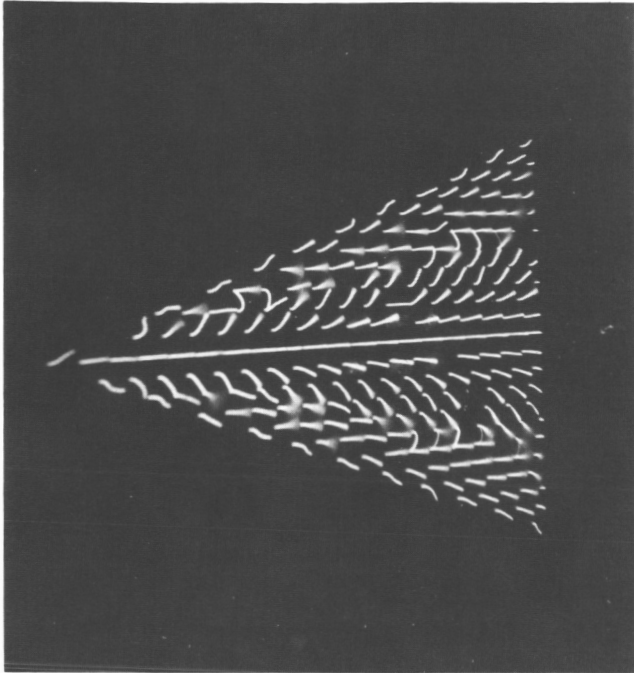
(j) $M = 2.0$, $\alpha = 12^\circ$.

Figure B2. Continued.

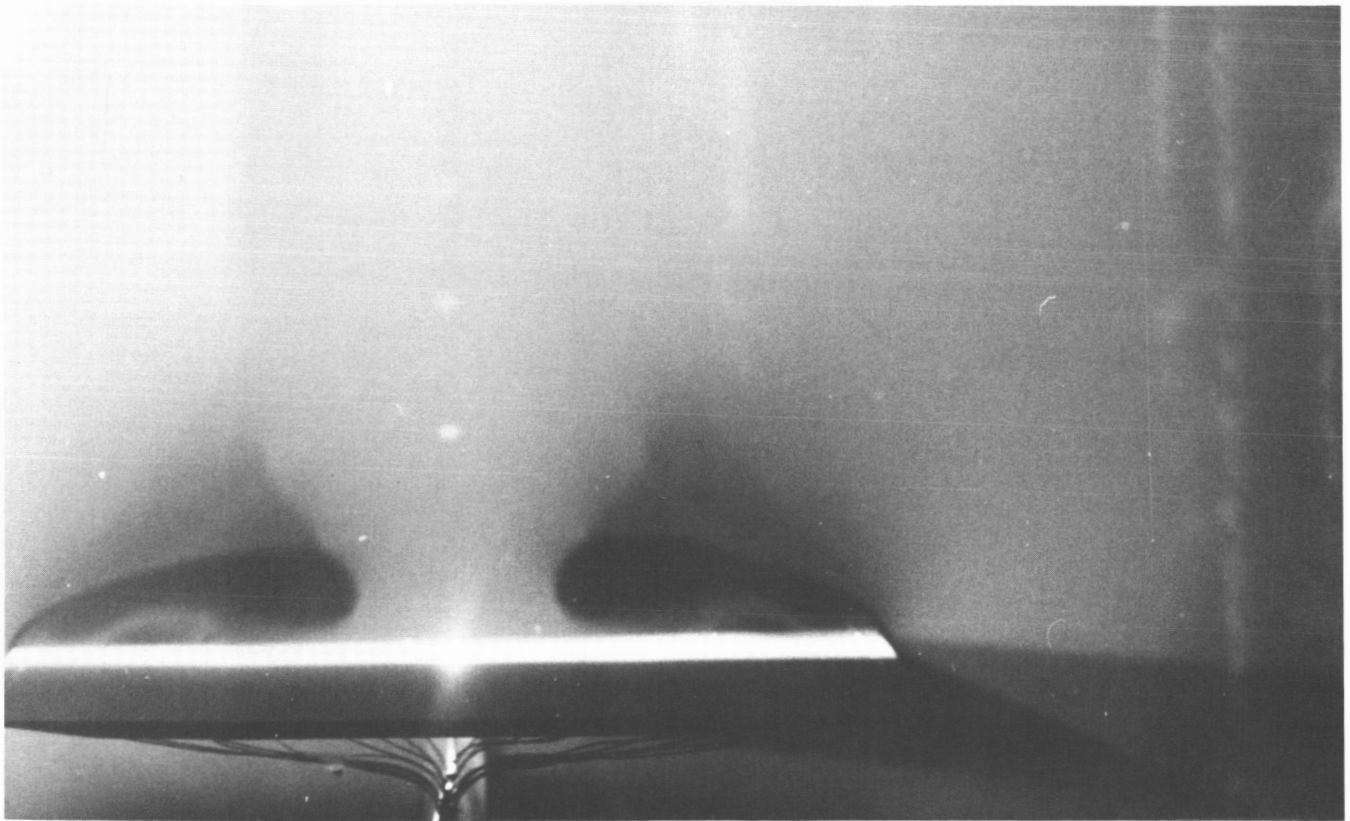


(k) $M = 2.0$, $\alpha = 16^\circ$.

Figure B2. Continued.

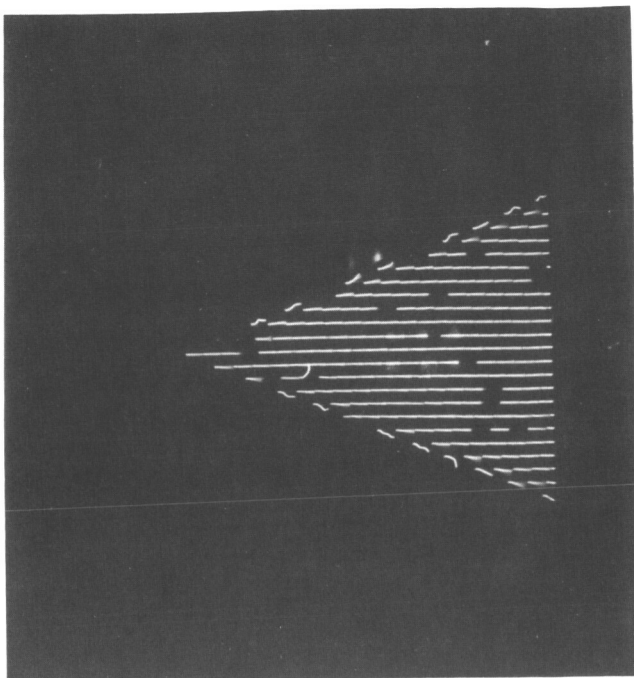


NO DATA



(1) $M = 2.0$, $\alpha = 20^\circ$.

Figure B2. Continued.

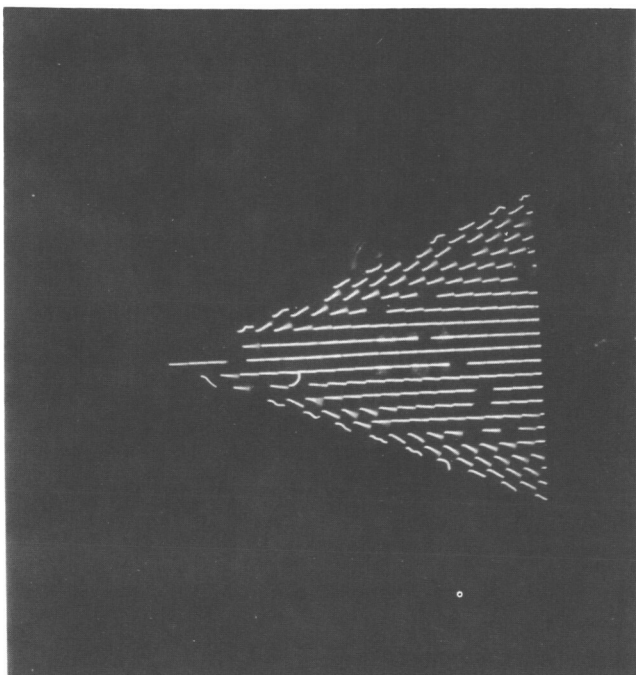


NO DATA

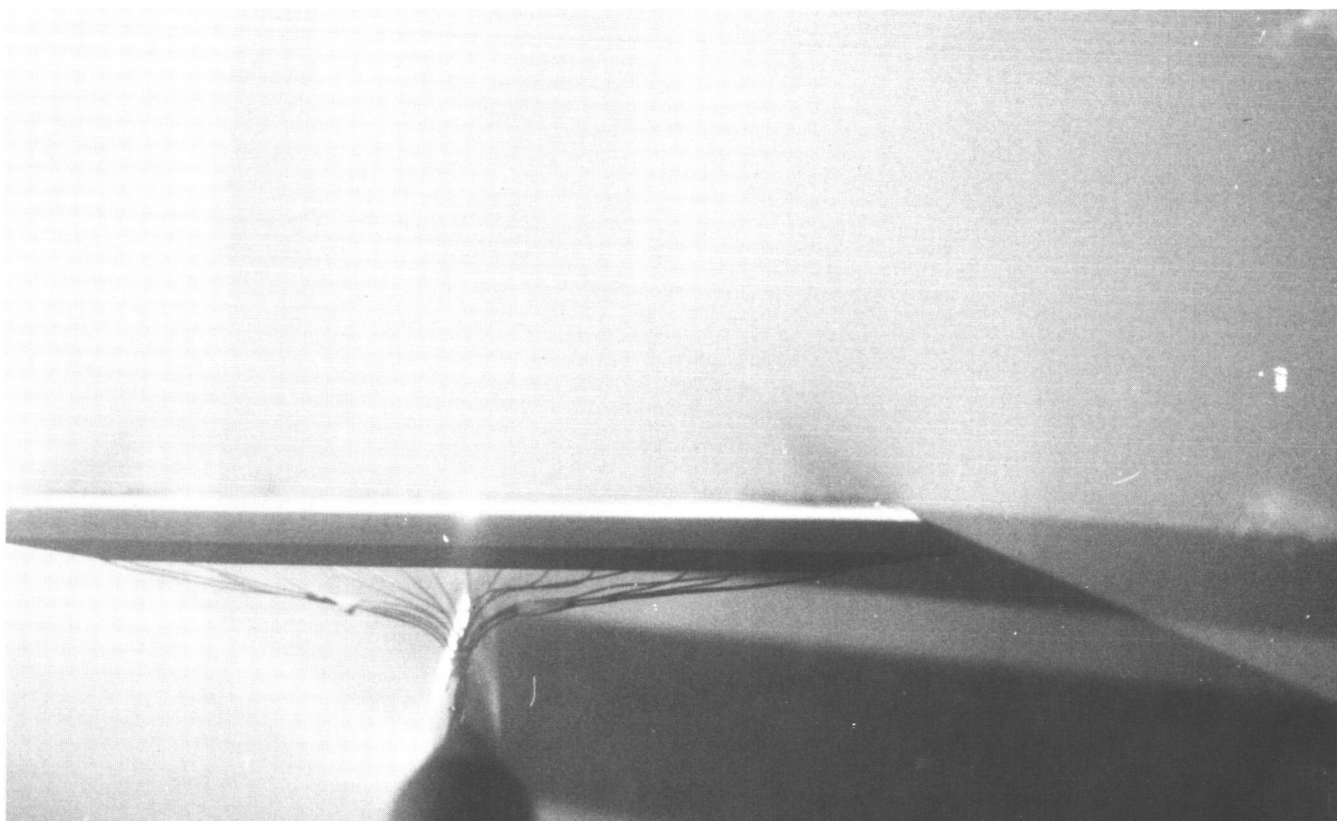


(m) $M = 2.4$, $\alpha = 0^\circ$.

Figure B2. Continued.

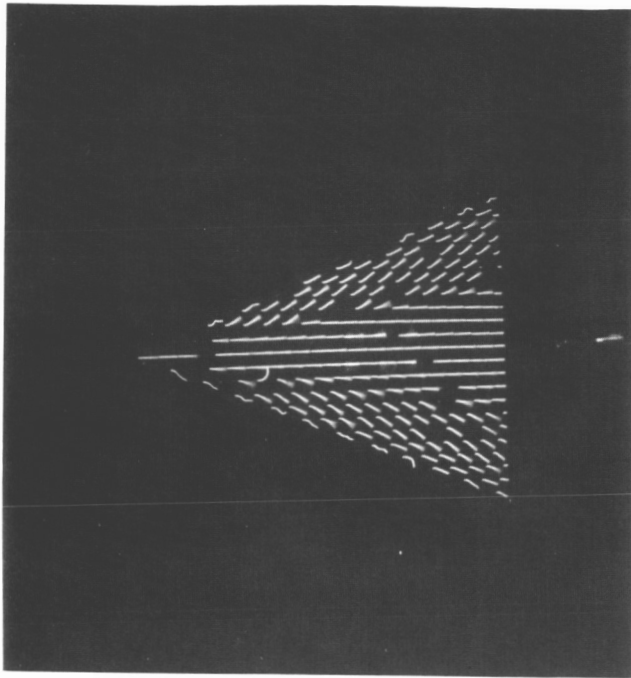


NO DATA

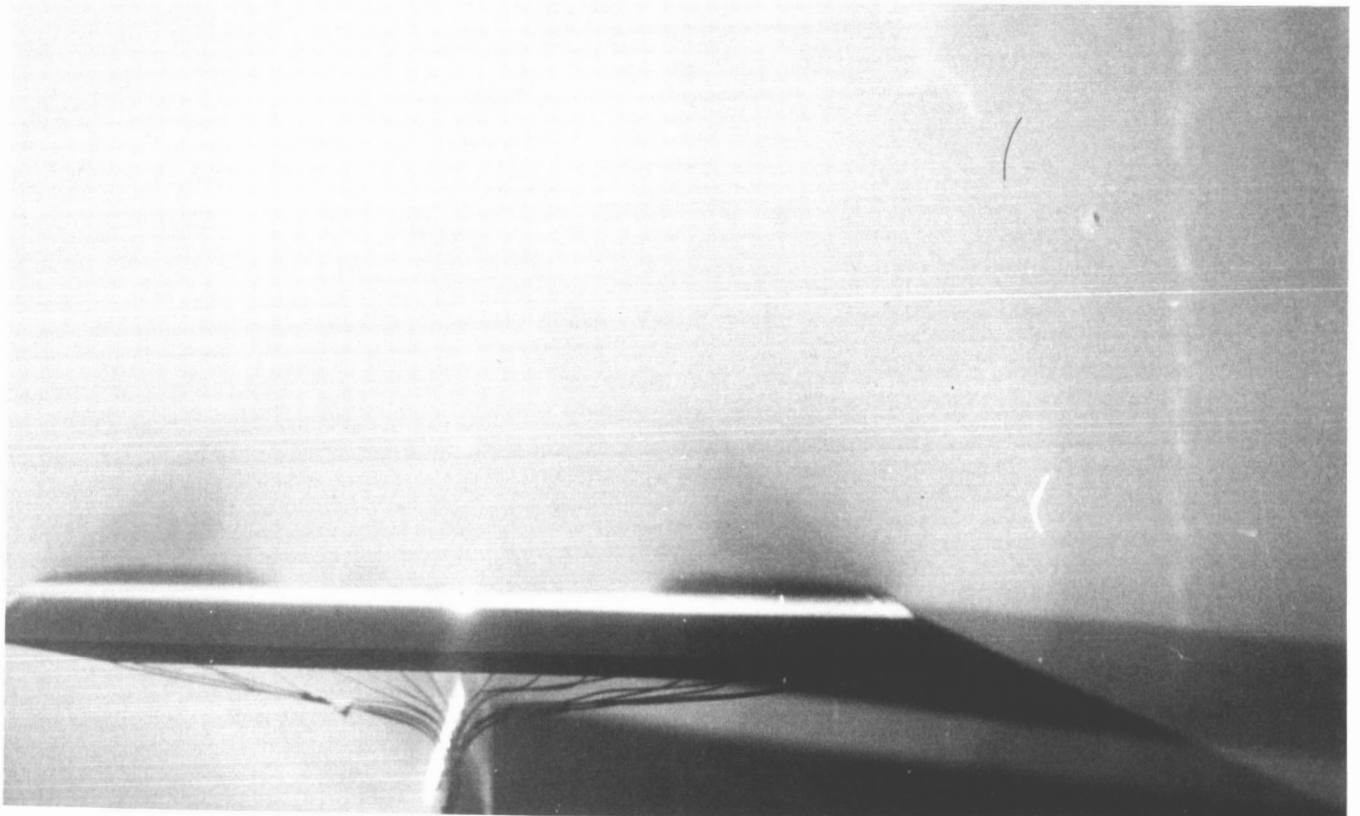


(n) $M = 2.4$, $\alpha = 4^\circ$.

Figure B2. Continued.

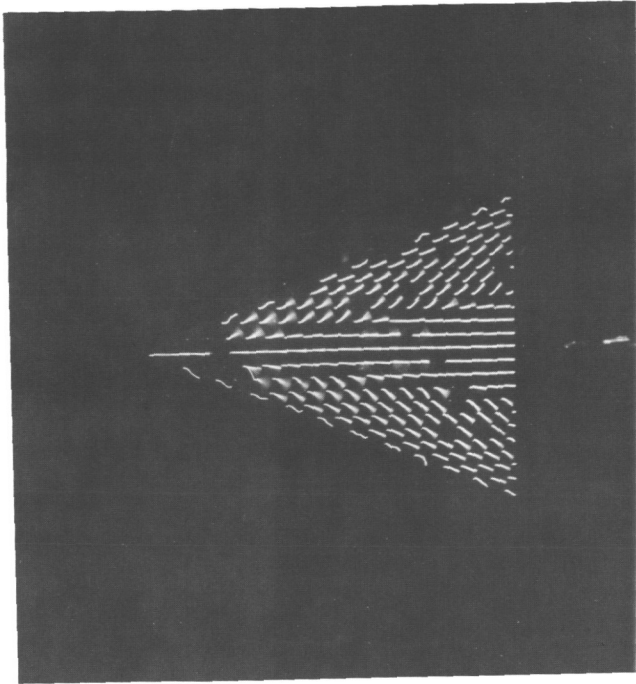


NO DATA

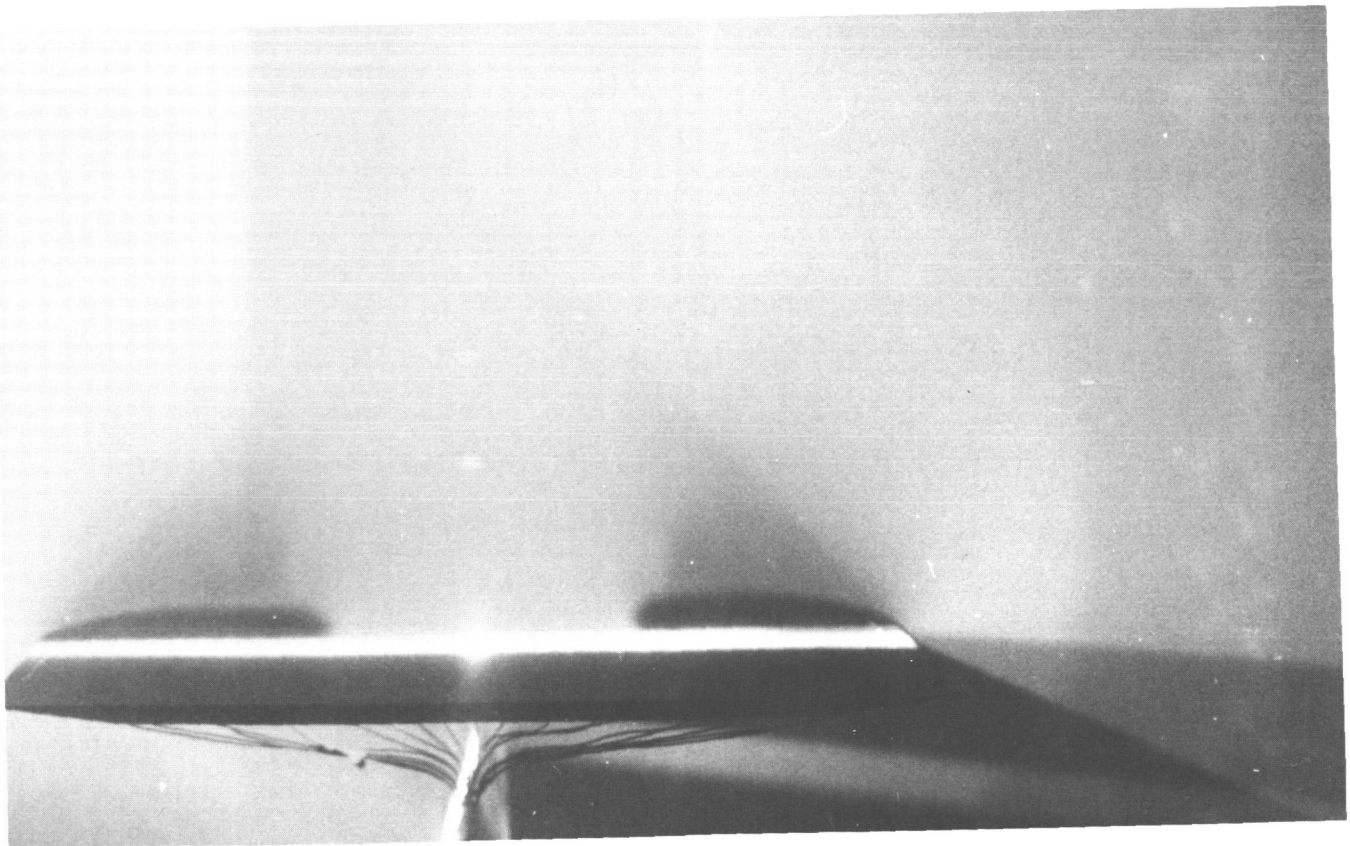


(o) $M = 2.4$, $\alpha = 8^\circ$.

Figure B2. Continued.

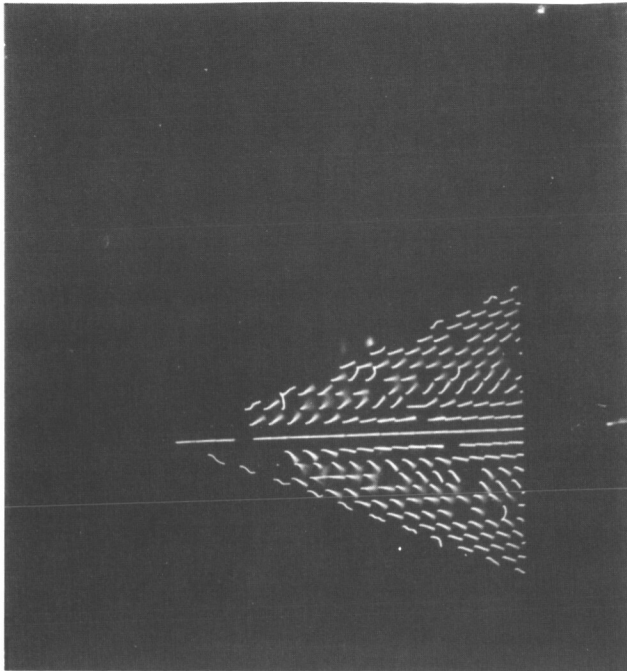


NO DATA

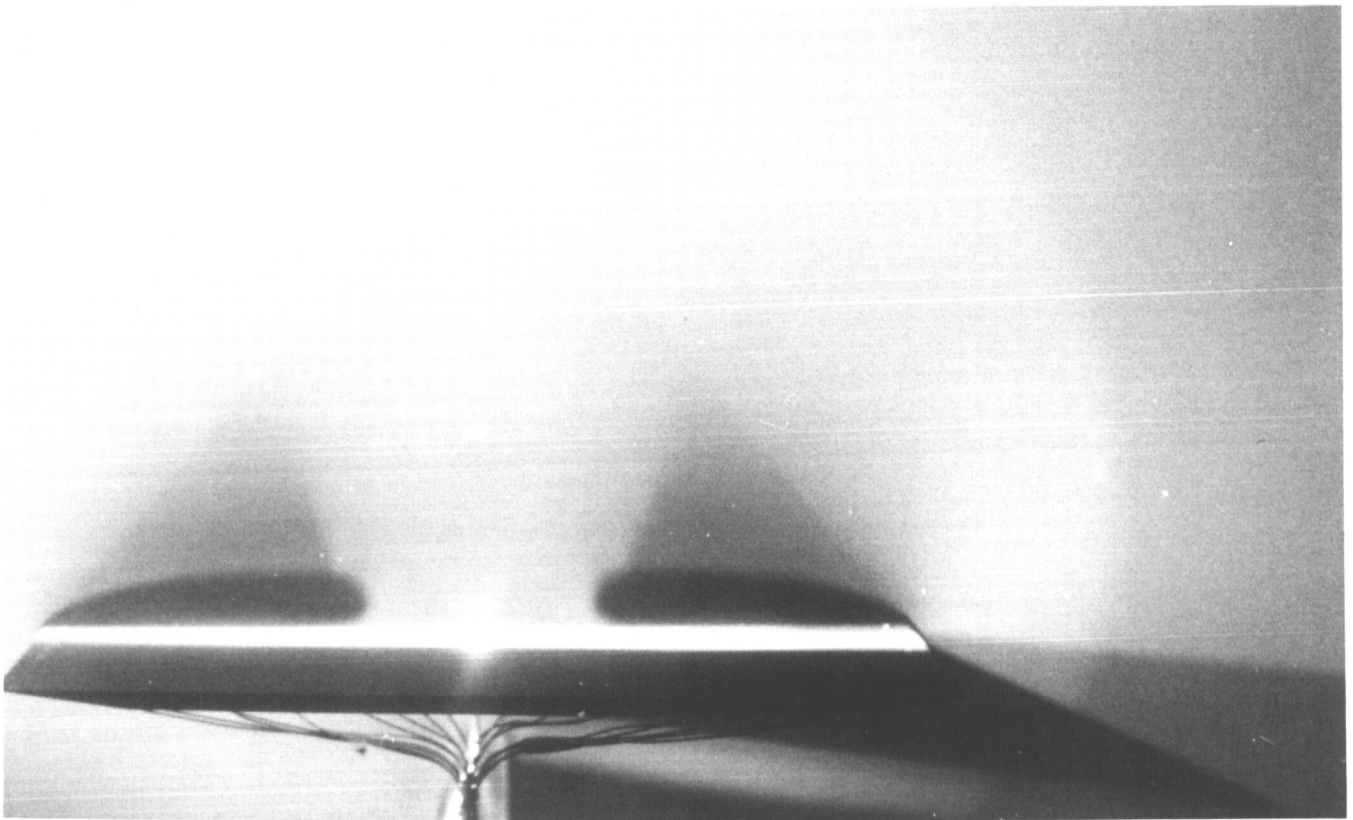


(p) $M = 2.4$, $\alpha = 12^\circ$.

Figure B2. Continued.

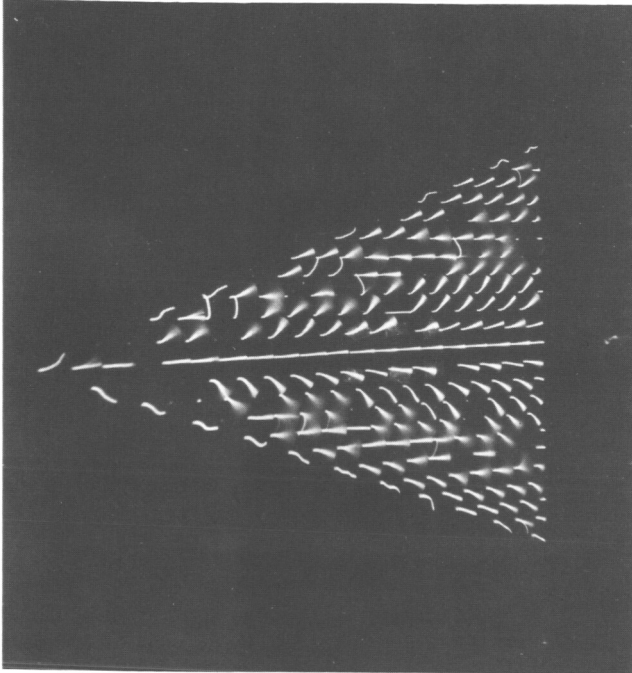


NO DATA

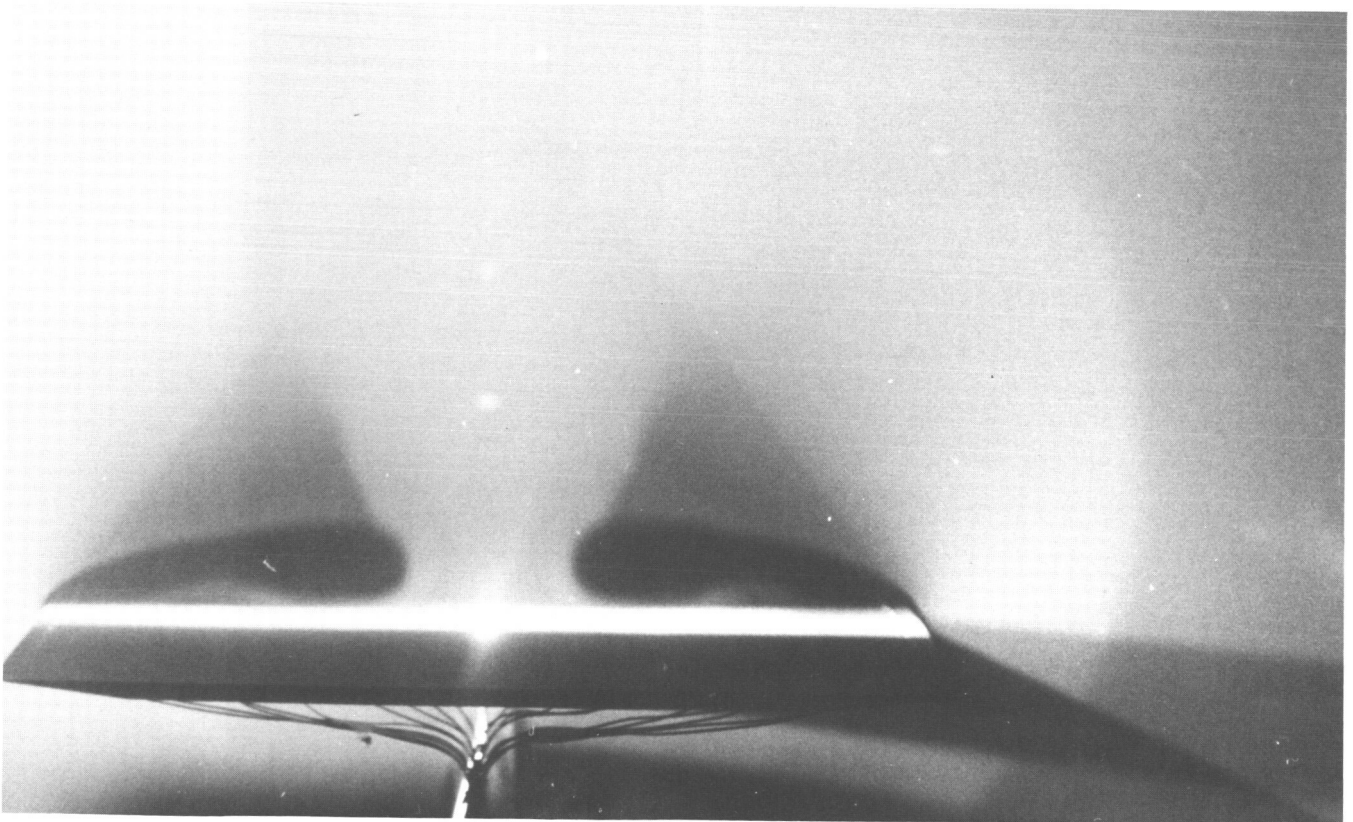


(q) $M = 2.4$, $\alpha = 16^\circ$.

Figure B2. Continued.

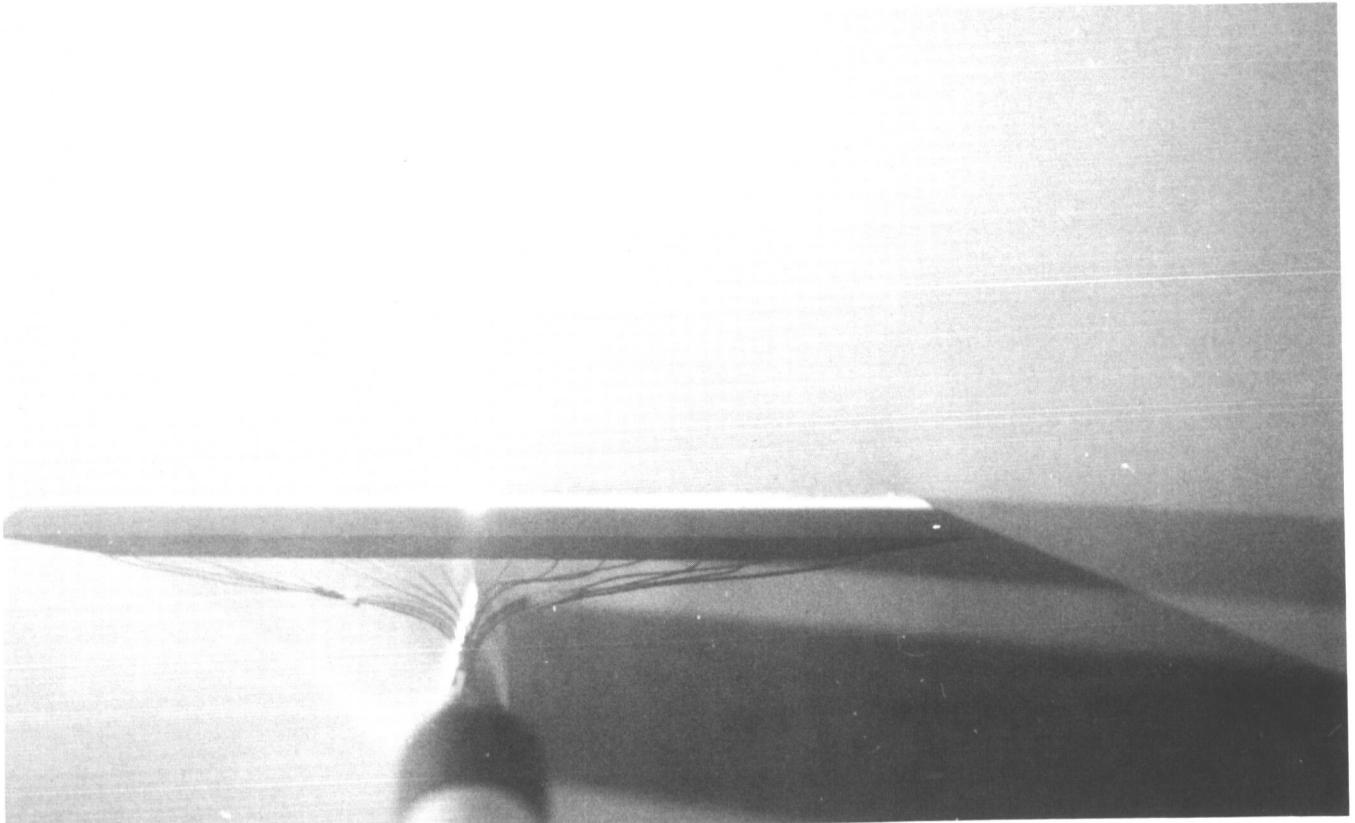
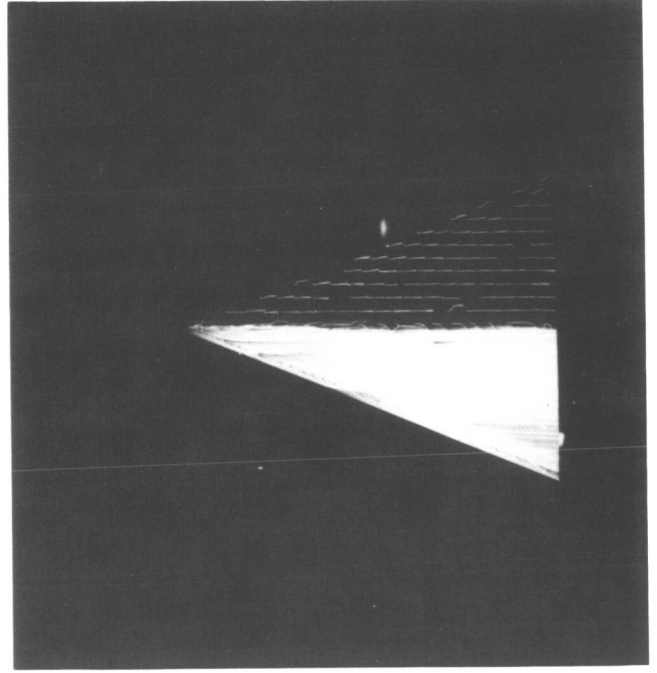
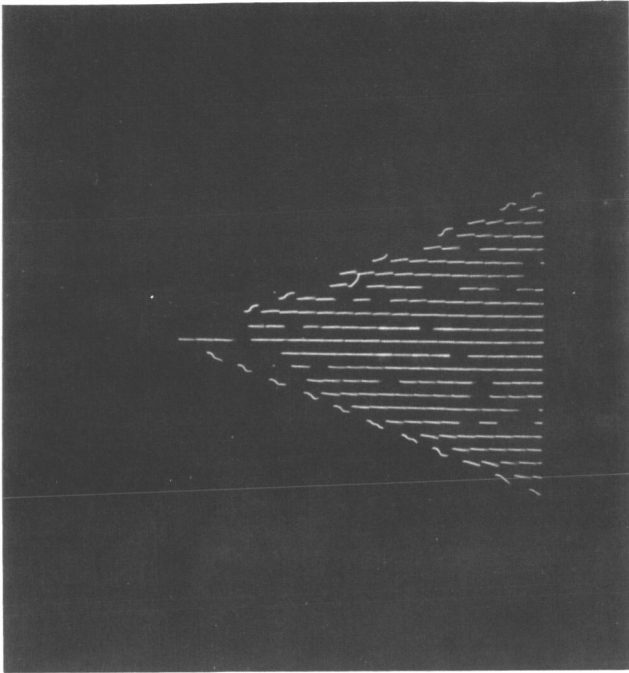


NO DATA



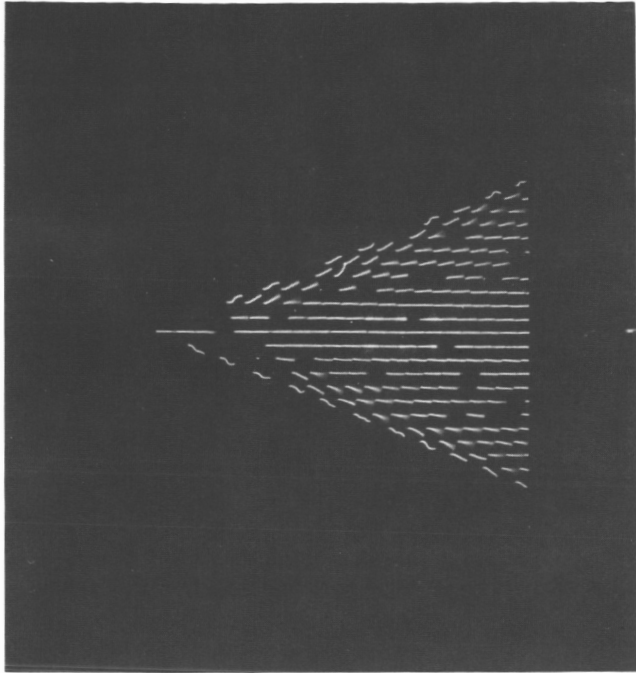
(r) $M = 2.4$, $\alpha = 20^\circ$.

Figure B2. Continued.

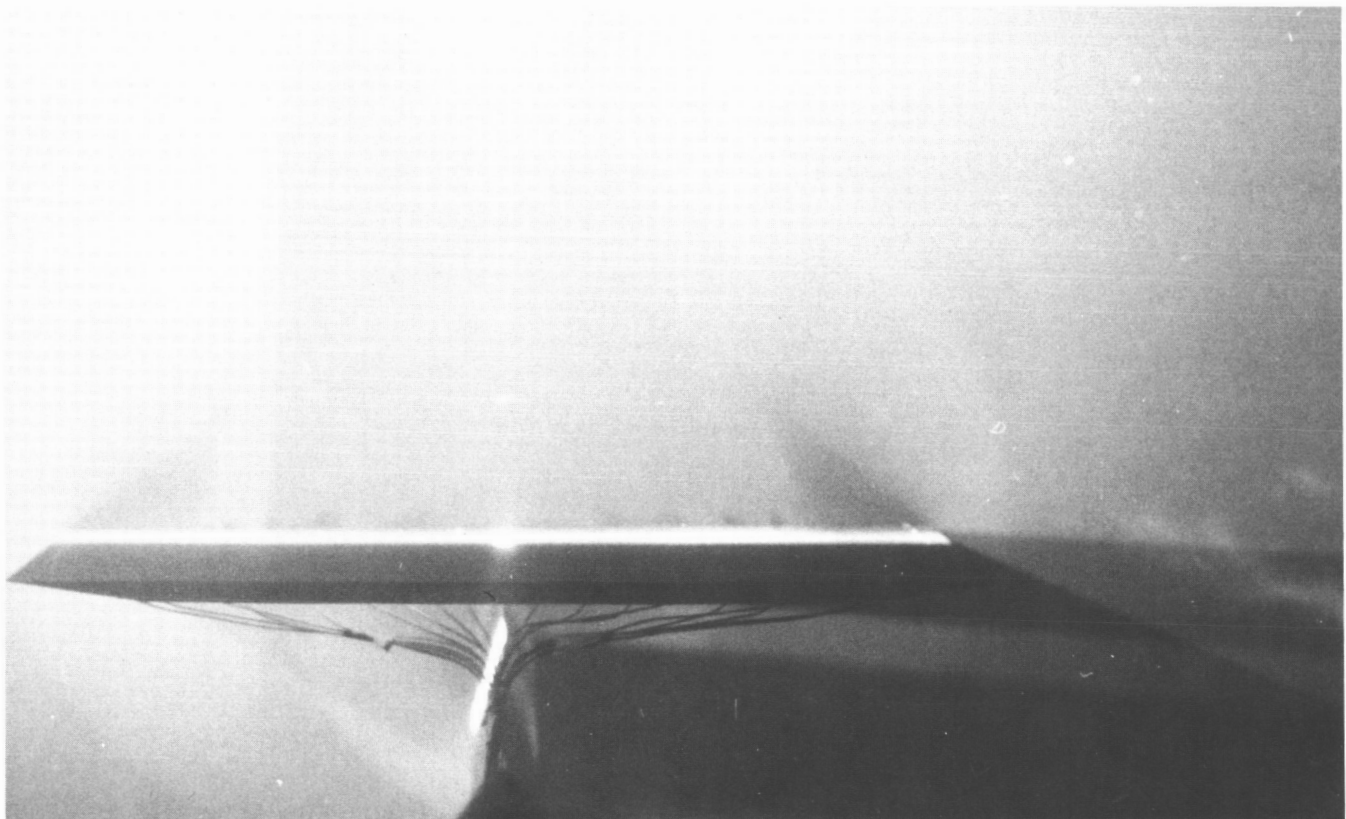


(s) $M = 2.8$, $\alpha = 0^\circ$.

Figure B2. Continued.

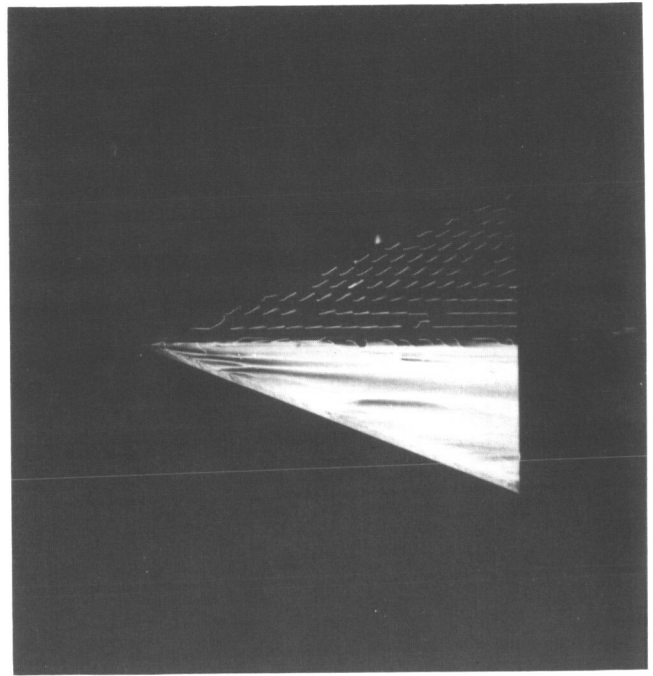
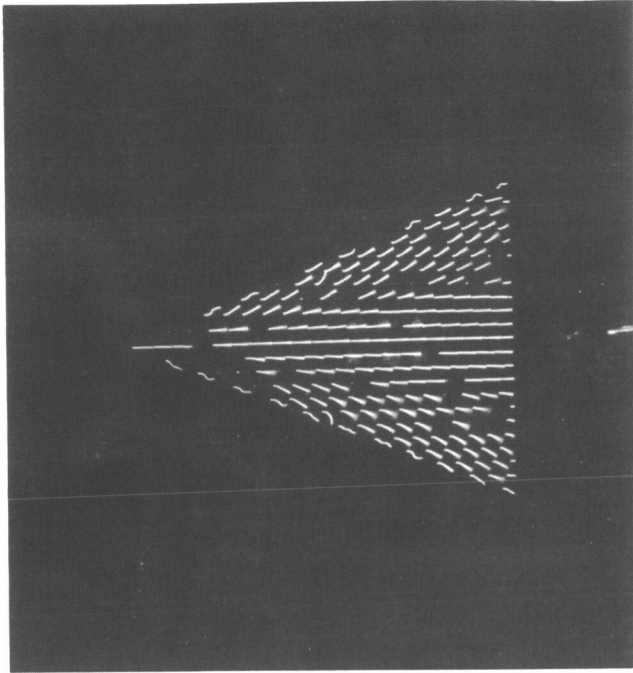


NO DATA



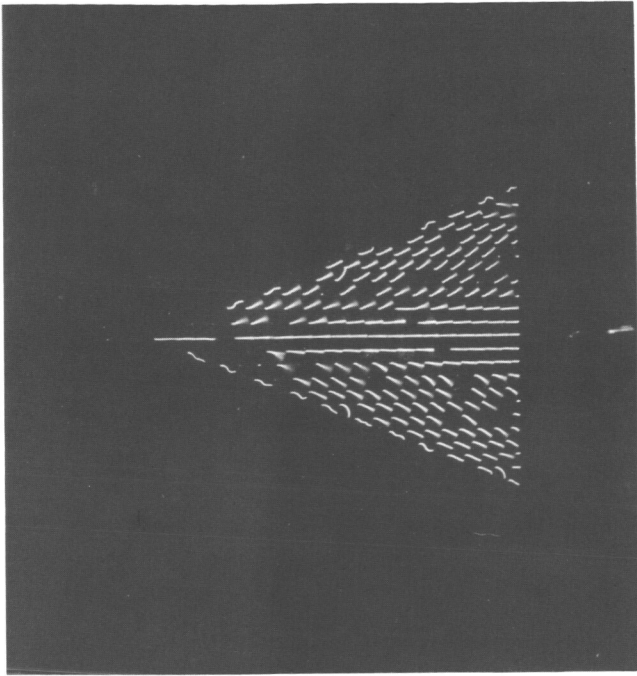
(t) $M = 2.8$, $\alpha = 4^\circ$.

Figure B2. Continued.

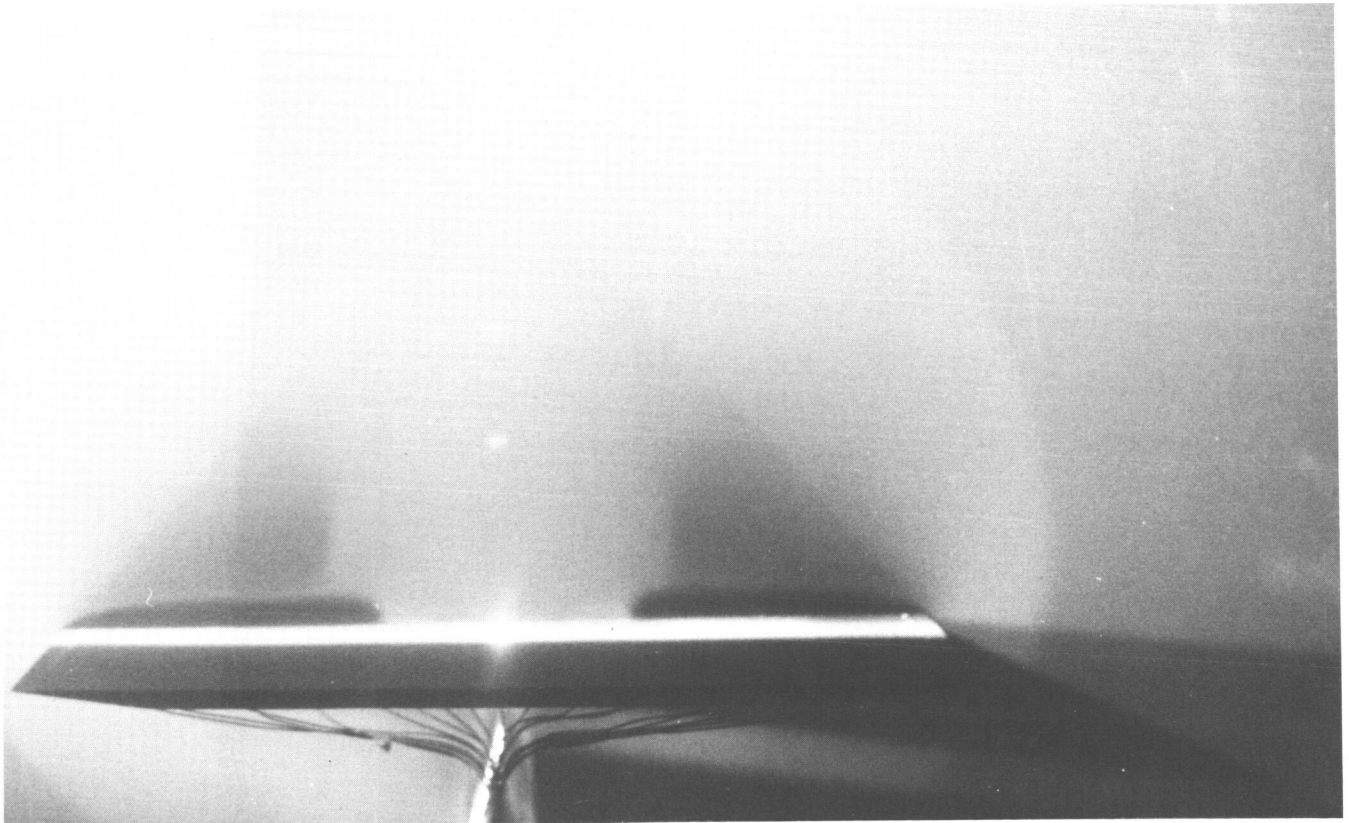


(u) $M = 2.8$, $\alpha = 8^\circ$.

Figure B2. Continued.

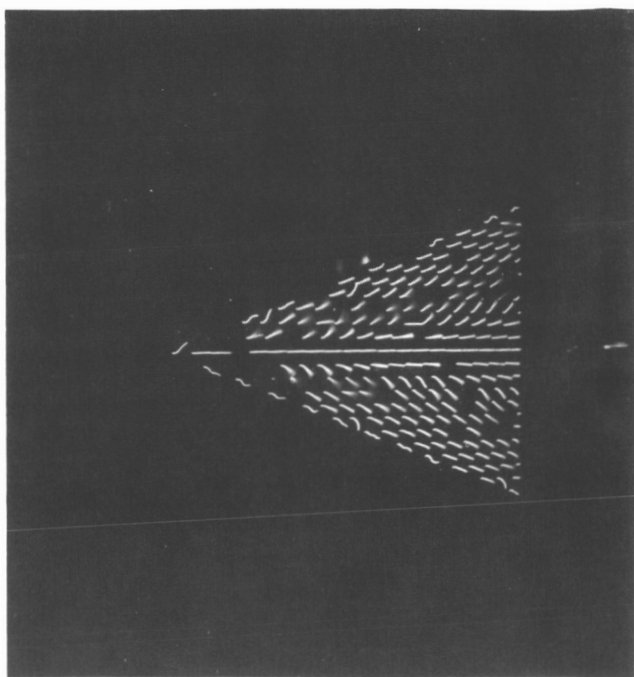


NO DATA



(v) $M = 2.8$, $\alpha = 12^\circ$.

Figure B2. Continued.

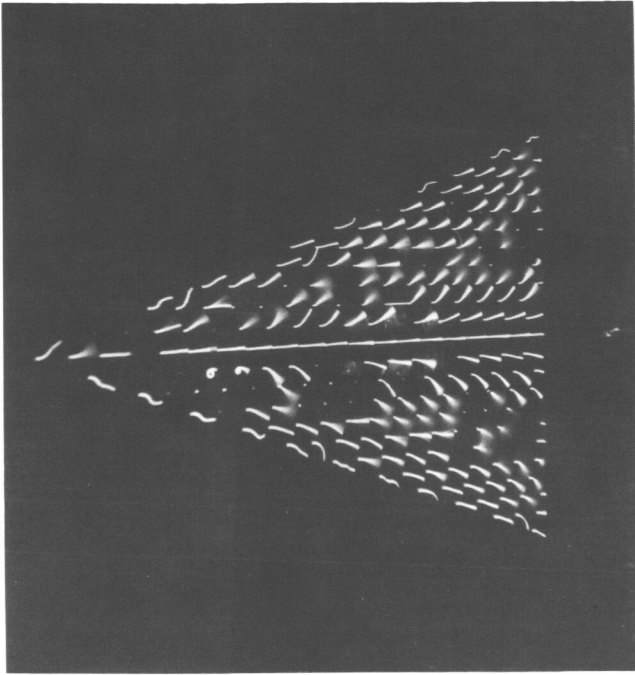


NO DATA

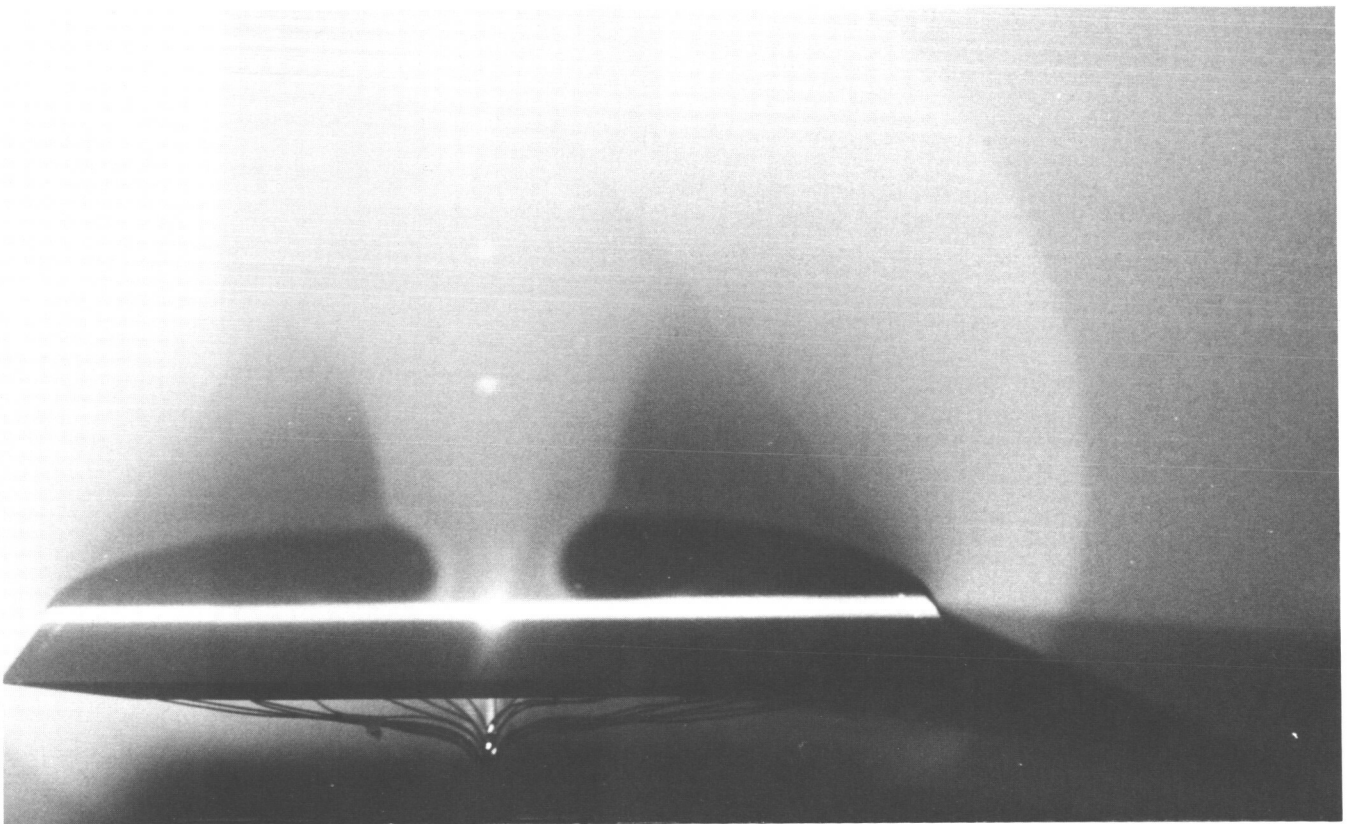


(w) $M = 2.8$, $\alpha = 16^\circ$.

Figure B2. Continued.

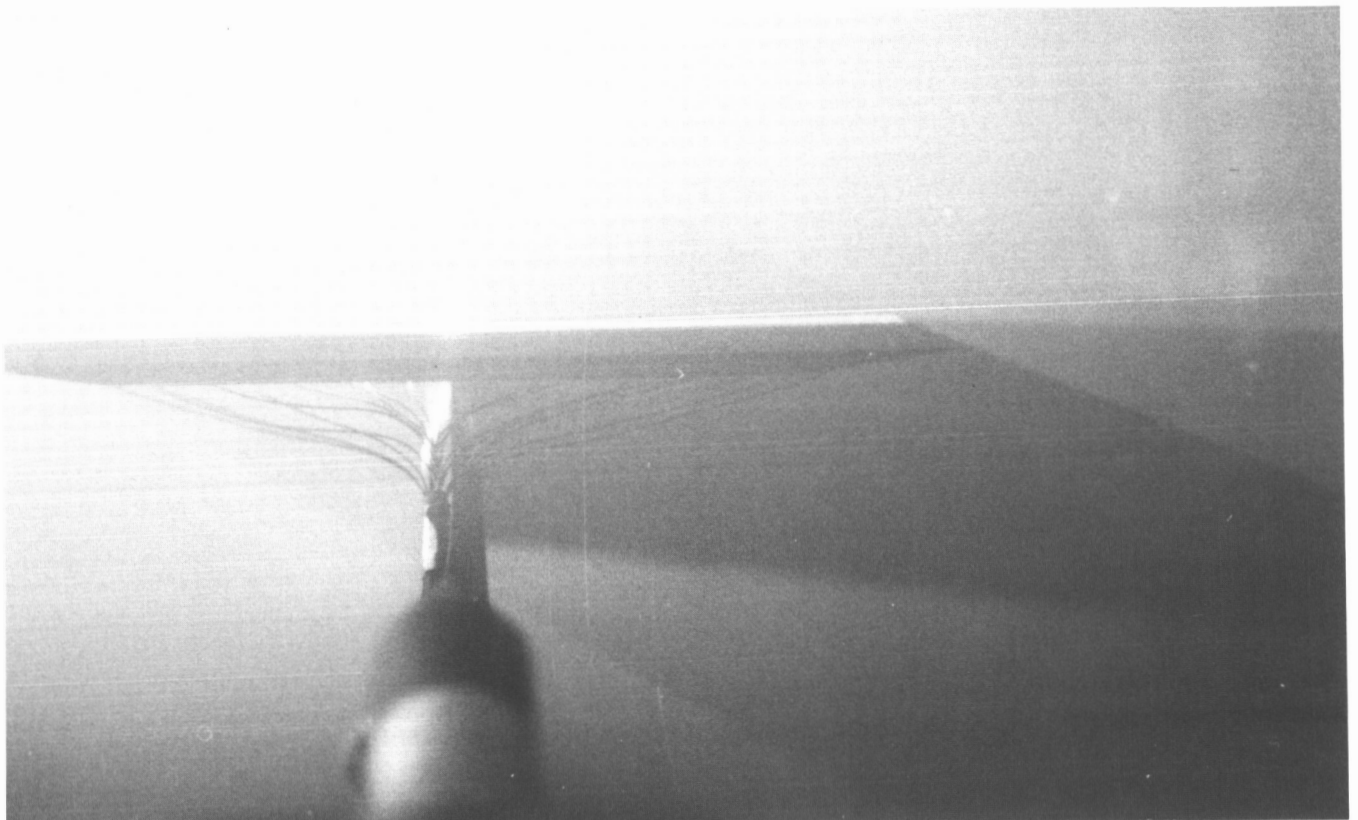
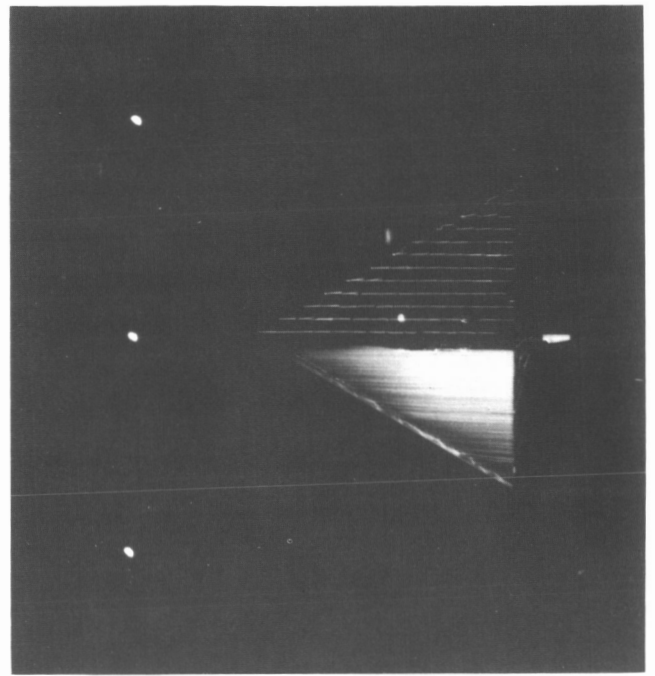
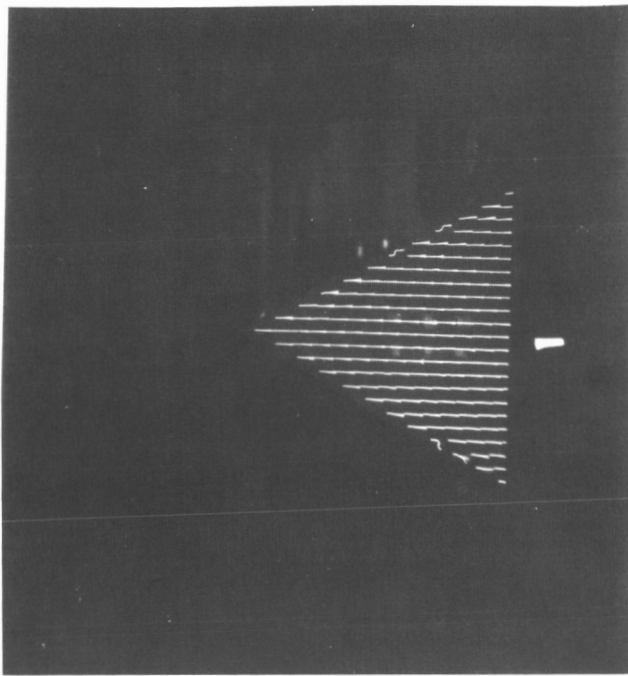


NO DATA



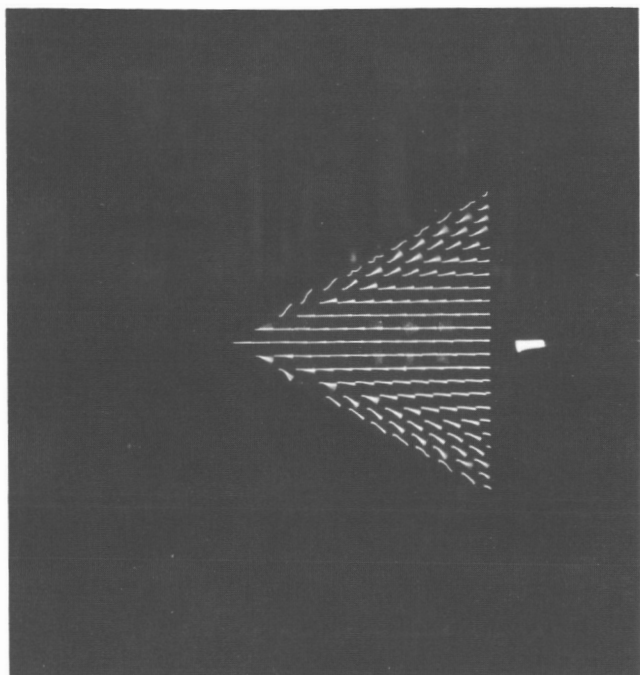
(x) $M = 2.8$, $\alpha = 20^\circ$.

Figure B2. Concluded.

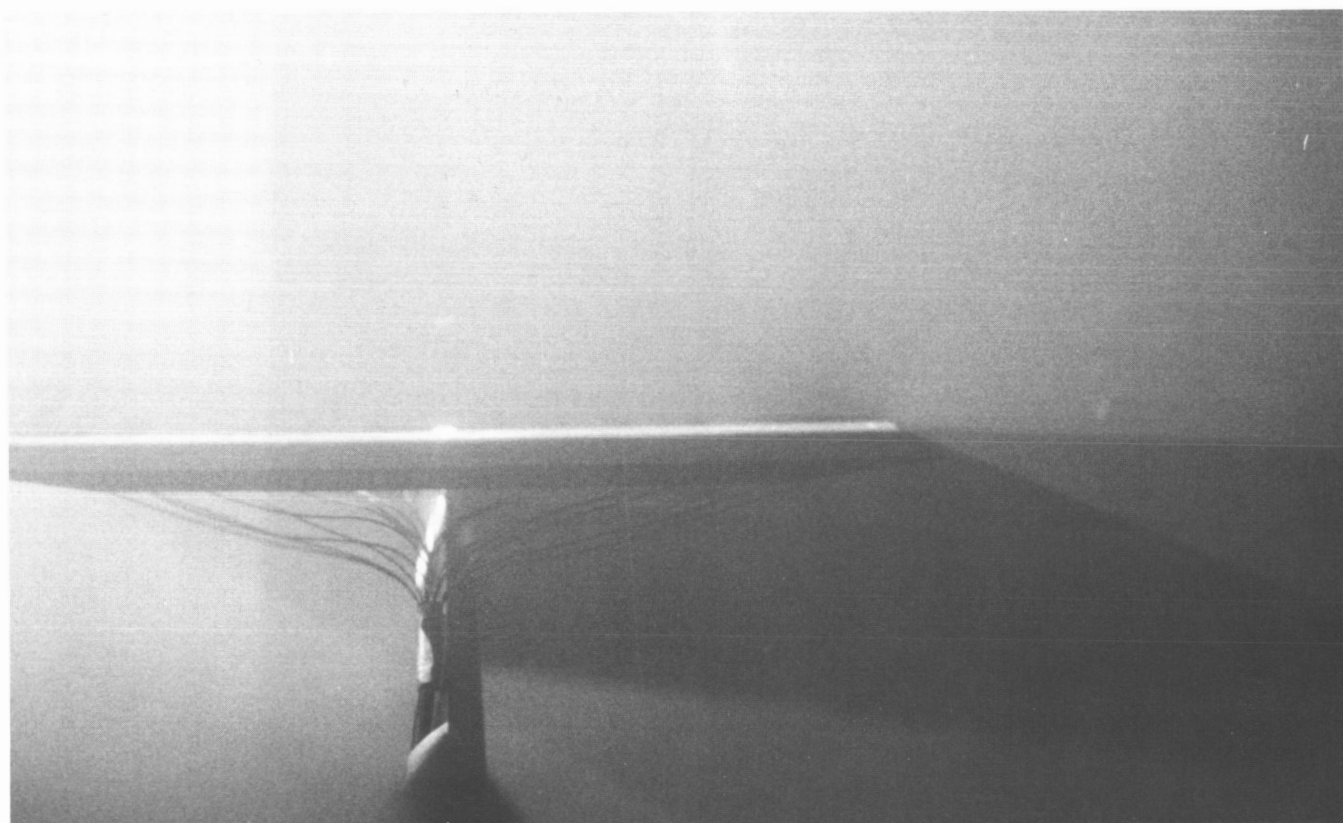


(a) $M = 1.7$, $\alpha = 0^\circ$.

Figure B3. Flow-visualization photographs for delta wing with $\Lambda_{LE} = 60^\circ$.

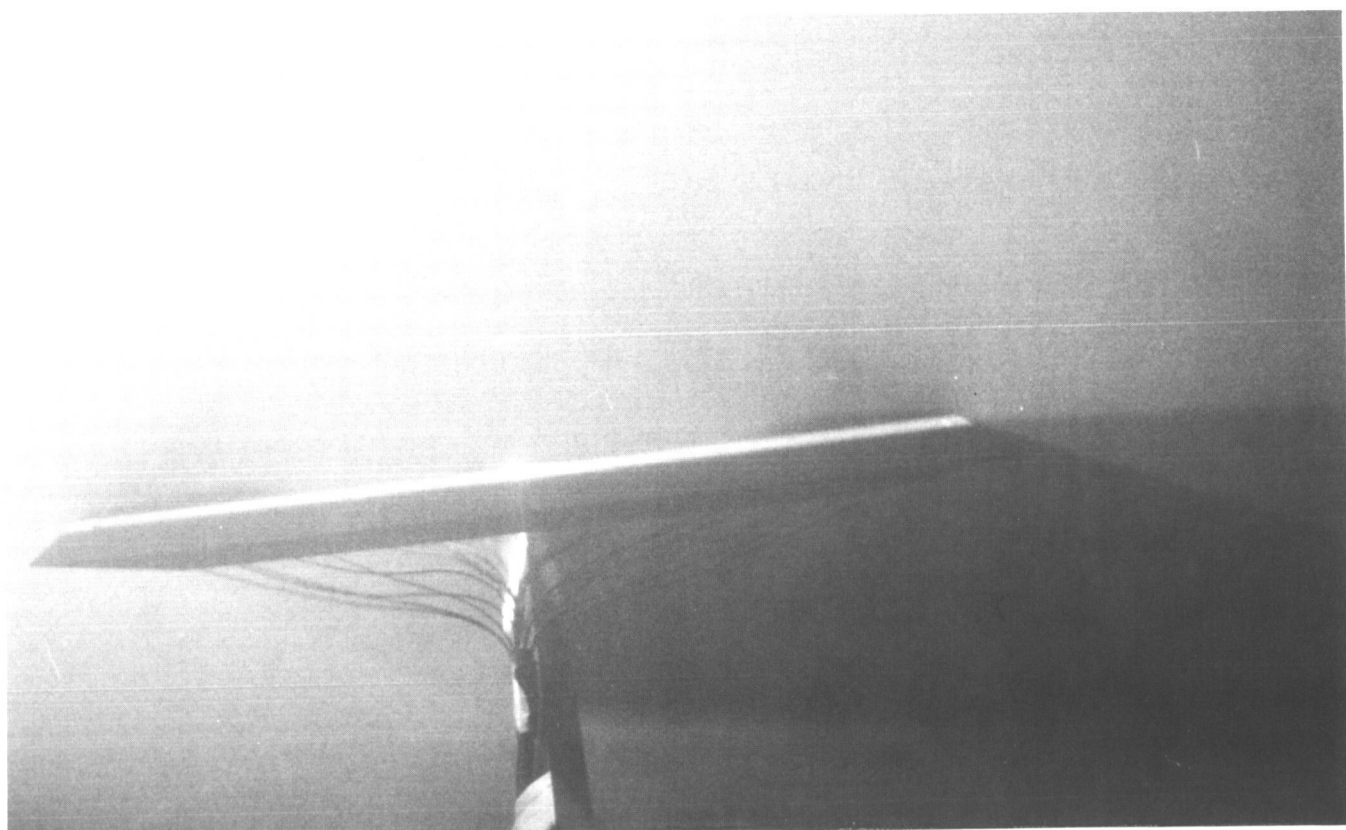
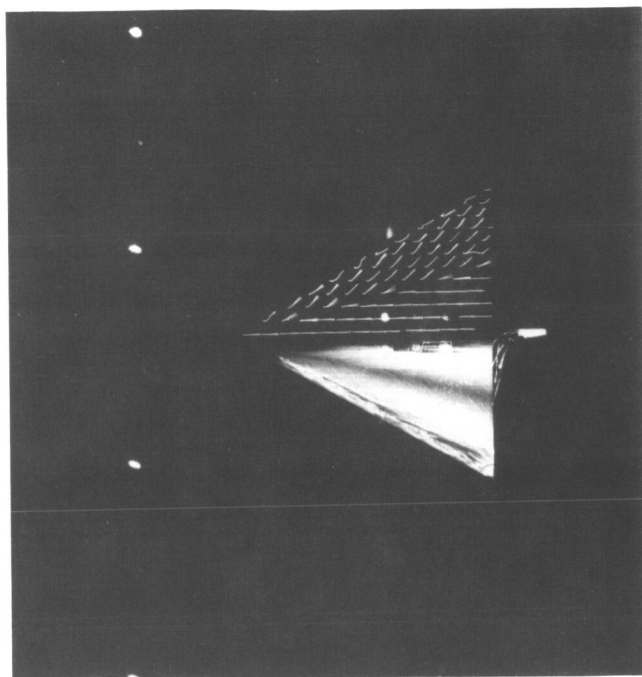
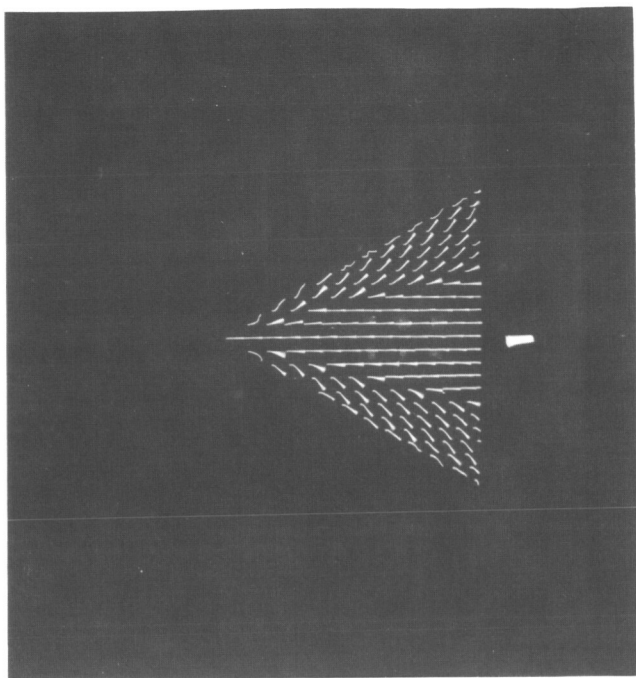


NO DATA



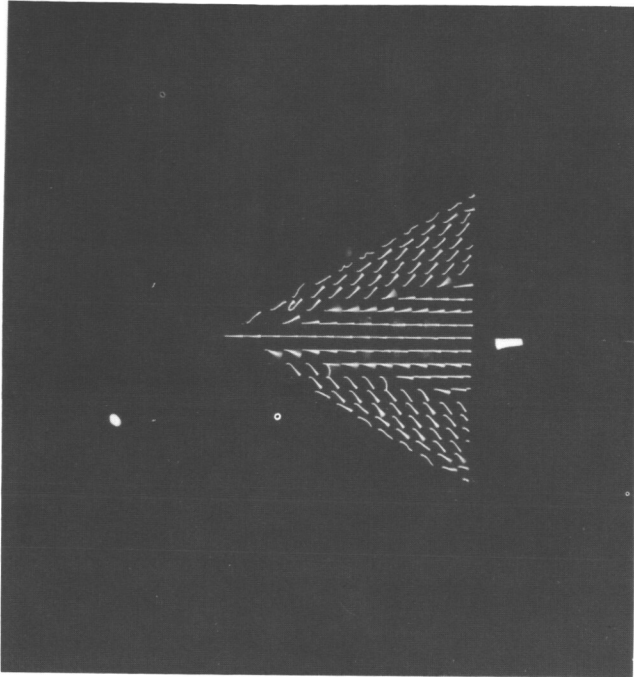
(b) $M = 1.7$, $\alpha = 4^\circ$.

Figure B3. Continued.

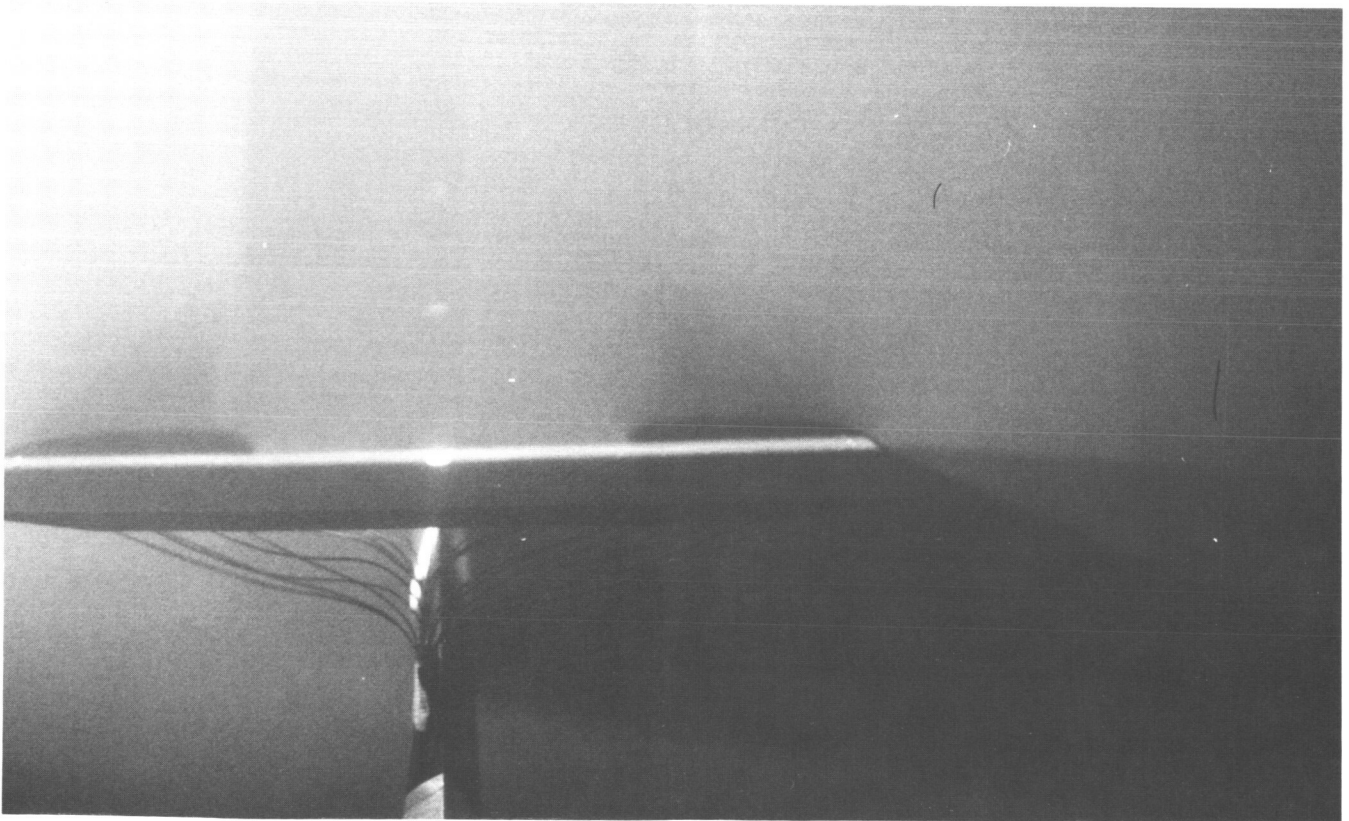


(c) $M = 1.7$, $\alpha = 8^\circ$.

Figure B3. Continued.

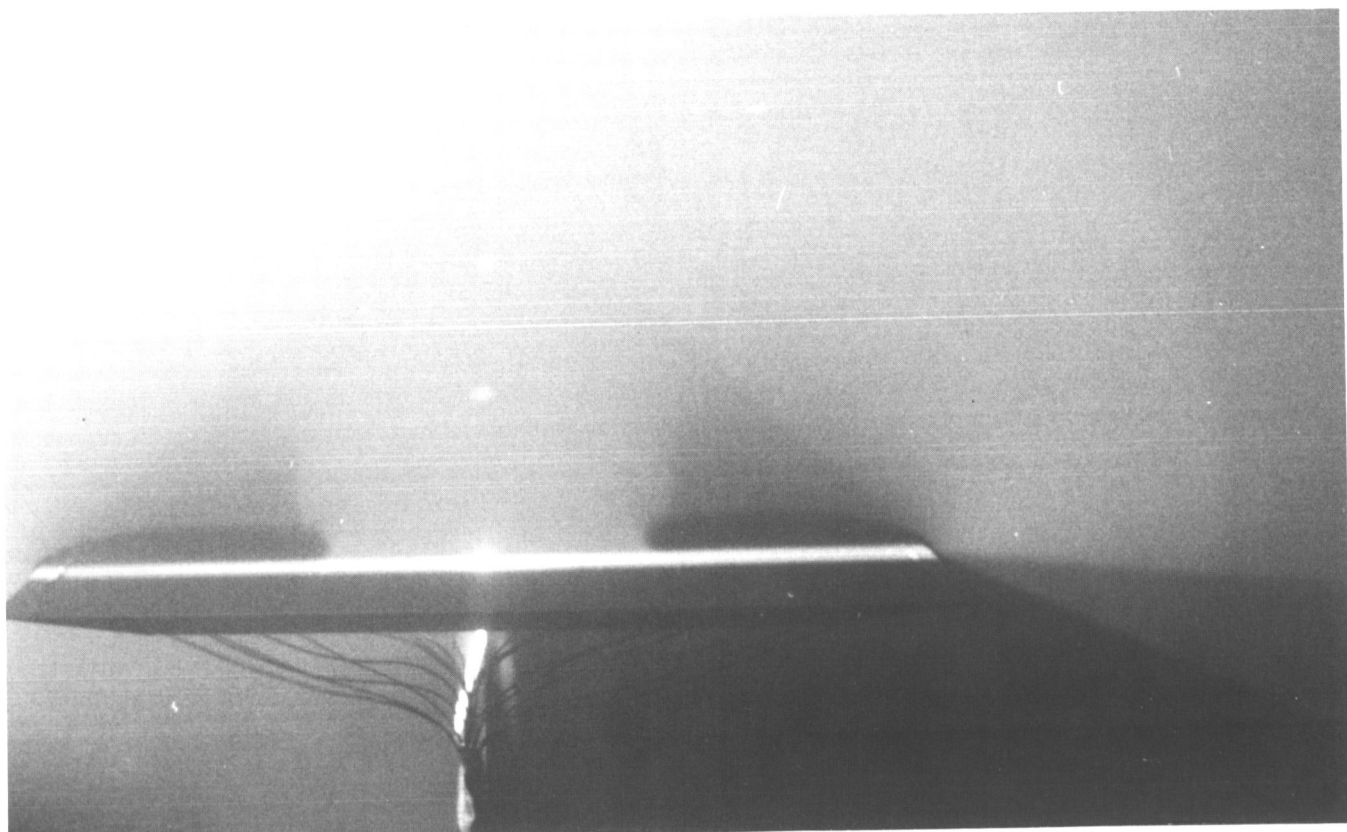
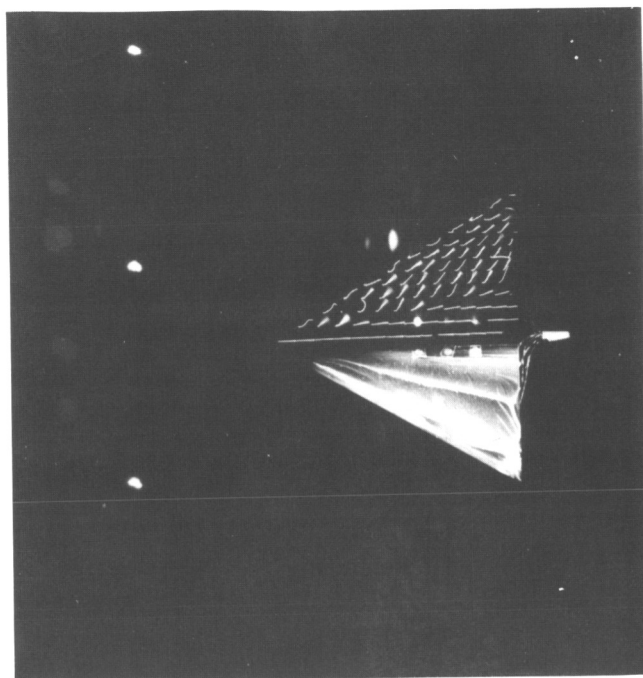
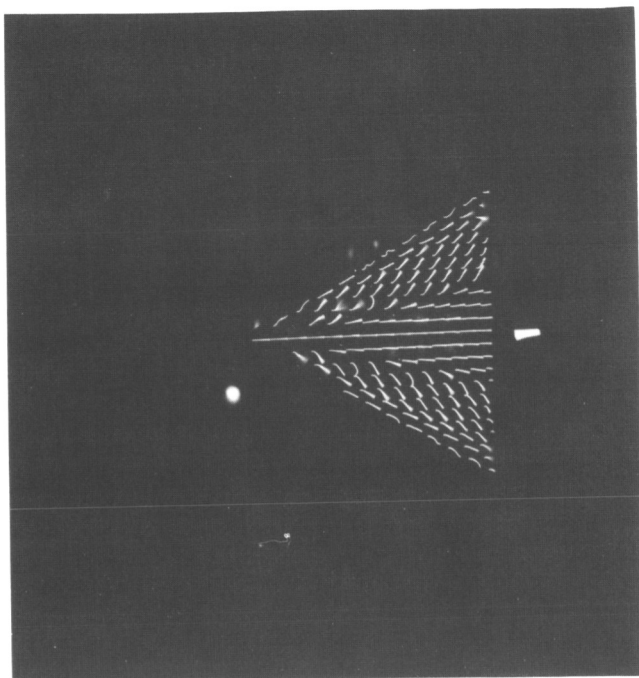


NO DATA



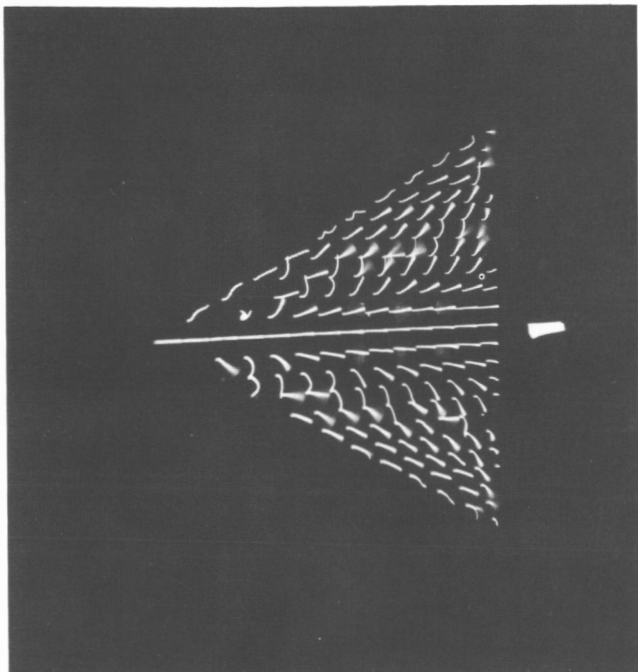
(d) $M = 1.7$, $\alpha = 12^\circ$.

Figure B3. Continued.

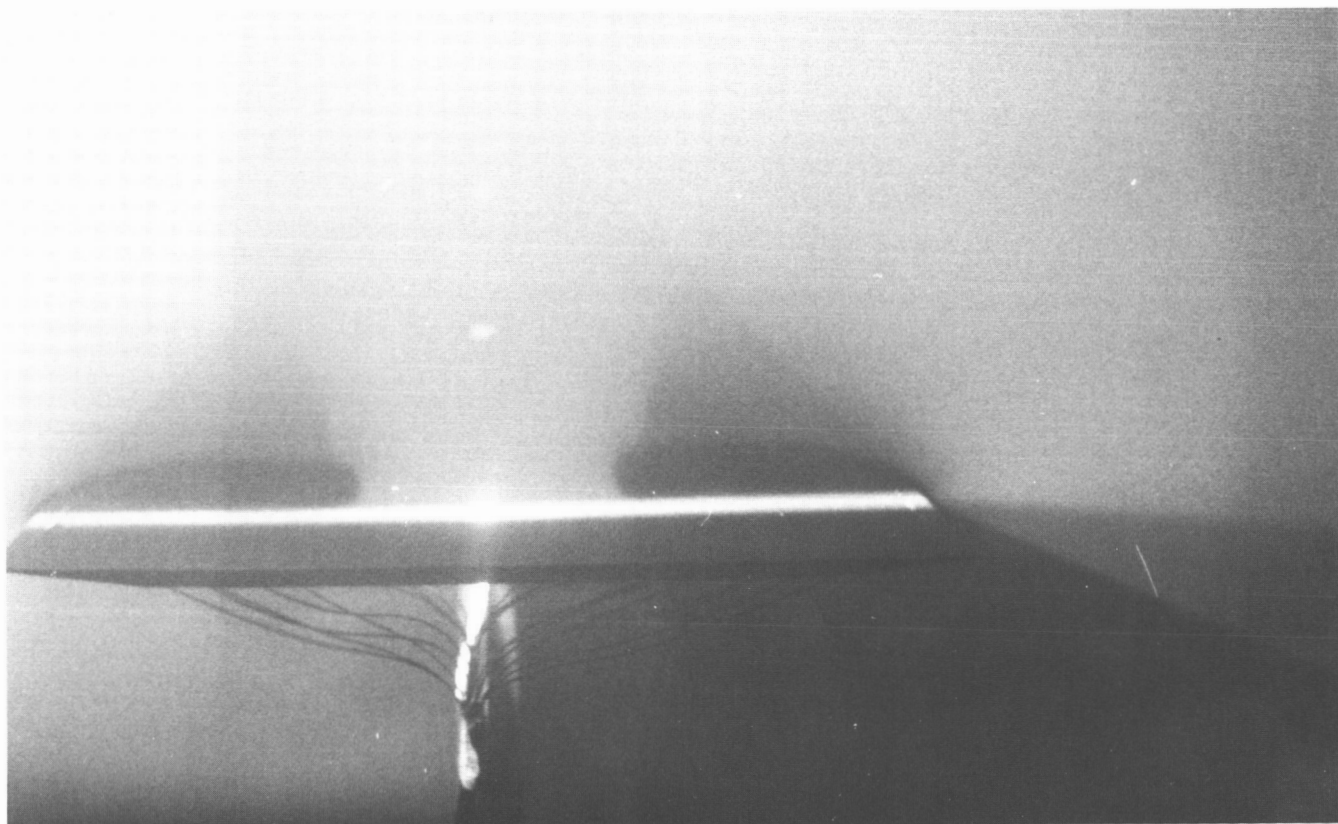


(e) $M = 1.7$, $\alpha = 16^\circ$.

Figure B3. Continued.

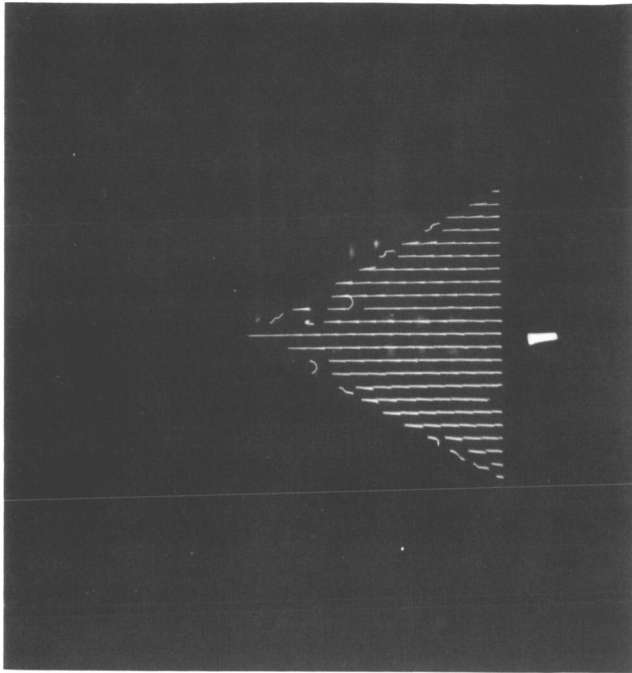


NO DATA

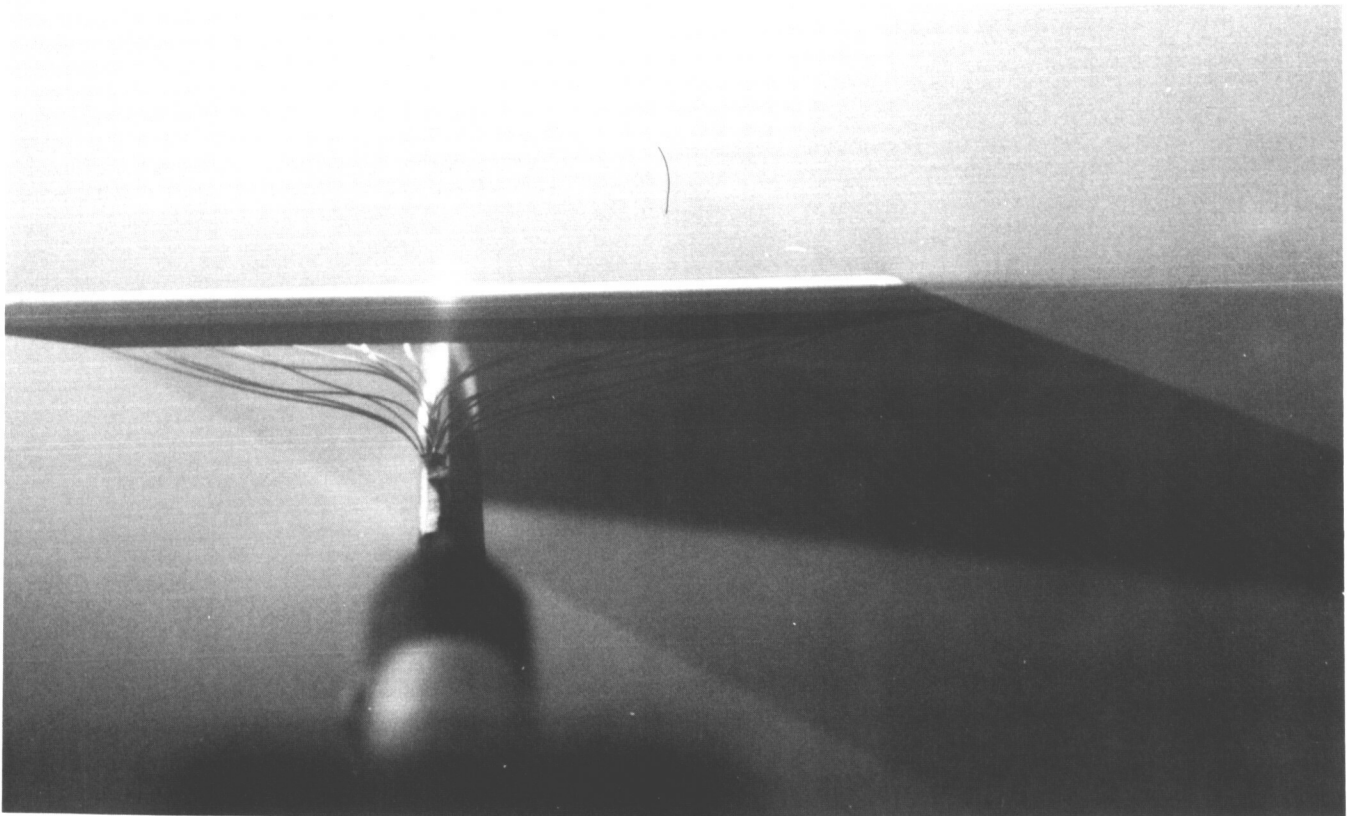


(f) $M = 1.7$, $\alpha = 20^\circ$.

Figure B3. Continued.

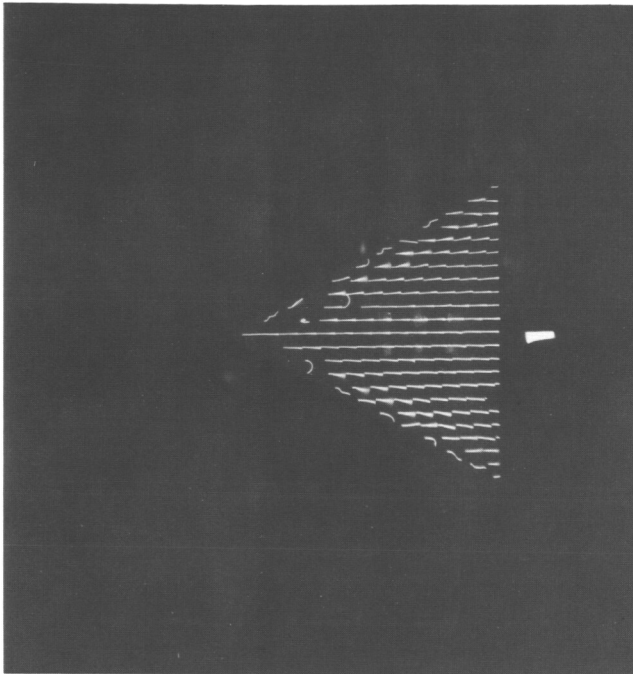


NO DATA

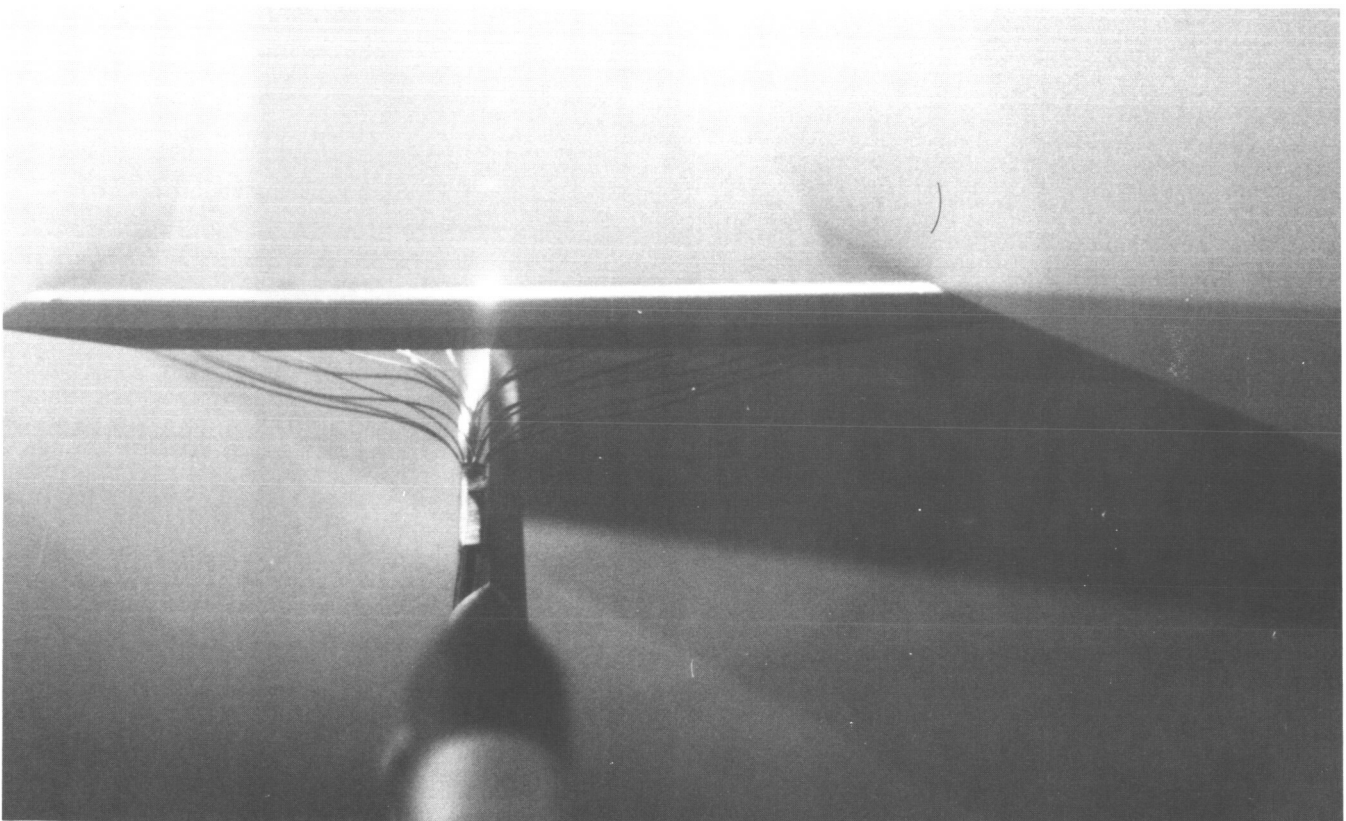


(g) $M = 2.0$, $\alpha = 0^\circ$.

Figure B3. Continued.

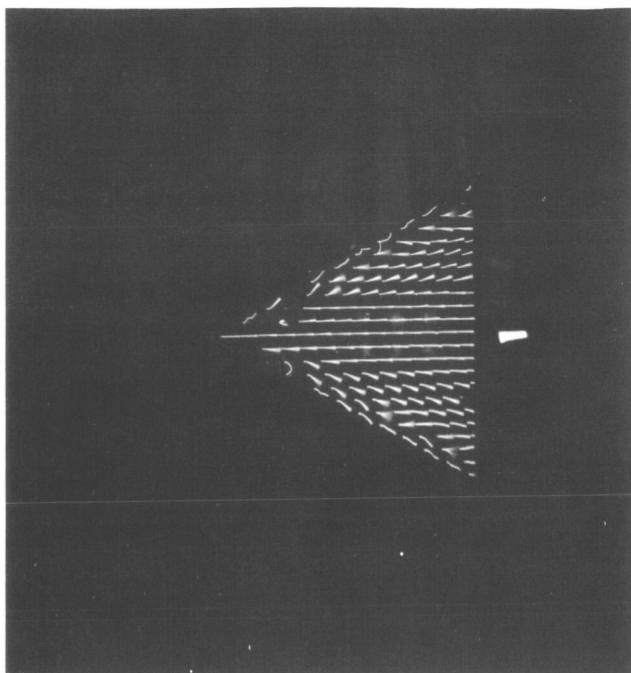


NO DATA

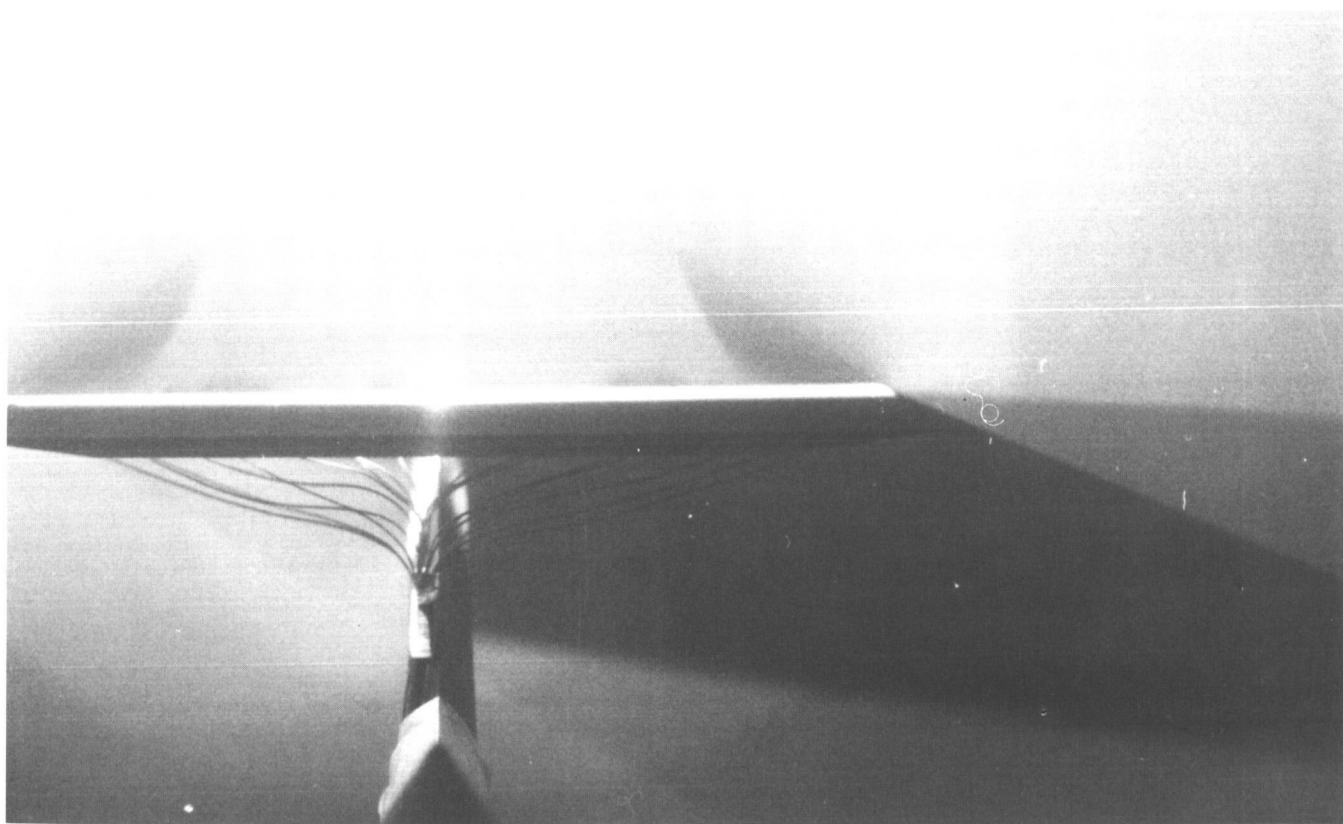


(h) $M = 2.0$, $\alpha = 4^\circ$.

Figure B3. Continued.

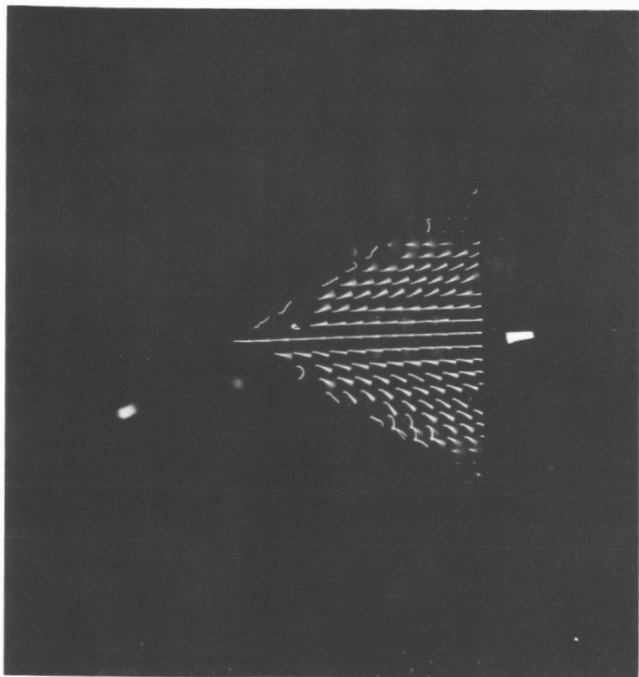


NO DATA

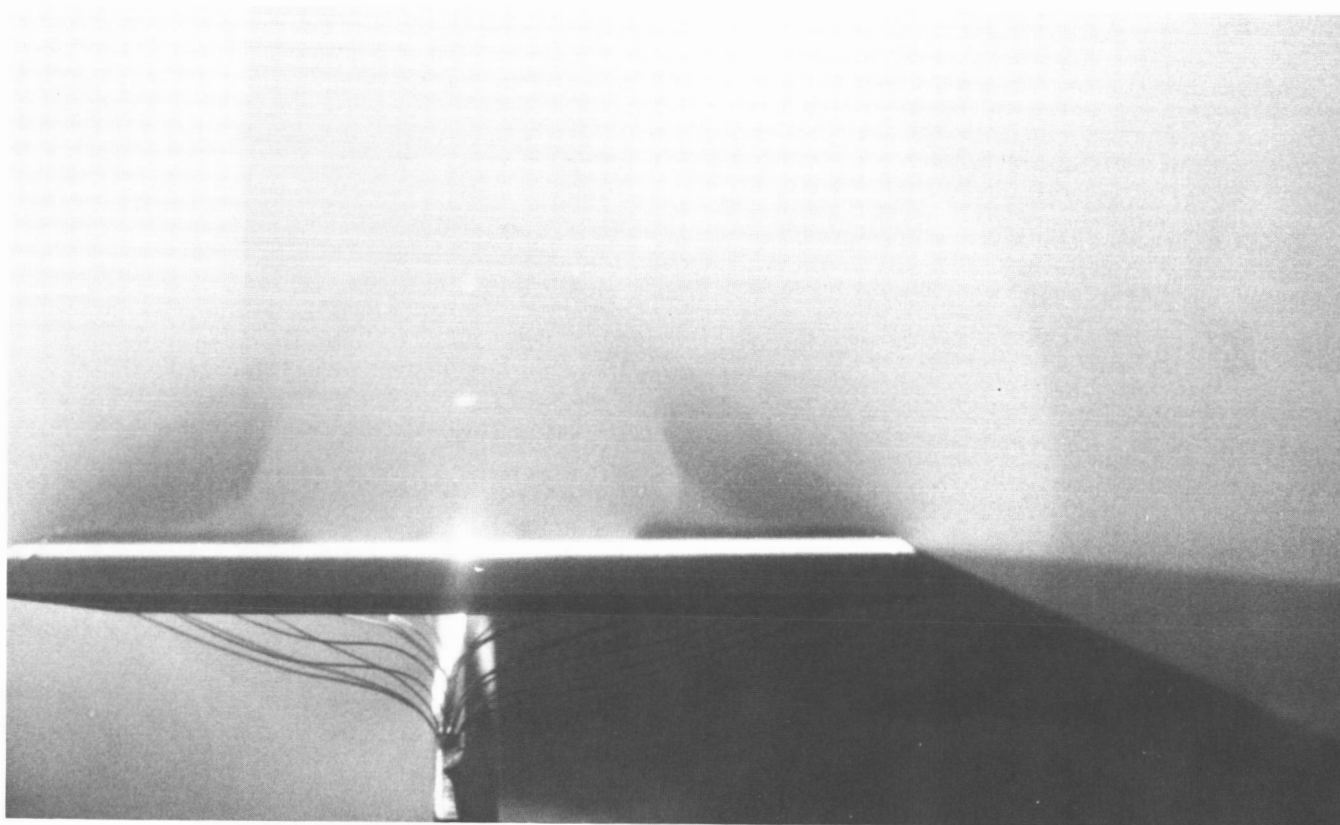


(i) $M = 2.0$, $\alpha = 8^\circ$.

Figure B3. Continued.

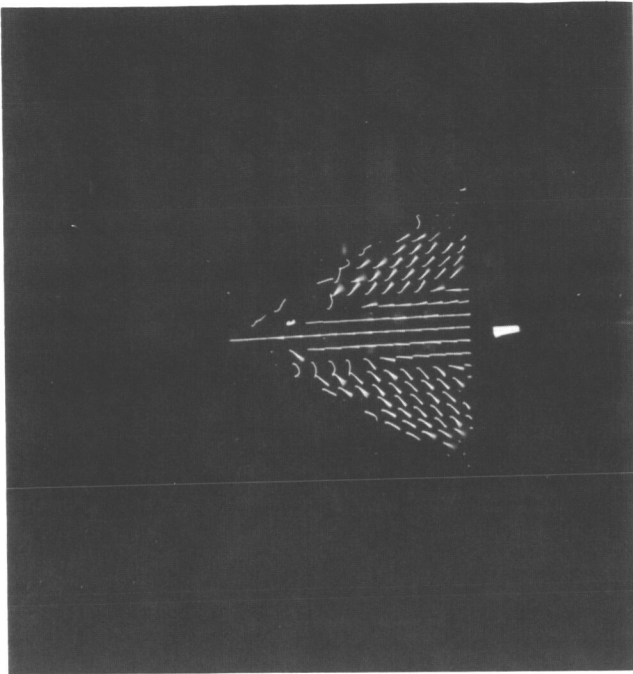


NO DATA

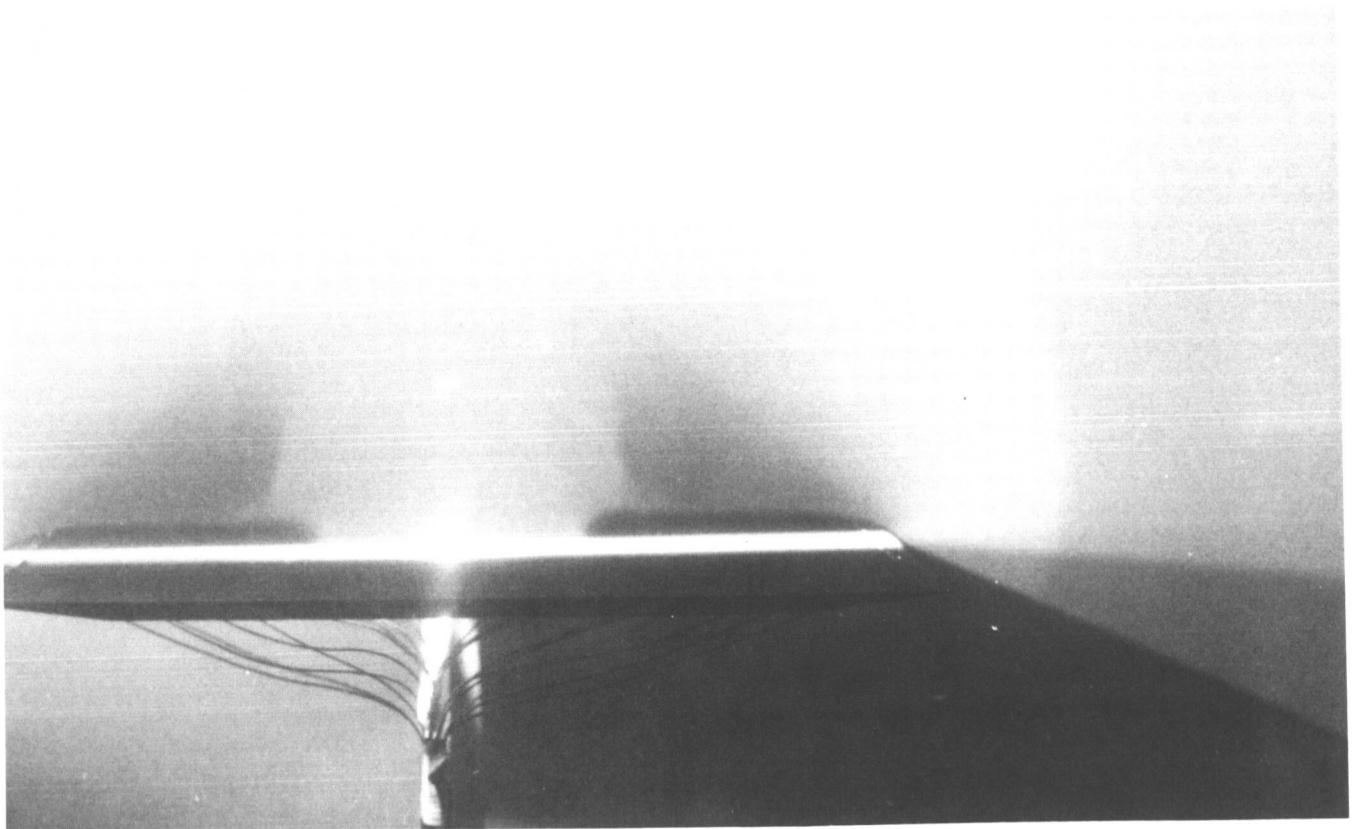


(j) $M = 2.0$, $\alpha = 12^\circ$.

Figure B3. Continued.

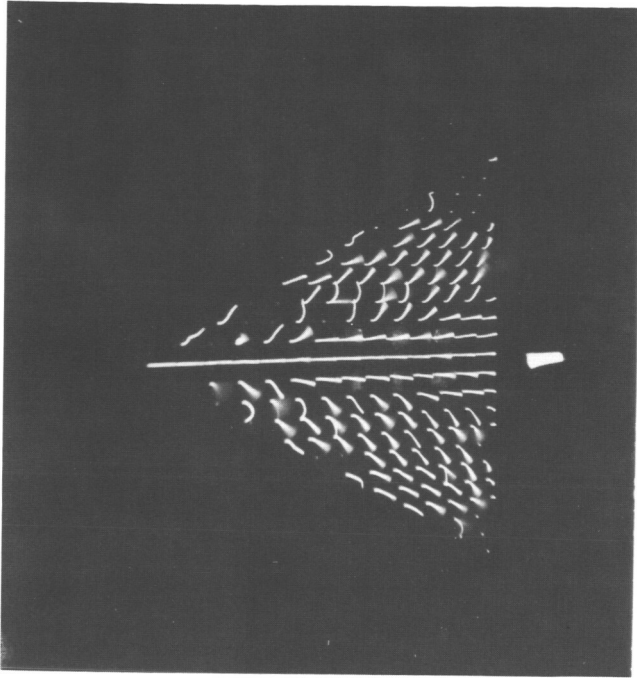


NO DATA



(k) $M = 2.0$, $\alpha = 16^\circ$.

Figure B3. Continued.

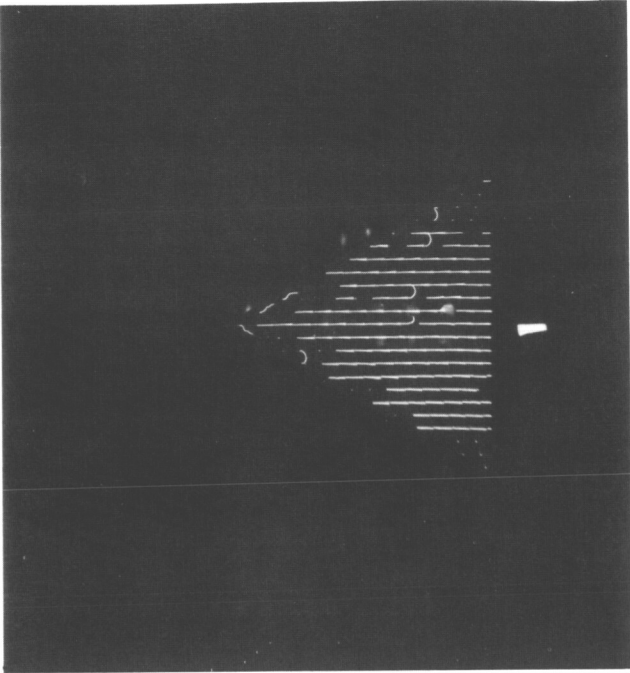


NO DATA

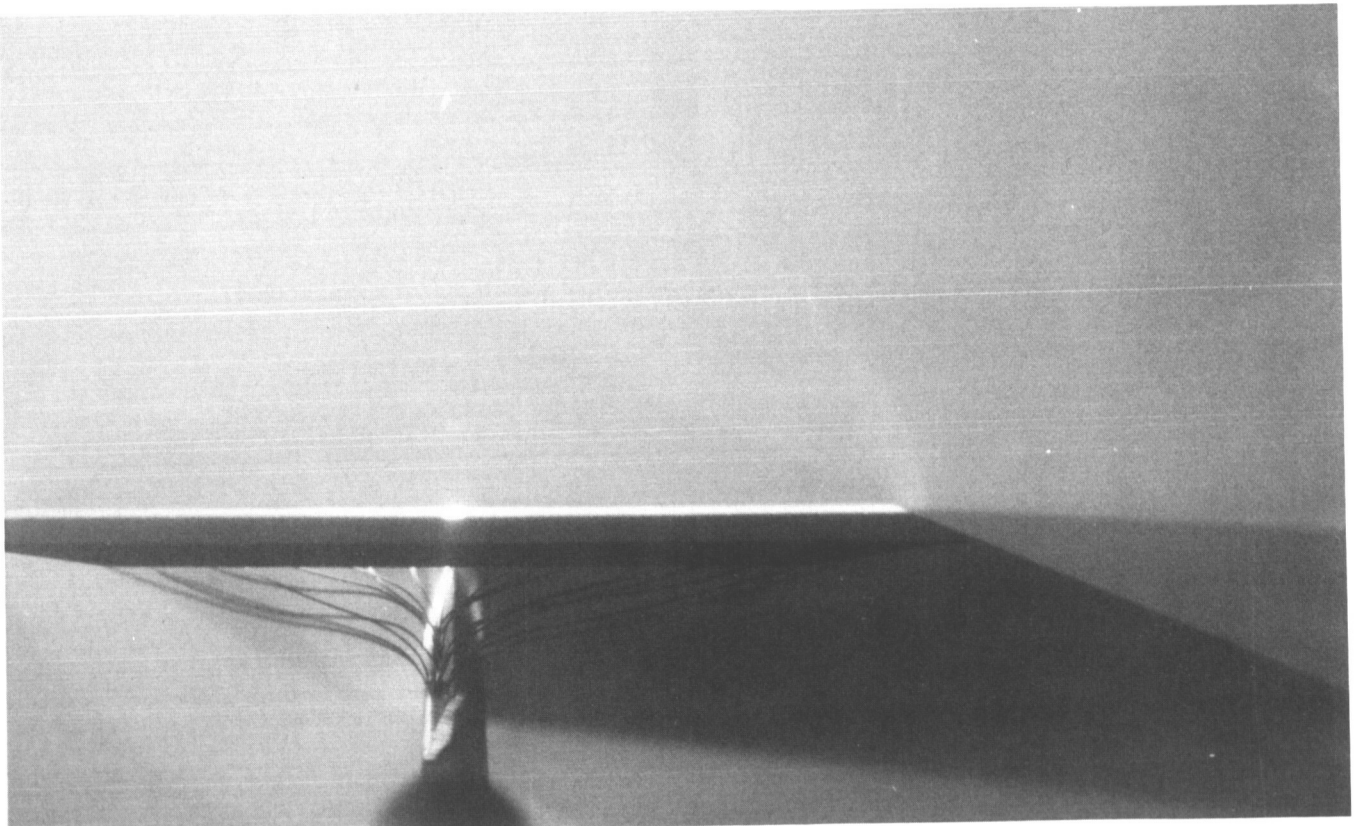


(1) $M = 2.0$, $\alpha = 20^\circ$.

Figure B3. Continued.

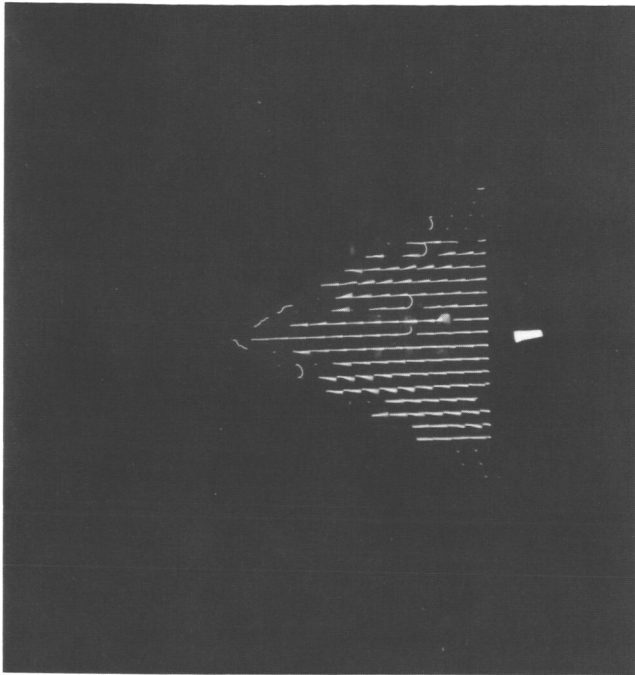


NO DATA

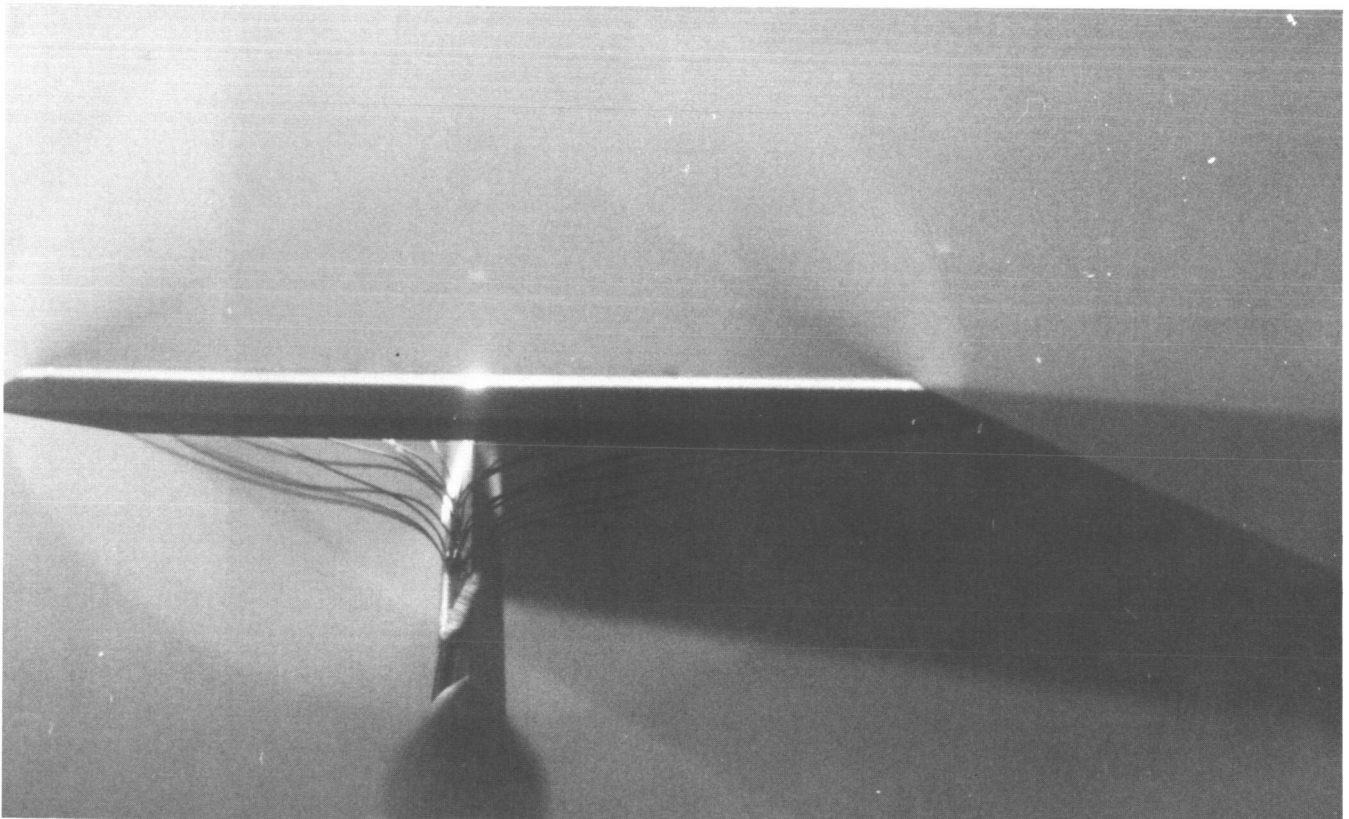


(m) $M = 2.4$, $\alpha = 0^\circ$.

Figure B3. Continued.

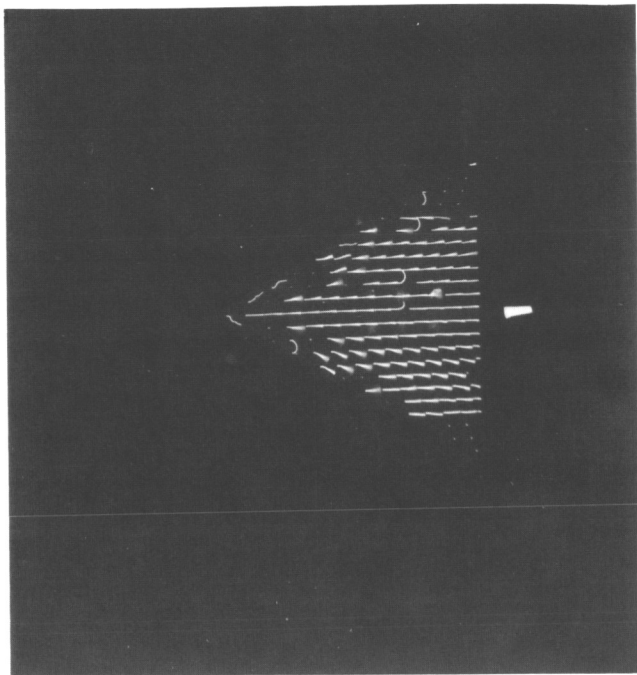


NO DATA

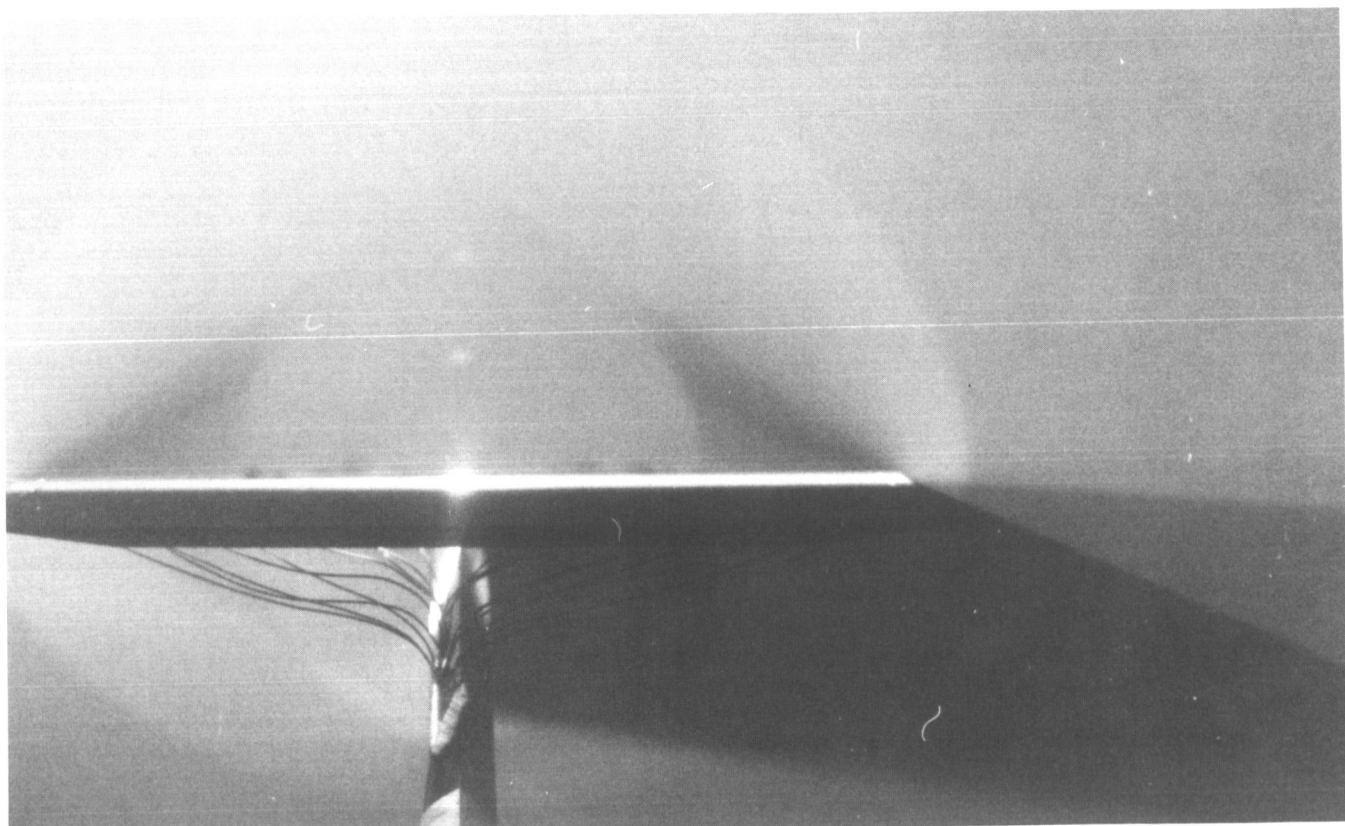


(n) $M = 2.4$, $\alpha = 4^\circ$.

Figure B3. Continued.

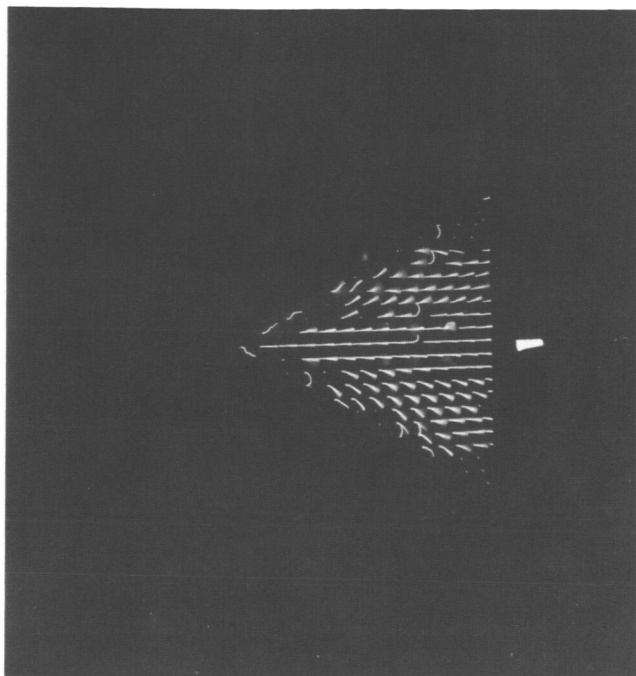


NO DATA

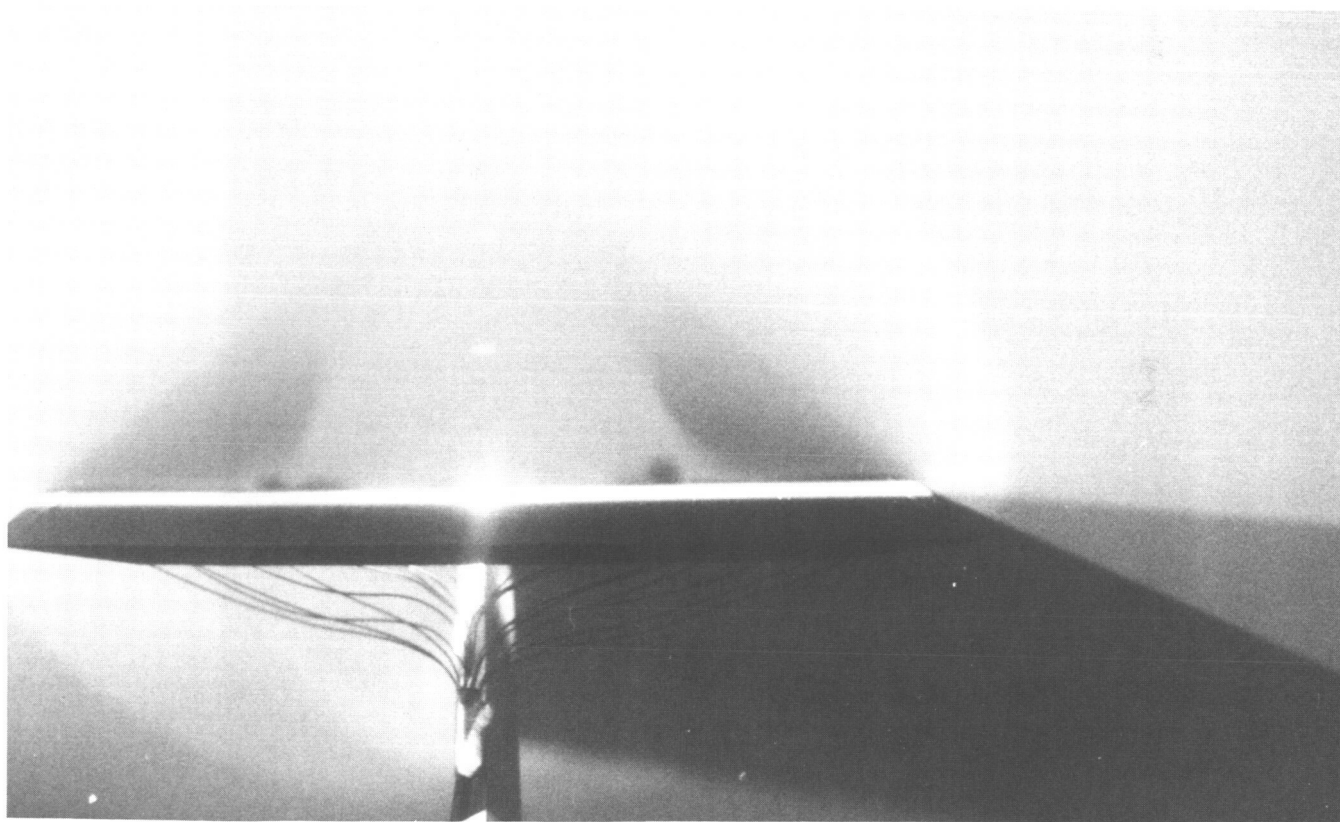


(o) $M = 2.4$, $\alpha = 8^\circ$.

Figure B3. Continued.

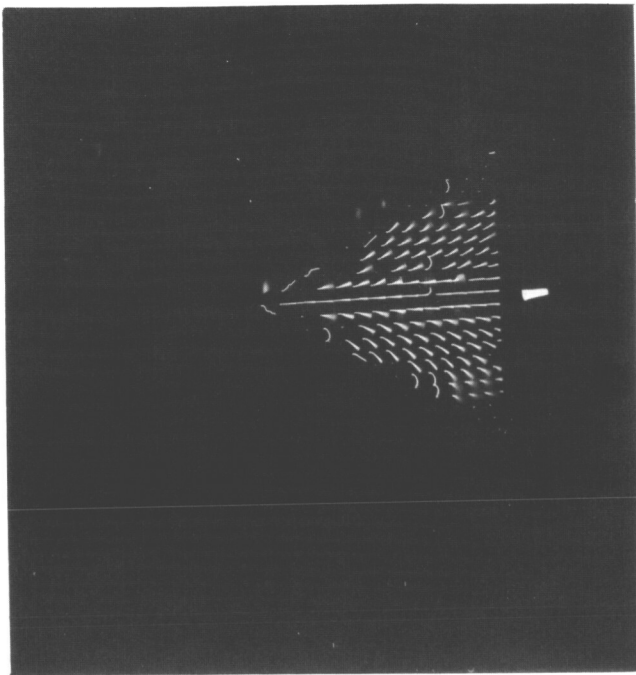


NO DATA

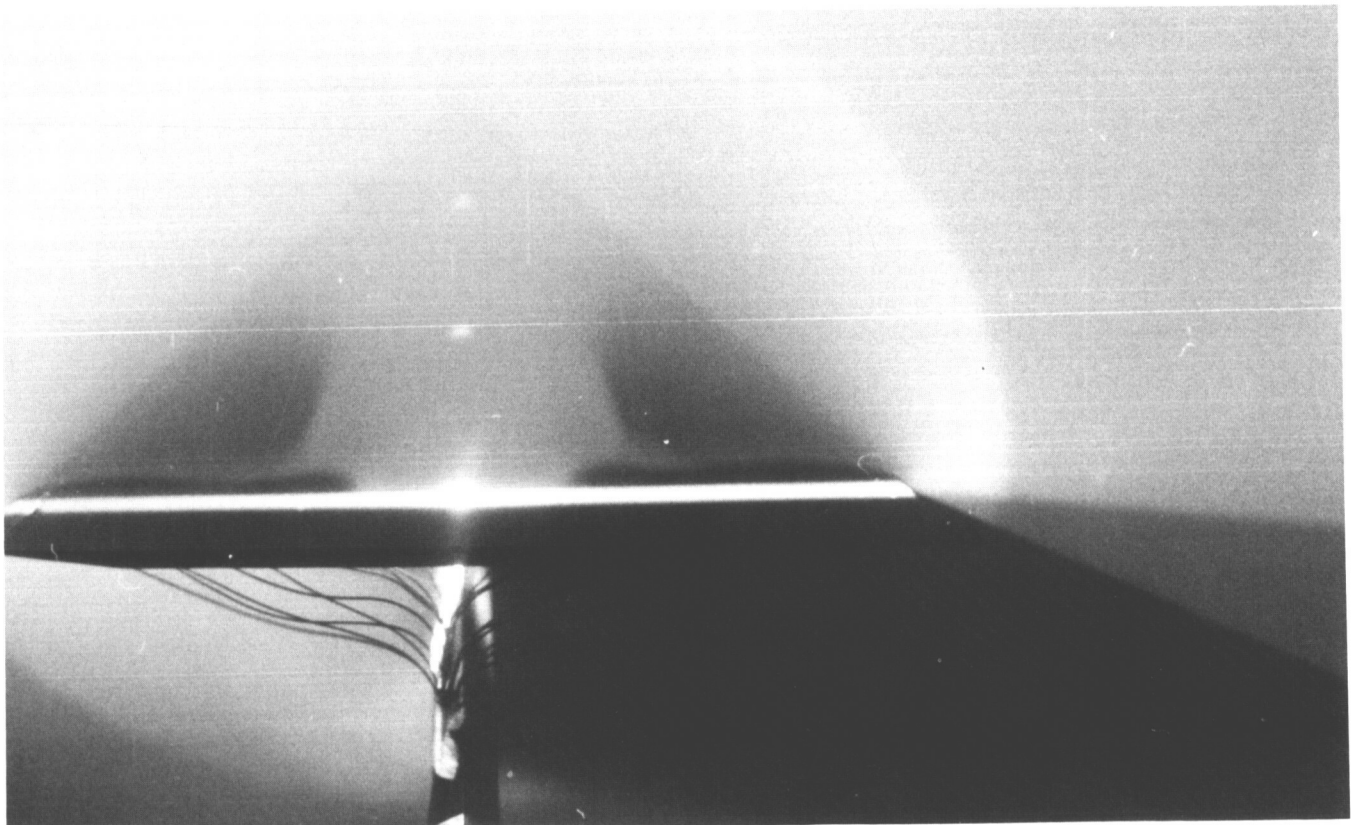


(p) $M = 2.4$, $\alpha = 12^\circ$.

Figure B3. Continued.

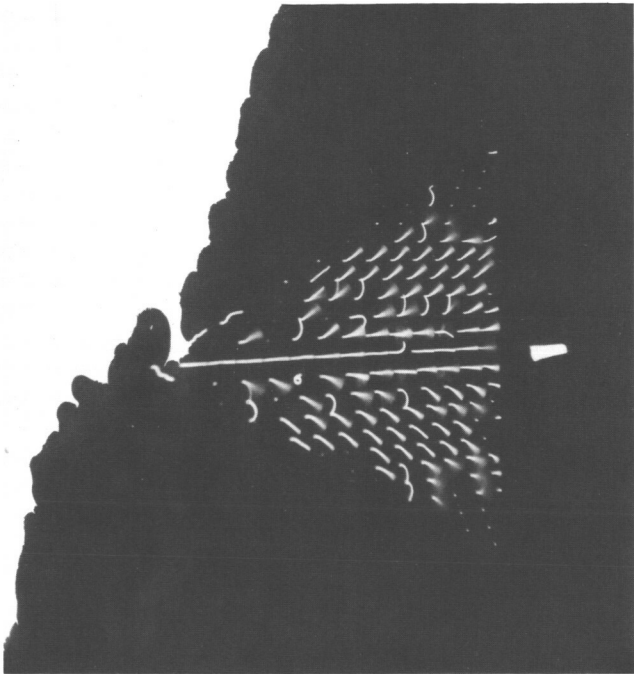


NO DATA

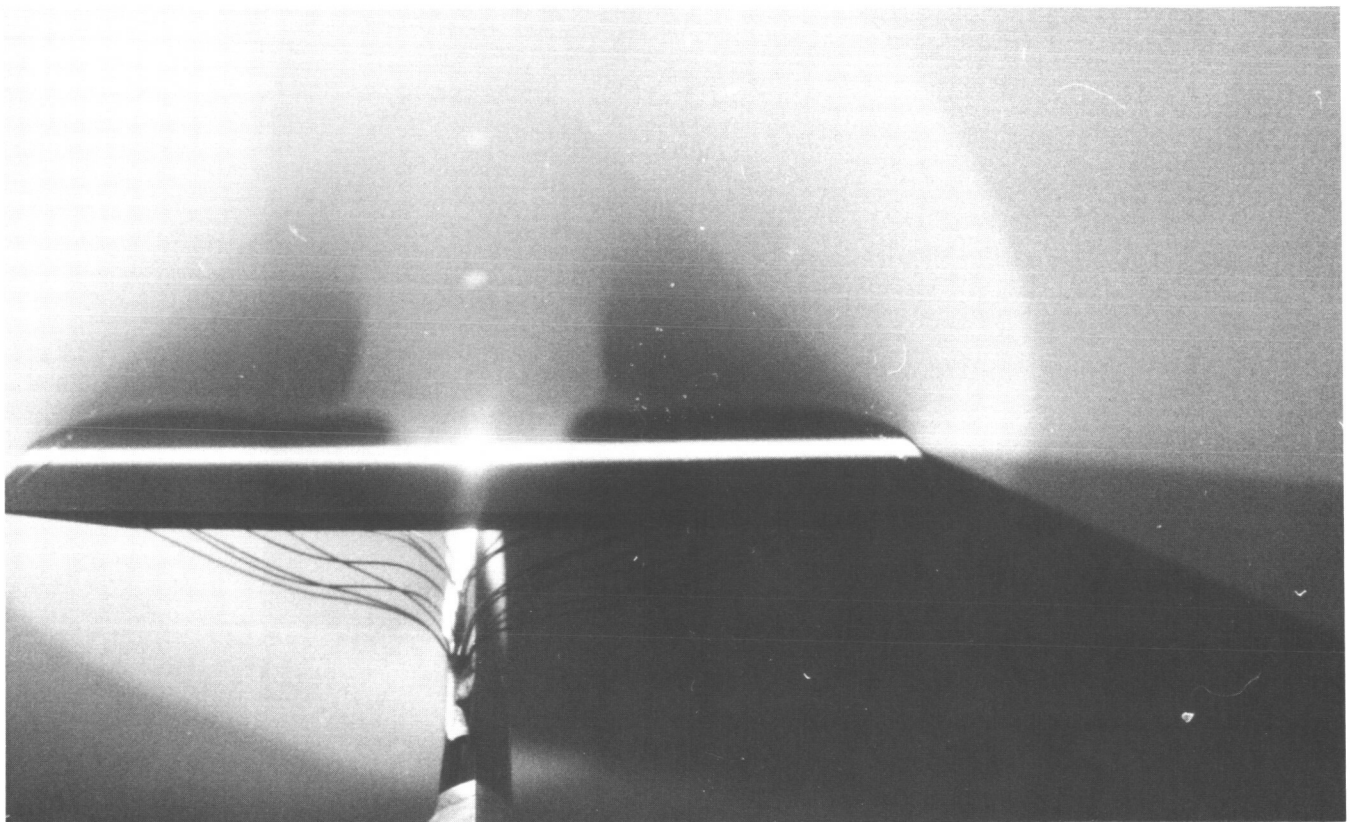


(q) $M = 2.4$, $\alpha = 16^\circ$.

Figure B3. Continued.

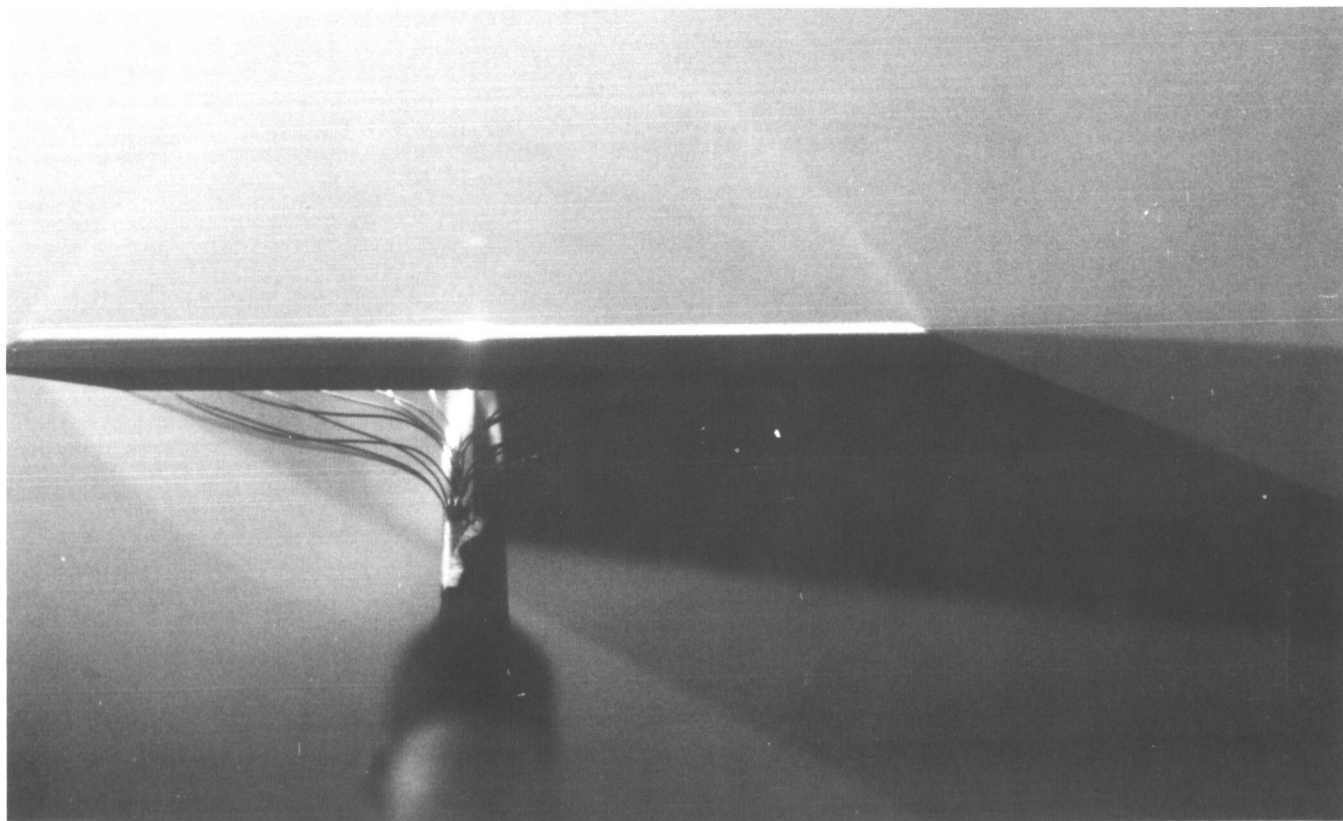
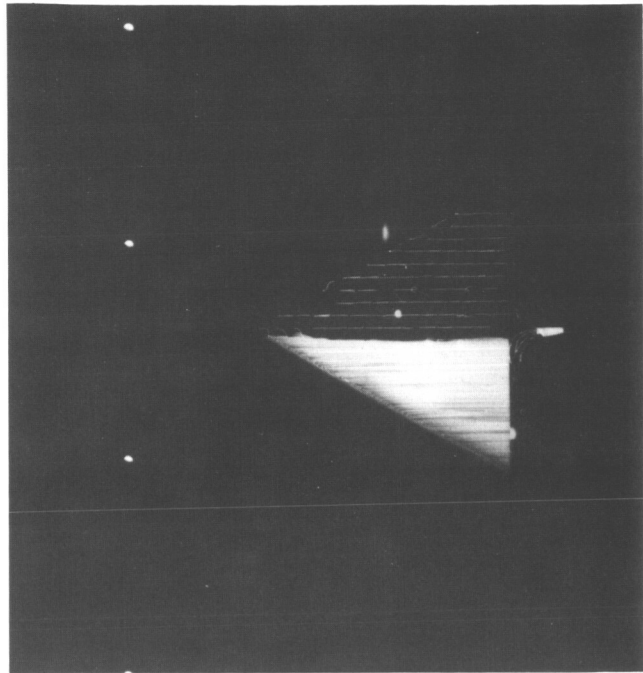
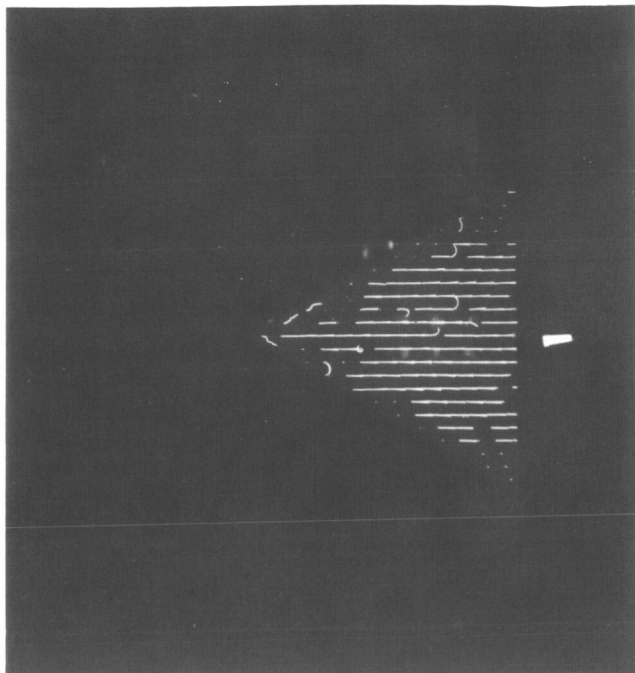


NO DATA



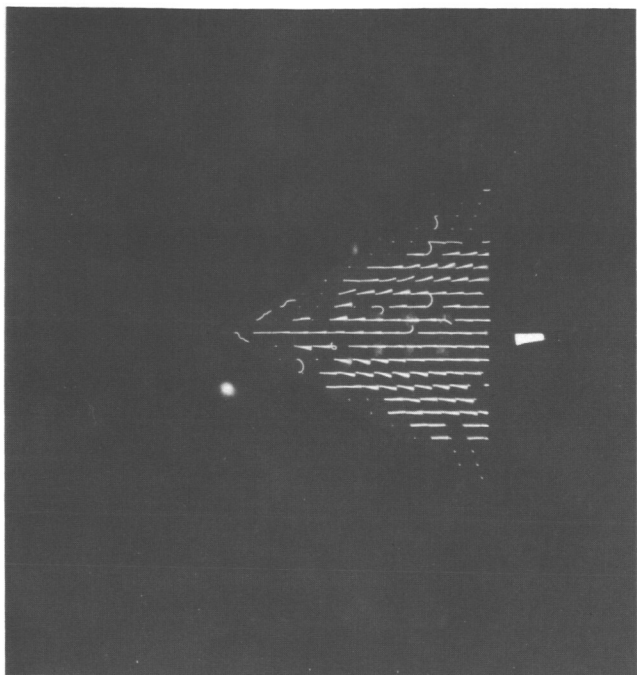
(r) $M = 2.4$, $\alpha = 20^\circ$.

Figure B3. Continued.

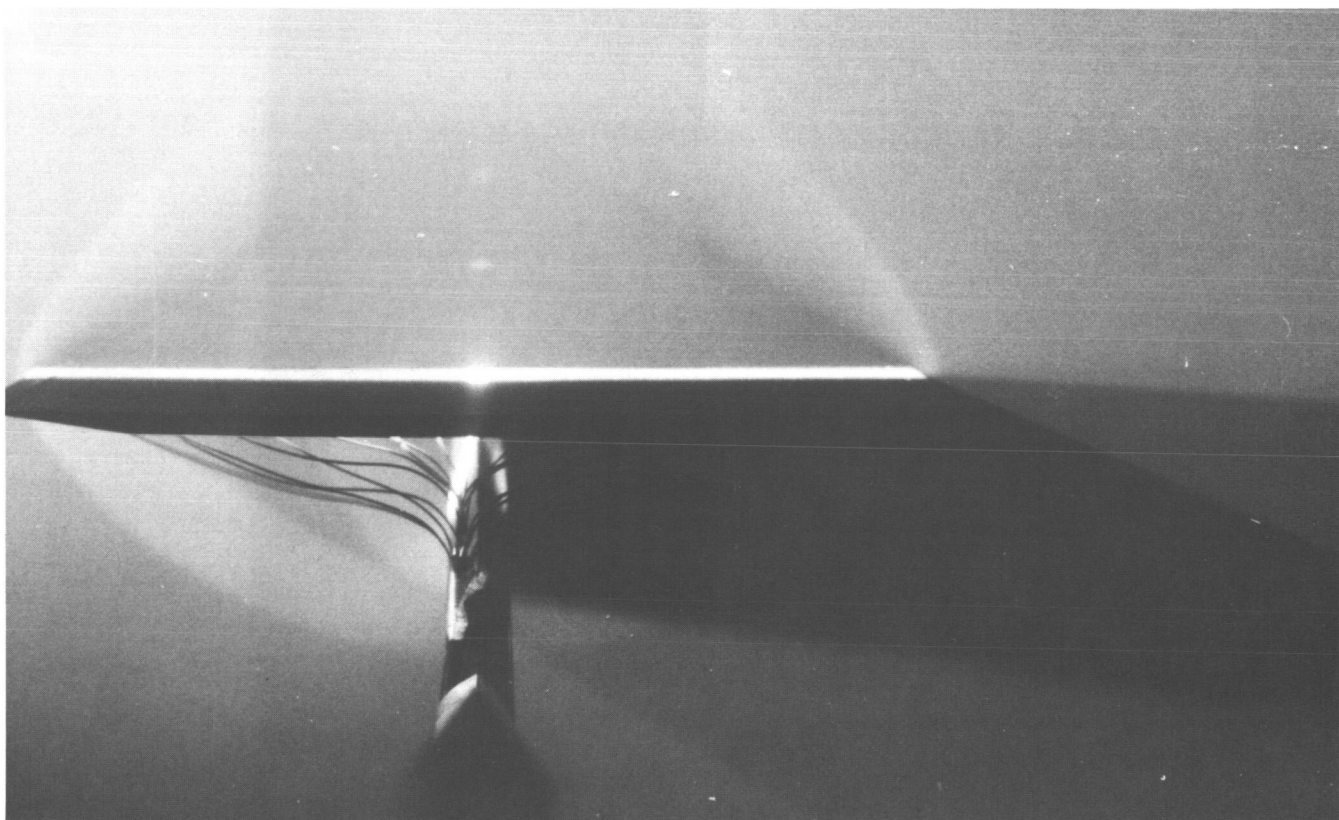


(s) $M = 2.8$, $\alpha = 0^\circ$.

Figure B3. Continued.

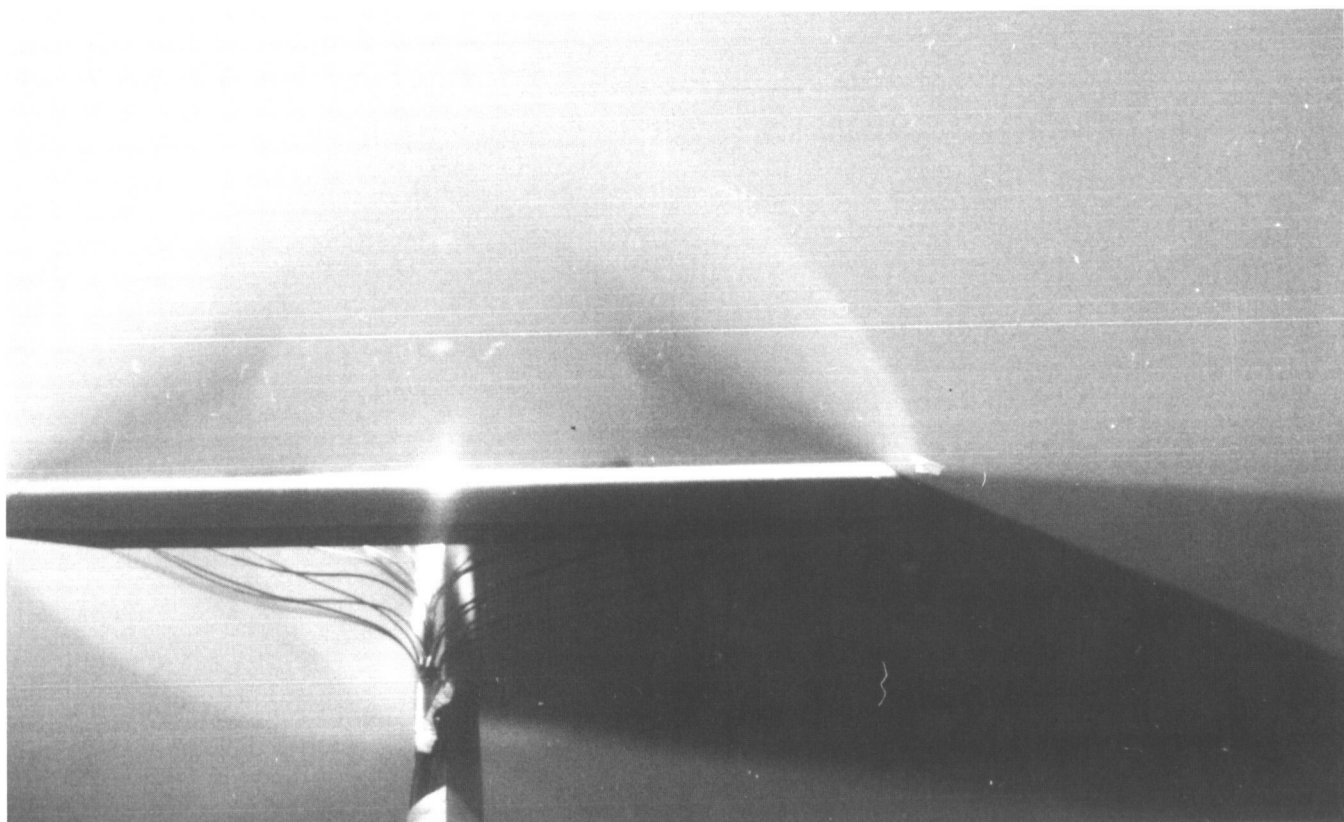
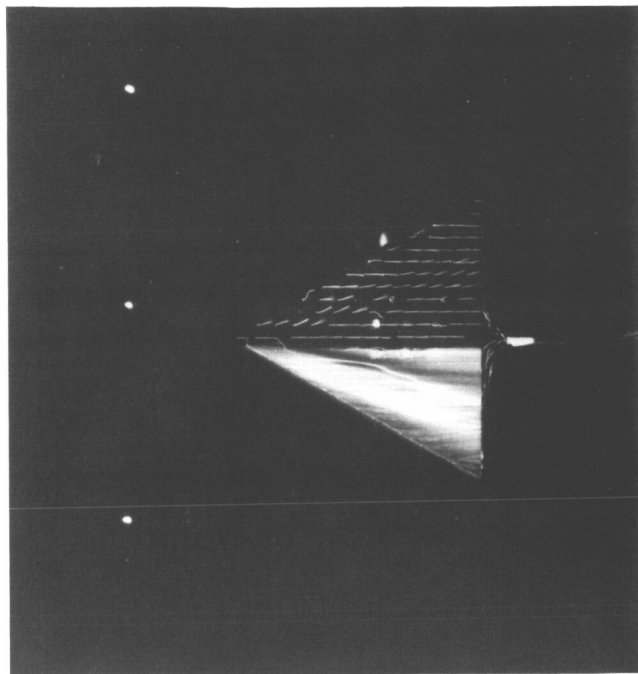
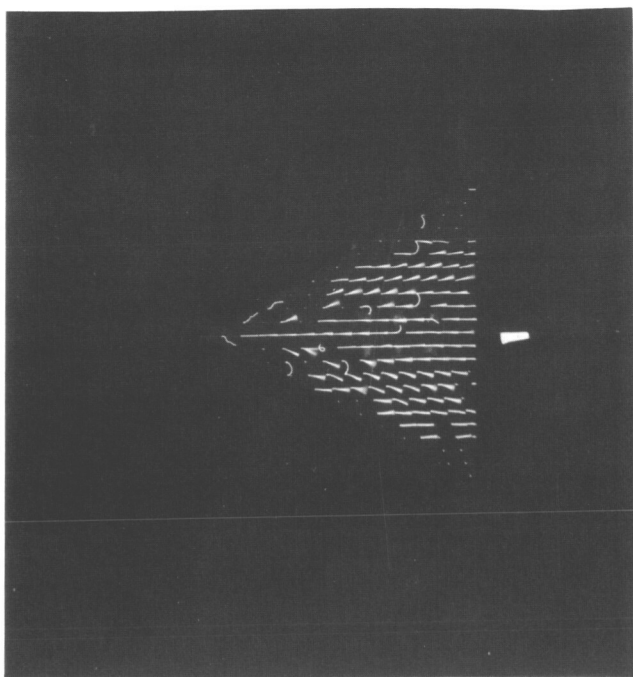


NO DATA



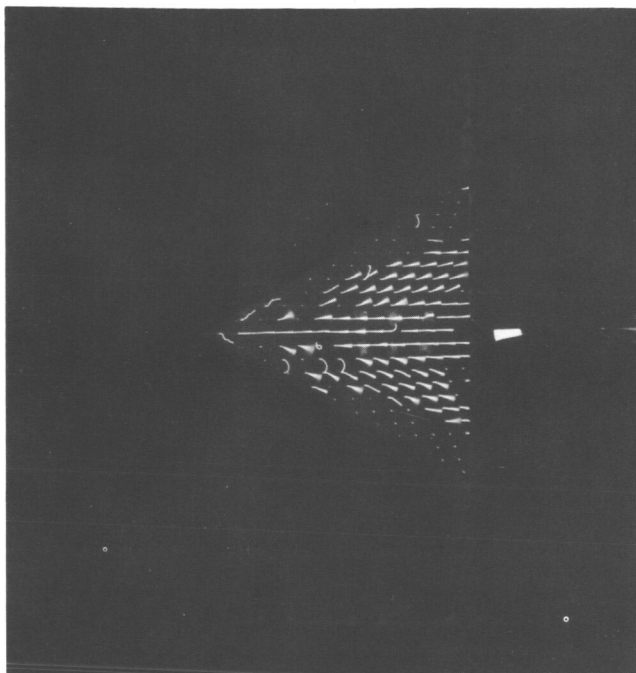
(t) $M = 2.8$, $\alpha = 4^\circ$.

Figure B3. Continued.

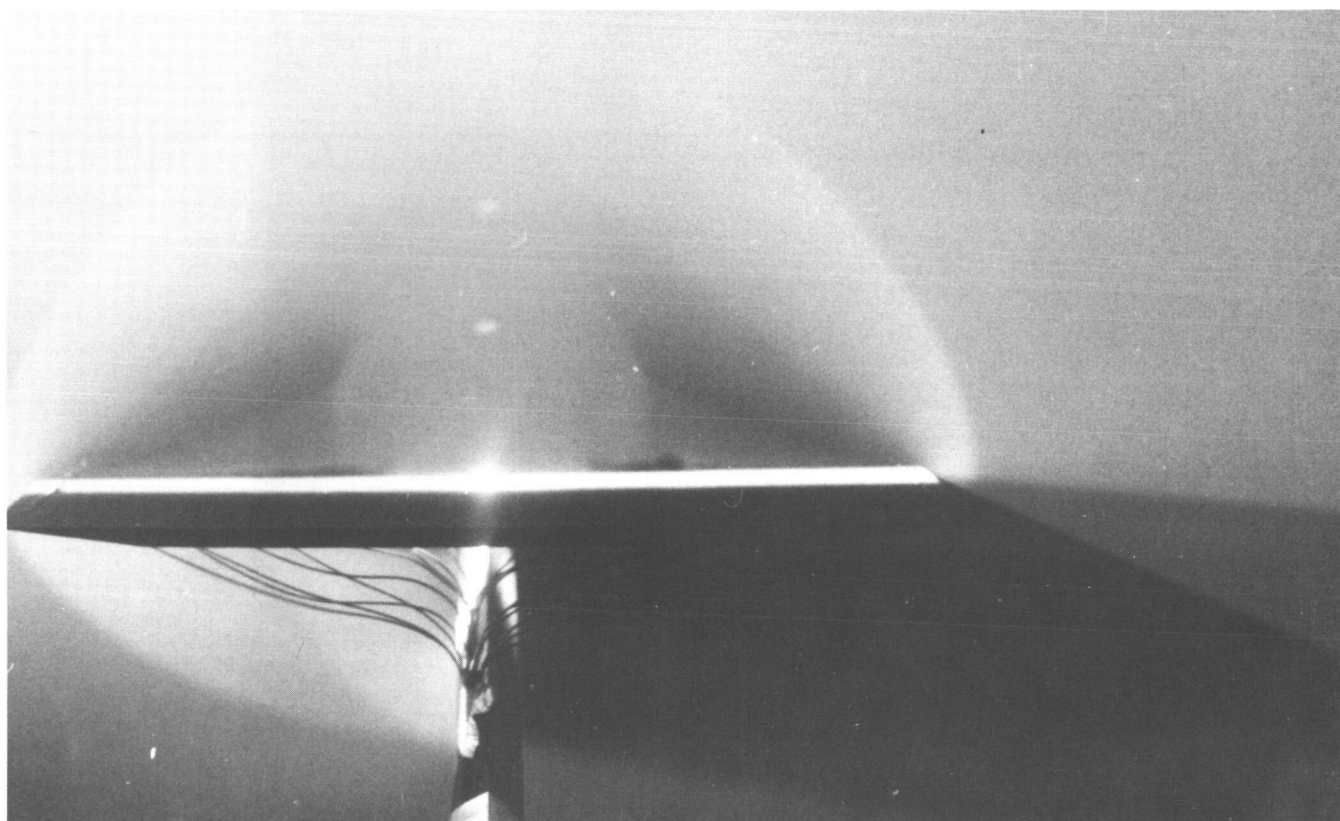


(u) $M = 2.8$, $\alpha = 8^\circ$.

Figure B3. Continued.

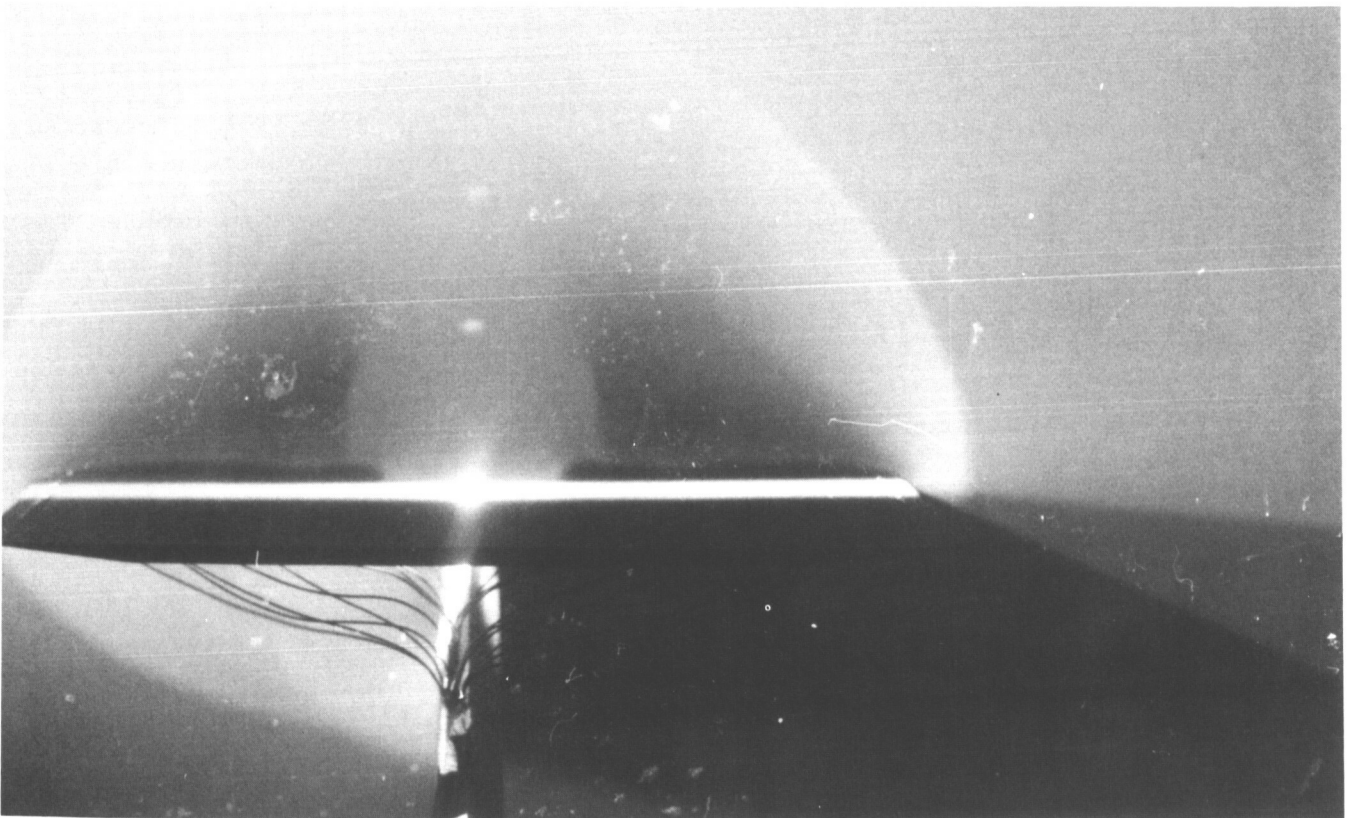
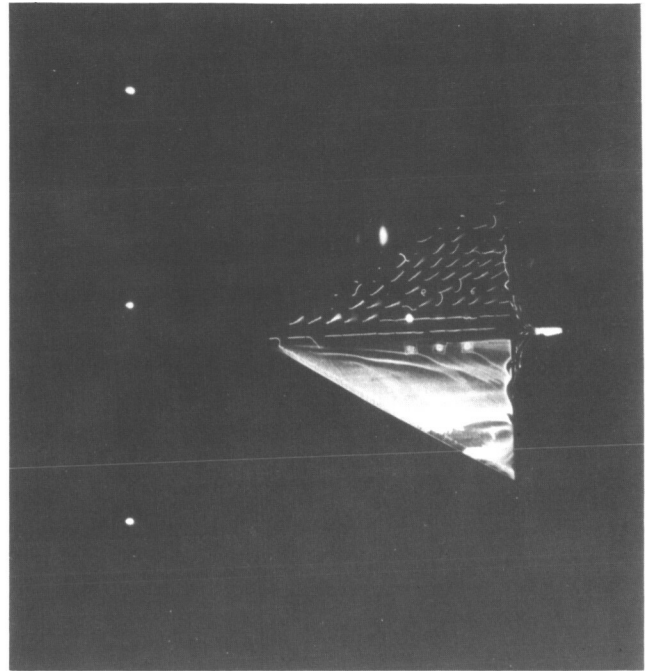
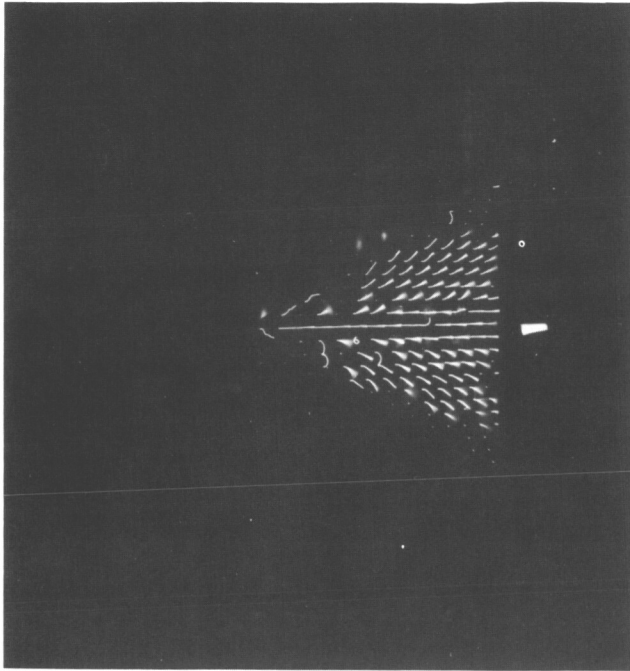


NO DATA



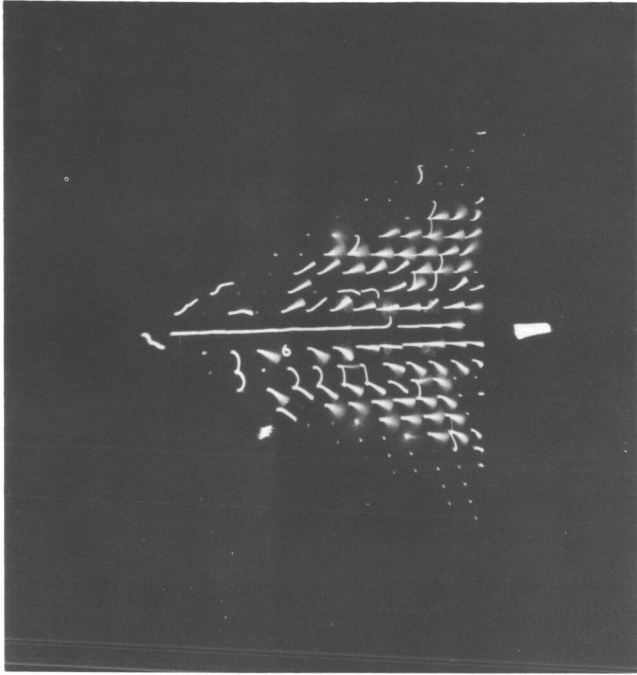
(v) $M = 2.8$, $\alpha = 12^\circ$.

Figure B3. Continued.

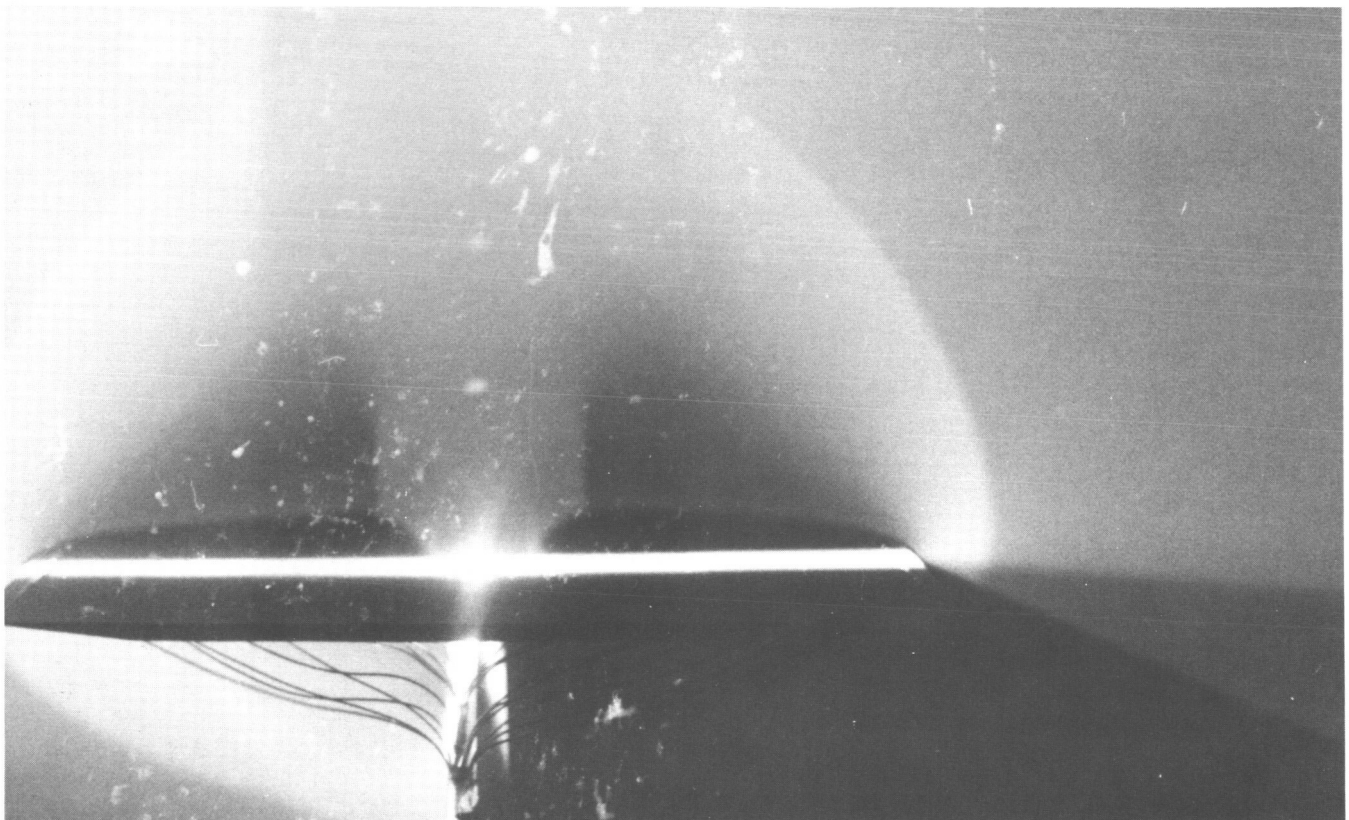


(w) $M = 2.8$, $\alpha = 16^\circ$.

Figure B3. Continued.

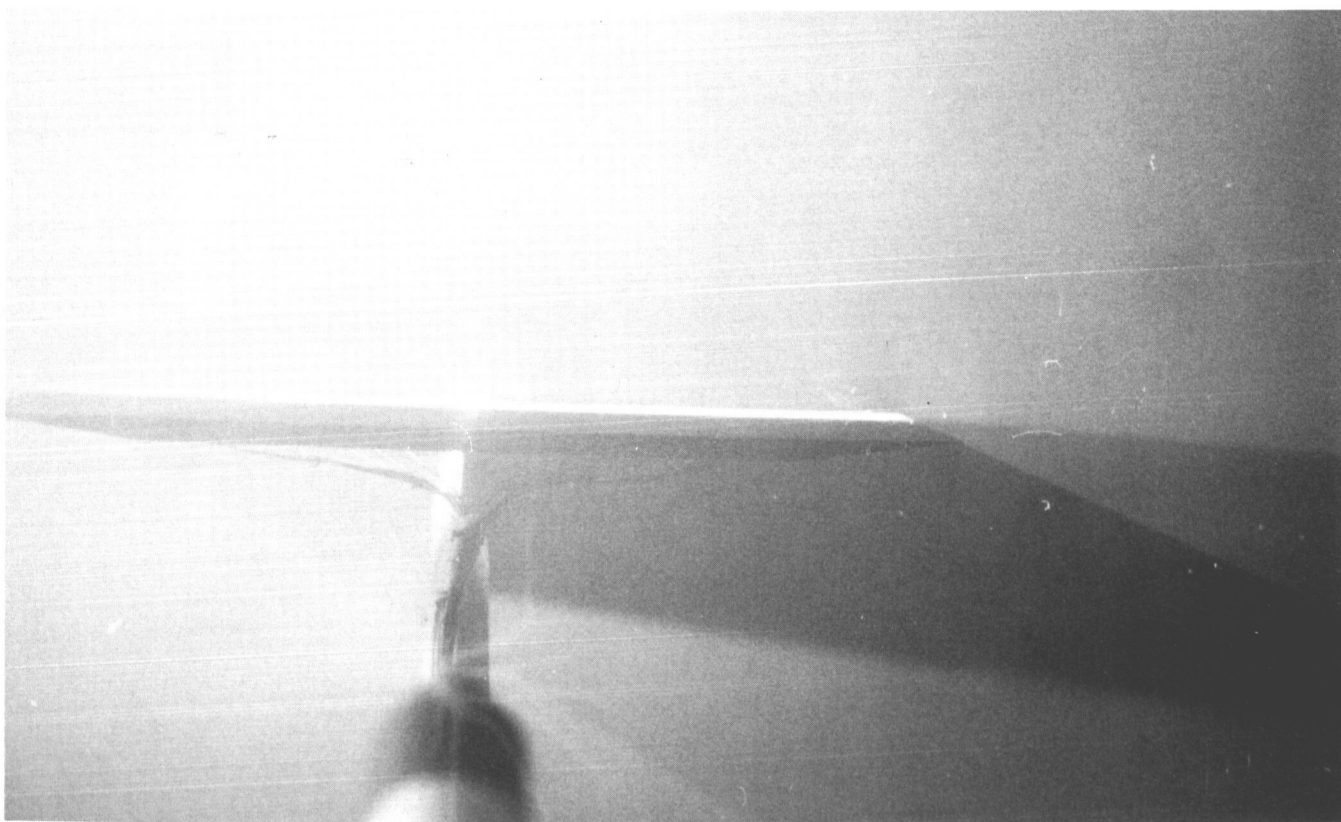
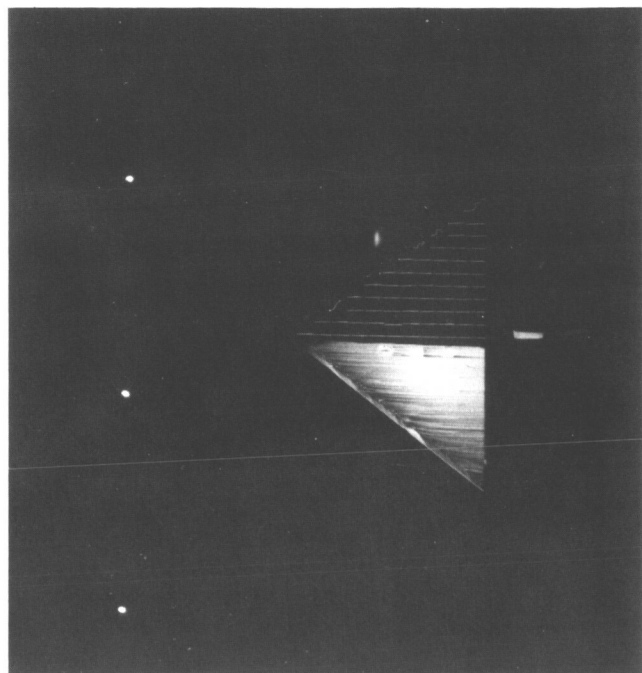
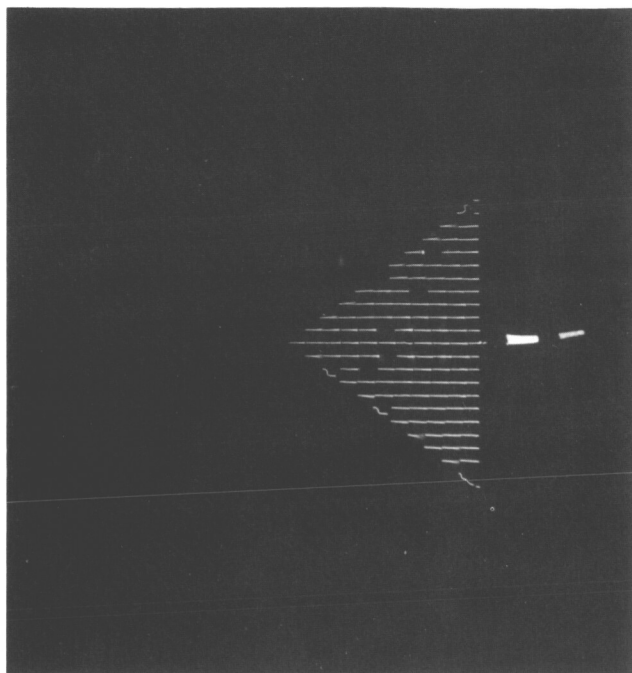


NO DATA



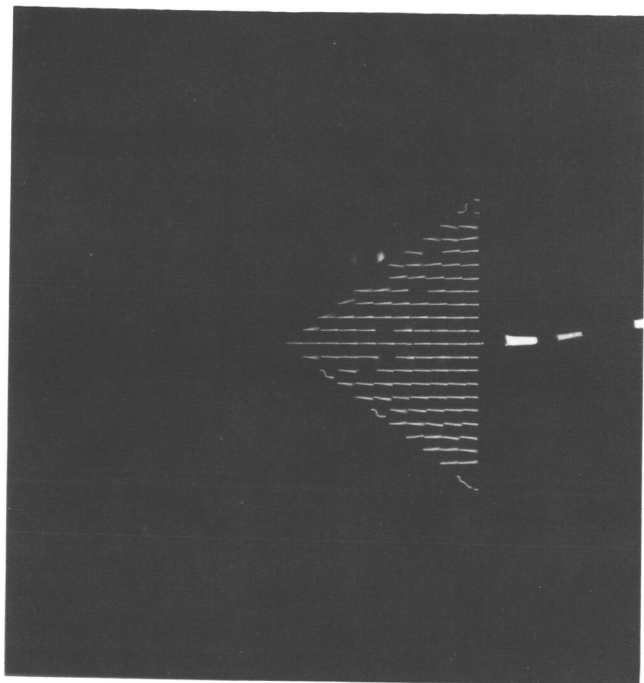
(x) $M = 2.8$, $\alpha = 20^\circ$.

Figure B3. Concluded.

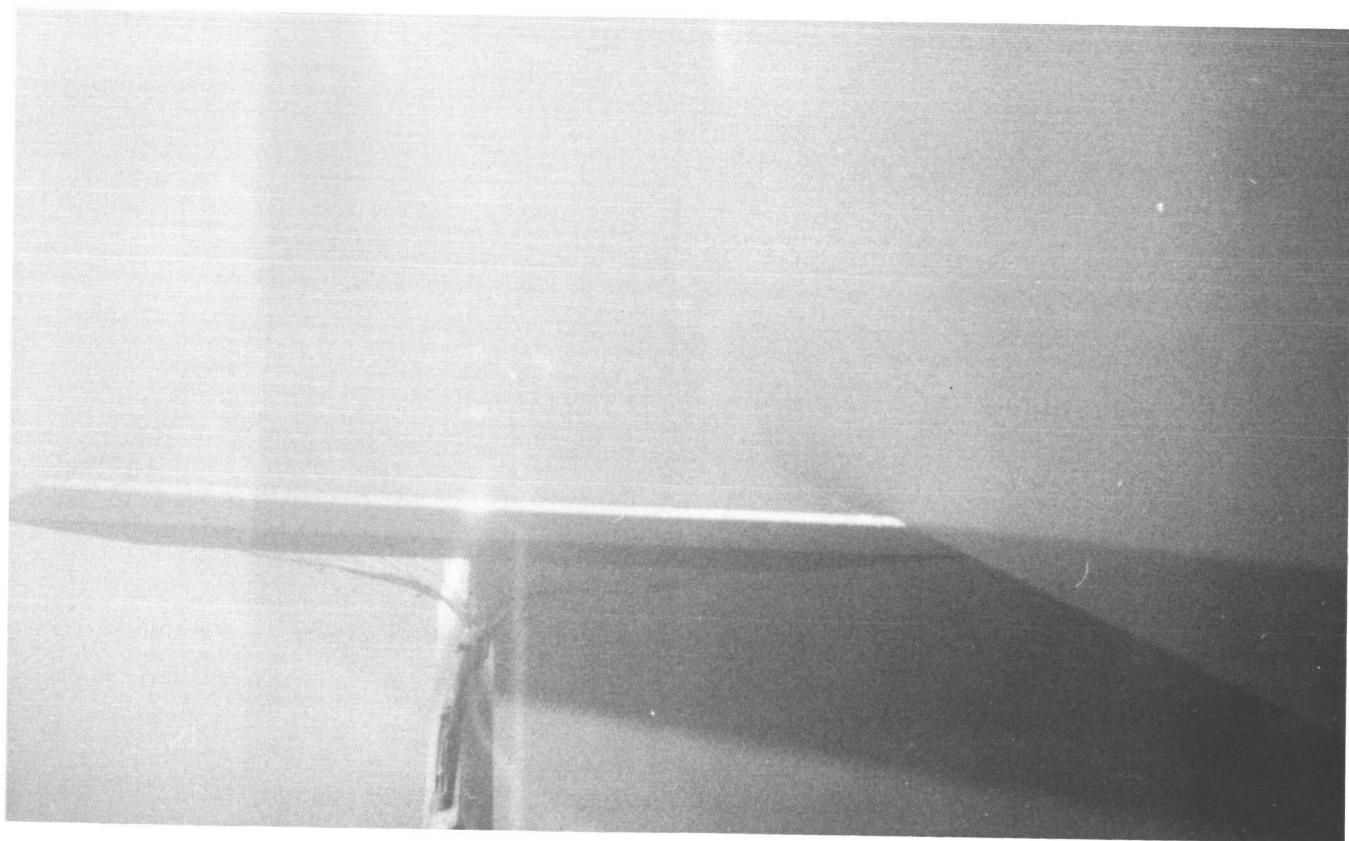


(a) $M = 1.7$, $\alpha = 0^\circ$.

Figure B4. Flow-visualization photographs for delta wing with $\Lambda_{LE} = 52.5^\circ$.

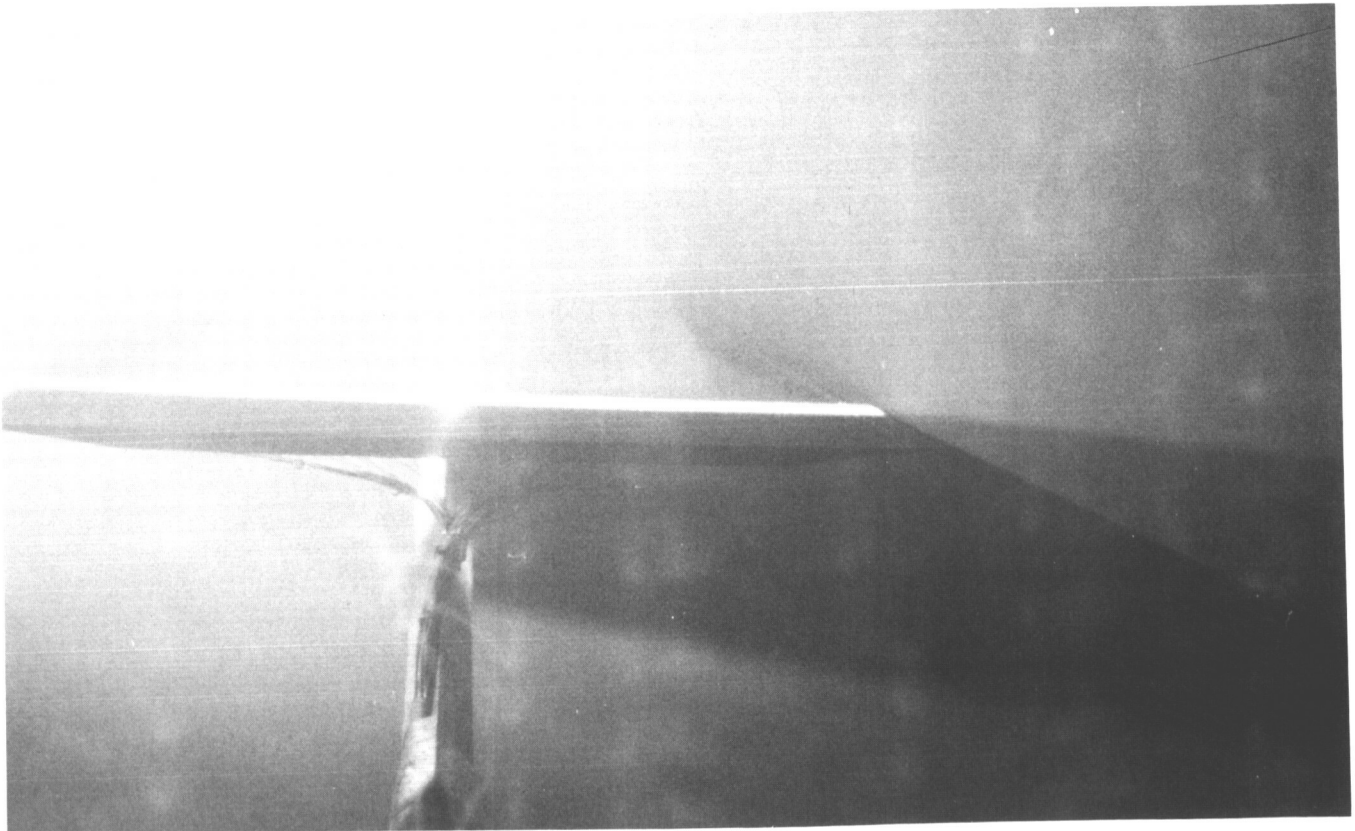
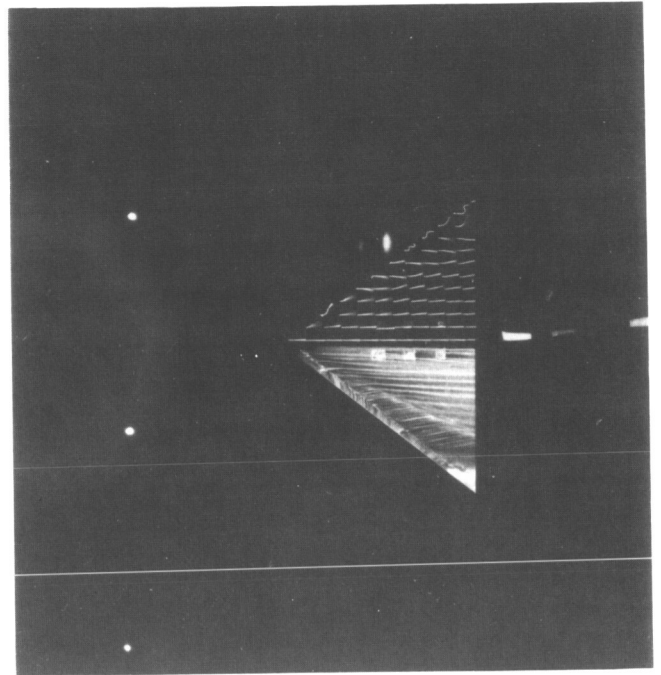
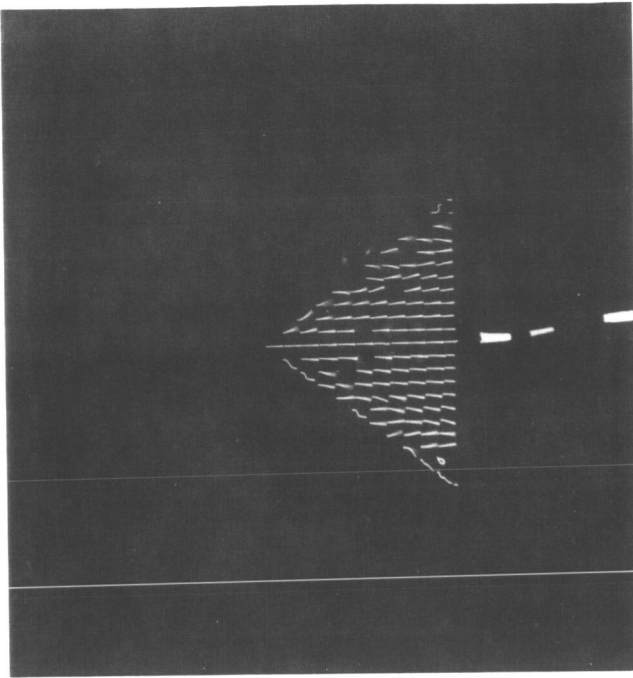


NO DATA



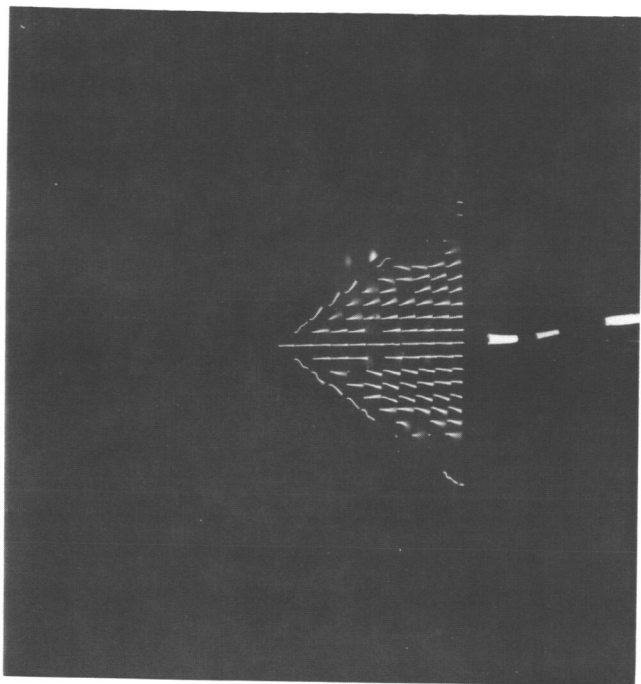
(b) $M = 1.7$, $\alpha = 4^\circ$.

Figure B4. . Continued.

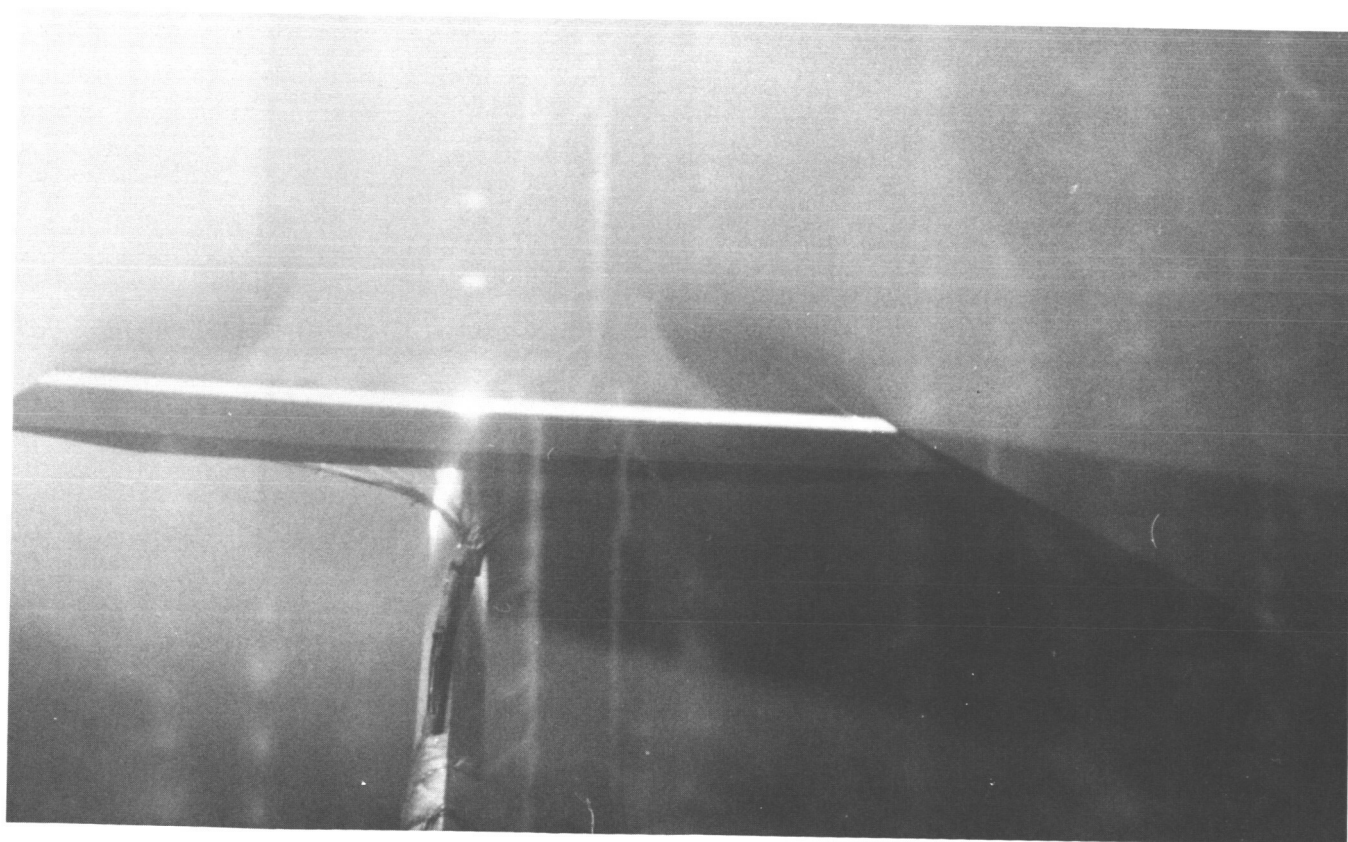


(c) $M = 1.7$, $\alpha = 8^\circ$.

Figure B4. Continued.

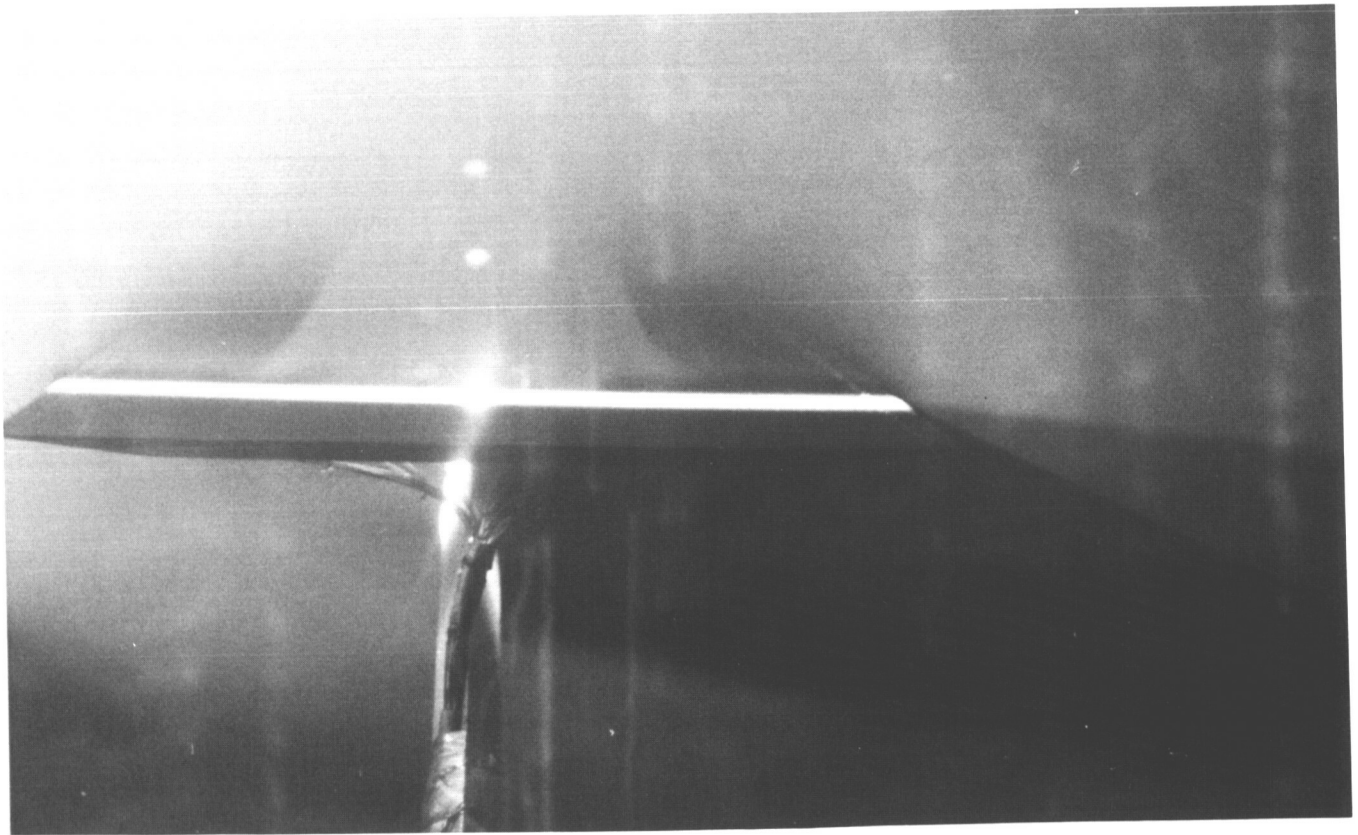
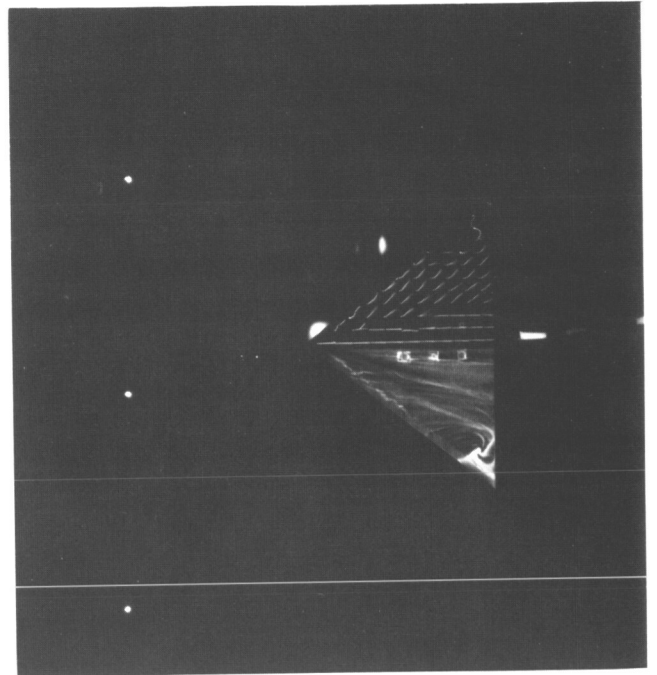
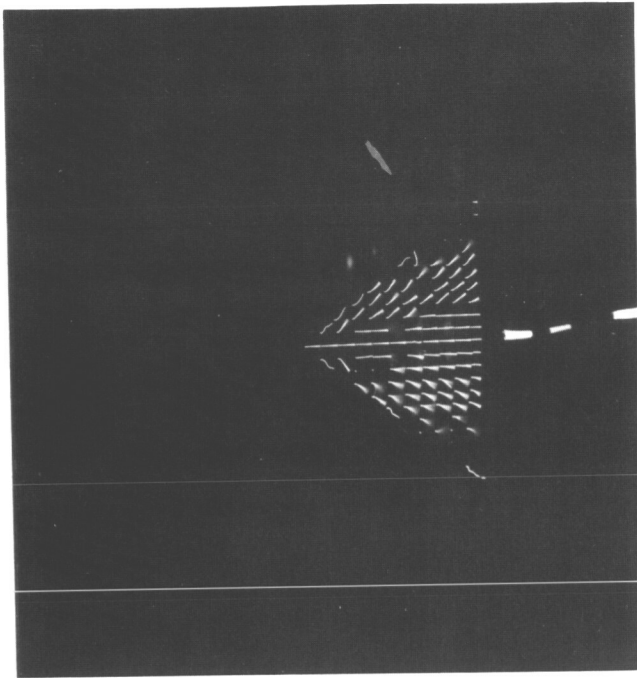


NO DATA



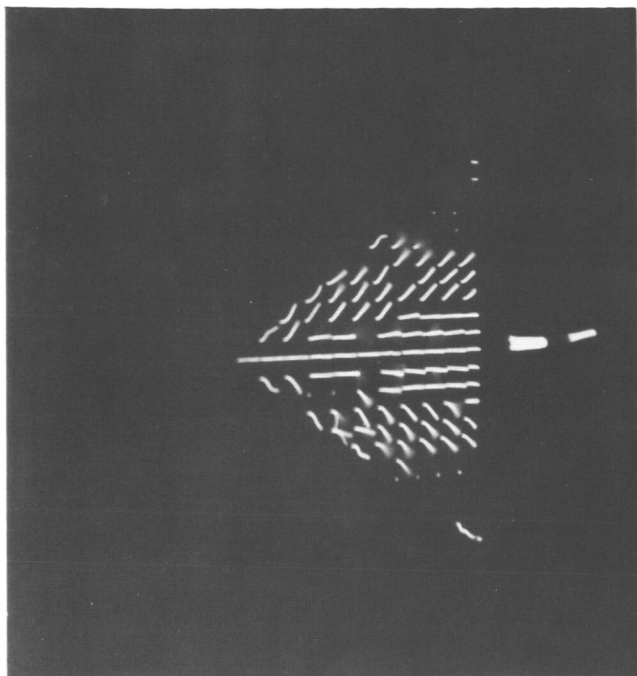
(d) $M = 1.7$, $\alpha = 12^\circ$.

Figure B4. Continued.

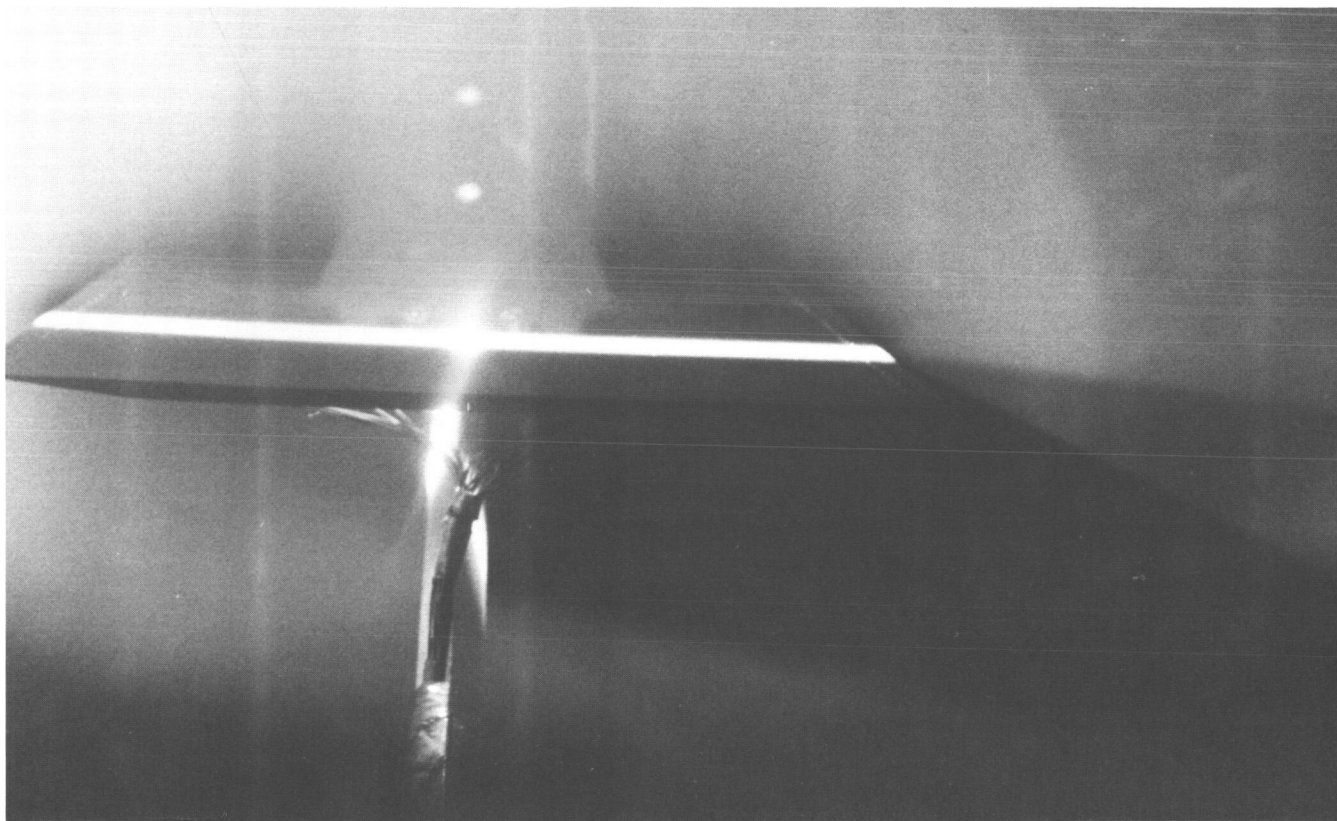


(e) $M = 1.7$, $\alpha = 16^\circ$.

Figure B4. Continued.

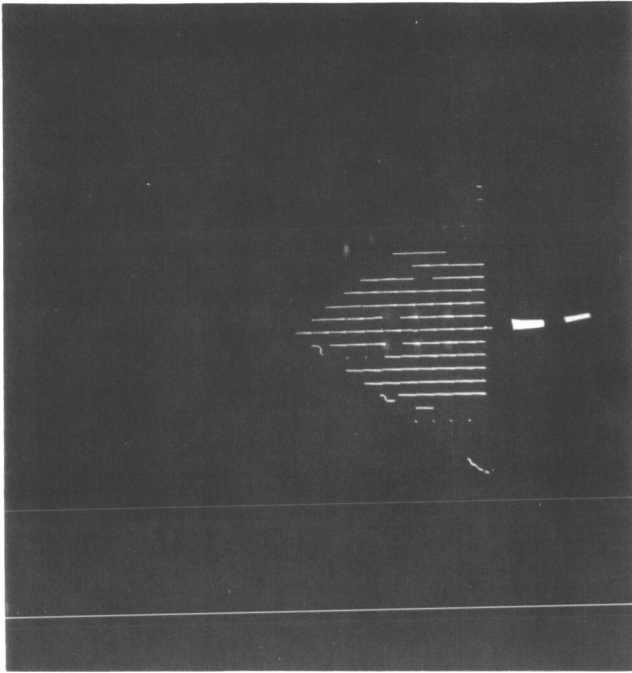


NO DATA

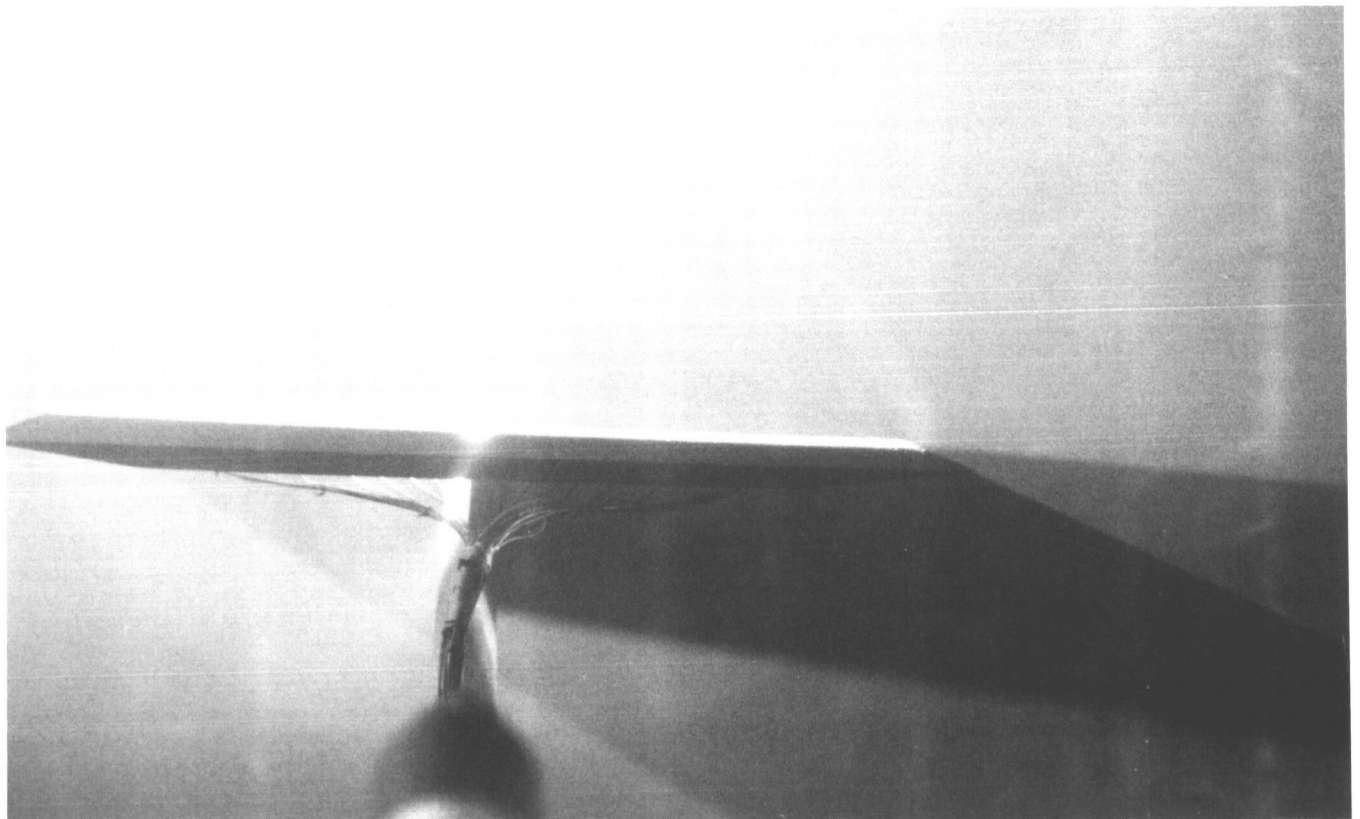


(f) $M = 1.7$, $\alpha = 20^\circ$.

Figure B4. Continued.

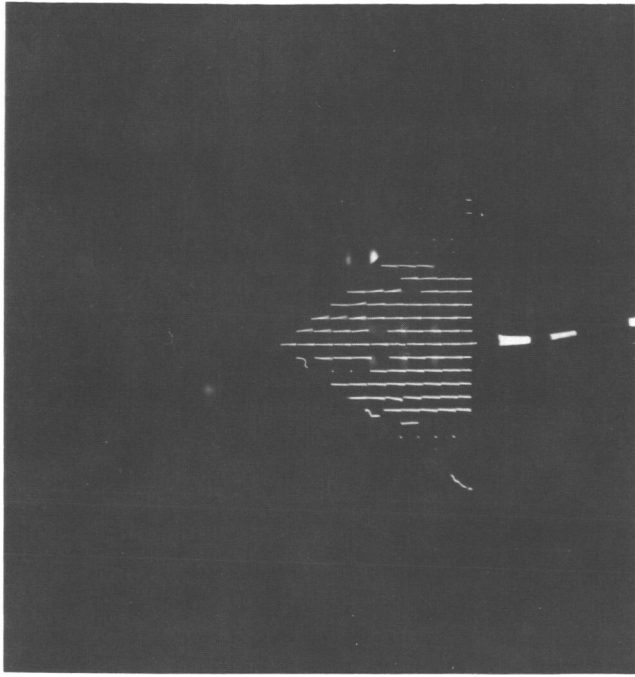


NO DATA

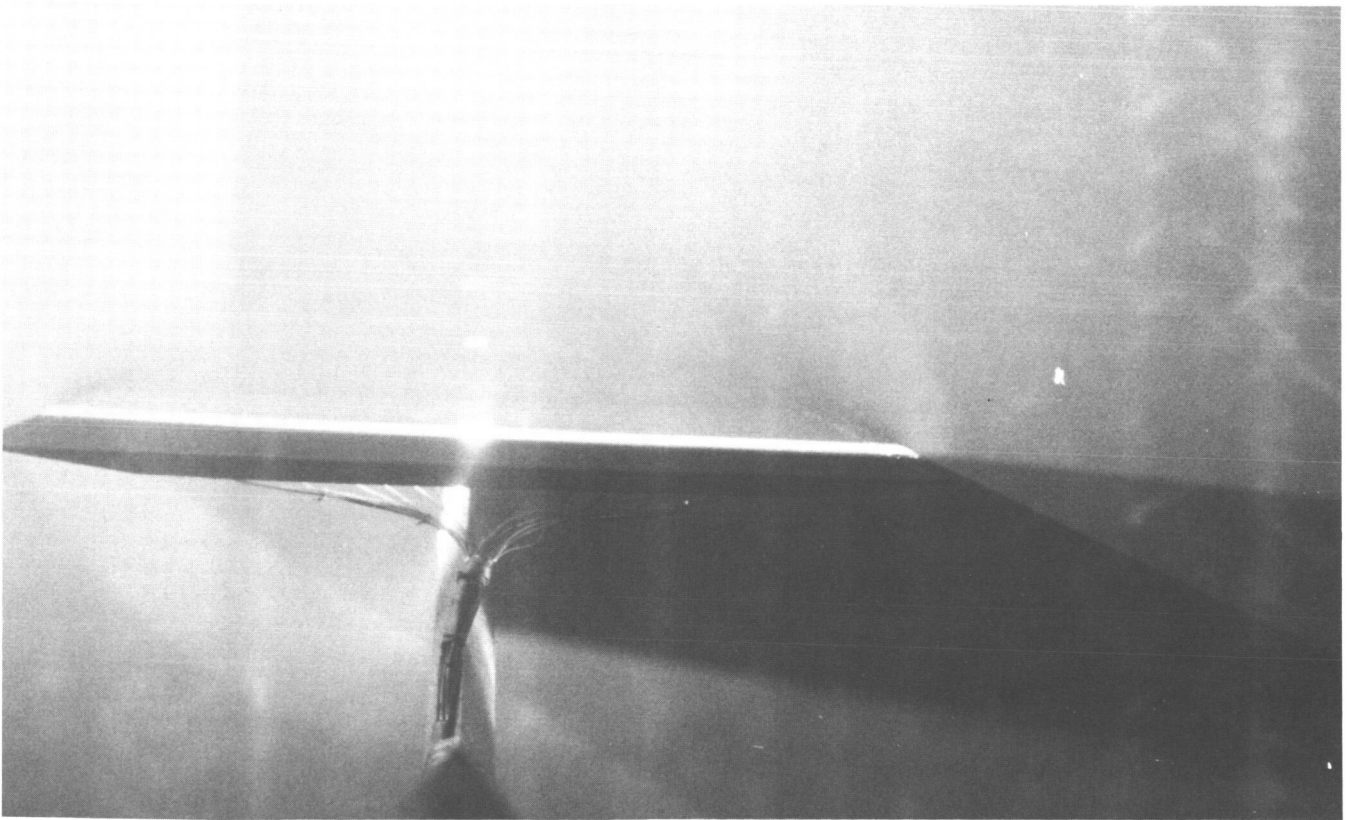


(g) $M = 2.0$, $\alpha = 0^\circ$.

Figure B4. Continued.

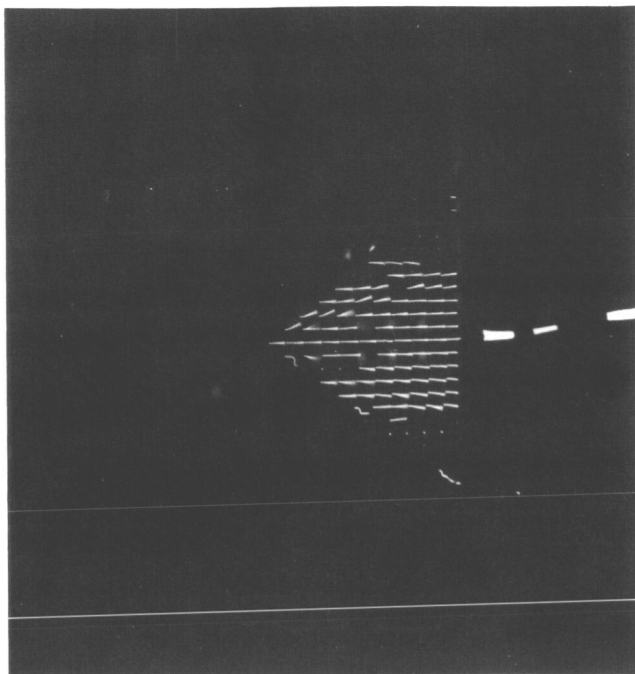


NO DATA

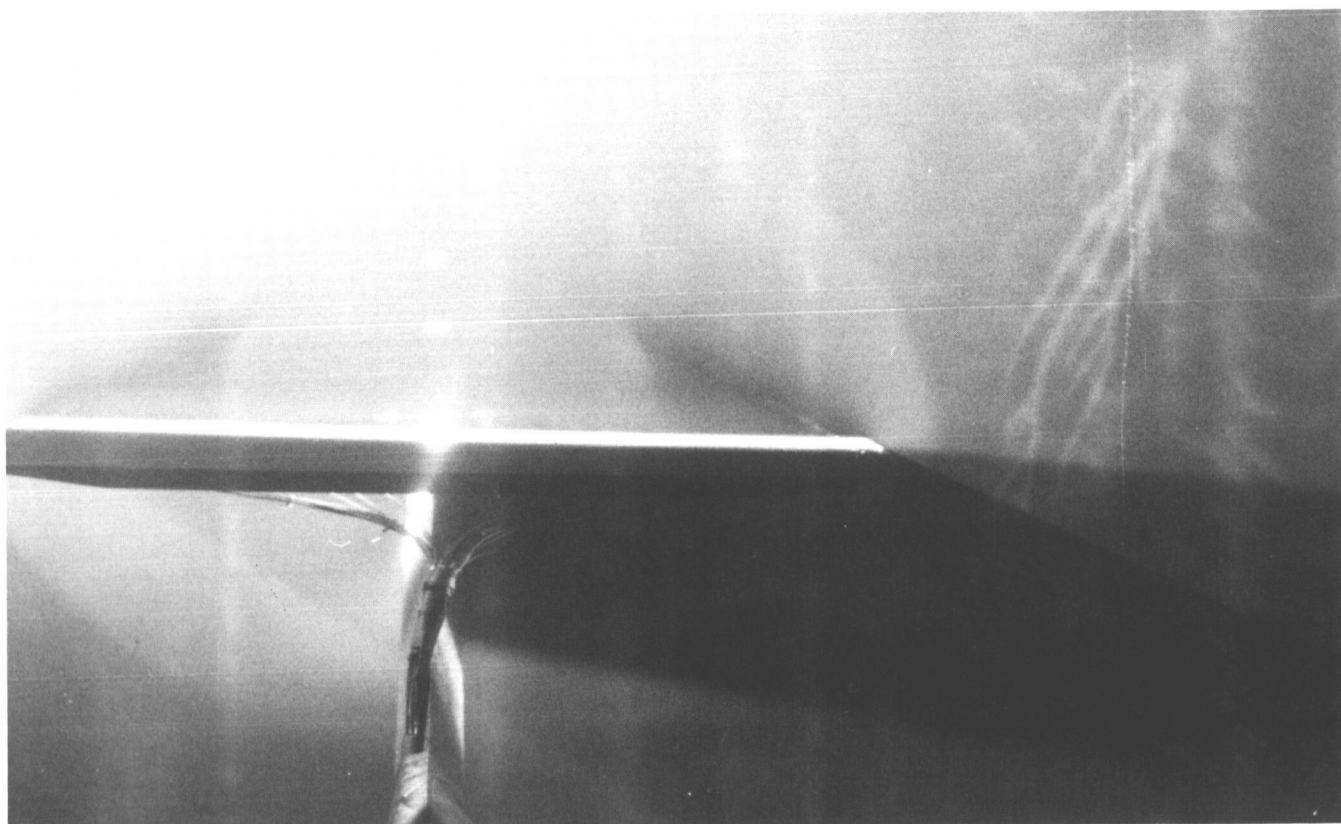


(h) $M = 2.0$, $\alpha = 4^\circ$.

Figure B4. Continued.

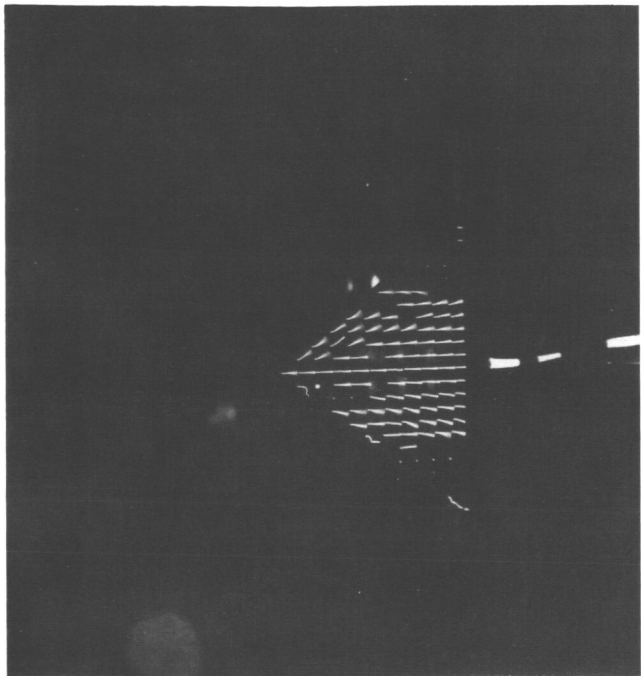


NO DATA



(i) $M = 2.0$, $\alpha = 8^\circ$.

Figure B4. Continued.

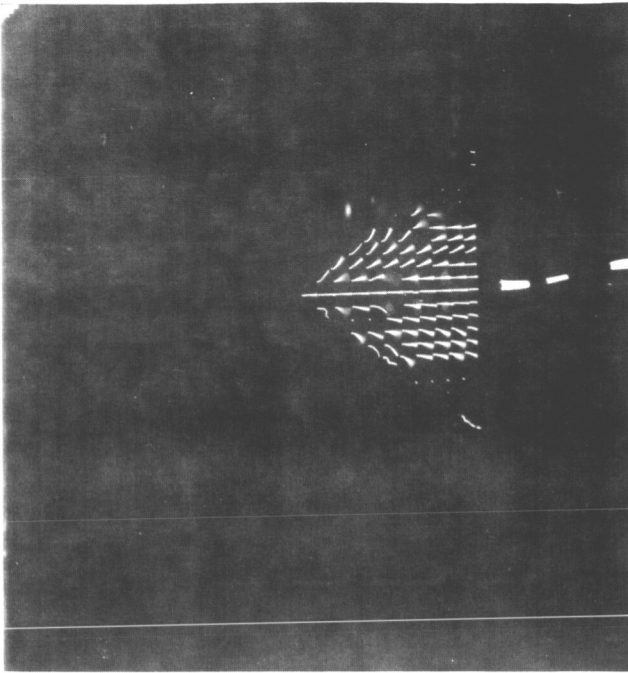


NO DATA

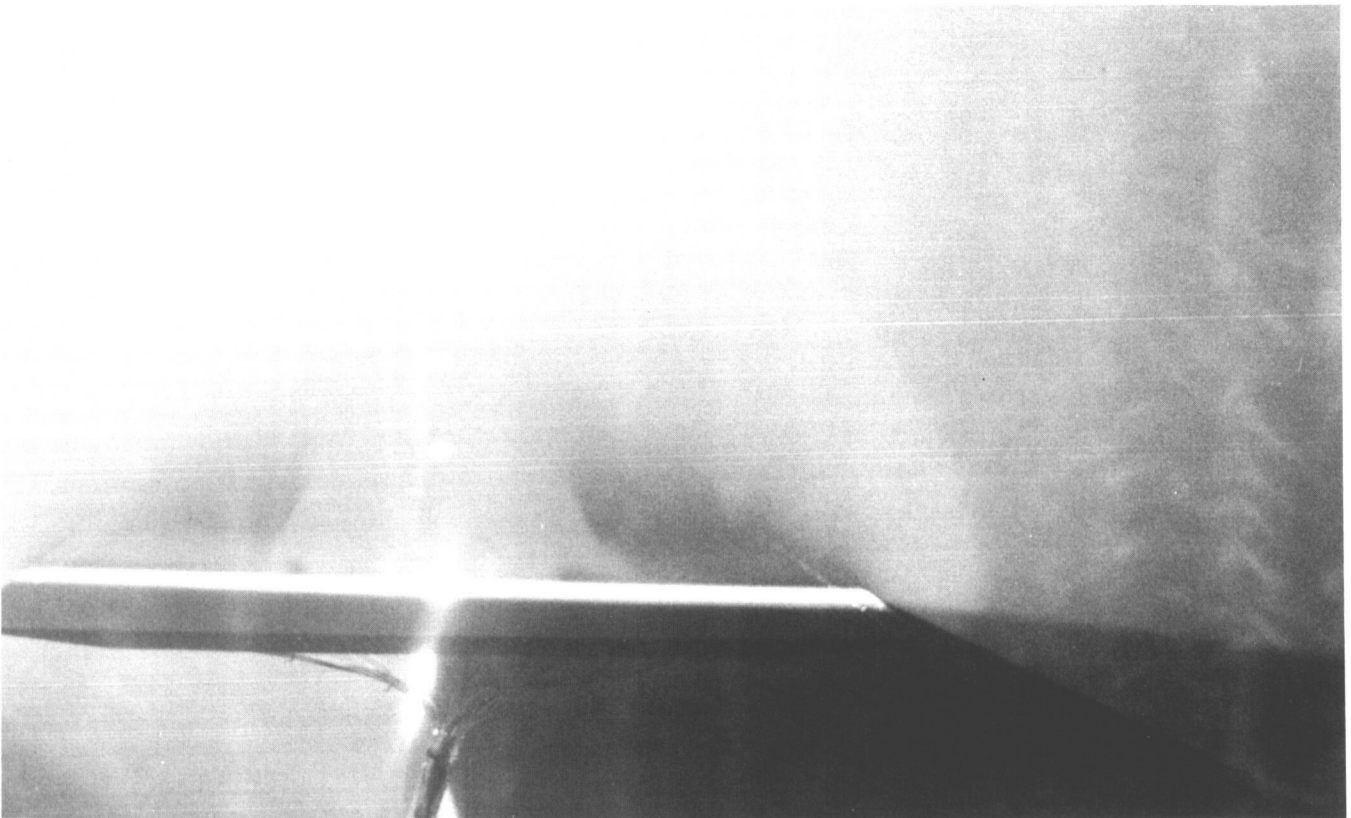


(j) $M = 2.0$, $\alpha = 12^\circ$.

Figure B4. Continued.

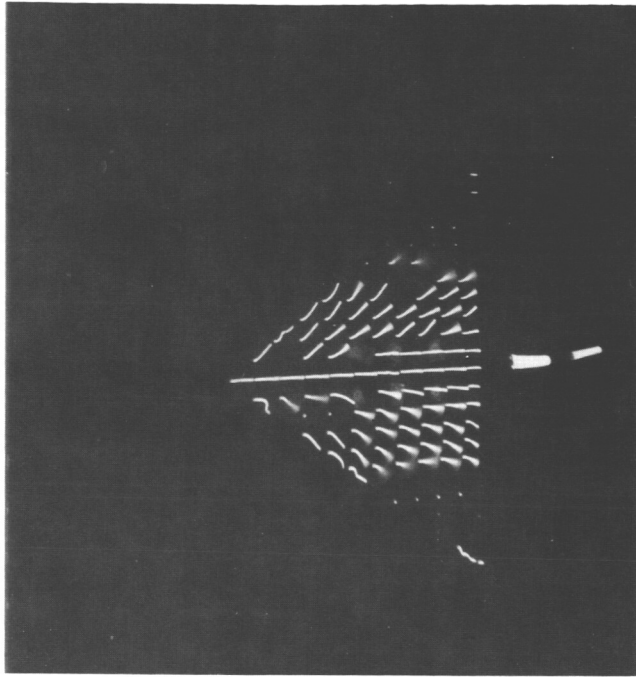


NO DATA



(k) $M = 2.0$, $\alpha = 16^\circ$.

Figure B4. Continued.



NO DATA

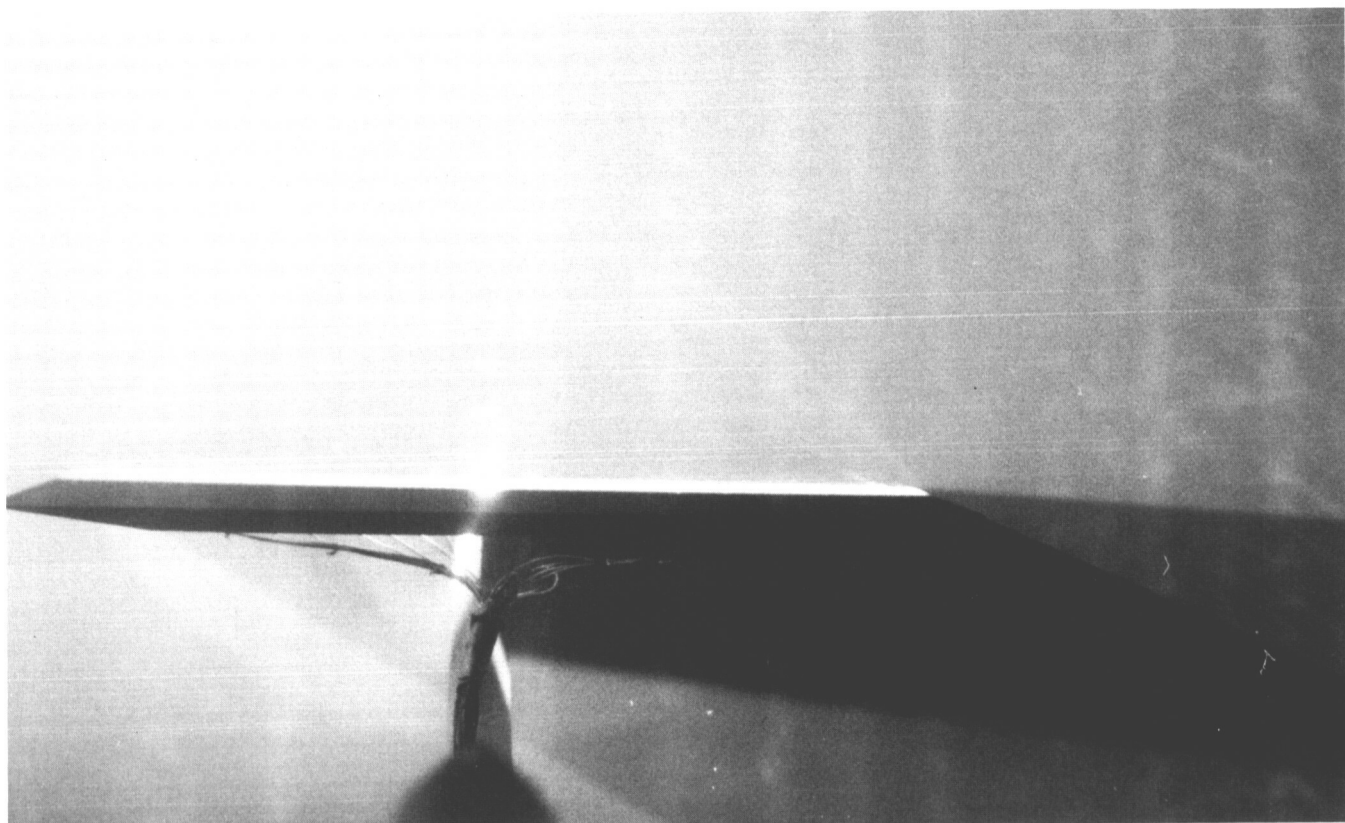


(1) $M = 2.0$, $\alpha = 20^\circ$.

Figure B4. Continued.

NO DATA

NO DATA



(m) $M = 2.4$, $\alpha = 0^\circ$.

Figure B4. Continued.

NO DATA

NO DATA

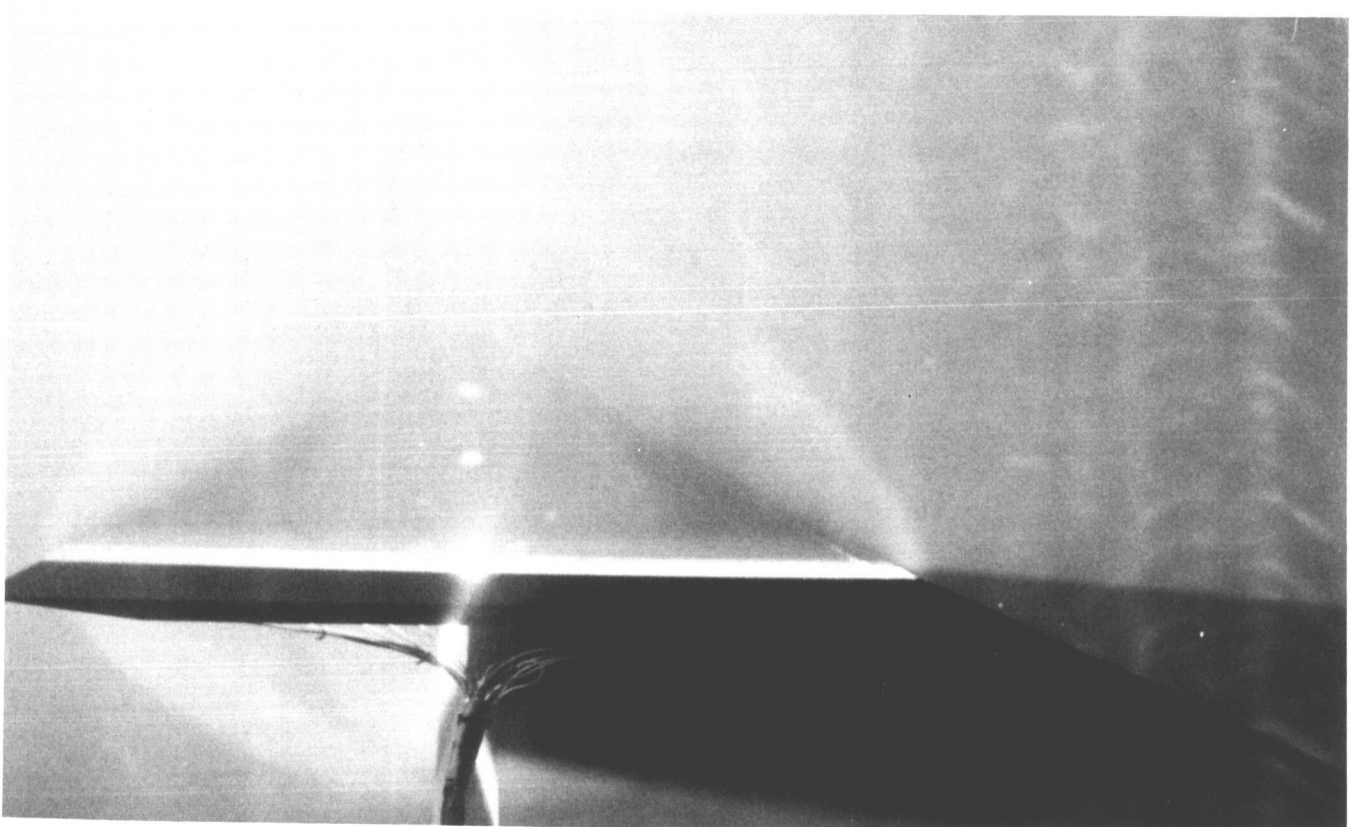


(n) $M = 2.4$, $\alpha = 4^\circ$.

Figure B4. Continued.

NO DATA

NO DATA



(o) $M = 2.4$, $\alpha = 8^\circ$.

Figure B4. Continued.

NO DATA

NO DATA

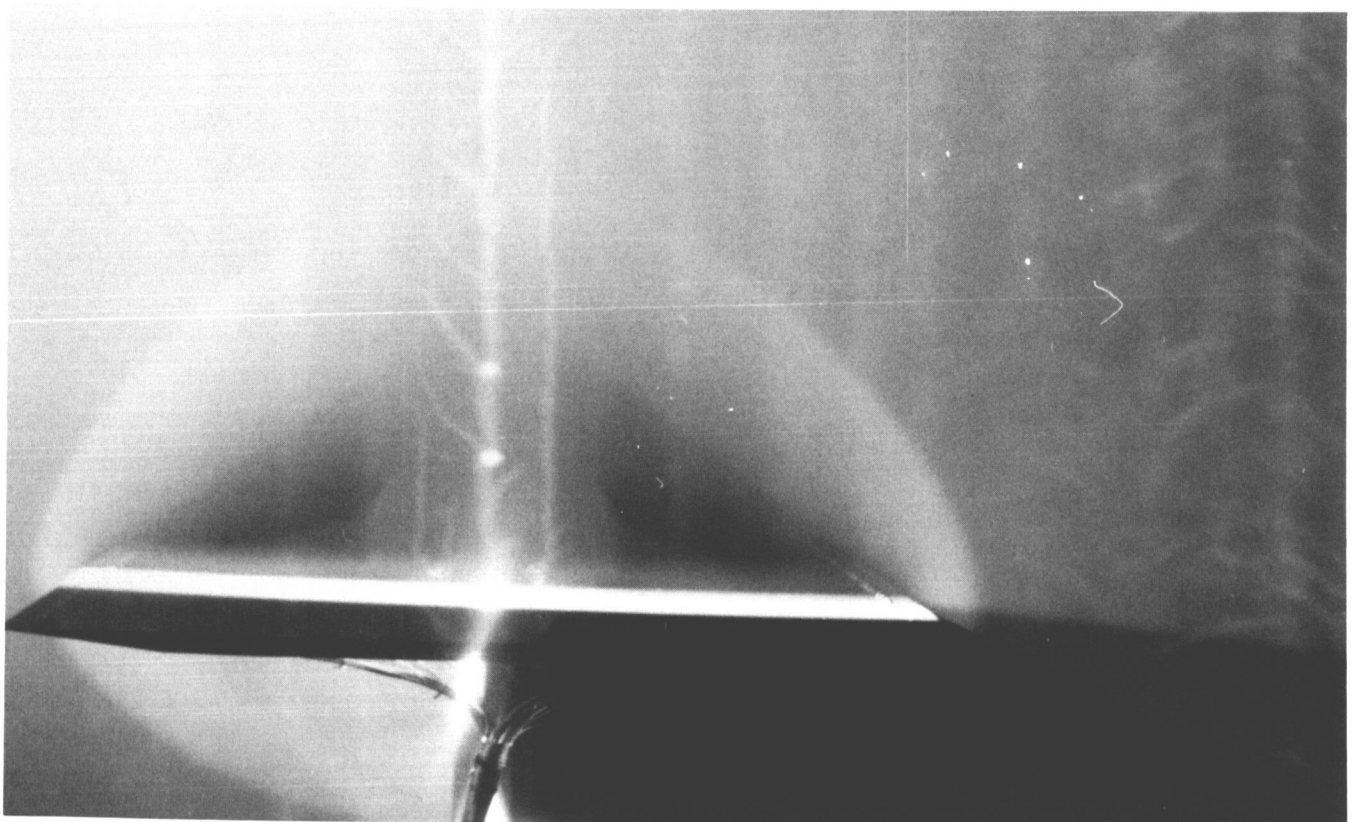


(p) $M = 2.4$, $\alpha = 12^\circ$.

Figure B4. Continued.

NO DATA

NO DATA

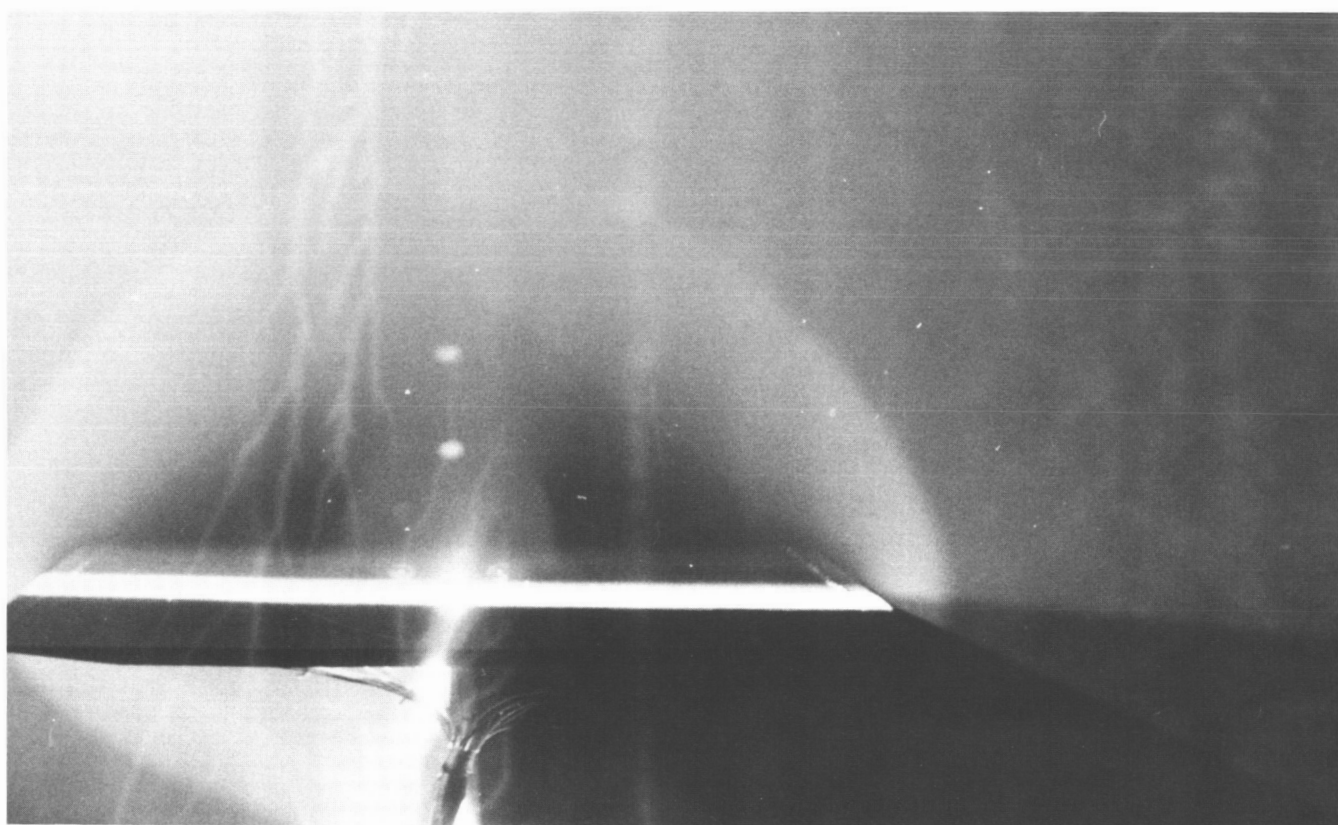


(q) $M = 2.4$, $\alpha = 16^\circ$.

Figure B4. Continued.

NO DATA

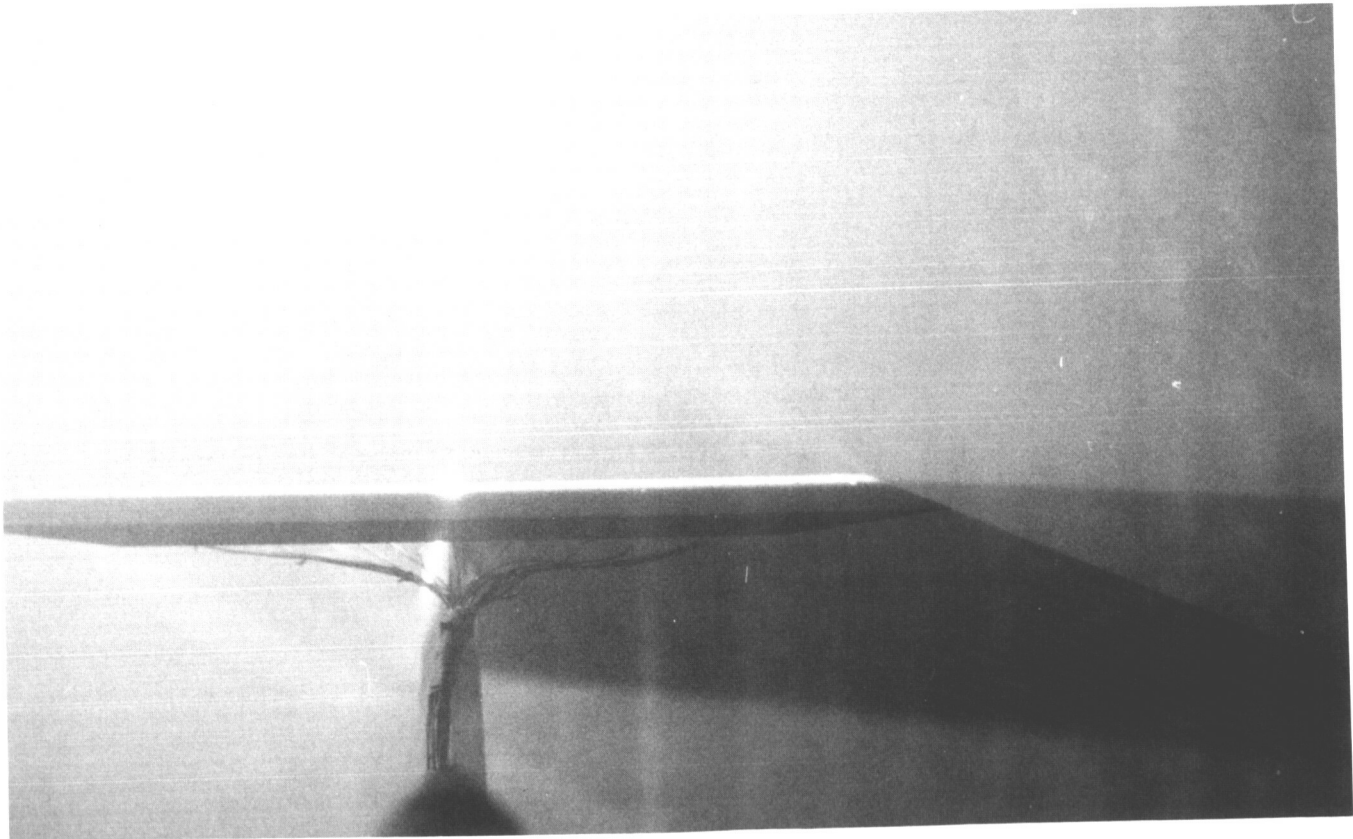
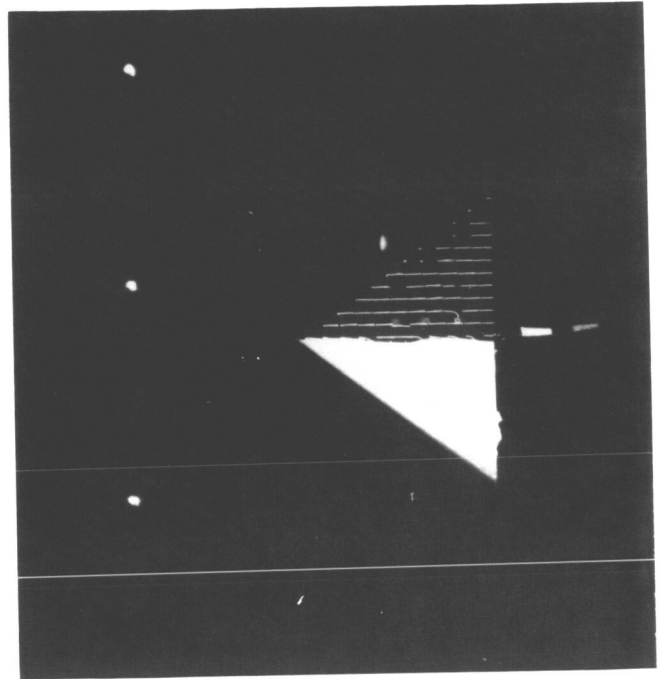
NO DATA



(r) $M = 2.4$, $\alpha = 20^\circ$.

Figure B4. Continued.

NO DATA

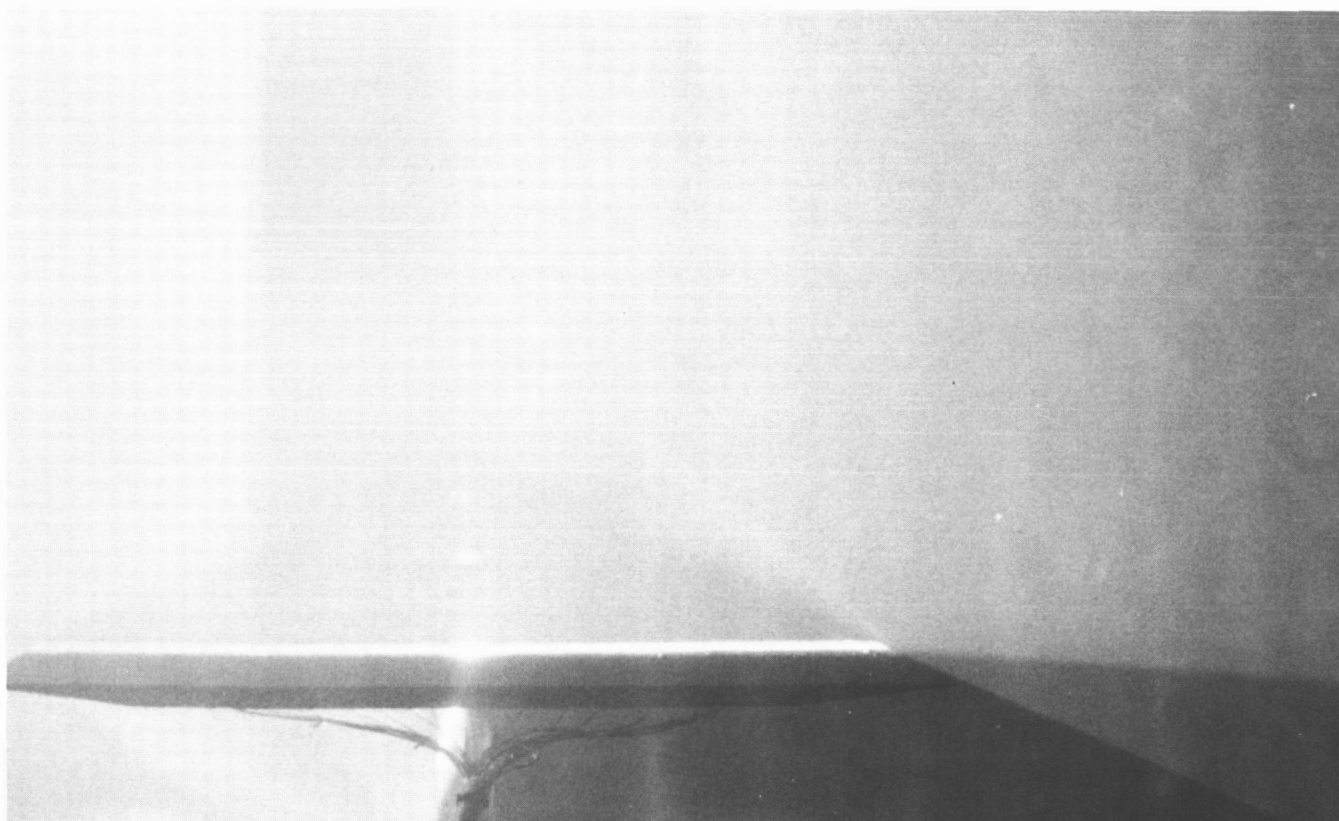


(s) $M = 2.8$, $\alpha = 0^\circ$.

Figure B4. Continued.

NO DATA

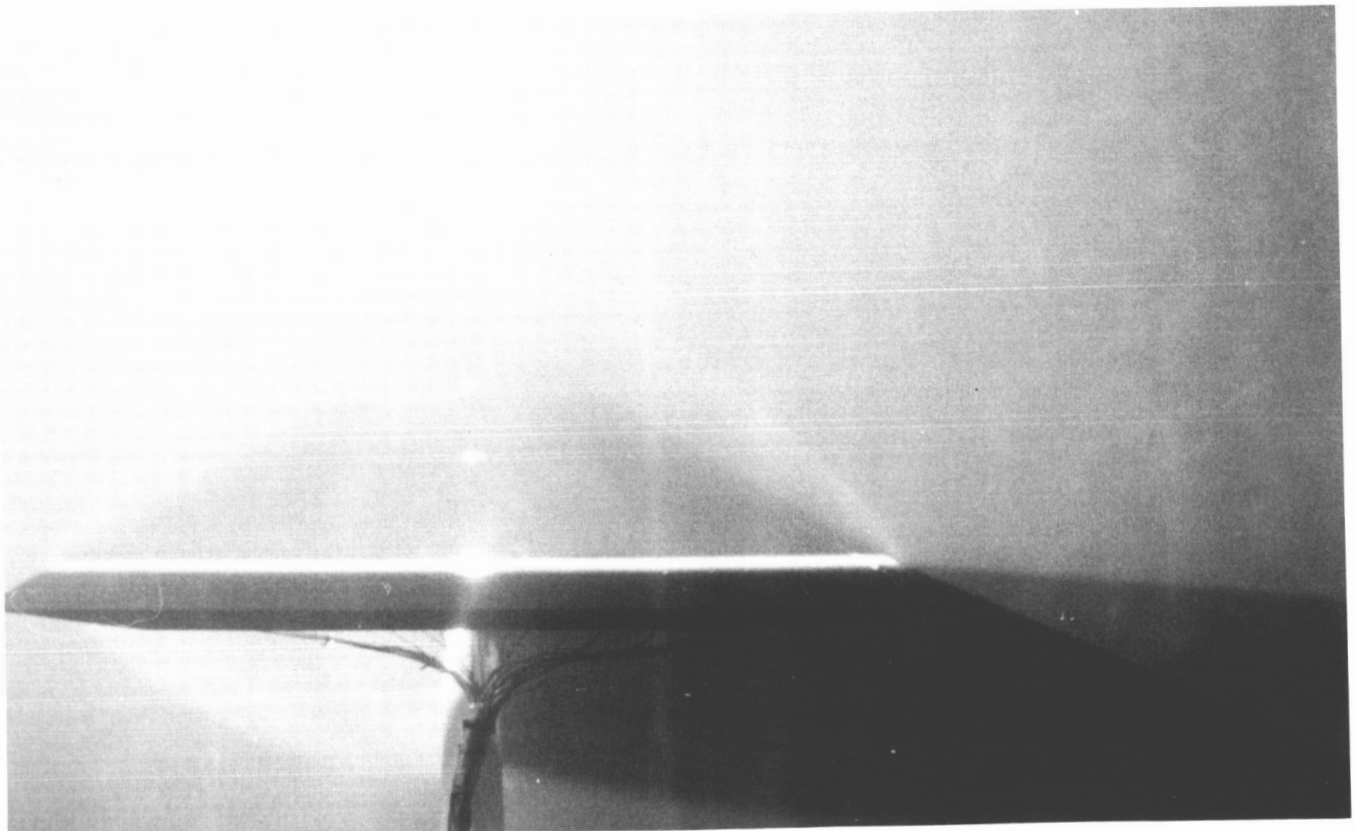
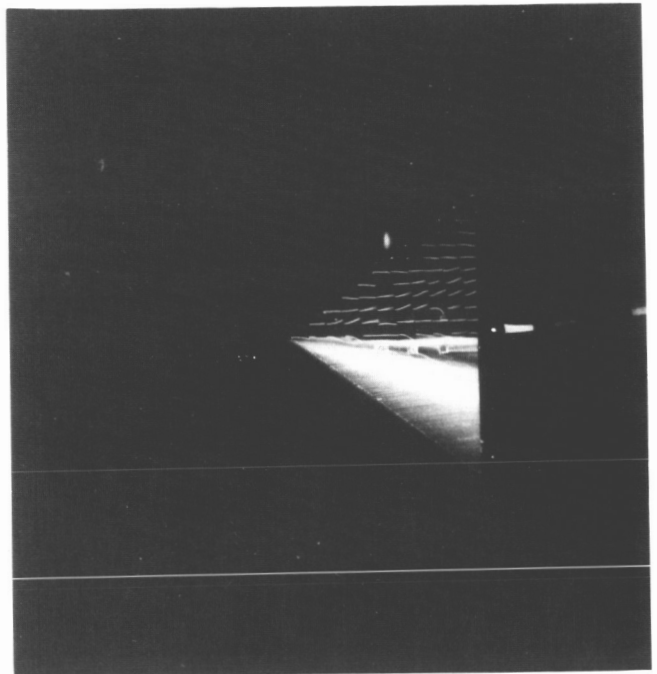
NO DATA



(t) $M = 2.8$, $\alpha = 4^\circ$.

Figure B4. Continued.

NO DATA



(u) $M = 2.8$, $\alpha = 8^\circ$.

Figure B4. Continued.

NO DATA

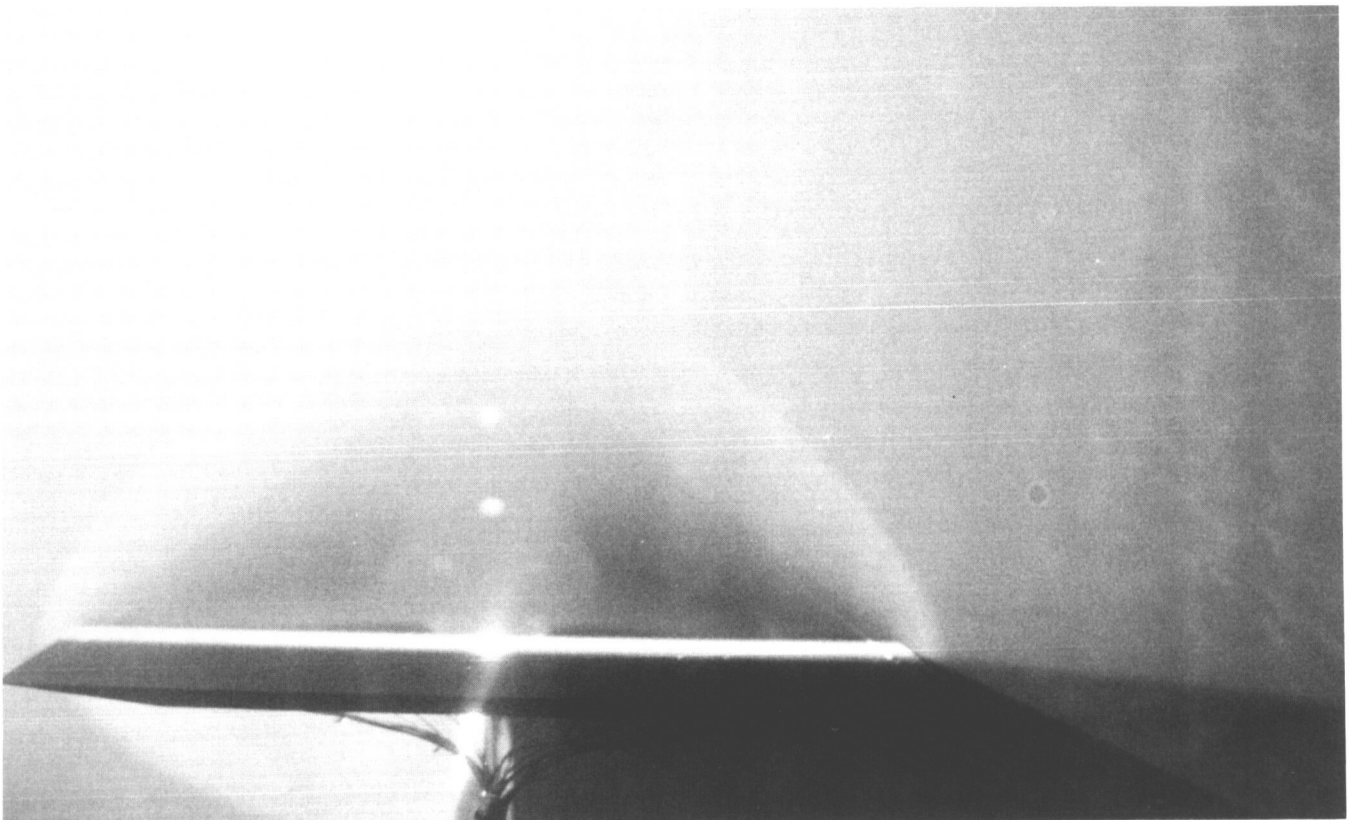
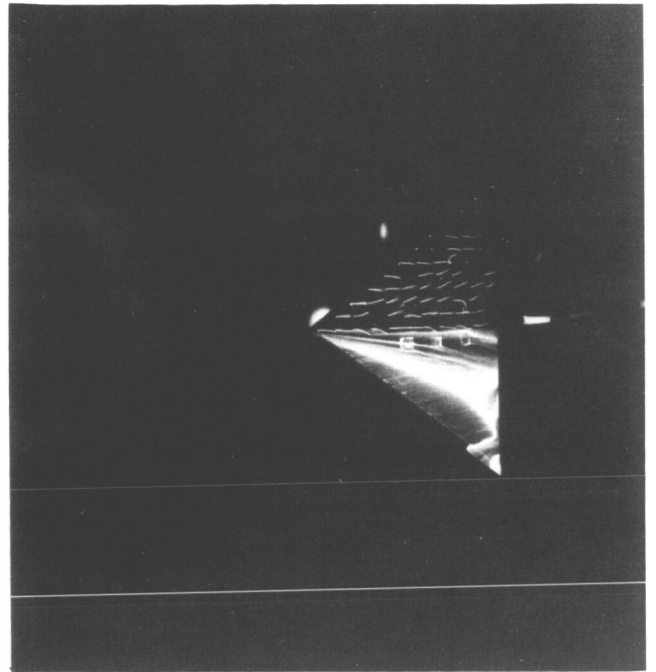
NO DATA



(v) $M = 2.8$, $\alpha = 12^\circ$.

Figure B4. Continued.

NO DATA

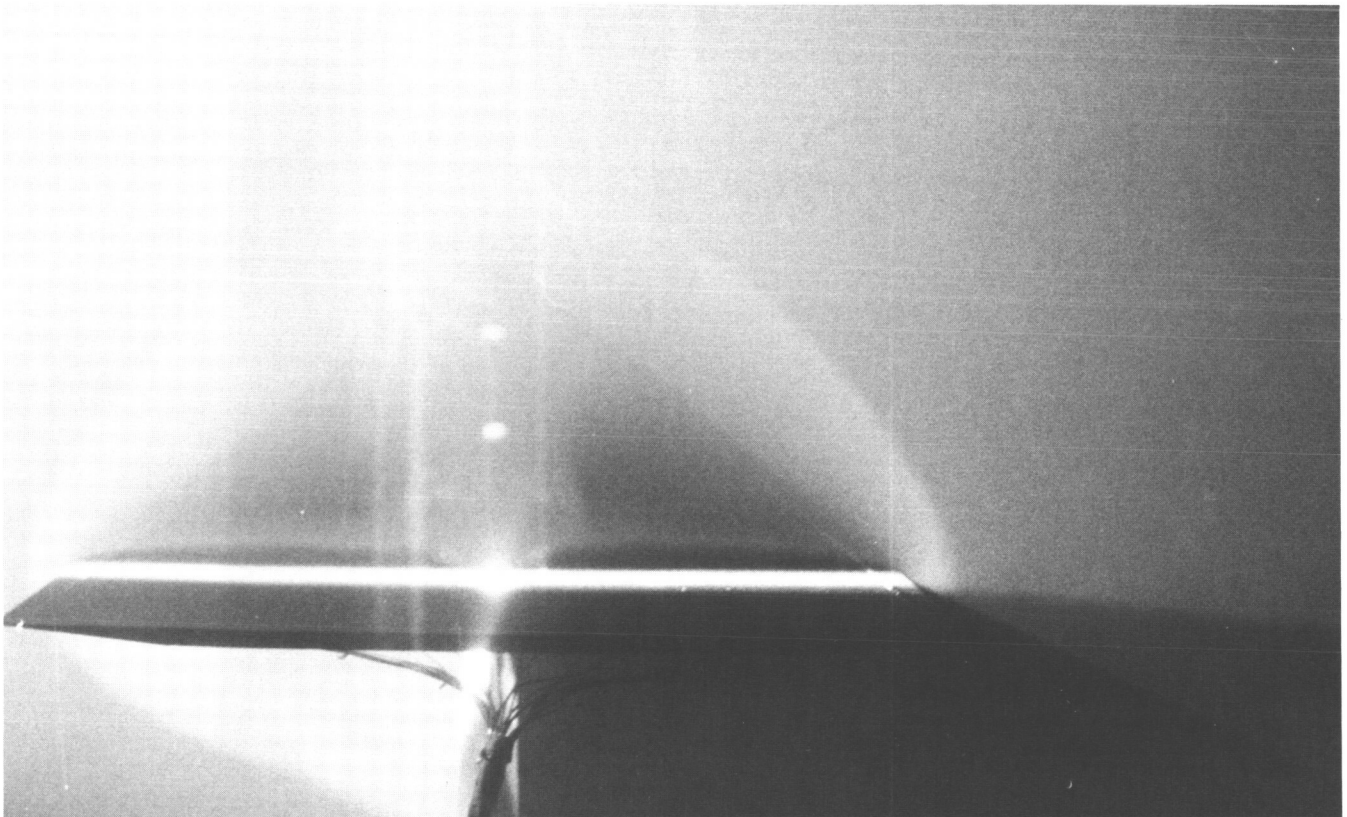


(w) $M = 2.8$, $\alpha = 16^\circ$.

Figure B4. Continued.

NO DATA

NO DATA



(x) $M = 2.8$, $\alpha = 20^\circ$.

Figure B4. Concluded.

Appendix C—Pressure-Coefficient Tables

Pressure-coefficient data for the four delta wings with leading-edge sweep angles of 75.0° , 67.5° , 60.0° , and 52.5° are presented in tables C1, C2, C3, and C4, respectively.

TABLE C1. PRESSURE-COEFFICIENT DATA FOR DELTA WING WITH $\Lambda_{LE} = 75.0^\circ$ (a) $M = 1.5$

| ALPHA = ETA | 4.01 | 7.09 | 12.00 | 16.00 | 20.00 |
|----------------|---------|---------|---------|-------|-------|
| -0.9 | -0.1557 | -0.2426 | -0.3153 | N | N |
| -0.8 | -0.2143 | -0.2499 | -0.3319 | N | N |
| -0.7 | -0.1557 | -0.3225 | -0.3380 | | |
| -0.6 | -0.0004 | -0.2911 | -0.4363 | D | D |
| -0.5 | -0.0142 | -0.0992 | -0.3131 | A | A |
| -0.4 | -0.0215 | -0.0571 | -0.1753 | T | T |
| -0.3 | -0.0245 | -0.0564 | -0.1172 | A | A |
| -0.2 | -0.0251 | -0.0588 | -0.1016 | | |
| -0.1 | -0.0242 | -0.0581 | -0.0972 | | |
| 0.0 | -0.0242 | -0.0589 | -0.0977 | | |
| 0.1 | -0.0238 | -0.0573 | -0.0969 | | |
| 0.2 | -0.0235 | -0.0572 | -0.1006 | | |
| 0.3 | -0.0249 | -0.0570 | -0.1142 | | |
| 0.4 | -0.0232 | -0.0566 | -0.1607 | | |
| 0.5 | -0.0179 | -0.0892 | -0.2762 | | |
| 0.6 | -0.0042 | -0.2571 | -0.4222 | | |
| 0.7 | -0.1417 | -0.3322 | -0.3346 | | |
| 0.8 | -0.2200 | -0.2497 | -0.3227 | | |
| 0.9 | -0.1542 | -0.2450 | -0.3199 | | |

(b) $M = 1.7$

| ALPHA = ETA | 4.00 | 8.00 | 12.00 | 16.00 | 20.01 |
|----------------|---------|---------|---------|---------|---------|
| -0.9 | -0.1457 | -0.2119 | -0.2686 | -0.3194 | -0.3644 |
| -0.8 | -0.1734 | -0.2357 | -0.3141 | -0.3570 | -0.3877 |
| -0.7 | -0.1677 | -0.2478 | -0.2975 | -0.3465 | -0.3838 |
| -0.6 | -0.0015 | -0.2852 | -0.3334 | -0.3649 | -0.3984 |
| -0.5 | -0.0091 | -0.1133 | -0.2928 | -0.3683 | -0.4060 |
| -0.4 | -0.0171 | -0.0535 | -0.1704 | -0.2833 | -0.3488 |
| -0.3 | -0.0204 | -0.0524 | -0.1082 | -0.1982 | -0.2696 |
| -0.2 | -0.0224 | -0.0564 | -0.0946 | -0.1525 | -0.2064 |
| -0.1 | -0.0229 | -0.0576 | -0.0915 | -0.1351 | -0.1742 |
| 0.0 | -0.0234 | -0.0578 | -0.0916 | -0.1316 | -0.1646 |
| 0.1 | -0.0224 | -0.0556 | -0.0908 | -0.1328 | -0.1711 |
| 0.2 | -0.0208 | -0.0528 | -0.0920 | -0.1838 | -0.1947 |
| 0.3 | -0.0217 | -0.0521 | -0.1051 | -0.1823 | -0.2464 |
| 0.4 | -0.0205 | -0.0518 | -0.1519 | -0.2592 | -0.3233 |
| 0.5 | -0.0122 | -0.0925 | -0.2630 | -0.3467 | -0.3888 |
| 0.6 | -0.0002 | -0.2590 | -0.3445 | -0.3711 | -0.4008 |
| 0.7 | -0.1588 | -0.2480 | -0.2926 | -0.3406 | -0.3789 |
| 0.8 | -0.1751 | -0.2298 | -0.3036 | -0.3458 | -0.3793 |
| 0.9 | -0.1447 | -0.2128 | -0.2731 | -0.3257 | -0.3688 |

TABLE C1. Continued

(c) $M = 2.0$

| ALPHA = ETA | 4.00 | 8.00 | 12.01 | 16.00 | 20.01 |
|----------------|---------|---------|---------|---------|---------|
| -0.9 | -0.1167 | -0.1789 | -0.2179 | -0.2478 | -0.2754 |
| -0.8 | -0.1347 | -0.2008 | -0.2543 | -0.2876 | -0.3031 |
| -0.7 | -0.1516 | -0.1986 | -0.2464 | -0.2802 | -0.2995 |
| -0.6 | -0.0262 | -0.2466 | -0.2527 | -0.2814 | -0.3082 |
| -0.5 | -0.0139 | -0.1362 | -0.2596 | -0.2978 | -0.3149 |
| -0.4 | -0.0208 | -0.0544 | -0.1740 | -0.2522 | -0.2873 |
| -0.3 | -0.0231 | -0.0499 | -0.1087 | -0.1858 | -0.2399 |
| -0.2 | -0.0242 | -0.0524 | -0.0899 | -0.1391 | -0.1898 |
| -0.1 | -0.0245 | -0.0535 | -0.0864 | -0.1203 | -0.1589 |
| 0.0 | -0.0246 | -0.0541 | -0.0862 | -0.1155 | -0.1480 |
| 0.1 | -0.0245 | -0.0546 | -0.0865 | -0.1191 | -0.1538 |
| 0.2 | -0.0236 | -0.0530 | -0.0884 | -0.1328 | -0.1756 |
| 0.3 | -0.0238 | -0.0521 | -0.1016 | -0.1694 | -0.2178 |
| 0.4 | -0.0217 | -0.0554 | -0.1527 | -0.2310 | -0.2681 |
| 0.5 | -0.0147 | -0.1065 | -0.2371 | -0.2846 | -0.3041 |
| 0.6 | -0.0126 | -0.2365 | -0.2558 | -0.2816 | -0.3107 |
| 0.7 | -0.1489 | -0.1990 | -0.2422 | -0.2751 | -0.2993 |
| 0.8 | -0.1386 | -0.2017 | -0.2562 | -0.2853 | -0.2955 |
| 0.9 | -0.1199 | -0.1800 | -0.2169 | -0.2533 | -0.2846 |

(d) $M = 2.4$

| ALPHA = ETA | 4.00 | 8.00 | 12.00 | 16.00 | 20.01 |
|----------------|---------|---------|---------|---------|---------|
| -0.9 | -0.1017 | -0.1400 | -0.1685 | -0.1846 | -0.1973 |
| -0.8 | -0.1130 | -0.1553 | -0.1789 | -0.2041 | -0.2176 |
| -0.7 | -0.1210 | -0.1638 | -0.1941 | -0.2113 | -0.2183 |
| -0.6 | -0.0746 | -0.1842 | -0.1951 | -0.2118 | -0.2186 |
| -0.5 | -0.0159 | -0.1460 | -0.2030 | -0.2151 | -0.2205 |
| -0.4 | -0.0228 | -0.0592 | -0.1661 | -0.2080 | -0.2155 |
| -0.3 | -0.0251 | -0.0488 | -0.1066 | -0.1672 | -0.1941 |
| -0.2 | -0.0261 | -0.0503 | -0.0825 | -0.1254 | -0.1637 |
| -0.1 | -0.0265 | -0.0513 | -0.0773 | -0.1057 | -0.1418 |
| 0.0 | -0.0261 | -0.0516 | -0.0756 | -0.1002 | -0.1287 |
| 0.1 | -0.0259 | -0.0516 | -0.0763 | -0.1027 | -0.1325 |
| 0.2 | -0.0252 | -0.0506 | -0.0793 | -0.1160 | -0.1503 |
| 0.3 | -0.0247 | -0.0494 | -0.0934 | -0.1481 | -0.1790 |
| 0.4 | -0.0232 | -0.0525 | -0.1428 | -0.1897 | -0.2053 |
| 0.5 | -0.0154 | -0.1173 | -0.1949 | -0.2140 | -0.2191 |
| 0.6 | -0.0420 | -0.1755 | -0.1884 | -0.2084 | -0.2169 |
| 0.7 | -0.1180 | -0.1627 | -0.1912 | -0.2085 | -0.2155 |
| 0.8 | -0.1116 | -0.1579 | -0.1871 | -0.2097 | -0.2170 |
| 0.9 | -0.1016 | -0.1472 | -0.1740 | -0.1928 | -0.2103 |

TABLE C1. Concluded

(e) $M = 2.8$

| ALPHA = ETA | 4.01 | 8.00 | 11.99 | 16.00 | 20.01 |
|----------------|---------|---------|---------|---------|---------|
| -0.9 | -0.0810 | -0.1084 | -0.1258 | -0.1366 | -0.1428 |
| -0.8 | -0.0918 | -0.1209 | -0.1351 | -0.1508 | -0.1546 |
| -0.7 | -0.0877 | -0.1279 | -0.1473 | -0.1544 | -0.1580 |
| -0.6 | -0.0671 | -0.1378 | -0.1467 | -0.1544 | -0.1595 |
| -0.5 | -0.0197 | -0.1339 | -0.1465 | -0.1550 | -0.1593 |
| -0.4 | -0.0200 | -0.0601 | -0.1447 | -0.1563 | -0.1603 |
| -0.3 | -0.0229 | -0.0413 | -0.1008 | -0.1439 | -0.1552 |
| -0.2 | -0.0231 | -0.0429 | -0.0716 | -0.1100 | -0.1336 |
| -0.1 | -0.0235 | -0.0443 | -0.0666 | -0.0903 | -0.1165 |
| 0.0 | -0.0239 | -0.0448 | -0.0657 | -0.0854 | -0.1104 |
| 0.1 | -0.0241 | -0.0448 | -0.0662 | -0.0884 | -0.1117 |
| 0.2 | -0.0238 | -0.0440 | -0.0690 | -0.1022 | -0.1260 |
| 0.3 | -0.0238 | -0.0424 | -0.0873 | -0.1295 | -0.1442 |
| 0.4 | -0.0223 | -0.0499 | -0.1318 | -0.1528 | -0.1569 |
| 0.5 | -0.0148 | -0.1204 | -0.1447 | -0.1560 | -0.1589 |
| 0.6 | -0.0644 | -0.1377 | -0.1457 | -0.1558 | -0.1599 |
| 0.7 | -0.0877 | -0.1278 | -0.1473 | -0.1558 | -0.1592 |
| 0.8 | -0.0906 | -0.1220 | -0.1363 | -0.1542 | -0.1589 |
| 0.9 | -0.0877 | -0.1191 | -0.1392 | -0.1515 | -0.1589 |

TABLE C2. PRESSURE-COEFFICIENT DATA FOR DELTA WING WITH $\Lambda_{LE} = 67.5^\circ$

| (a) $M = 1.5$ | | | | | |
|---------------|---------|---------|---------|-------|-------|
| ALPHA = | 4.01 | 8.00 | 12.00 | 16.00 | 20.00 |
| ETA | | | | | |
| -0.9 | -0.2185 | -0.3221 | -0.3950 | N | N |
| -0.8 | -0.2361 | -0.3463 | -0.4392 | N | N |
| -0.7 | -0.2134 | -0.3996 | -0.4324 | | |
| -0.6 | 0.0227 | -0.3356 | -0.4778 | D | D |
| -0.5 | -0.0253 | -0.0543 | -0.3610 | A | A |
| -0.4 | -0.0334 | -0.0667 | -0.1394 | T | T |
| -0.3 | -0.0354 | -0.0777 | -0.1208 | A | A |
| -0.2 | -0.0350 | -0.0804 | -0.1239 | | |
| -0.1 | -0.0350 | -0.0813 | -0.1265 | | |
| 0.0 | -0.0359 | -0.0820 | -0.1286 | | |
| 0.1 | -0.0360 | -0.0822 | -0.1285 | | |
| 0.2 | -0.0362 | -0.0823 | -0.1271 | | |
| 0.3 | -0.0376 | -0.0801 | -0.1243 | | |
| 0.4 | -0.0368 | -0.0698 | -0.1339 | | |
| 0.5 | -0.0288 | -0.0548 | -0.3146 | | |
| 0.6 | 0.0028 | -0.3212 | -0.4845 | | |
| 0.7 | -0.1911 | -0.3873 | -0.4348 | | |
| 0.8 | -0.2407 | -0.3465 | -0.4434 | | |
| 0.9 | -0.2173 | -0.3231 | -0.3920 | | |

| (b) $M = 1.7$ | | | | | |
|---------------|---------|---------|---------|---------|---------|
| ALPHA = | 4.00 | 8.00 | 12.00 | 16.00 | 20.00 |
| ETA | | | | | |
| -0.9 | -0.1936 | -0.2737 | -0.3304 | -0.3708 | -0.3949 |
| -0.8 | -0.2045 | -0.3033 | -0.3516 | -0.3856 | -0.4205 |
| -0.7 | -0.1910 | -0.3383 | -0.3599 | -0.4137 | -0.4378 |
| -0.6 | 0.0098 | -0.3261 | -0.3974 | -0.4111 | -0.4344 |
| -0.5 | -0.0220 | -0.0513 | -0.3551 | -0.4283 | -0.4450 |
| -0.4 | -0.0306 | -0.0607 | -0.1408 | -0.3246 | -0.4013 |
| -0.3 | -0.0338 | -0.0727 | -0.1084 | -0.1867 | -0.2952 |
| -0.2 | -0.0330 | -0.0740 | -0.1115 | -0.1549 | -0.2152 |
| -0.1 | -0.0317 | -0.0733 | -0.1125 | -0.1510 | -0.1914 |
| 0.0 | -0.0306 | -0.0720 | -0.1122 | -0.1508 | -0.1875 |
| 0.1 | -0.0314 | -0.0731 | -0.1126 | -0.1521 | -0.1920 |
| 0.2 | -0.0329 | -0.0742 | -0.1125 | -0.1557 | -0.2109 |
| 0.3 | -0.0342 | -0.0731 | -0.1103 | -0.1783 | -0.2767 |
| 0.4 | -0.0326 | -0.0640 | -0.1274 | -0.2955 | -0.3843 |
| 0.5 | -0.0257 | -0.0489 | -0.3235 | -0.4181 | -0.4440 |
| 0.6 | 0.0076 | -0.3150 | -0.3933 | -0.4117 | -0.4334 |
| 0.7 | -0.1780 | -0.3347 | -0.3633 | -0.4114 | -0.4353 |
| 0.8 | -0.2042 | -0.3000 | -0.3571 | -0.3958 | -0.4276 |
| 0.9 | -0.1863 | -0.2724 | -0.3292 | -0.3684 | -0.3929 |

TABLE C2. Continued

(c) $M = 2.0$

| ALPHA = ETA | 4.00 | 8.00 | 12.00 | 16.00 | 20.00 |
|----------------|---------|---------|---------|---------|---------|
| -0.9 | -0.1742 | -0.2204 | -0.2564 | -0.2812 | -0.3011 |
| -0.8 | -0.1627 | -0.2323 | -0.2627 | -0.2902 | -0.3024 |
| -0.7 | -0.1332 | -0.2393 | -0.2823 | -0.3019 | -0.3156 |
| -0.6 | -0.0424 | -0.2364 | -0.2878 | -0.3096 | -0.3167 |
| -0.5 | -0.0296 | -0.1685 | -0.2998 | -0.3132 | -0.3174 |
| -0.4 | -0.0304 | -0.0483 | -0.1688 | -0.2932 | -0.3189 |
| -0.3 | -0.0331 | -0.0633 | -0.0914 | -0.1803 | -0.2666 |
| -0.2 | -0.0347 | -0.0665 | -0.0958 | -0.1329 | -0.1874 |
| -0.1 | -0.0334 | -0.0673 | -0.0989 | -0.1293 | -0.1658 |
| 0.0 | -0.0333 | -0.0680 | -0.1001 | -0.1306 | -0.1610 |
| 0.1 | -0.0338 | -0.0685 | -0.1006 | -0.1314 | -0.1651 |
| 0.2 | -0.0344 | -0.0686 | -0.0988 | -0.1337 | -0.1864 |
| 0.3 | -0.0347 | -0.0662 | -0.0952 | -0.1660 | -0.2502 |
| 0.4 | -0.0331 | -0.0549 | -0.1368 | -0.2766 | -0.3121 |
| 0.5 | -0.0266 | -0.1058 | -0.2937 | -0.3121 | -0.3165 |
| 0.6 | -0.0536 | -0.2397 | -0.2901 | -0.3081 | -0.3151 |
| 0.7 | -0.1263 | -0.2437 | -0.2836 | -0.3058 | -0.3138 |
| 0.8 | -0.1618 | -0.2361 | -0.2636 | -0.2910 | -0.3027 |
| 0.9 | -0.1676 | -0.2224 | -0.2581 | -0.2832 | -0.3045 |

(d) $M = 2.4$

| ALPHA = ETA | 4.00 | 8.00 | 12.00 | 16.00 | 20.00 |
|----------------|---------|---------|---------|---------|---------|
| -0.9 | -0.1485 | -0.1734 | -0.1920 | -0.2038 | -0.2116 |
| -0.8 | -0.1382 | -0.1786 | -0.1973 | -0.2109 | -0.2178 |
| -0.7 | -0.0679 | -0.1717 | -0.2028 | -0.2131 | -0.2184 |
| -0.6 | -0.0327 | -0.1441 | -0.1965 | -0.2114 | -0.2198 |
| -0.5 | -0.0353 | -0.1209 | -0.1886 | -0.2105 | -0.2206 |
| -0.4 | -0.0378 | -0.0738 | -0.1805 | -0.2136 | -0.2217 |
| -0.3 | -0.0332 | -0.0584 | -0.0866 | -0.1791 | -0.2090 |
| -0.2 | -0.0333 | -0.0613 | -0.0819 | -0.1141 | -0.1637 |
| -0.1 | -0.0330 | -0.0616 | -0.0844 | -0.1082 | -0.1390 |
| 0.0 | -0.0321 | -0.0608 | -0.0849 | -0.1073 | -0.1312 |
| 0.1 | -0.0327 | -0.0609 | -0.0849 | -0.1082 | -0.1359 |
| 0.2 | -0.0327 | -0.0610 | -0.0841 | -0.1147 | -0.1547 |
| 0.3 | -0.0332 | -0.0583 | -0.0812 | -0.1593 | -0.2008 |
| 0.4 | -0.0329 | -0.0561 | -0.1699 | -0.2137 | -0.2219 |
| 0.5 | -0.0338 | -0.1278 | -0.1914 | -0.2108 | -0.2209 |
| 0.6 | -0.0457 | -0.1468 | -0.1961 | -0.2090 | -0.2188 |
| 0.7 | -0.0685 | -0.1678 | -0.2022 | -0.2109 | -0.2144 |
| 0.8 | -0.1247 | -0.1759 | -0.1971 | -0.2101 | -0.2135 |
| 0.9 | -0.1404 | -0.1732 | -0.1949 | -0.2097 | -0.2157 |

TABLE C2. Concluded

| ALPHA = ETA | (e) $M = 2.8$ | | | | |
|----------------|---------------|---------|---------|---------|---------|
| | 4.00 | 8.00 | 12.00 | 16.00 | 20.00 |
| -0.9 | -0.0963 | -0.1269 | -0.1355 | -0.1445 | -0.1487 |
| -0.8 | -0.0873 | -0.1325 | -0.1436 | -0.1541 | -0.1580 |
| -0.7 | -0.0668 | -0.1298 | -0.1478 | -0.1569 | -0.1591 |
| -0.6 | -0.0413 | -0.1176 | -0.1455 | -0.1564 | -0.1588 |
| -0.5 | -0.0327 | -0.0893 | -0.1349 | -0.1513 | -0.1588 |
| -0.4 | -0.0312 | -0.0630 | -0.1211 | -0.1504 | -0.1587 |
| -0.3 | -0.0291 | -0.0543 | -0.1071 | -0.1476 | -0.1582 |
| -0.2 | -0.0294 | -0.0553 | -0.0729 | -0.1016 | -0.1360 |
| -0.1 | -0.0289 | -0.0538 | -0.0715 | -0.0919 | -0.1127 |
| 0.0 | -0.0288 | -0.0526 | -0.0713 | -0.0905 | -0.1069 |
| 0.1 | -0.0287 | -0.0529 | -0.0712 | -0.0920 | -0.1118 |
| 0.2 | -0.0289 | -0.0528 | -0.0697 | -0.0959 | -0.1288 |
| 0.3 | -0.0294 | -0.0514 | -0.0982 | -0.1430 | -0.1584 |
| 0.4 | -0.0310 | -0.0684 | -0.1254 | -0.1507 | -0.1595 |
| 0.5 | -0.0333 | -0.0915 | -0.1356 | -0.1499 | -0.1592 |
| 0.6 | -0.0371 | -0.1145 | -0.1453 | -0.1556 | -0.1574 |
| 0.7 | -0.0617 | -0.1289 | -0.1484 | -0.1574 | -0.1582 |
| 0.8 | -0.0858 | -0.1282 | -0.1450 | -0.1551 | -0.1567 |
| 0.9 | -0.0987 | -0.1271 | -0.1418 | -0.1529 | -0.1553 |

TABLE C3. PRESSURE-COEFFICIENT DATA FOR DELTA WING WITH $\Lambda_{LE} = 60.0^\circ$ (a) $M = 1.5$

| ALPHA = ETA | 4.01 | 8.01 | 12.00 | 16.00 | 20.00 |
|----------------|---------|---------|---------|---------|-------|
| -0.9 | -0.2864 | -0.3794 | -0.4476 | -0.4937 | N |
| -0.8 | -0.2525 | -0.3858 | -0.4681 | -0.5076 | O |
| -0.7 | -0.1766 | -0.3894 | -0.4839 | -0.5299 | |
| -0.6 | -0.0429 | -0.3721 | -0.4852 | -0.5330 | D |
| -0.5 | -0.0429 | -0.0381 | -0.4392 | -0.5523 | A |
| -0.4 | -0.0473 | -0.0866 | -0.1178 | -0.3451 | T |
| -0.3 | -0.0476 | -0.0983 | -0.1401 | -0.1880 | A |
| -0.2 | -0.0445 | -0.0994 | -0.1472 | -0.1911 | |
| -0.1 | -0.0434 | -0.0976 | -0.1472 | -0.1924 | |
| 0.0 | -0.0433 | -0.0985 | -0.1501 | -0.1948 | |
| 0.1 | -0.0434 | -0.0998 | -0.1492 | -0.1922 | |
| 0.2 | -0.0456 | -0.1018 | -0.1503 | -0.1920 | |
| 0.3 | -0.0480 | -0.1003 | -0.1421 | -0.1871 | |
| 0.4 | -0.0496 | -0.0892 | -0.1187 | -0.3420 | |
| 0.5 | -0.0409 | -0.0359 | -0.4281 | -0.5558 | |
| 0.6 | -0.0301 | -0.3772 | -0.4876 | -0.5388 | |
| 0.7 | -0.1954 | -0.4016 | -0.4900 | -0.5319 | |
| 0.8 | -0.2549 | -0.3920 | -0.4653 | -0.5043 | |
| 0.9 | -0.2901 | -0.3759 | -0.4416 | -0.4890 | |

(b) $M = 1.7$

| ALPHA = ETA | 4.00 | 8.01 | 12.00 | 16.00 | 20.01 |
|----------------|---------|---------|---------|---------|---------|
| -0.9 | -0.3175 | -0.3345 | -0.3735 | -0.4018 | -0.4209 |
| -0.8 | -0.1389 | -0.3091 | -0.3829 | -0.4110 | -0.4325 |
| -0.7 | -0.0995 | -0.2841 | -0.3735 | -0.4204 | -0.4417 |
| -0.6 | -0.0570 | -0.2493 | -0.3526 | -0.4132 | -0.4415 |
| -0.5 | -0.0484 | -0.1695 | -0.3410 | -0.4038 | -0.4384 |
| -0.4 | -0.0469 | -0.0752 | -0.1384 | -0.3794 | -0.4456 |
| -0.3 | -0.0452 | -0.0890 | -0.1278 | -0.1683 | -0.3064 |
| -0.2 | -0.0425 | -0.0895 | -0.1335 | -0.1709 | -0.2114 |
| -0.1 | -0.0388 | -0.0873 | -0.1296 | -0.1681 | -0.2046 |
| 0.0 | -0.0388 | -0.0871 | -0.1302 | -0.1694 | -0.2042 |
| 0.1 | -0.0386 | -0.0866 | -0.1300 | -0.1683 | -0.2046 |
| 0.2 | -0.0419 | -0.0897 | -0.1347 | -0.1707 | -0.2108 |
| 0.3 | -0.0423 | -0.0871 | -0.1291 | -0.1692 | -0.3029 |
| 0.4 | -0.0471 | -0.0739 | -0.1169 | -0.3707 | -0.4419 |
| 0.5 | -0.0511 | -0.1680 | -0.3474 | -0.4081 | -0.4426 |
| 0.6 | -0.0513 | -0.2611 | -0.3618 | -0.4169 | -0.4384 |
| 0.7 | -0.1207 | -0.2881 | -0.3763 | -0.4235 | -0.4406 |
| 0.8 | -0.1757 | -0.3214 | -0.3844 | -0.4088 | -0.4294 |
| 0.9 | -0.2897 | -0.3223 | -0.3684 | -0.3915 | -0.4044 |

TABLE C3. Continued

(c) $M = 2.0$

| ALPHA = | 4.00 | 8.00 | 12.01 | 16.01 | 20.00 |
|---------|---------|---------|---------|---------|---------|
| ETA | | | | | |
| -0.9 | -0.1907 | -0.2705 | -0.2735 | -0.2810 | -0.2941 |
| -0.8 | -0.1434 | -0.2333 | -0.2781 | -0.2849 | -0.3080 |
| -0.7 | -0.0644 | -0.2127 | -0.2862 | -0.2950 | -0.3172 |
| -0.6 | -0.0454 | -0.1303 | -0.2096 | -0.2973 | -0.3177 |
| -0.5 | -0.0413 | -0.0990 | -0.1956 | -0.2644 | -0.3118 |
| -0.4 | -0.0396 | -0.0893 | -0.1844 | -0.2455 | -0.3042 |
| -0.3 | -0.0377 | -0.0800 | -0.1204 | -0.2081 | -0.2766 |
| -0.2 | -0.0354 | -0.0779 | -0.1102 | -0.1357 | -0.1725 |
| -0.1 | -0.0336 | -0.0737 | -0.1088 | -0.1418 | -0.1724 |
| 0.0 | -0.0349 | -0.0750 | -0.1088 | -0.1425 | -0.1707 |
| 0.1 | -0.0337 | -0.0748 | -0.1094 | -0.1438 | -0.1721 |
| 0.2 | -0.0354 | -0.0757 | -0.1113 | -0.1524 | -0.1822 |
| 0.3 | -0.0363 | -0.0785 | -0.1196 | -0.1542 | -0.2660 |
| 0.4 | -0.0394 | -0.0961 | -0.1860 | -0.2774 | -0.3081 |
| 0.5 | -0.0414 | -0.1000 | -0.1982 | -0.2844 | -0.3116 |
| 0.6 | -0.0478 | -0.1302 | -0.2094 | -0.2966 | -0.3196 |
| 0.7 | -0.0701 | -0.2154 | -0.2862 | -0.3062 | -0.3198 |
| 0.8 | -0.1449 | -0.2505 | -0.2811 | -0.3017 | -0.3141 |
| 0.9 | -0.1884 | -0.2704 | -0.2764 | -0.2835 | -0.2950 |

(d) $M = 2.4$

| ALPHA = | 3.99 | 7.99 | 12.00 | 16.00 | 20.01 |
|---------|---------|---------|---------|---------|---------|
| ETA | | | | | |
| -0.9 | -0.0967 | -0.1624 | -0.1898 | -0.1925 | -0.1952 |
| -0.8 | -0.0882 | -0.1510 | -0.1933 | -0.1981 | -0.2019 |
| -0.7 | -0.0809 | -0.1428 | -0.1875 | -0.1989 | -0.2035 |
| -0.6 | -0.0717 | -0.1342 | -0.1811 | -0.2018 | -0.2076 |
| -0.5 | -0.0485 | -0.1100 | -0.1546 | -0.1972 | -0.2101 |
| -0.4 | -0.0399 | -0.0834 | -0.1371 | -0.1791 | -0.2047 |
| -0.3 | -0.0375 | -0.0706 | -0.1119 | -0.1533 | -0.2020 |
| -0.2 | -0.0362 | -0.0693 | -0.0960 | -0.1311 | -0.1592 |
| -0.1 | -0.0346 | -0.0669 | -0.0933 | -0.1162 | -0.1414 |
| 0.0 | -0.0350 | -0.0669 | -0.0924 | -0.1172 | -0.1384 |
| 0.1 | -0.0343 | -0.0664 | -0.0937 | -0.1171 | -0.1405 |
| 0.2 | -0.0361 | -0.0698 | -0.0951 | -0.1244 | -0.1536 |
| 0.3 | -0.0366 | -0.0730 | -0.1095 | -0.1662 | -0.2002 |
| 0.4 | -0.0390 | -0.0772 | -0.1392 | -0.1747 | -0.2055 |
| 0.5 | -0.0413 | -0.1038 | -0.1610 | -0.1994 | -0.2141 |
| 0.6 | -0.0681 | -0.1338 | -0.1849 | -0.2026 | -0.2115 |
| 0.7 | -0.0816 | -0.1458 | -0.1929 | -0.2010 | -0.2080 |
| 0.8 | -0.0905 | -0.1531 | -0.1922 | -0.2003 | -0.2044 |
| 0.9 | -0.1035 | -0.1710 | -0.1899 | -0.1970 | -0.1973 |

TABLE C3. Concluded

(e) $M = 2.8$

| ALPHA = ETA | 4.00 | 8.00 | 12.00 | 16.00 | 19.99 |
|----------------|---------|---------|---------|---------|---------|
| -0.9 | -0.0552 | -0.1030 | -0.1292 | -0.1320 | -0.1363 |
| -0.8 | -0.0567 | -0.1018 | -0.1284 | -0.1384 | -0.1437 |
| -0.7 | -0.0566 | -0.0985 | -0.1216 | -0.1380 | -0.1449 |
| -0.6 | -0.0537 | -0.0944 | -0.1203 | -0.1381 | -0.1472 |
| -0.5 | -0.0499 | -0.0913 | -0.1202 | -0.1389 | -0.1447 |
| -0.4 | -0.0466 | -0.0896 | -0.1196 | -0.1380 | -0.1448 |
| -0.3 | -0.0364 | -0.0638 | -0.1128 | -0.1327 | -0.1460 |
| -0.2 | -0.0324 | -0.0583 | -0.0783 | -0.1073 | -0.1406 |
| -0.1 | -0.0315 | -0.0598 | -0.0803 | -0.0978 | -0.1112 |
| 0.0 | -0.0321 | -0.0593 | -0.0808 | -0.0976 | -0.1105 |
| 0.1 | -0.0318 | -0.0597 | -0.0804 | -0.0975 | -0.1112 |
| 0.2 | -0.0316 | -0.0586 | -0.0787 | -0.1000 | -0.1366 |
| 0.3 | -0.0343 | -0.0704 | -0.1087 | -0.1314 | -0.1453 |
| 0.4 | -0.0448 | -0.0901 | -0.1202 | -0.1376 | -0.1445 |
| 0.5 | -0.0497 | -0.0915 | -0.1225 | -0.1428 | -0.1472 |
| 0.6 | -0.0528 | -0.0940 | -0.1228 | -0.1398 | -0.1474 |
| 0.7 | -0.0568 | -0.0981 | -0.1249 | -0.1406 | -0.1476 |
| 0.8 | -0.0576 | -0.1024 | -0.1300 | -0.1396 | -0.1451 |
| 0.9 | -0.0571 | -0.1086 | -0.1370 | -0.1360 | -0.1386 |

TABLE C4. PRESSURE-COEFFICIENT DATA FOR DELTA WING WITH $\Lambda_{LE} = 52.5^\circ$ (a) $M = 1.5$

| ALPHA = | 4.01 | 7.99 | 12.00 | 16.01 | 20.01 |
|---------|---------|---------|---------|---------|-------|
| ETA | | | | | |
| -0.9 | -0.3521 | -0.4790 | -0.5022 | -0.5102 | N |
| -0.8 | -0.2494 | -0.4485 | -0.5115 | -0.4989 | D |
| -0.7 | -0.0837 | -0.3246 | -0.4630 | -0.5056 | |
| -0.6 | -0.0712 | -0.1736 | -0.3855 | -0.4940 | D |
| -0.5 | -0.0638 | -0.1589 | -0.3117 | -0.4544 | A |
| -0.4 | -0.0598 | -0.1275 | -0.2048 | -0.4267 | T |
| -0.3 | -0.0553 | -0.1228 | -0.1742 | -0.1896 | A |
| -0.2 | -0.0547 | -0.1213 | -0.1709 | -0.2113 | |
| -0.1 | -0.0509 | -0.1141 | -0.1669 | -0.2121 | |
| 0.0 | -0.0538 | -0.1152 | -0.1671 | -0.2127 | |
| 0.1 | -0.0508 | -0.1140 | -0.1658 | -0.2133 | |
| 0.2 | -0.0623 | -0.1278 | -0.1719 | -0.2199 | |
| 0.3 | -0.0586 | -0.1234 | -0.1591 | -0.1923 | |
| 0.4 | -0.0648 | -0.1252 | -0.2294 | -0.4238 | |
| 0.5 | -0.0666 | -0.1768 | -0.3555 | -0.4760 | |
| 0.6 | | | | | |
| 0.7 | -0.0842 | -0.2696 | -0.4595 | -0.5318 | |
| 0.8 | -0.2188 | -0.4538 | -0.4600 | -0.4881 | |
| 0.9 | | | | | |

(b) $M = 1.7$

| ALPHA = | 4.00 | 8.00 | 12.00 | 16.01 | 20.01 |
|---------|---------|---------|---------|---------|---------|
| ETA | | | | | |
| -0.9 | -0.2375 | -0.3564 | -0.3848 | -0.4129 | -0.3889 |
| -0.8 | -0.1908 | -0.3061 | -0.3931 | -0.4239 | -0.4054 |
| -0.7 | -0.1065 | -0.2778 | -0.3805 | -0.4242 | -0.4070 |
| -0.6 | -0.0670 | -0.1875 | -0.3391 | -0.4079 | -0.4078 |
| -0.5 | -0.0570 | -0.1329 | -0.2256 | -0.3028 | -0.4070 |
| -0.4 | -0.0532 | -0.1127 | -0.1726 | -0.2607 | -0.3886 |
| -0.3 | -0.0524 | -0.1076 | -0.1563 | -0.2256 | -0.3180 |
| -0.2 | -0.0502 | -0.1038 | -0.1592 | -0.2009 | -0.2370 |
| -0.1 | -0.0456 | -0.0975 | -0.1477 | -0.1902 | -0.2283 |
| 0.0 | -0.0450 | -0.0966 | -0.1458 | -0.1870 | -0.2243 |
| 0.1 | -0.0455 | -0.0969 | -0.1467 | -0.1899 | -0.2278 |
| 0.2 | -0.0540 | -0.1064 | -0.1492 | -0.1890 | -0.2336 |
| 0.3 | -0.0530 | -0.1079 | -0.1630 | -0.2188 | -0.2768 |
| 0.4 | -0.0558 | -0.1107 | -0.2073 | -0.3145 | -0.3886 |
| 0.5 | -0.0595 | -0.1215 | -0.2187 | -0.3343 | -0.4062 |
| 0.6 | | | | | |
| 0.7 | -0.0938 | -0.2730 | -0.3750 | -0.4023 | -0.4036 |
| 0.8 | -0.1873 | -0.3052 | -0.3962 | -0.4103 | -0.3996 |
| 0.9 | | | | | |

TABLE C4. Continued

(c) $M = 2.0$

| ALPHA = ETA | 4.00 | 8.01 | 11.99 | 16.00 | 20.00 |
|----------------|---------|---------|---------|---------|---------|
| -0.9 | -0.1135 | -0.2025 | -0.2682 | -0.2740 | -0.2951 |
| -0.8 | -0.1012 | -0.1888 | -0.2545 | -0.2856 | -0.3103 |
| -0.7 | -0.0964 | -0.1794 | -0.2410 | -0.2873 | -0.3165 |
| -0.6 | -0.0777 | -0.1718 | -0.2336 | -0.2838 | -0.3143 |
| -0.5 | -0.0521 | -0.1364 | -0.2019 | -0.2752 | -0.3037 |
| -0.4 | -0.0445 | -0.0933 | -0.1702 | -0.2332 | -0.2812 |
| -0.3 | -0.0435 | -0.0901 | -0.1259 | -0.1661 | -0.2572 |
| -0.2 | -0.0410 | -0.0867 | -0.1298 | -0.1636 | -0.1954 |
| -0.1 | -0.0397 | -0.0844 | -0.1204 | -0.1535 | -0.1864 |
| 0.0 | -0.0396 | -0.0834 | -0.1212 | -0.1538 | -0.1847 |
| 0.1 | -0.0402 | -0.0851 | -0.1240 | -0.1562 | -0.1856 |
| 0.2 | -0.0436 | -0.0887 | -0.1250 | -0.1608 | -0.1828 |
| 0.3 | -0.0437 | -0.0915 | -0.1383 | -0.1875 | -0.2751 |
| 0.4 | -0.0460 | -0.0976 | -0.1519 | -0.2126 | -0.2857 |
| 0.5 | -0.0492 | -0.1365 | -0.2116 | -0.2760 | -0.2941 |
| 0.6 | | | | | |
| 0.7 | -0.0984 | -0.1832 | -0.2431 | -0.2865 | -0.3167 |
| 0.8 | -0.1063 | -0.1920 | -0.2557 | -0.2865 | -0.3121 |
| 0.9 | | | | | |

(d) $M = 2.4$

| ALPHA = ETA | 4.00 | 8.00 | 11.99 | 16.00 | 20.00 |
|----------------|---------|---------|---------|---------|---------|
| -0.9 | -0.0596 | -0.1187 | -0.1630 | -0.1772 | -0.1841 |
| -0.8 | -0.0595 | -0.1201 | -0.1646 | -0.1903 | -0.1978 |
| -0.7 | -0.0644 | -0.1208 | -0.1621 | -0.1899 | -0.2004 |
| -0.6 | -0.0654 | -0.1187 | -0.1585 | -0.1835 | -0.2002 |
| -0.5 | -0.0603 | -0.1122 | -0.1515 | -0.1800 | -0.2035 |
| -0.4 | -0.0474 | -0.1093 | -0.1472 | -0.1789 | -0.2039 |
| -0.3 | -0.0416 | -0.0827 | -0.1348 | -0.1759 | -0.1970 |
| -0.2 | -0.0401 | -0.0803 | -0.1108 | -0.1469 | -0.1868 |
| -0.1 | -0.0393 | -0.0755 | -0.1032 | -0.1269 | -0.1441 |
| 0.0 | -0.0396 | -0.0764 | -0.1027 | -0.1296 | -0.1442 |
| 0.1 | -0.0387 | -0.0737 | -0.1031 | -0.1271 | -0.1434 |
| 0.2 | -0.0385 | -0.0743 | -0.1005 | -0.1311 | -0.1737 |
| 0.3 | -0.0413 | -0.0848 | -0.1362 | -0.1727 | -0.1963 |
| 0.4 | -0.0476 | -0.1035 | -0.1474 | -0.1790 | -0.2002 |
| 0.5 | -0.0603 | -0.1131 | -0.1515 | -0.1788 | -0.1982 |
| 0.6 | | | | | |
| 0.7 | -0.0653 | -0.1217 | -0.1629 | -0.1905 | -0.2019 |
| 0.8 | -0.0642 | -0.1224 | -0.1677 | -0.1909 | -0.1985 |
| 0.9 | | | | | |

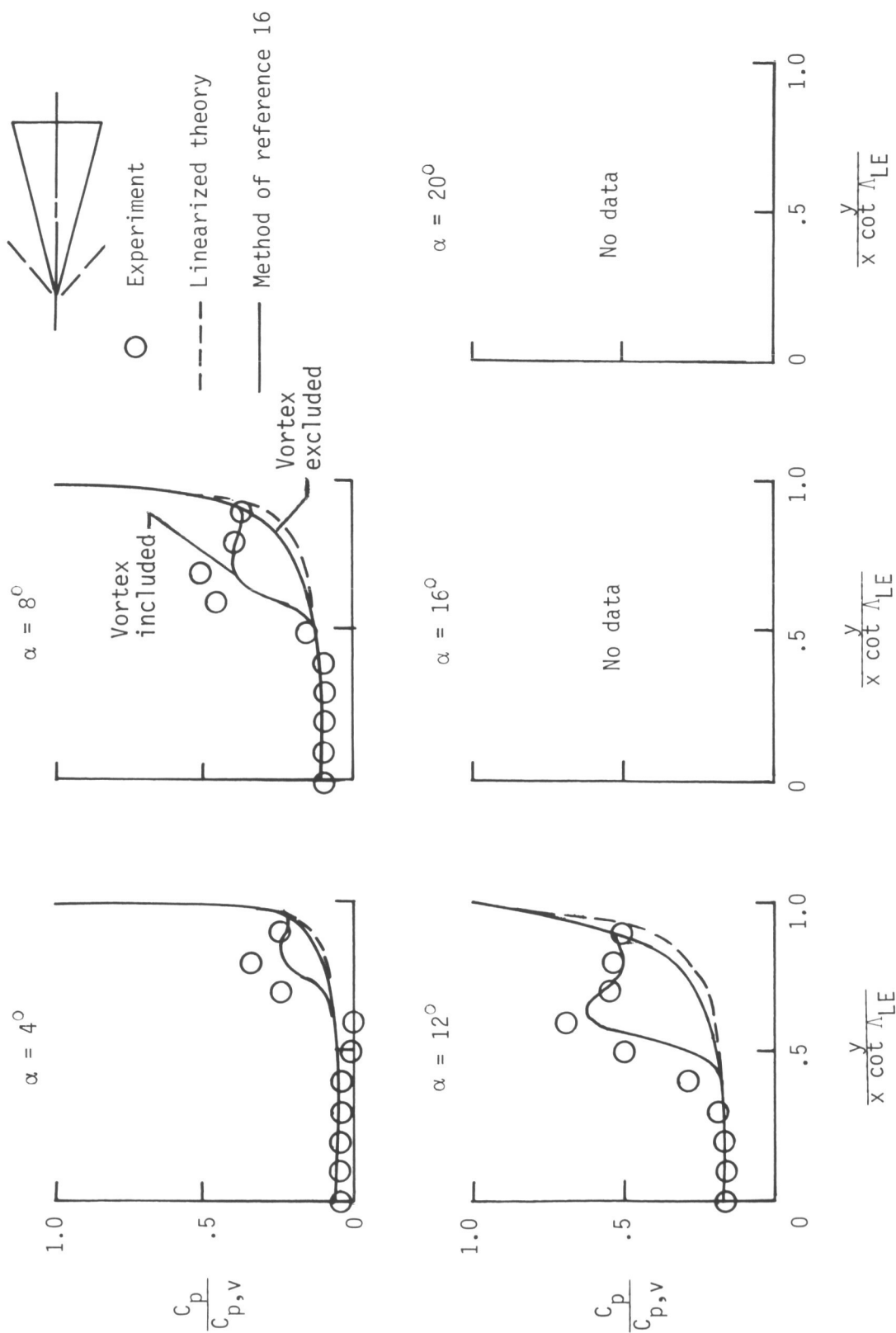
TABLE C4. Concluded

(e) $M = 2.8$

| ALPHA = ETA | 4.01 | 8.00 | 12.00 | 16.00 | 20.00 |
|----------------|---------|---------|---------|---------|---------|
| -0.9 | -0.0378 | -0.0754 | -0.1025 | -0.1205 | -0.1235 |
| -0.8 | -0.0471 | -0.0862 | -0.1147 | -0.1348 | -0.1376 |
| -0.7 | -0.0491 | -0.0887 | -0.1188 | -0.1337 | -0.1391 |
| -0.6 | -0.0489 | -0.0910 | -0.1190 | -0.1278 | -0.1407 |
| -0.5 | -0.0486 | -0.0864 | -0.1137 | -0.1261 | -0.1385 |
| -0.4 | -0.0459 | -0.0829 | -0.1107 | -0.1252 | -0.1365 |
| -0.3 | -0.0416 | -0.0808 | -0.1137 | -0.1274 | -0.1384 |
| -0.2 | -0.0359 | -0.0722 | -0.1121 | -0.1285 | -0.1398 |
| -0.1 | -0.0339 | -0.0625 | -0.0859 | -0.1043 | -0.1152 |
| 0.0 | -0.1365 | -0.0660 | -0.0895 | -0.1017 | -0.1095 |
| 0.1 | -0.0363 | -0.0636 | -0.0854 | -0.1018 | -0.1155 |
| 0.2 | -0.0378 | -0.0709 | -0.1063 | -0.1279 | -0.1379 |
| 0.3 | -0.0422 | -0.0772 | -0.1079 | -0.1262 | -0.1377 |
| 0.4 | -0.0449 | -0.0797 | -0.1073 | -0.1242 | -0.1374 |
| 0.5 | -0.0480 | -0.0851 | -0.1087 | -0.1221 | -0.1350 |
| 0.6 | | | | | |
| 0.7 | -0.0483 | -0.0881 | -0.1185 | -0.1269 | -0.1381 |
| 0.8 | -0.0469 | -0.0871 | -0.1168 | -0.1320 | -0.1365 |
| 0.9 | | | | | |

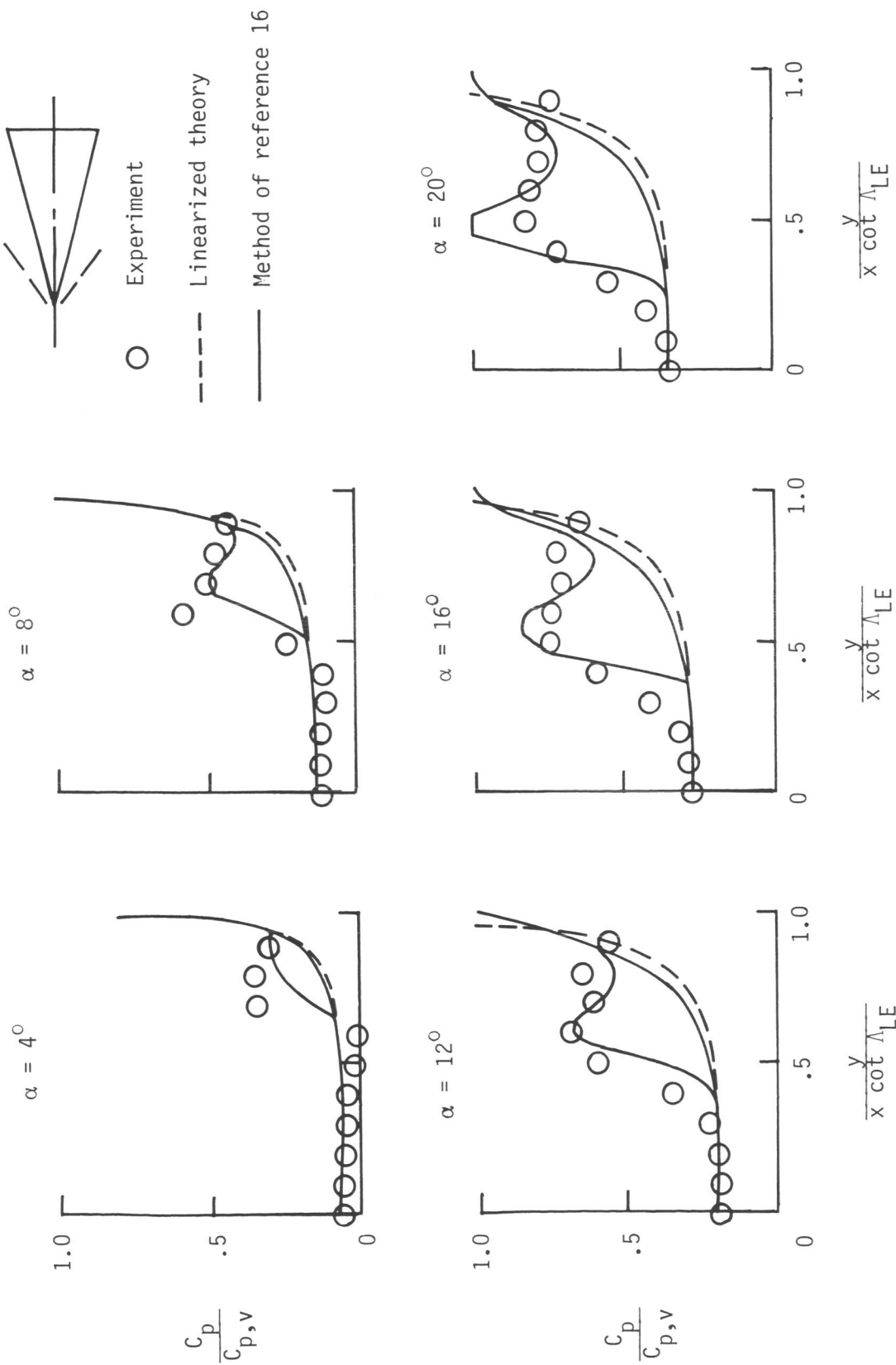
Appendix D—Pressure-Coefficient Plots

Experimental pressure-distribution plots for the four delta wings with leading-edge sweep angles of 75.0° , 67.5° , 60.0° , and 52.5° are presented in figures D1, D2, D3, and D4, respectively. Also presented are pressure distributions predicted by linearized theory and by a modified linearized theory in which the vortex effects can be included or excluded. (See fig. D1(a), $\alpha = 8^\circ$.) All the predicted results were obtained from the computer code described in reference 16.



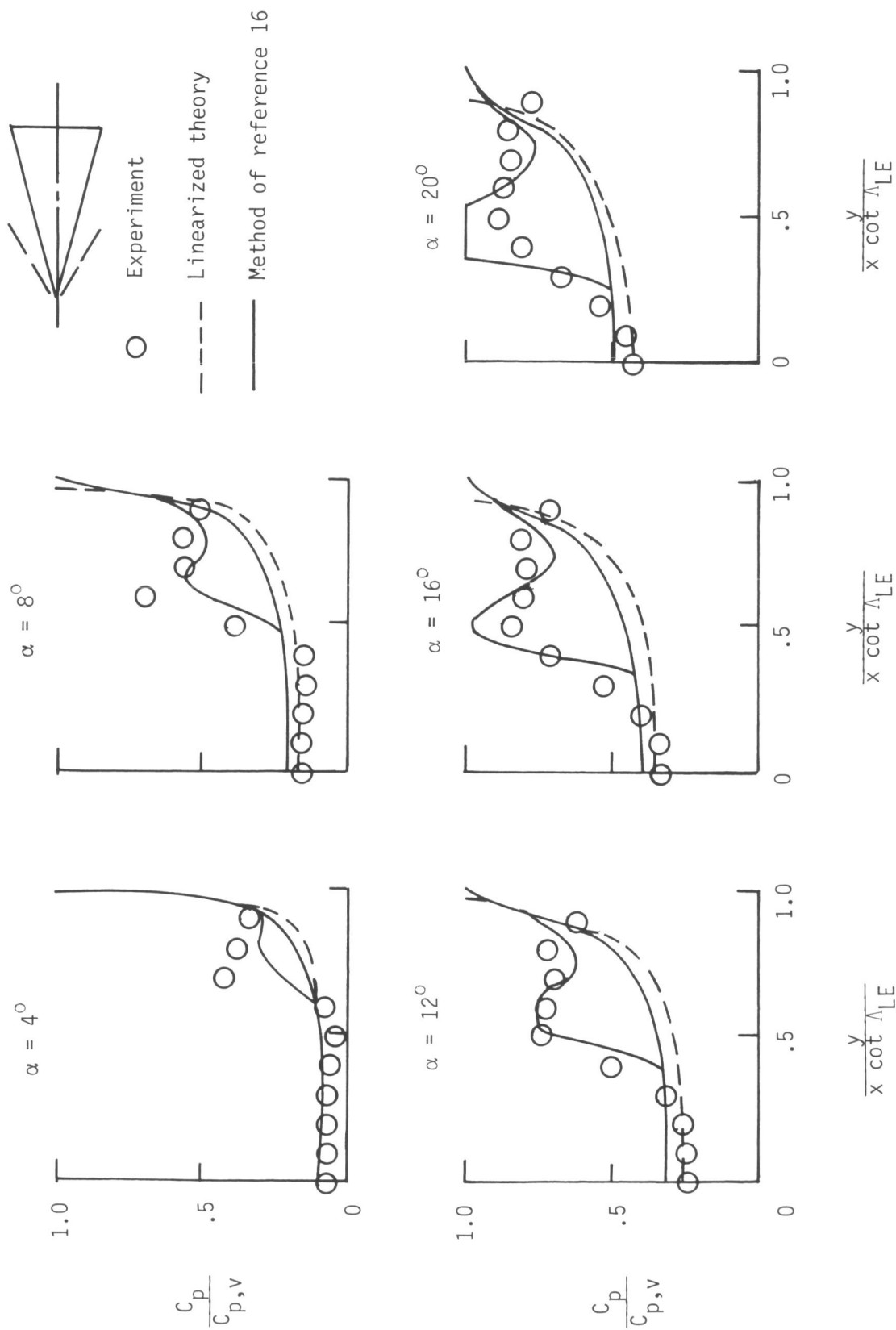
(a) $M = 1.5$.

Figure D1. Spanwise pressure distributions for delta wing with $\Lambda_{LE} = 75.0^\circ$.



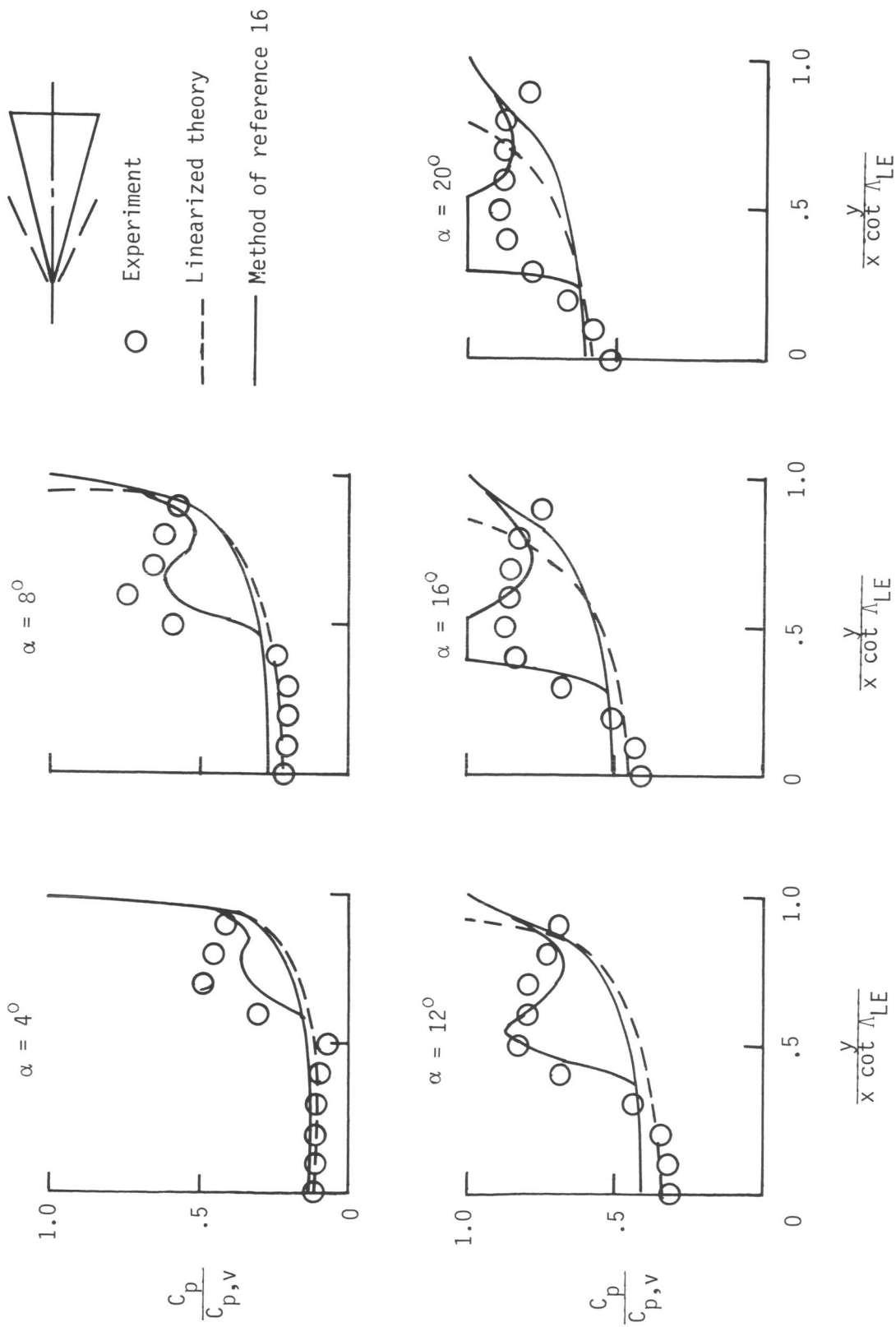
(b) $M = 1.7$.

Figure D1. Continued.



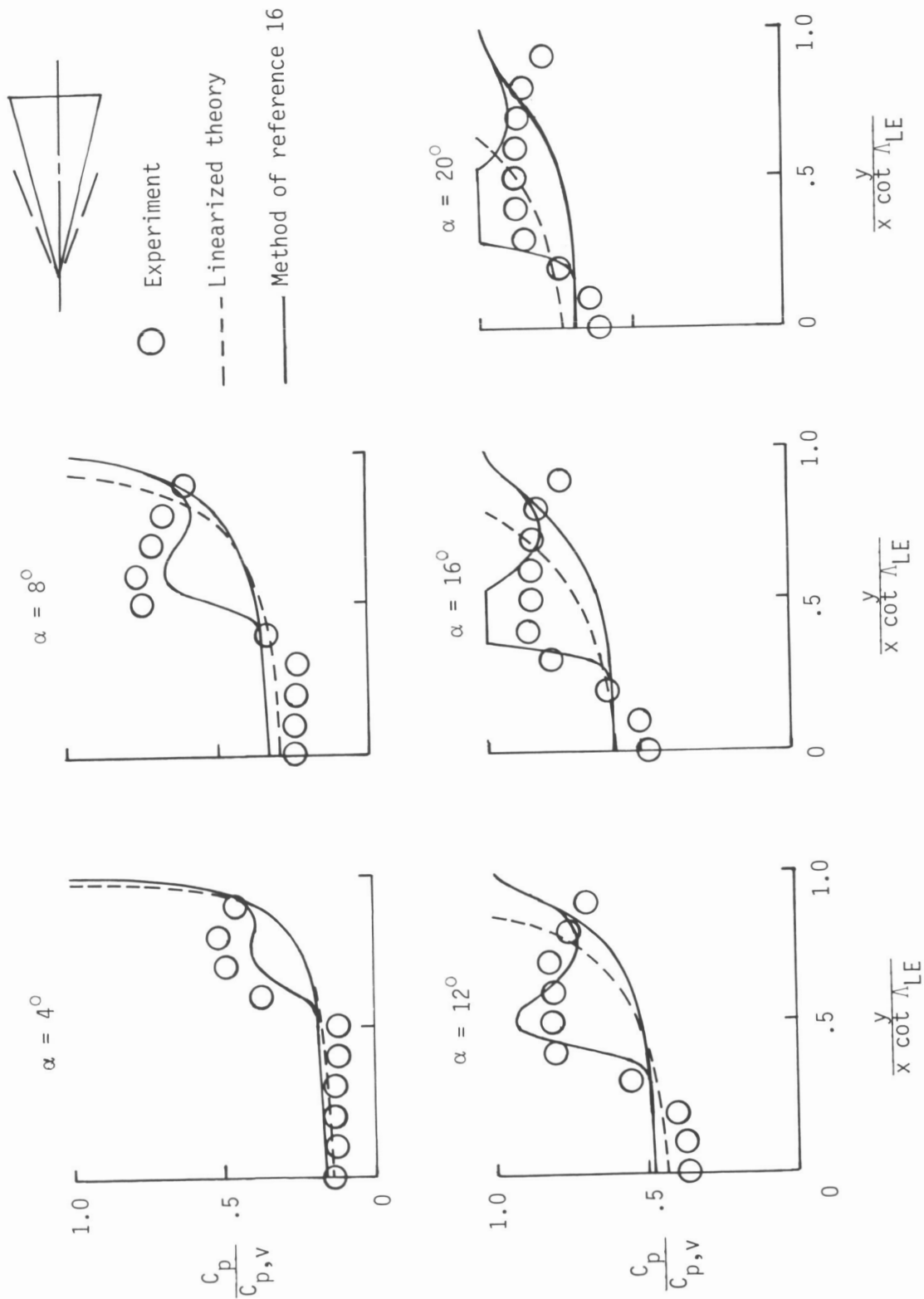
(c) $M = 2.0$.

Figure D1. Continued.



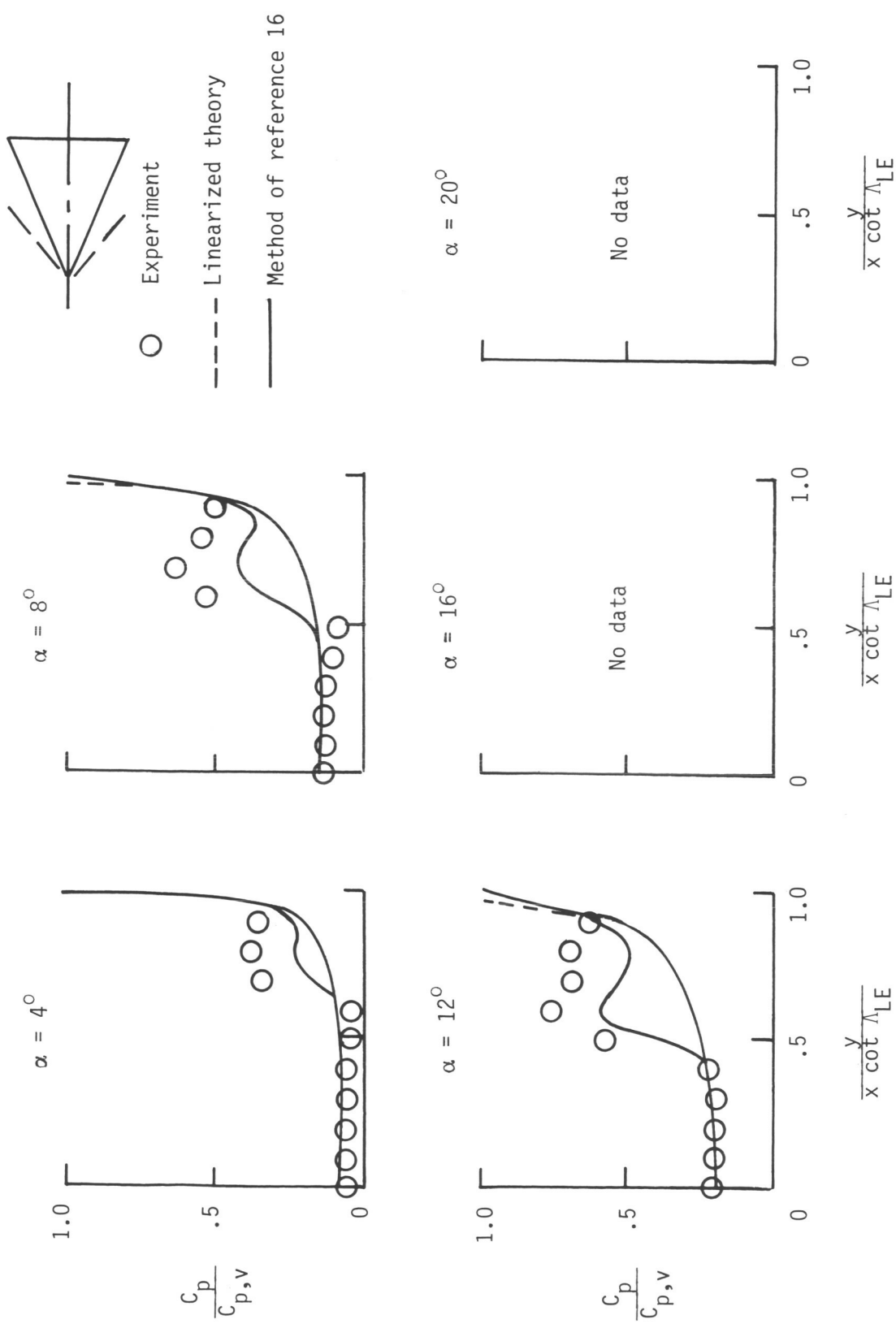
(d) $M = 2.4$.

Figure D1. Continued.



(e) $M = 2.8$.

Figure D1. Concluded.



(a) $M = 1.5$.

Figure D2. Spanwise pressure distributions for delta wing with $\Lambda_{LE} = 67.5^\circ$.

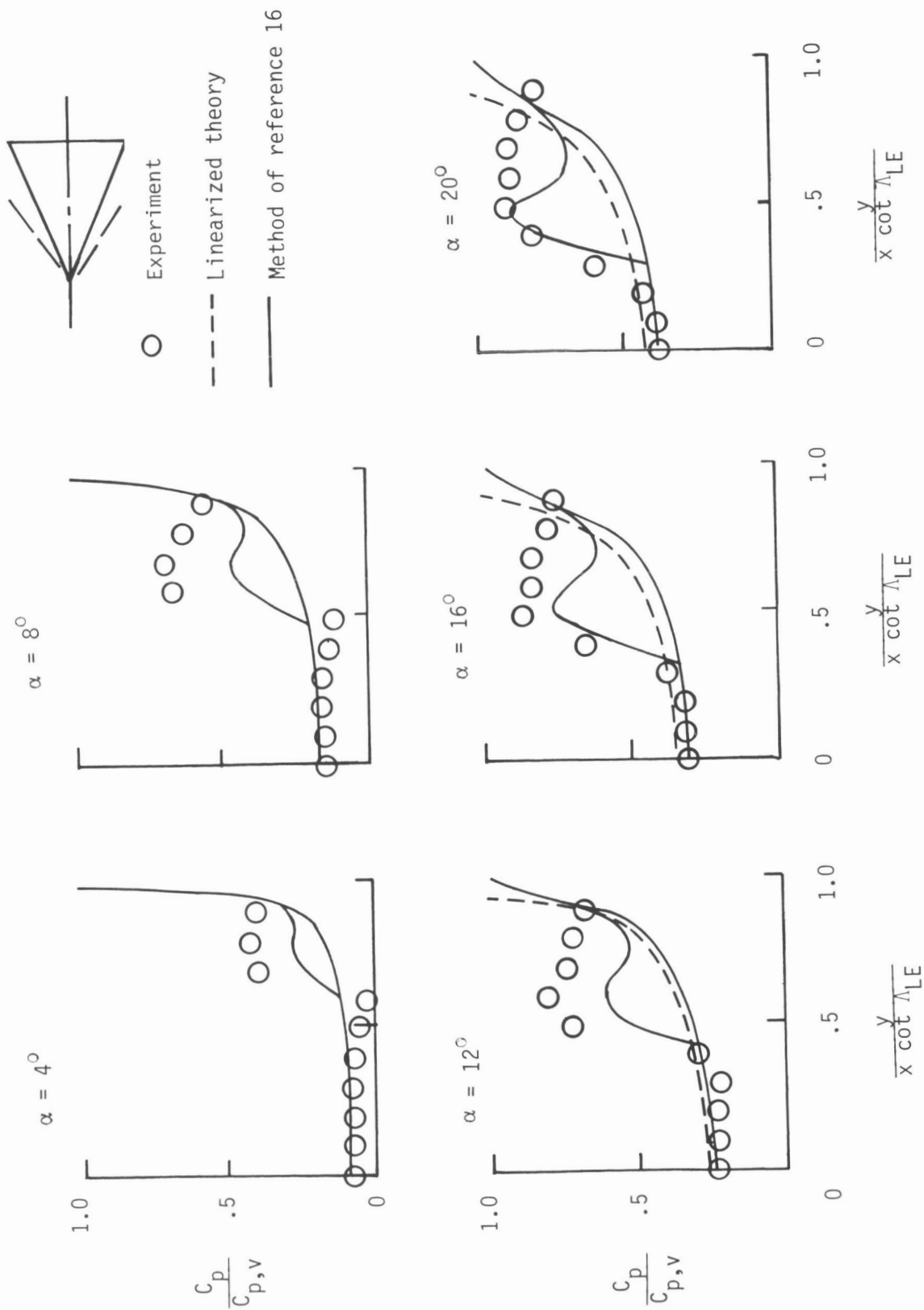
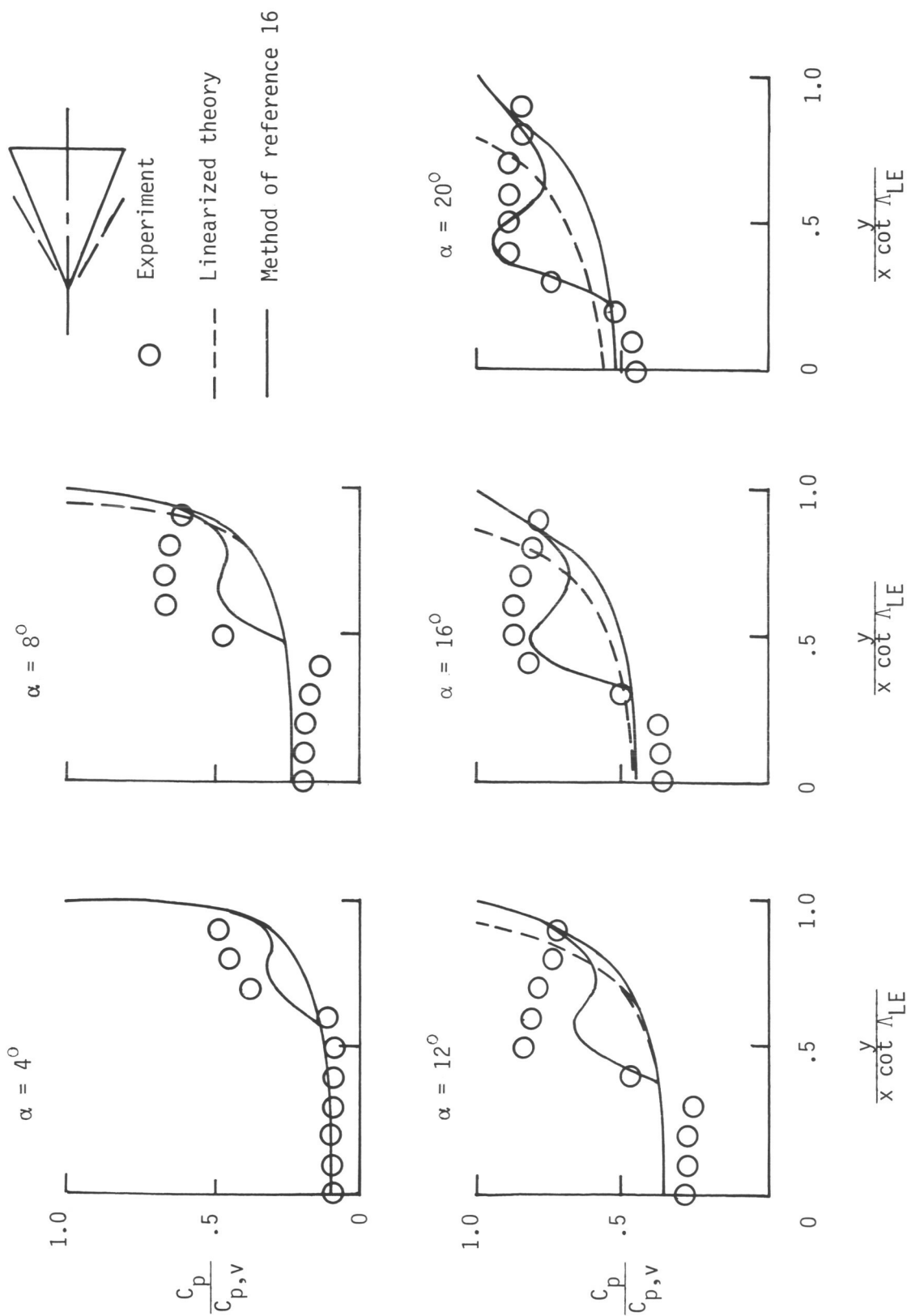
(b) $M = 1.7$.

Figure D2. Continued.



(c) $M = 2.0$.

Figure D2. Continued.

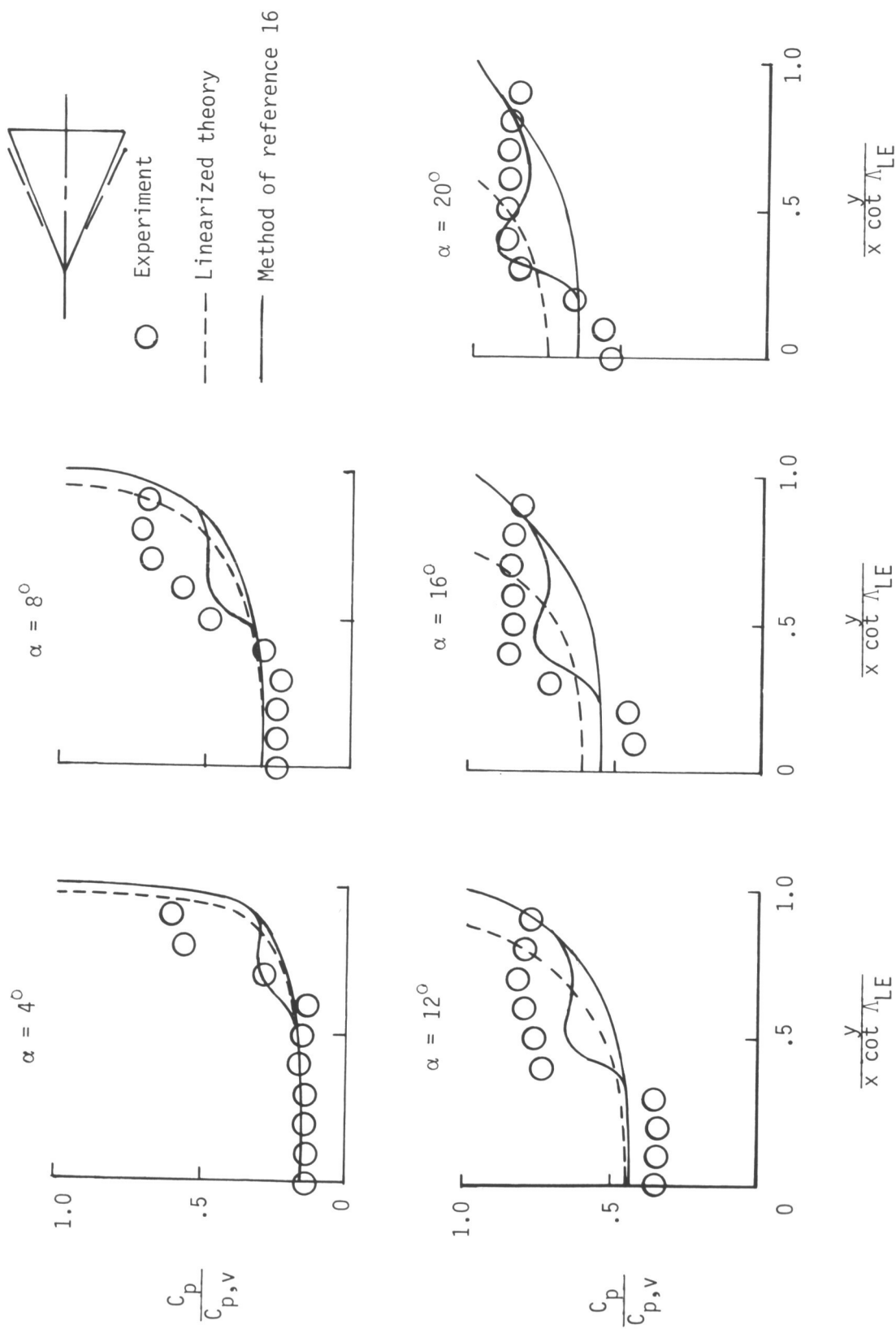
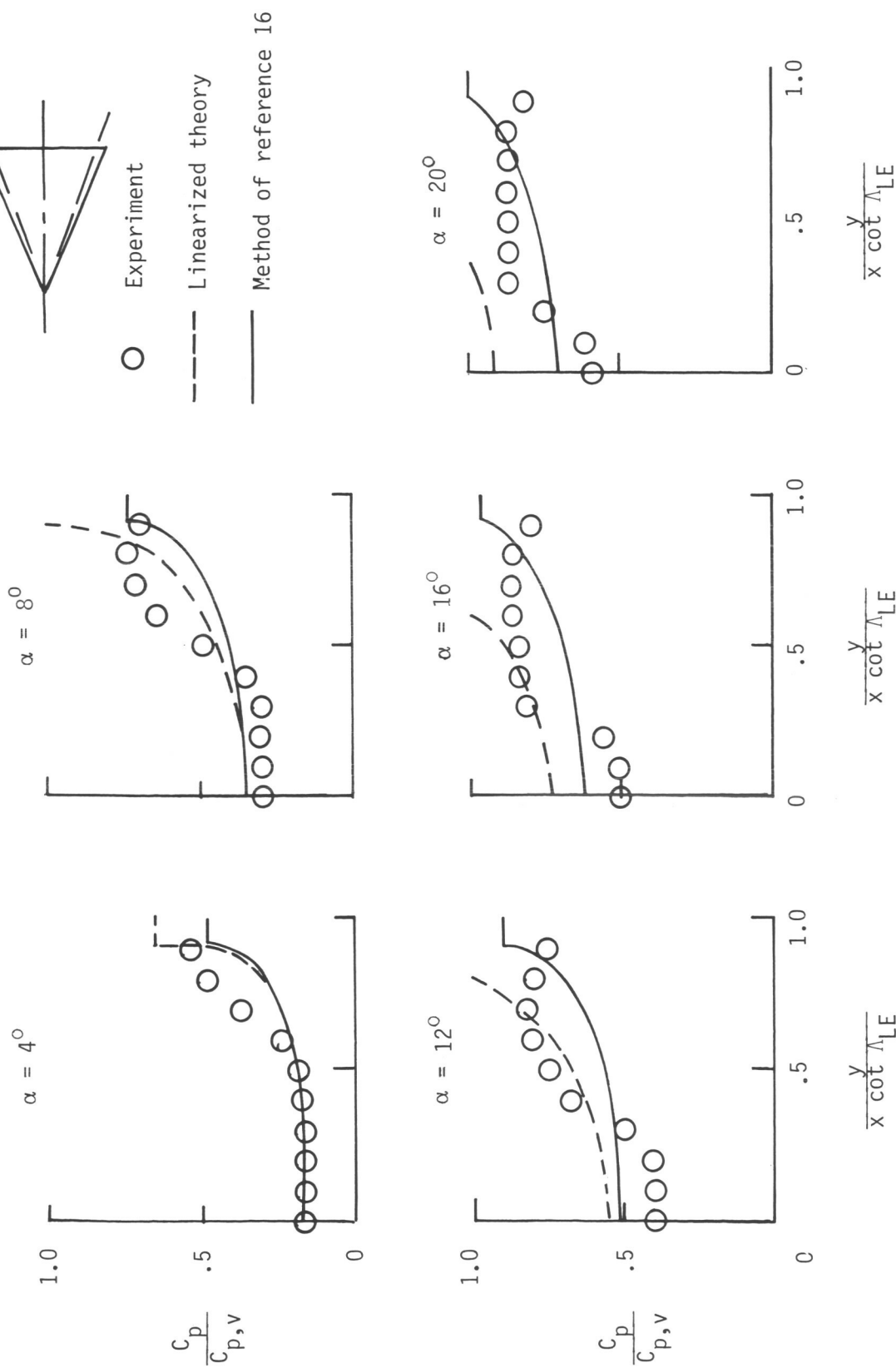
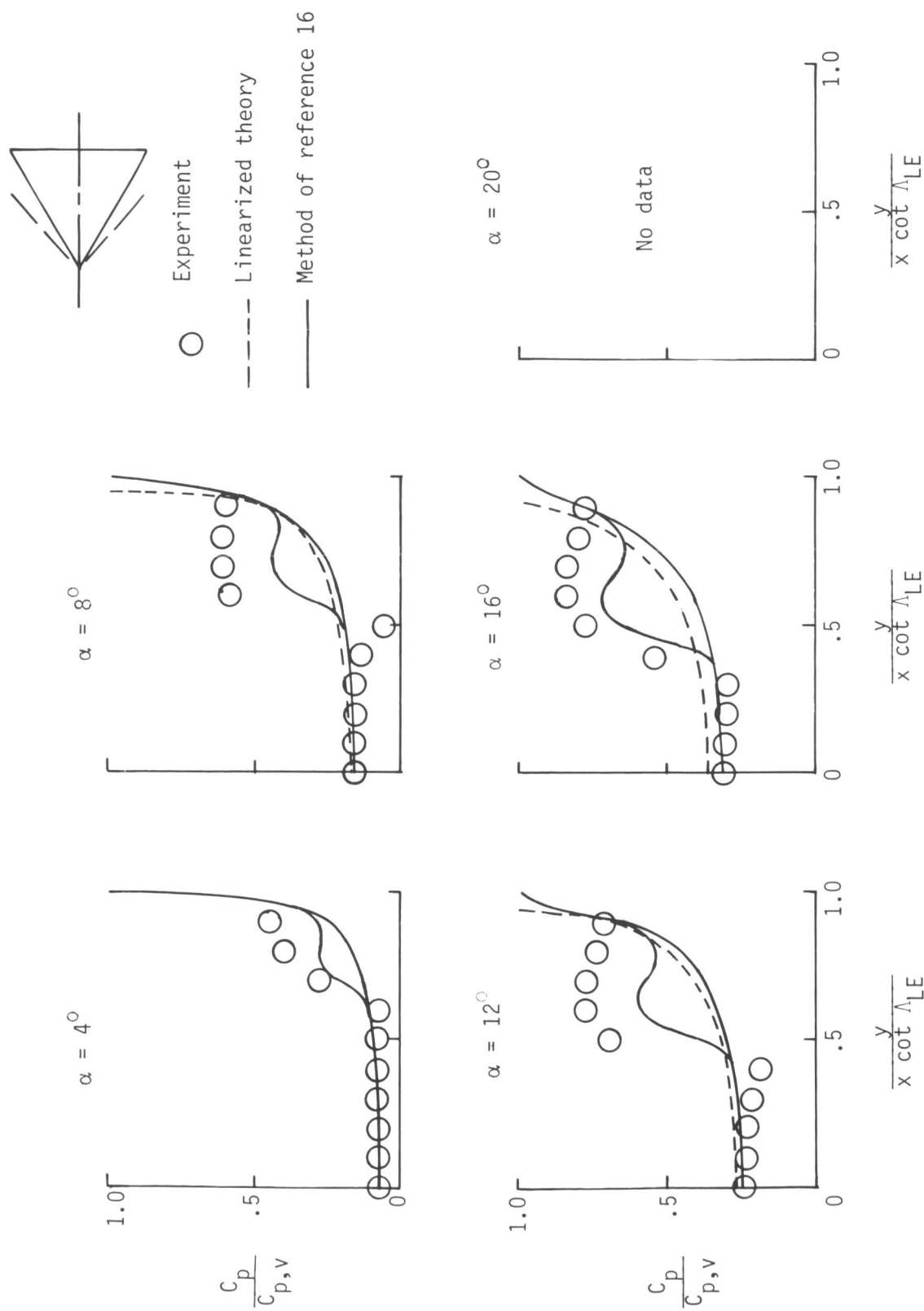
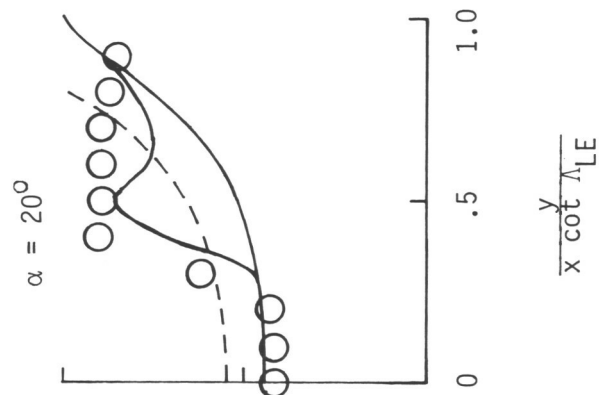
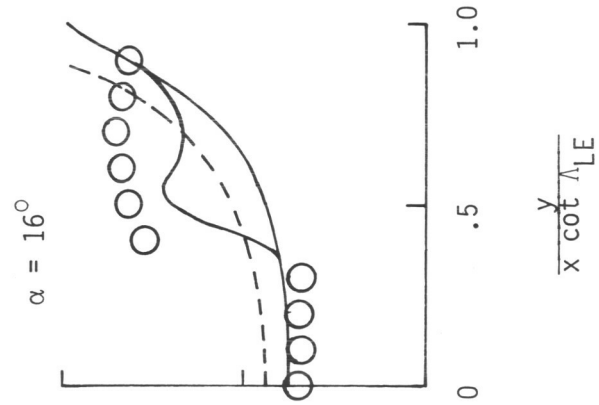
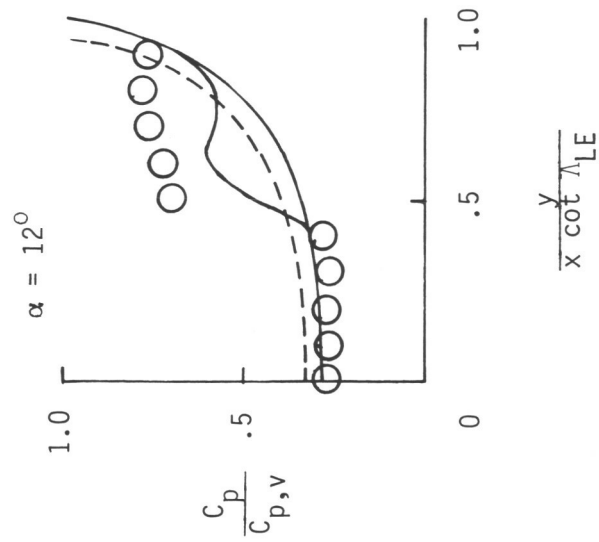
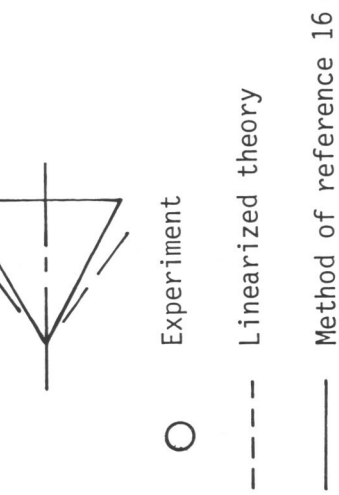
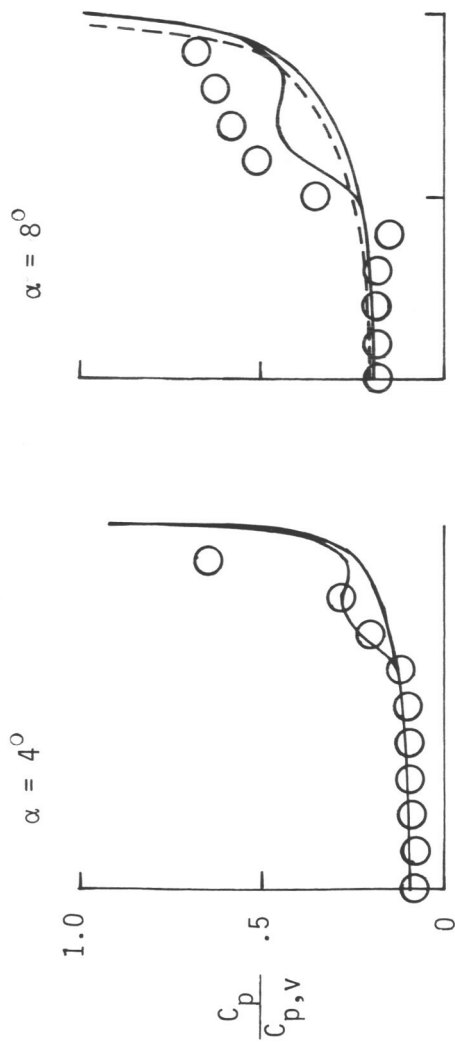
(d) $M = 2.4$.

Figure D2. Continued.



(e) $M = 2.8$.
Figure D2. Concluded.

(a) $M = 1.5$.Figure D3. Spanwise pressure distributions for delta wing with $\Lambda_{LE} = 60.0^\circ$.



(b) $M = 1.7$.
Figure D3. Continued.

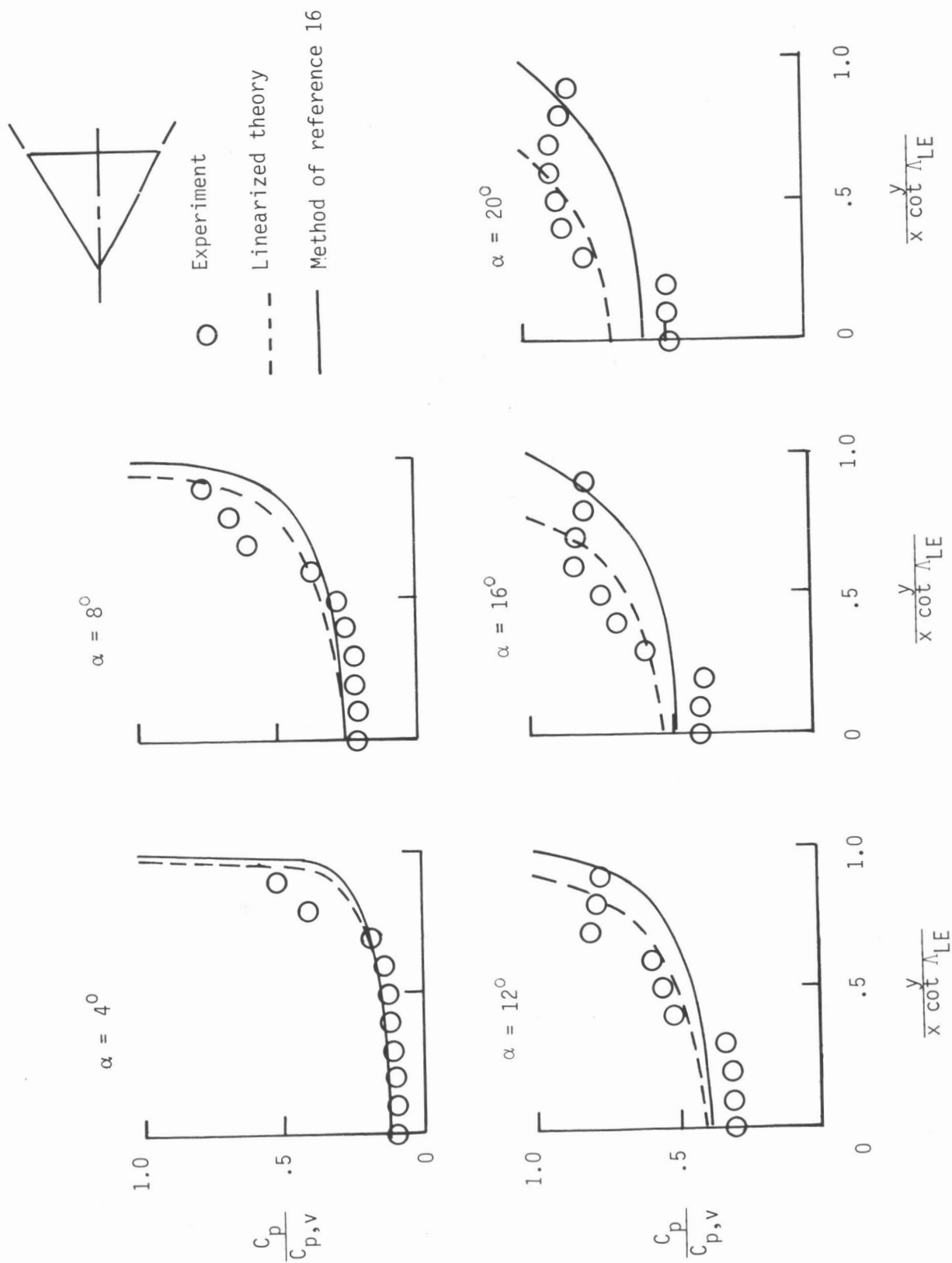
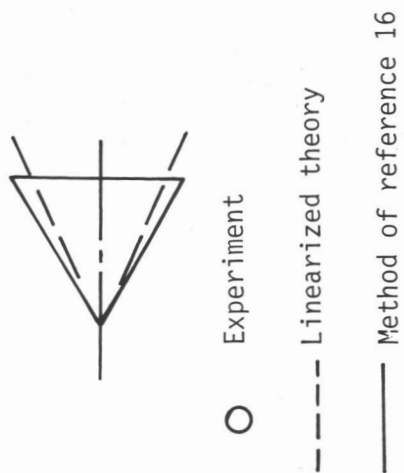
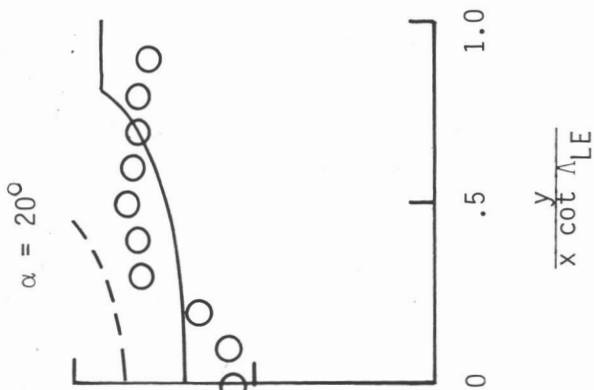
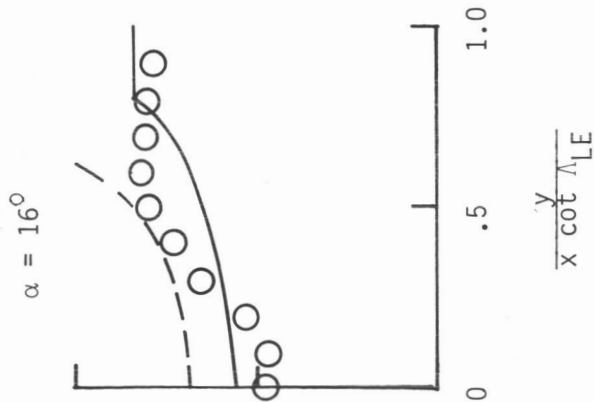
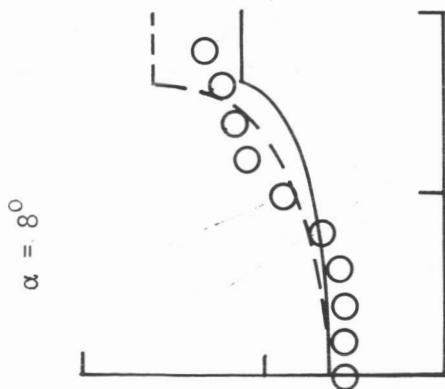
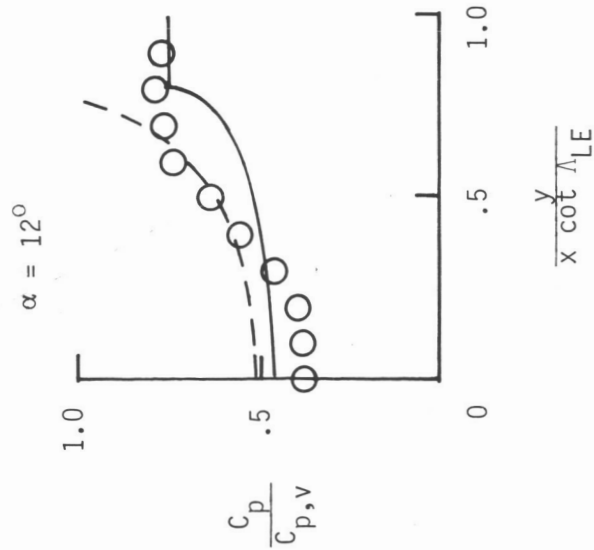
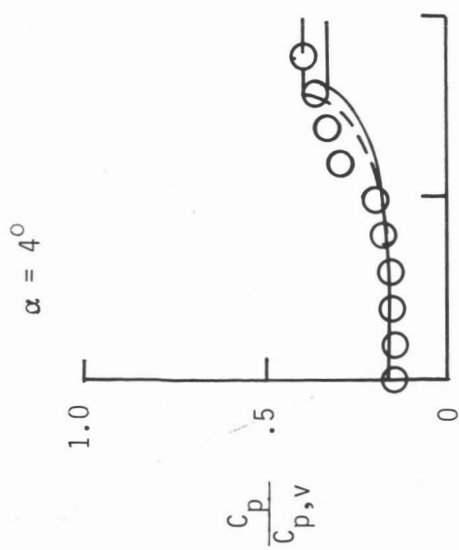
(c) $M = 2.0$.

Figure D3. Continued.



(d) $M = 2.4$.

Figure D3. Continued.

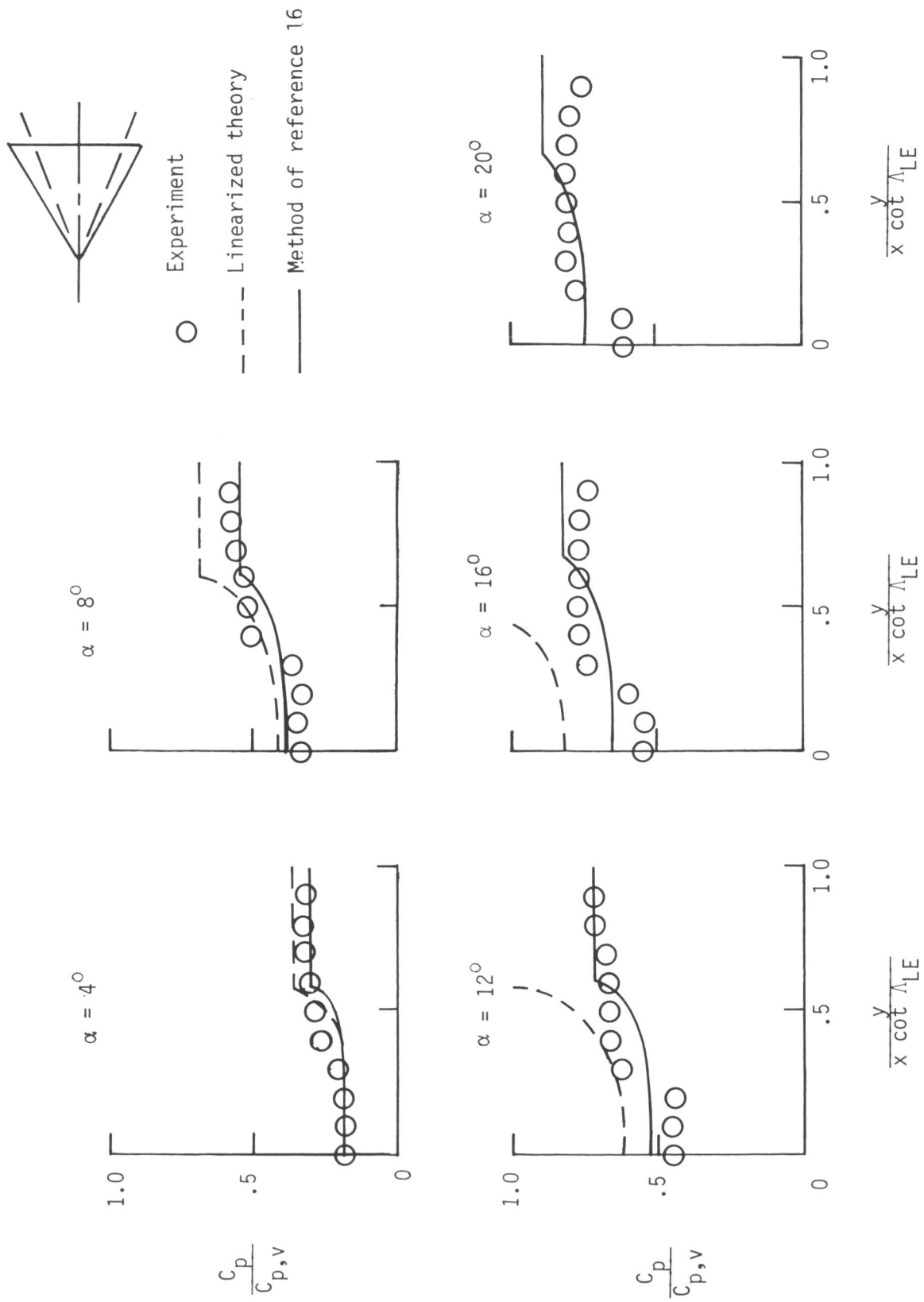
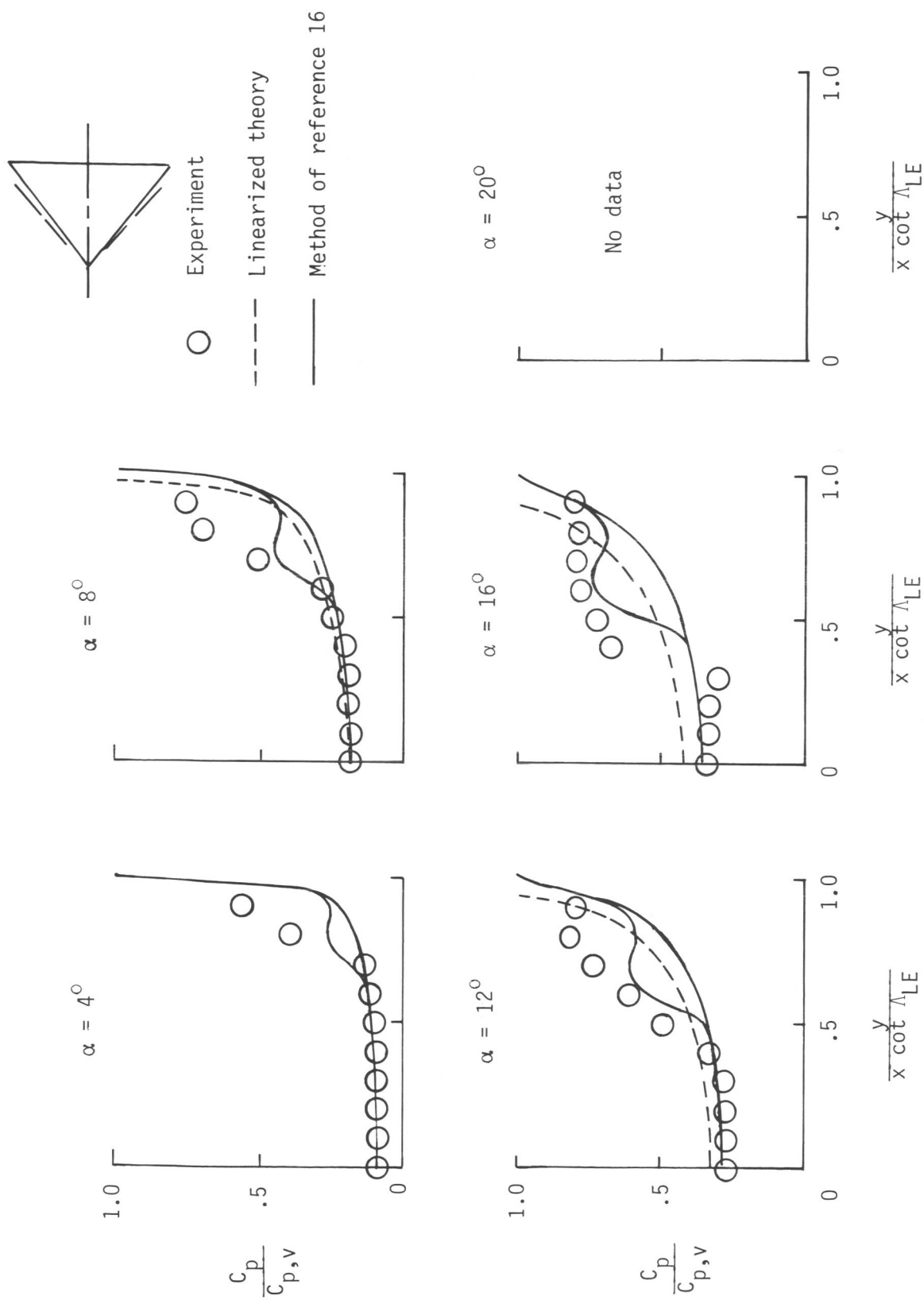
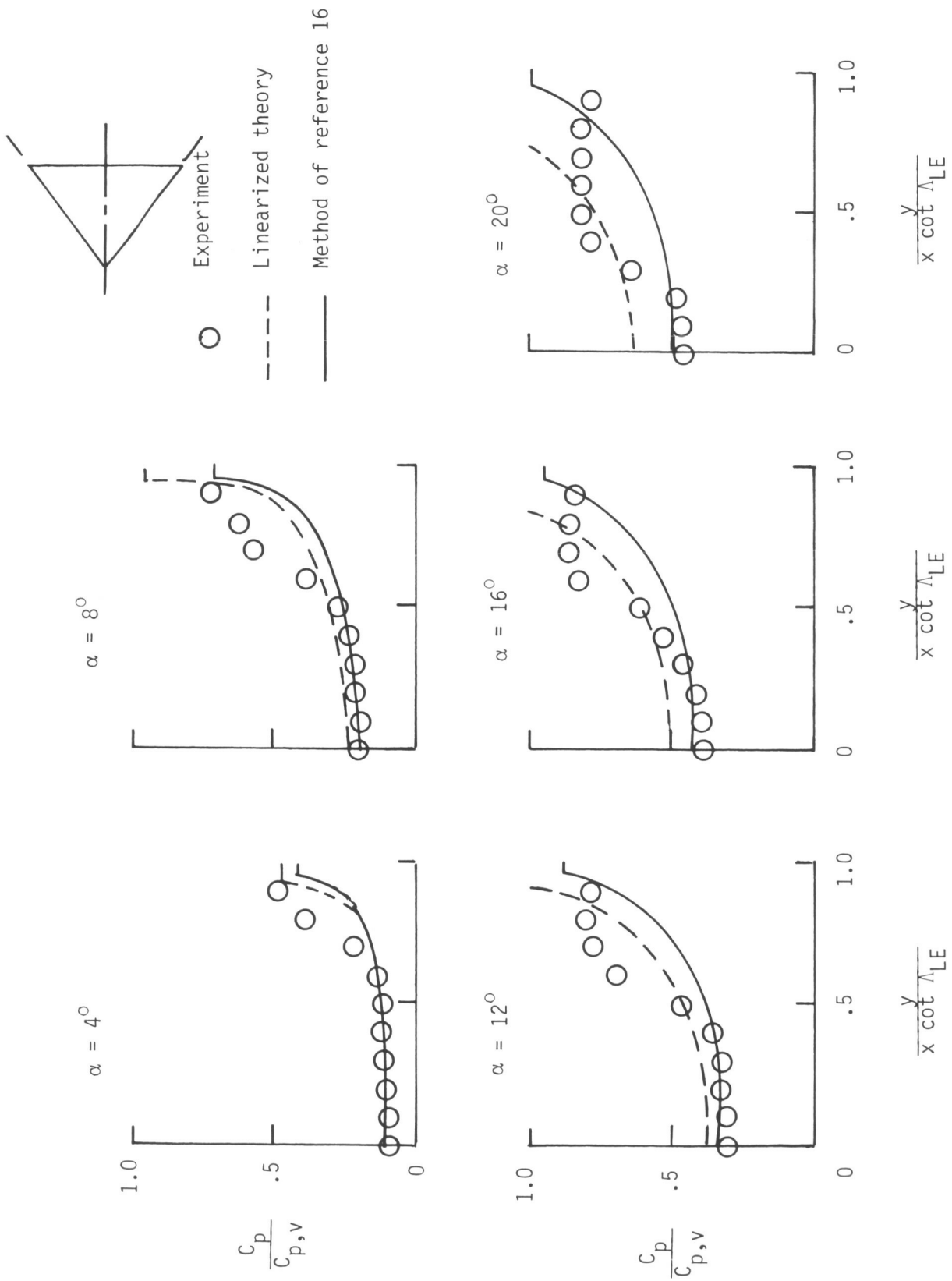
(e) $M = 2.8$.

Figure D3. Concluded.

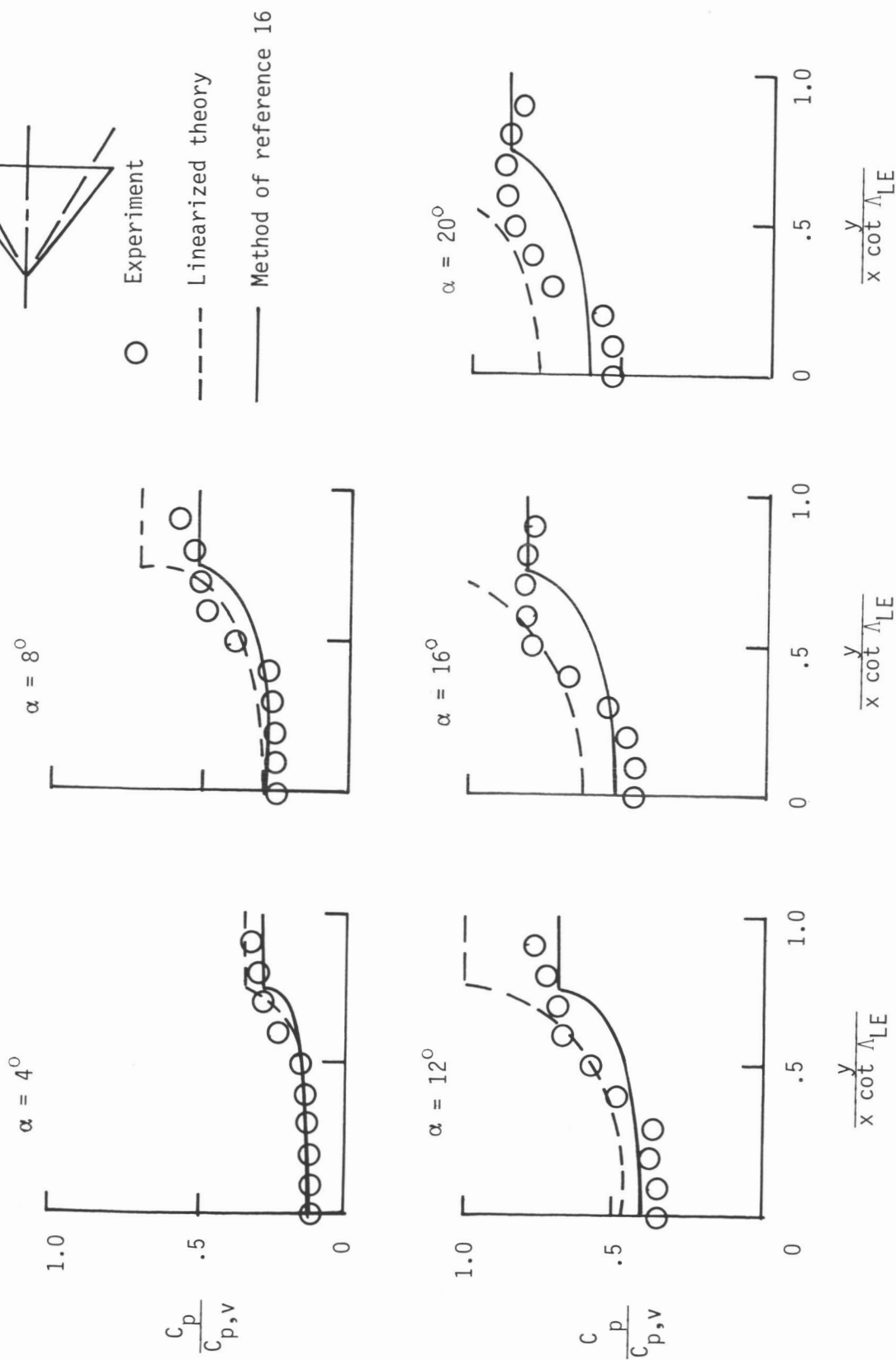


(a) $M = 1.5$.

Figure D4. Spanwise pressure distributions for delta wing with $\Lambda_{LE} = 52.5^\circ$.



(b) $M = 1.7$.
Figure D4. Continued.



(c) $M = 2.0$.
Figure D4. Continued.

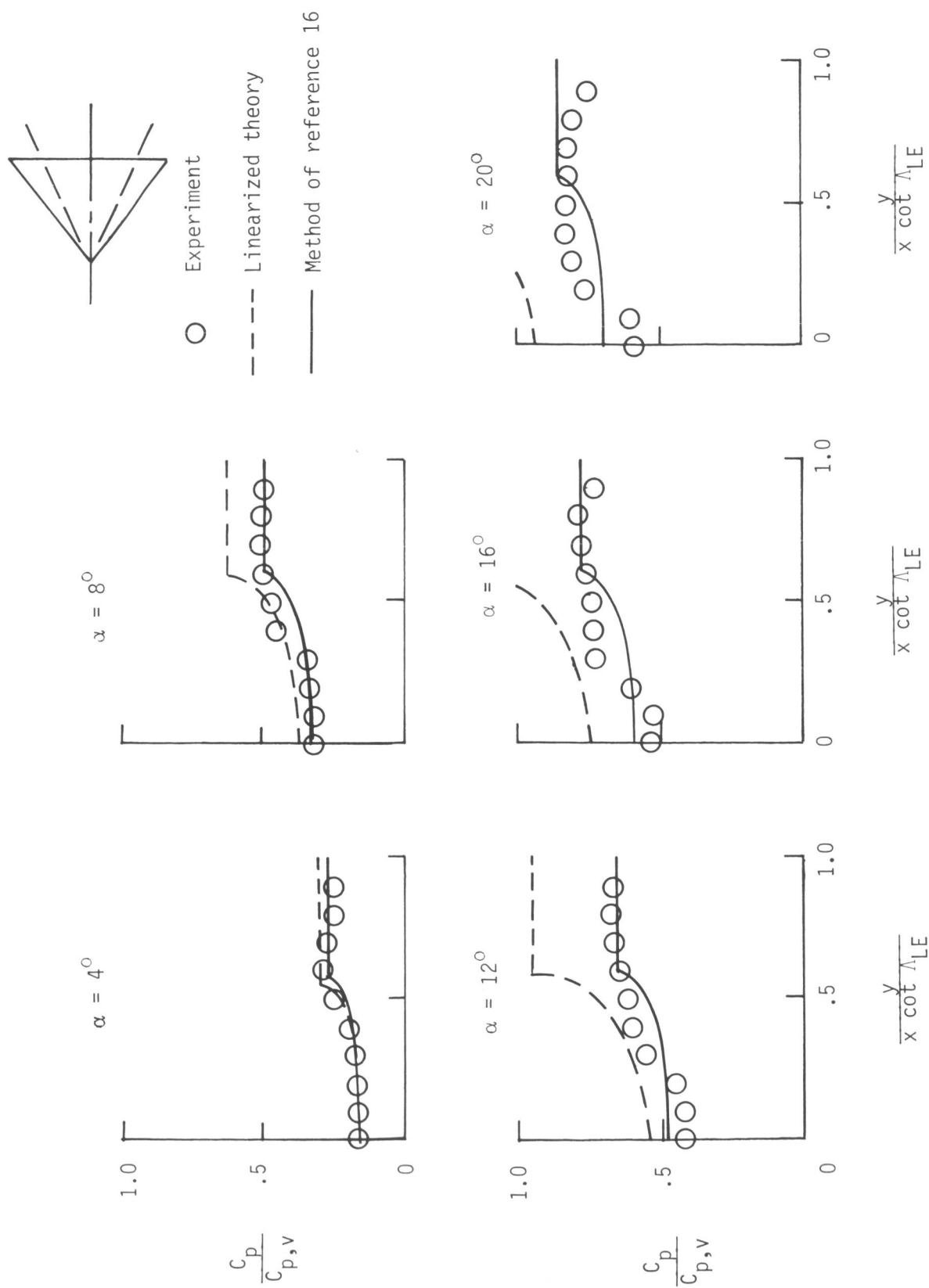
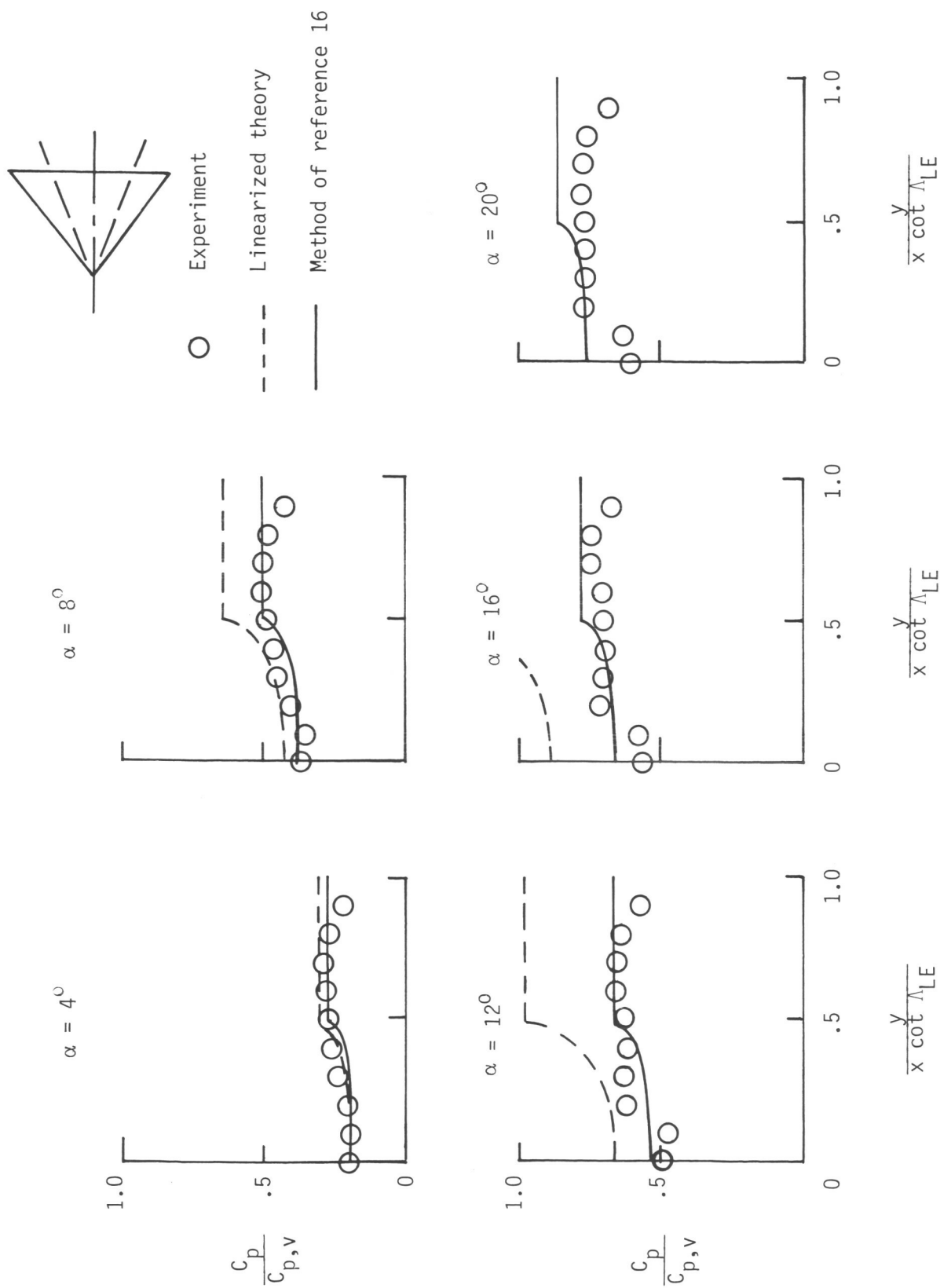
(d) $M = 2.4$.

Figure D4. Continued.



(e) $M = 2.8$.

Figure D4. Concluded.

References

1. Carlson, Harry W.; and Middleton, Wilbur D.: *A Numerical Method for the Design of Camber Surfaces of Supersonic Wings With Arbitrary Planforms*. NASA TN D-2341, 1964.
2. Carlson, Harry W.; and Miller, David S.: *Numerical Methods for the Design and Analysis of Wings at Supersonic Speeds*. NASA TN D-7713, 1974.
3. Mack, Robert J.: *A Numerical Method for Evaluation and Utilization of Supersonic Nacelle-Wing Interference*. NASA TN D-5057, 1969.
4. Kulfan, R. M.; and Sigalla A.: Real Flow Limitations in Supersonic Airplane Design. AIAA Paper 78-147, Jan. 1978.
5. Carlson, Harry W.; and Miller, David S.: The Influence of Leading-Edge Thrust on Twisted and Cambered Wing Design for Supersonic Cruise. AIAA-81-1656, Aug. 1981.
6. Carlson, Harry W.: *Aerodynamic Characteristics at Mach Number 2.05 of a Series of Highly Swept Arrow Wings Employing Various Degrees of Twist and Camber*. NASA TM X-332, 1960.
7. Morris, Odell A.; and Fournier, Roger H.: *Aerodynamic Characteristics at Mach Numbers 2.30, 2.60, and 2.96 of a Supersonic Transport Model Having a Fixed, Warped Wing*. NASA TM X-1115, 1965.
8. Miller, David S.; and Schemensky, Roy T.: Design Study Results of a Supersonic Cruise Fighter Wing. AIAA Paper 79-0062, Jan. 1979.
9. Miller, David S.; Pittman, Jimmy L.; and Wood, Richard M.: An Overview of Two Nonlinear Supersonic Wing Design Studies. AIAA-83-0182, Jan. 1983.
10. Lamar, John E.; and Campbell, James F.: Recent Studies at NASA-Langley of Vortical Flows Interacting With Neighboring Surfaces. *Aerodynamics of Vortical Type Flows in Three Dimensions*, AGARD-CP-342, July 1983, pp. 10-1-10-32.
11. Stallings, Robert L., Jr.; and Lamb, Milton: *Wing-Alone Aerodynamic Characteristics for High Angles of Attack at Supersonic Speeds*. NASA TP-1889, 1981.
12. Jackson, Charlie M., Jr.; Corlett, William A.; and Monta, William J.: *Description and Calibration of the Langley Unitary Plan Wind Tunnel*. NASA TP-1905, 1981.
13. Braslow, Albert L.; and Knox, Eugene C.: *Simplified Method for Determination of Critical Height of Distributed Roughness Particles for Boundary-Layer Transition at Mach Numbers From 0 to 5*. NACA TN 4363, 1958.
14. Stanbrook, A.; and Squire, L. C.: Possible Types of Flow at Swept Leading Edges. *Aeronaut. Q.*, vol. XV, pt. 1, Feb. 1964, pp. 72-82.
15. Ganzer, U.; Hoder, H.; and Szodruch, J.: On the Aerodynamics of Hypersonic Cruise Vehicles at Off-Design Conditions. *ICAS Proceedings—1978, Volume 1—Fuel Conservation, Hypersonic Vehicles, Environmental Effects, Materials and Structures, Computational Aerodynamics, Wind Tunnels, Flight Testing, Stability and Control*, J. Singer and R. Staufenbiel, eds., 1978, pp. 152-161.
16. Carlson, Harry W.; and Mack, Robert J.: *Estimation of Wing Nonlinear Aerodynamic Characteristics at Supersonic Speeds*. NASA TP-1718, 1980.

| | | | | | |
|--|--|---|--|---|--|
| 1. Report No. NASA TP-2430 | | 2. Government Accession No. | | 3. Recipient's Catalog No. | |
| 4. Title and Subtitle Lee-Side Flow Over Delta Wings at Supersonic Speeds | | | | 5. Report Date June 1985 | |
| | | | | 6. Performing Organization Code 505-43-23-02 | |
| 7. Author(s) David S. Miller and Richard M. Wood | | | | 8. Performing Organization Report No. L-15888 | |
| | | | | 10. Work Unit No. | |
| 9. Performing Organization Name and Address NASA Langley Research Center Hampton, VA 23665 | | | | 11. Contract or Grant No. | |
| | | | | 13. Type of Report and Period Covered Technical Paper | |
| 12. Sponsoring Agency Name and Address National Aeronautics and Space Administration Washington, DC 20546 | | | | 14. Sponsoring Agency Code | |
| | | | | | |
| 15. Supplementary Notes | | | | | |
| 16. Abstract <p>An experimental investigation of the lee-side flow on sharp leading-edge delta wings at supersonic speeds has been conducted. Pressure data were obtained at Mach numbers from 1.5 to 2.8, and three types of flow-visualization data (oil-flow, tuft, and vapor-screen) were obtained at Mach numbers from 1.7 to 2.8 for wing leading-edge sweep angles from 52.5° to 75°. From the flow-visualization data, the lee-side flows were classified into seven distinct types and a chart was developed that defines the flow mechanism as a function of the conditions normal to the wing leading edge, specifically, angle of attack and Mach number. Pressure data obtained experimentally and by a semiempirical prediction method were employed to investigate the effects of angle of attack, leading-edge sweep, and Mach number on vortex strength and vortex position. In general, the predicted and measured values of vortex-induced normal force and vortex position obtained from experimental data have the same trends with angle of attack, Mach number, and leading-edge sweep; however, the vortex-induced normal force is underpredicted by 15 to 30 percent, and the vortex spanwise location is overpredicted by approximately 15 percent.</p> | | | | | |
| 17. Key Words (Suggested by Authors(s)) Lee-side flow Delta wing Supersonic Leading-edge vortex | | | | 18. Distribution Statement Unclassified—Unlimited Subject Category 02 | |
| 19. Security Classif.(of this report) Unclassified | | 20. Security Classif.(of this page) Unclassified | | 22. Price A08 | |
| | | | | 21. No. of Pages 153 | |

National Aeronautics and
Space Administration

Washington, D.C.
20546

Official Business

Penalty for Private Use, \$300

SPECIAL FOURTH CLASS MAIL
BOOK

Postage and Fees Paid
National Aeronautics and
Space Administration
NASA-451



3 2 1J,A, 850603 S00161DSR
DEPT OF THE AIR FORCE
ARNOLD ENG DEVELOPMENT CENTER (AFSC)
ATTN: LIBRARY/DOCUMENTS
ARNOLD AF STA TN 37389

NASA

POSTMASTER:

If Undeliverable (Section 158
Postal Manual) Do Not Return